ORGANIC MATERIALS AS SATURABLE ABSORBER FOR PULSE GENERATION AT TELECOMMUNICATION WINDOW

SAMEER SALAM M.H. MOHAMMED HUSSEIN

FACULTY OF ENGINEERING
UNIVERSITY OF MALAYA
KUALA LUMPUR

2020

ORGANIC MATERIALS AS SATURABLE ABSORBER FOR PULSE GENERATION AT TELECOMMUNICATION WINDOW

SAMEER SALAM M.H. MOHAMMED HUSSEIN

THESIS SUBMITTED IN FULFILMENT OF THE REQUIREMENTS FOR THE DEGREE OF DOCTOR OF PHILOSOPHY

FACULTY OF ENGINEERING
UNIVERSITY OF MALAYA
KUALA LUMPUR

2020

UNIVERSITY OF MALAYA

ORIGINAL LITERARY WORK DECLARATION

Name of Candidate: SAMEER SALAM M.H. MOHAMMED HUSSEIN

Registration/Matric No: KVA170071

Name of Degree: DOCTOR OF PHILOSOPHY

Title of Project Paper/Research Report/Dissertation/Thesis ("this Work"):

ORGANIC MATERIALS AS SATURABLE ABSORBER FOR PULSE GENERATION AT TELECOMMUNICATION WINDOW

Field of Study: PHOTONICS

I do solemnly and sincerely declare that:

(1) I am the sole author/writer of this Work;
(2) This Work is original;
(3) Any use of any work in which copyright exists was done by way of fair dealing and for permitted purposes and any excerpt or extract from, or reference to or reproduction of any copyright work has been disclosed expressly and sufficiently and the title of the Work and its authorship have been acknowledged in this Work;
(4) I do not have any actual knowledge nor do I ought reasonably to know that the making of this work constitutes an infringement of any copyright work;
(5) I hereby assign all and every rights in the copyright to this Work to the University of Malaya ("UM"), who henceforth shall be owner of the copyright in this Work and that any reproduction or use in any form or by any means whatsoever is prohibited without the written consent of UM having been first had and obtained;
(6) I am fully aware that if in the course of making this work, I have infringed any copyright whether intentionally or otherwise, I may be subject to legal action or any other action as may be determined by UM.

Candidate's Signature Date: *6/August/2020*

Subscribed and solemnly declared before,

Witness's Signature Date:

Name:

Designation:

ORGANIC MATERIALS AS SATURABLE ABSORBER FOR PULSE GENERATION AT TELECOMMUNICATION WINDOW

ABSTRACT

This thesis demonstrates several types of fiber lasers based on newly developed organic materials as saturable absorbers (SAs). We used these SAs in all-fiber based erbium-doped fiber laser (EDFL) ring cavity to produce Q-switched and mode-locked pulses at telecommunication window, at ~ 1560 nm. Three different organic materials were used in this thesis: Bis[2-(4,6-difluorophenyl)pyridinato-C^2,N](picolinato)iridium(III) (FIrpic), bis(8-hydroxyquinoline)zinc (Znq_2) and Tris(8-hydroxyquinoline)aluminum (Alq_3). Finding new materials is still one of the defining characteristics of nonlinear optics field, as the rapid development of SAs has provided several new opportunities for nonlinear optics. Throughout this work, organic material showed a very interesting performance in terms of pulse duration, pulse energy, damage threshold, stability, spectral tunability, nonlinear response and proved to have a great potential in fiber laser technology. Organic materials are bio-compatible, environment-friendly, light-weight and mechanically flexible. The SA thin-films based on FIrpic, Znq_2 and Alq_3 in conjunction with polyvinyl alcohol (PVA) were successfully fabricated, in a simple, straight and low-cost process. A small piece of fabricated SA thin-film was inserted between two ferrules to form SA device. A set of measurements were taken to characterize the fabricated SAs, such as Fourier transform infrared (FTIR) spectrometer, optical absorption, linear and non-linear transmission. Different kinds of Q-switched fiber lasers with very high stability were successfully demonstrated using these materials. At first, FIrpic was used to develop a Q-switched laser with single- and dual-wavelength operation. Then, Znq_2 was used to demonstrate Q-switching pulsing with fixed and tunable wavelength operation. The produced pulse width was decreased from 6.6 µs to 2.8 µs, while the repetition rate was increased from 45 kHz to 85 kHz. Finally, Alq_3 was used as a Q-switcher to produce pulses at 1.5 µm and 1.0

µm regions. At 1.5 µm region, the pulse width and repetition rate were tunable within 1.2 µs to 6.65 µs and 31.65 kHz to 144.5 kHz, respectively. At 1 µm region, Alq_3 produced high pulse energy and high peak power of 0.8 µJ and 237.62 mW, respectively, in two different setups. Stable ultrafast soliton laser operations were also achieved by using the developed SAs. At first, FIrpic was used to demonstrate a mode-locked laser with pulse width and repetition rate of 120 ns and 3.43 MHz, respectively. Similarly, Znq_2 was also successful as a mode-locker, where it was used to produce a laser with a pulse width of 1.46 ps and a repetition rate of 3.5 MHz. Finally, a pulse width of 820 fs and a repetition rate of 4.9 MHz was achieved by using Alq_3. Alq_3 produced mode-locking operation with single and multi-wavelength operation at 1.0 µm with pulse width and repetition rate of 5.96 ps and 6.84 MHz, respectively. In conclusion, this work has successfully drawn attention to the potentials that organic materials have in fiber laser technology especially for Q-switching and mode-locking applications.

Keywords: Organic materials, Q-switched fiber laser, mode-locked fiber laser

BAHAN-BAHAN ORGANIK SEBAGAI PENYERAP BOLEH TEPU UNTUK PENJANAAN DENYUT PADA TETINGKAP TELEKOMUNIKASI

ABSTRAK

Disertasi ini mendemonstrasikan beberapa jenis laser gentian berasaskan penghasilan baru baham organic sebaga penyerap boleh tepu (SAs). Kami menggunakan SAs ini di dalam semua kaviti cincin gentian asas laser gentian ion erbium yang didopkan (EDFL) untuk menghasilkan denyut suis-q dan selakan –mod di tingkap telekomunikasi, pada ~ 1560 nm. Tiga bahan organic yang berlainan telah digunakan dalam disertasi ini; Bis[2-(4,6-difluorophenyl)pyridinato-C^2,N](picolinato)iridium(III) (FIrpic), bis(8-hydroxyquinoline)zinc (Znq_2) and Tris(8-hydroxyquinoline)aluminum (Alq_3). Pencarian bahan baru masih lagi satu ciri-ciri khusus kepada bidang tak linear optik, pembangunan pesat SAs telah menyediakan banyak peluang baru untuk optik tak linear. Melalui kerja ini, bahan organik menunjukkan prestasi yang sangat bagus dalam terma tempoh denyut, denyut tenaga, ambang kerosakan, kestabilan, spektrum boleh tala, tindakbalas tak linear dan terbukti mempunyai potensi bagus dalam teknologi laser gentian. Bahan-bahan organik adalah serasi-bio, endah alam sekitar, ringan dan boleh suai mekanikal. Filem SA berasaskan pada bahan FIrpic, Znq_2 and Alq_3 berhubung dengan polivinil alcohol (PVA) telah berjaya difabrikkan, ringkas, lurus dan proses kos rendah. Satu bahagian kecil SA-filem yang telah difabrikkan telah dimasukkan diaantara dua ferrule dalam turutan menhasilkan peranti SA. Satu set pengukuran telah diambil untuk mencirikan turutan SAs yang telah difabrikkan, seperti Transformasi Fourier Inframerah Spektroskopi (FTIR) Spektrometer, penyerapan optic, tranmisi linear dan tak linear. Berlainan jenis laser gentian suis-q dengan kestabilan yang tinggi telah Berjaya Berjaya didemostratkan menggunakan bahan-bahan ini. Mula-mula, FIrpic telah digunakan untuk menghasilkan laser suis-q dengan operasi jarak gelombang tunggal dan dual. Kemudian, Znq_2 telah digunakan untuk mendemost operasi denyut suis-q dengan tetap dan operasi jarak gelombang bola tala. Penghasilan denyut lebar

telah menurun dari 6.6 µs kepas 2.8 µs, manakala kadar ulangan telah menaik dari 45 kHz ke 85 kHz. Akhir sekali, Alq_3 telah digunakan sebagi suis-q untuk menghasilkan denyut-denyut pada bahagian 1.5 µm da 1.0 µm. Pada bahagian 1.5 µm, masing-masing denyut lebar dan kadar ulangan telah boleh tala diantara 1.2 ke 6.65 µs dan 31.65 sehingga 144.5 kHz. Pada bahagian 1 µm, Alq_3 telah menghasilkan tenaga tinggi dan kuasa puncak yang tinggi iaitu 0.8 µJ dan 237.62 mW dalam dua tatacara yang berbeza. Operasi laser *Ultrafast Soliton* yang stabil juga tercapai dengan menggunakan pembangunan SAs. Pada mulanya, FIrpic telah digunakan untuk mendemonstrat laser selakan-mod dengan denyut lebar dan kadar ulangan 120 ns dan 3.43 MHz. Akhirnya, denyut lebar 820 fs dan kadar ulangan of 4.9 MHz telah tercapai dengan menggunakan Alq_3. Alq_3 menghasilkan operasi selakan-mod tunggal dan pelbagai jarak gelombang pada operasi 1.0 µm dengan masing-masing denyut lebar dan kadar ulangan 5.96 ps dan 6.84 MHz. Sebagai kesimpulan, kerja ini berjaya menarik perhatian kepada potensi bahan-bahan organic yang terdapat di dalam teknologi gentian laser terutama untuk aplikasi suis-q dan selakan-mod

Kata kunci: Bahan organik, laser gentian bersuis-Q, laser gentian selakan mod

ACKNOWLEDGEMENTS

To my parents, to my family. I must be the luckiest man to have you, I feel a deep sense of gratitude. Thank you for being in my life. Thank you for your unlimited love and support.

To my mentor, Prof. Sulaiman Wadi Harun. I am very blessed and privileged to have you as a supervisor. Thank you for ever-present kindness and generosity.

To my second supervisor, Dr. Wong Wei Ru. I am grateful for your support and help. I have learned a lot from you.

To Al-Sadiq university, thank you for all the support you gave me.

TABLE OF CONTENTS

LIST OF FIGURES

LIST OF TABLES

LIST OF SYMBOLS AND ABBREVIATIONS

2D	:	Two-dimensional
Alq_3	:	Tris(8-hydroxyquinoline)aluminum
BP	:	Black Phosphorus
c	:	Speed of light
CNTs	:	Carbon Nanotubes
CVD	:	chemical vapour deposition
CW	:	Continues Wave
dB	:	Decibel
DI	:	Deionized Water
DWQS	:	Dual-Wavelength Q-Switch
EDF	:	Erbium-Doped Fiber
EDFA	:	Erbium-Doped Fiber Amplifier
EDFL	:	Erbium-Doped Fiber Laser
E_g	:	Optical Band Gap
FESEM	:	Field Emission Scanning Microscopy
FIrpic	:	Bis[2-(4,6-difluorophenyl) pyridinato-C^2,N] (picolinato)iridium(III)
FTIR	:	Fourier-Transform Infrared Spectroscopy
FWHM	:	Full-Width at Half Maximum
GVD	:	Group Velocity Dispersion
HNLF	:	Highly Nonlinear Fiber
hv	:	Photon Energy
I	:	Light intensity
ISO	:	Optical Isolator

LASER	:	Light Amplification by Stimulated Emission of Radiation
LD	:	Laser Diode
LPE	:	Liquid Phase Exfoliation
MWCNTs	:	Multi-Walled Carbon Nanotubes
n	:	Refractive index
NA	:	Numerical Aperture
NLPs	:	Noise-Like Pulses
nm	:	Nanometer
NOLM	:	Nonlinear Optical Loop Mirror
NPR	:	Nonlinear Polarization Rotation
OC	:	Optical Coupler
OSA	:	Optical Spectrum Analyzer
OSC	:	Oscilloscope
OTDM	:	Optical Time Division Multiplexing
PC	:	Polarization Controller
PCF	:	Photonic Crystal Fiber
ps	:	Picosecond
PVA	:	Polyvinyl Alcohol
PZT	:	Piezoelectric Transducer
RF	:	Radio Frequency
RFSA	:	RF Spectrum Analyzer
SA	:	Saturable Absorber
SC	:	Supercontinuum
$Sech^2$	:	Secant hyperbolic
SEM		Scanning Electron Microscope
SESAMs	:	Semiconductor Saturable Absorption Mirrors

SMF	:	Single Mode Fiber
SNR	:	Signal to Noise Ratio
SPM	:	Self-Phase Modulation
SWCNT	:	Single-Walled Carbon Nanotubes
TBF	:	Tunable Bandpass Filter
TBP	:	Time-Bandwidth Product
TI	:	Topological Insulator
TMD	:	Transition Metal Dichalcogenide
WDM	:	Wavelength Division Multiplexing
XPM	:	Cross-Phase Modulation
YDF	:	Ytterbium-Doped Fiber
YDFL	:	Ytterbium-Doped Fiber Laser
Znq_2	:	bis(8-hydroxyquinoline)zinc

CHAPTER 1: INTRODUCTION

1. 1 Background and Motivation

Pulsed fiber lasers are extremely important in many fields in science and engineering technology. Fiber lasers have extensive applications in many areas such as telecommunications (O'Mahony, Simeonidou, Hunter, & Tzanakaki, 2001), signal processing (Ghelfi et al., 2014; Khilo et al., 2012), optical frequency measurements (Jones et al., 2000; Udem, Holzwarth, & Hänsch, 2002), ranging metrology (Coddington, Swann, Nenadovic, & Newbury, 2009; Joohyung Lee, Kim, Lee, Lee, & Kim, 2010), high-resolution atomic clocks (Bloom et al., 2014; Nemitz et al., 2016), and astronomy (C.-H. Li et al., 2008; Steinmetz et al., 2008). In comparison with other types of lasers, fiber lasers are compact, reliable, highly efficient, robust, and always deliver high-quality laser beams (Fermann & Hartl, 2013; X. Liu, Cui, Han, Yao, & Sun, 2015; Nishizawa, 2014; C. Zhao et al., 2012). Additionally, they have the advantages of alignment-free, small size, simple structure, high environmental stability, and low cost (Cai, Chen, Chen, & Hou, 2018; Y. Chen, G. Jiang, S. Chen, Z. Guo, X. Yu, C. Zhao, H. Zhang, Q. Bao, S. Wen, & D. Tang, 2015; Sheng et al., 2013; J. Xu, Liu, Wu, Yang, & Wang, 2012).

Fiber lasers have been developed rapidly over the past decade. It is worth noting that fiber lasers have been revolutionized by the advances in fiber optics. Fiber optics provides an appropriate platform and has a significant impact on fiber lasers developments. A fiber laser uses rare-earth doped fiber as a gain medium. Rare-earth ions such as erbium (Er), ytterbium (Yb), holmium (Ho), thulium (Tm) and neodymium (Nd) are doped into the fiber to provide a gain in various wavelength regions. Specifically, erbium-doped fiber laser (EDFL), which is operating at 1.5 µm region, is considered as one of the most widely developed fiber lasers and have received huge interest from the researchers. They have many practical advantages such as compact, efficient heat dissipation, inexpensive and

robust (Chong, 2008). Additionally, EDFL operates at wavelength region around 1550 nm, which falls in a low loss window of standard single-mode fiber (SMF).

The pulsed fiber laser can be realized by either active or passive techniques. The active technique achieved by inserting an optical modulator into the laser cavity (Alvarez-Chavez et al., 2000; Kee, Lee, & Newson, 1998). On the other hand, the passive technique does not require an external device, instead, it is obtained through incorporating a saturable absorber (SA) inside the laser cavity. The passive techniques are, in general, cost-effective and more useful than active approaches which require additional switching electronics (Svelto & Hanna, 2013). Additionally, passive techniques are more compact, simple, and flexible to be implemented compared to the active method (Shi-Xiang, Wen-Xue, Qiang, Hui, & He-Ping, 2008).

To date, several types of passive SAs have been intensively investigated for generating Q-switched and mode-locked fiber lasers, including semiconductor saturable absorber mirrors (SESAMs) (J. Y. Huang et al., 2008; Ursula Keller, 2003; Lecourt, Martel, Guezo, Labbe, & Loualiche, 2006; J. Liu, J. Xu, & P. Wang, 2012; Z.-C. Luo et al., 2015; Nodop et al., 2007; Spühler et al., 2001), carbon nanotubes (CNT), (Ahmed et al., 2015; X. Xu et al., 2014; U. Zhang et al., 2013; Zhou, Wei, Dong, & Liu, 2010), and two-dimensional (2D) nanomaterials such as graphene and transition-metal di-chalcogenides (TMDs) (Cao, Wang, Luo, Luo, & Xu, 2011; Jiang Liu, Jia Xu, & Pu Wang, 2012; Popa et al., 2011).

SESAMs, however, demand an expensive and complex fabrication. Additionally, they have limited applications as they are not compatible with optical fiber. The CNTs, on the other hand, have the advantages of fiber compatibility, low cost and ease of fabrication over the traditional SAs (J. Y. Huang et al., 2008; Lecourt et al., 2006; D. Lin et al., 2010; Philippov, Kir'yanov, & Unger, 2004). CNTs also have a wide operating bandwidth, low saturation intensity and sub-picosecond recovery time. CNTs, however,

require a complex band gap control which limits their operation at certain wavelengths (Q. L. Bao et al., 2009). The dominance of CNTs was reduced with the introduction of graphene, as it has a cost-efficient and simple fabrication and manufacturing processes and ultrafast recovery time. Consequently, graphene became the dominant choice for SAs (J. Liu, Wu, Yang, & Wang, 2011; L. Zhang et al., 2012). In comparison to CNT, graphene has a higher damage threshold and a super broad bandwidth. But, graphene, however, has the drawbacks of low modulation depth as well as a small optical absorption range which posed a limitation in many applications (Luo et al., 2010).

Recently, black phosphorous (BP) have also attracted much attention as it has the potential of a promising SA for both Q-switched and mode-locked fiber laser applications (Y. Chen, G. Jiang, S. Chen, Z. Guo, X. Yu, C. Zhao, H. Zhang, Q. Bao, S. Wen, D. Tang, et al., 2015; Jiang, Yin, Zheng, Yu, & Cheng, 2015; L. Kong et al., 2016). BP has a highly useful property of a controllable band gap through the control of its thickness. However, BP oxidation could be accelerated in the air when it illuminated to high power illuminates, which could lead to reducing the damage threshold (Feng et al., 2016). Moreover, BP is a hydrophilic material (J. Li et al., 2016) which is easily damaged when exposed to water and oxygen.

Lately, TMDs have been extensively studied as SAs for both Q-switching and mode-locking operations (Heping Li et al., 2015; Zhengqian Luo et al., 2014; S. Wang et al., 2014; H Zhang et al., 2014; Meng Zhang et al., 2015). For instance, molybdenum disulfide (MoS_2) has attracted much attention as it has a unique absorption property and also a thickness-dependent band gap (Du et al., 2014; Hao Liu et al., 2014). Yet, TMDs have a low impurity and uniformity and low damage threshold which restricts the long-term stability of the pulsed fiber laser.

Nevertheless, there have been increasing concerns about the effect of long-term exposure of the nanomaterials on human health (Nel, Xia, Mädler, & Li, 2006). On the

other hand, many attempts in the last few years have been carried out to find new materials to be used as a high-performance SAs. In that regards, organics material might be a promising candidate as new SA as they are biocompatible (Šafaříková et al., 2018) and have a broad spectral tunability. Additionally, organic material have a large and ultrafast nonlinear response and they can be solution-processed at low cost. Moreover, organic material would be a highly desirable alternative for developing non-hazardous and environmentally-friendly photonic devices which could find increasing applications in biomedical lasers.

In comparison with traditional inorganic materials, organic materials have the advantages of simple and low-cost manufacturing process and easy control of physical properties (Nel et al., 2006). Despite numerous works reported on the use of organic materials in the linear regimes, the applications of organic materials in nonlinear optics, especially in the fiber lasers pulse generation, have yet to be fully explored.

Bis[2-(4,6-difluorophenyl)pyridinato-C^2,N](picolinato)iridium(III) (FIrpic), bis(8-hydroxyquinoline)zinc (Znq_2) and Tris(8-hydroxyquinoline)aluminum (Alq_3) might be a good candidate to be used as an efficient SA. They are widely utilized in the development of organic light-emitting diodes (Adachi, Kwong, et al., 2001; Jaewon Lee et al., 2008). Additionally, they have a straightforward synthesis process, excellent stability and favourable electrochemical properties. Furthermore, they have simple, low-cost and straightforward fabrication process, which would be very interesting for practical applications. They might be a strong potential candidate for developing pulsed fiber laser with a very interesting performance.

This research tries to draw attention to the potentials that organic materials have in fiber laser technology. The proposed organic materials were used in a simple all-compact EDFL cavity and produced a very interesting result. To the best of our knowledge, this

research will be the first to demonstrate the usage of these proposed materials as SAs in fiber laser cavity.

1. 2 Objectives of Research

This thesis has the goal of drawing attention to the potential that organic-based SAs have in pulse fiber laser technology. This thesis shows that these materials can be fabricated at a low-cost, easy and straight-forward process. Furthermore, this thesis shows that different types of Q-switched and mode-locked fiber lasers have been demonstrated based on organic materials, which further indicates their potentials. Several objectives have been outlined to guide the research direction toward the goal:

1. To fabricate and characterize newly developed organic materials, FIrpic, Znq_2 and Alq_3, to be used as a high-performance SAs.
2. To design an optimized fiber laser cavity to generate Q-switch and mode-locked pulses.
3. To develop single, dual-wavelength and tunable wavelength Q-switched fiber laser with high stability and wide tunability by using the fabricated organic SAs.
4. To generate a soliton mode-locked fiber laser with nanosecond, picoseconds and femtoseconds pulse width by using the developed organic SAs.

1. 3 Contributions

The contributions of this research work are summarized as follow:

1. A simple and compact Q-switched and mode-locked EDFL is successfully developed using organic materials-based SA. The newly thin-film SAs are prepared by drop-casting technique. A small piece of the prepared thin-film SAs was sandwiched between two ferrules and integrate into the EDFL ring cavity.

2. Demonstration of single, dual and tunable wavelength Q-switched fiber lasers by using the developed SAs.
3. Demonstration of various mode-locked EDFLs using the developed SAs. Soliton mode-locked EDFL lasers with nanosecond, picosecond and femtosecond were developed by using FIrpic, Znq_2 and Alq_3, respectively. Additionally, dark pulse-mode-locked fiber laser was demonstrated by managing the polarization of the cavity. Furthermore, supercontinuum wavelength with picosecond pulse width was obtained by using 100 m PCF fiber.
4. To the best of our knowledge, this is the first time that these organic materials were used in fiber laser technology.

1. 4 Thesis Overview

Though out this thesis, a comprehensive study of Q-switched and mode-locked pulse generation by using organic materials is presented. This thesis consists of six chapters. This chapter presents a background, motivation and objectives of this study.

Chapter 2 presents the literature review of this research work. Theoretical aspects for pulse propagation in optical fiber are addressed, along with a review on the recently used SAs. The important parameters of the pulsing operation of the fiber laser are also described.

Chapter 3 illustrates the fabrication process and characterization of FIrpic, Znq_2 and Alq_3 as SAs. All the SAs are fabricated in a simple, low cost, straight-forward process. Polyvinyl alcohol (PVA) was used to form the thin-film SAs. FTIR, absorption spectrum, SEM image, linear and non-linear absorption were used to characterize the SAs thin-films.

Chapter 4 reports various passively Q-switched EDFLs using the developed SAs. Firstly, FIrpic was used to produce a Q-switched laser with both single and dual-

wavelength operations. Secondly, Znq_2 was used to produce single and tunable-wavelength operation. Thirdly, Alq_3 was used to generate Q-switched pulsing at 1560 nm. Finally, Alq_3 was used to generate a Q-switched laser at 1067 nm to investigate the potential of organic materials at 1.0 µm region.

Chapter 5 demonstrates several types of mode-locked fiber lasers. FIrpic and Znq_2 were used to develop nanosecond and picosecond soliton mode-locking operation, respectively. Znq_2 was also used to produce dark pulses and supercontinuum mode-locking operations. A mode-locked with a femtosecond pulse width was demonstrated by using Alq_3. Alq_3 was also used to produce mode-locking operation at 1.0 µm region.

Finally, chapter 6 concludes the thesis and presents a summary of the research findings. The final chapter also provided a recommendation for future works.

CHAPTER 2: LITERATURE REVIEW

2. 1 Overview of Fiber Lasers

When the lasers were firstly developed in the 1960s, it was said that the laser was a solution in search of a problem. It was not clear how it would be used. The laser in the coming decades become an enabling technology with applications as diverse as optical communications, range finding, laser reflectometry, remote sensing, laser surgery, reading-writing data on CDs and DVDs, bar-code scanners and precision cutting device manufacturing (Quimby, 2006). It is not an exaggeration to state that the laser had made the modern technological world the way it is today.

The laser consists of three basic elements: a pumping power to supply energy, a gain medium to amplify the light and a feedback mechanism. The feedback will form an optical cavity, in which the light will be circulated back and forth through the gain medium. The amplification is achieved by stimulated emission. Albert Einstein has proposed this process in 1917. To understand stimulated emission, we need to consider the ways that light interacts with an atom, see Figure 2.1 below. There are three processes involved; absorption, spontaneous emission and stimulated emission. In absorption, an atom is raised to a higher energy level (excited state) from the lowest energy level (ground state) by absorbing an incident photon. That atom will fall back to the ground state and emits a photon, this is called spontaneous emission. The stimulated emission occurs when an atom that is already in the excited state is stimulated to drop to ground state and emit a photon (which is identical to the photon that was originally absorbed by the atom in the first place). Amplification is the process of duplicating the photons. As the number of photons increases, the intensity of light increases.

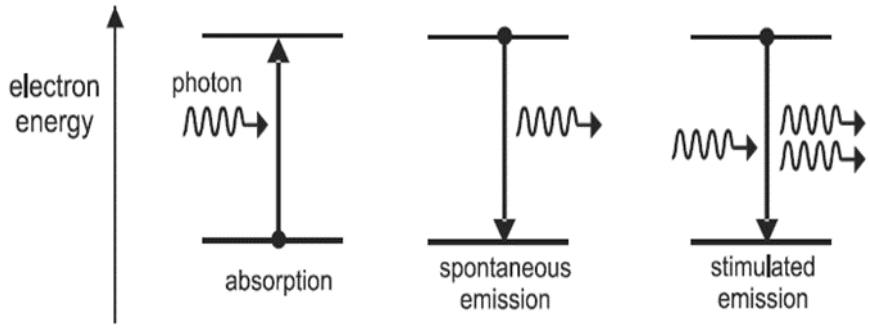

Figure 2.1: Amplification process in the laser's gain medium (Quimby, 2006)

A fiber laser is a type of laser in which the gain medium is an optical fiber doped with rare-earth elements such as erbium, ytterbium, and thulium. The fiber lasers technology was born in 1961 when Snitzer demonstrated a laser oscillation in glass (Snitzer, 1961a) and then in fiber laser (Snitzer, 1961b). In 1964, fiber laser oscillation in a gain fiber was demonstrated by Koester and Snitzer (Koester & Snitzer, 1964). In the 1980s and 1990s, fiber lasers have received a tremendous research interest due to the appearance of reliable and reasonably powerful diode-pumped laser technology. This was further motivated by the application of the erbium-doped fiber amplifier (EDFA) in optical telecommunication. The telecommunication age was and still contributing to the development of fiber laser technology. On the other hand, one can observe from reviewing the millstone of the fiber laser technology development, that fiber laser is a result of joint success in the field of optical fiber technology and solid-state lasers. Fiber lasers have adopted solutions from both fields. Today, fiber lasers complement gas and bulk solid-state high-power lasers (Ter-Mikirtychev, 2014).

2. 2 Light Amplification

To understand the principle of fiber laser, it is important to understand the basics of optical amplification. At thermal equilibrium, the atomic system is naturally relaxed, as the lower energy level is more populated than the higher energy level. High energy level might

increase its population at higher temperatures, but it never becomes higher than the lower level. In order to achieve an optical gain through stimulated emission, equilibrium status should be avoided and the population at high energy level should be higher than the lower level, this is known as population inversion. The population inversion can be realized by pumping method. The laser system can be classified into three-level and four-level systems depending on the active medium.

Figure 2.2 illustrates the four-energy-level system. As the pump energy is launched into the gain medium, atoms will be excited from level 1 (ground level) to level 2. Then the atoms will decay spontaneously to level 4 after fast relaxation to energy level 3 (non-radiative relaxation and takes only sub-nanosecond to picosecond). Then the atoms will have non-radiative relaxation from level 4 and returning to level 1. The amplification occurs during the slow spontaneous decay from level 3 to level 4 (with durations from milliseconds to nanoseconds). Atoms will be accumulated at level 3, while level 4 will remains unpopulated, due to the fast relaxation from Level 4 to level 3.

Amplification can be made in fiber laser by achieving population inversion in the gain medium. The amplification of lasing increases with the length of the gain medium until the saturation level is reached. The amplification in fiber lasers can be very high and it is only limited by the available light intensity or the laser oscillations inside the fiber laser cavity (in case the optical feedback becomes equal to the amplification). The optical feedback is build-up by either a ring or Fabry Perot resonator. The high gain of the gain medium enables the fiber laser to operate with a low optical feedback power, thus simplifies the developments of fiber lasers.

The gain medium, as mentioned above, are rare earth elements such as ytterbium, neodymium, erbium or thulium and are ionized in silica in order to form a trivalent state. In the next subsection, we will focus on erbium-doped fiber (EDF) as it is widely used as a gain medium in fiber laser that generates laser in 1550 nm region, which it is interest for communication applications.

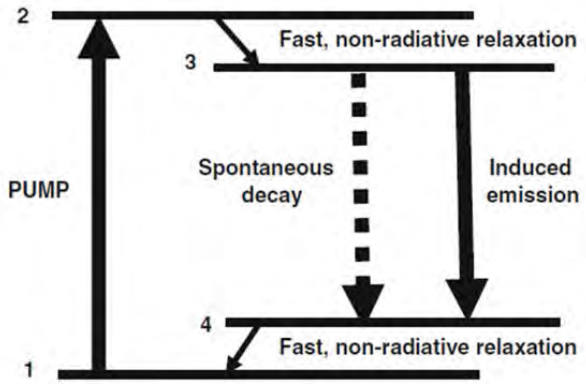

Figure 2.2: Four-energy-level scheme of laser operation

2. 3 Spectroscopic Properties of Erbium-Doped Fibers

EDFs have attracted much attention in the 1980s and they are probably the most studied in comparison with other rare earth materials, due to their importance in optical telecommunication. An enormous number of successful commercial development and research papers are triggered by the demand for optical amplifiers and fiber lasers that operating at 1.5 µm and for telecommunication applications (Ter-Mikirtychev, 2014). Figure 2.3 illustrates the energy level of the erbium ion (Er^{3+}). The transition in EDF from $^4I_{13/2}$ to $^4I_{15/2}$ is considered as the main transition since it provides a gain in the C-band region, as $^4I_{13/2}$ is the only metastable state at room temperature (Ngo, 2016). The EDF has the maximum emission and absorption peak at a wavelength around 1530 nm, therefore, the operating wavelength must be chosen in the band that the absorption cross-section is much smaller than the emission cross-section, which is around 1.55-µm. The EDF can be pumped with a laser diode at a wavelength of 810, 980, and 1480 nm. The pumping operation at 980 and 1480 nm are more preferred as the pumping at 810 nm is inefficient. This is attributed to excited-state absorption (ESA), which will cause an undesirable waste of pumping photons. Pumping at 980 nm is one of the most commonly used for EDFA as it has a high gain efficiency and high signal-to-noise ratio (SNR) (Digonnet, 2001). Additionally, it gives better quantum conversion efficiencies and better noise figures (NFs) for power amplifiers. On the

other hand, EDF is also widely used for ultrashort pulse generation as the fiber dispersion at 1.5 μm is irregular and the EDF has a broad spectrum range.

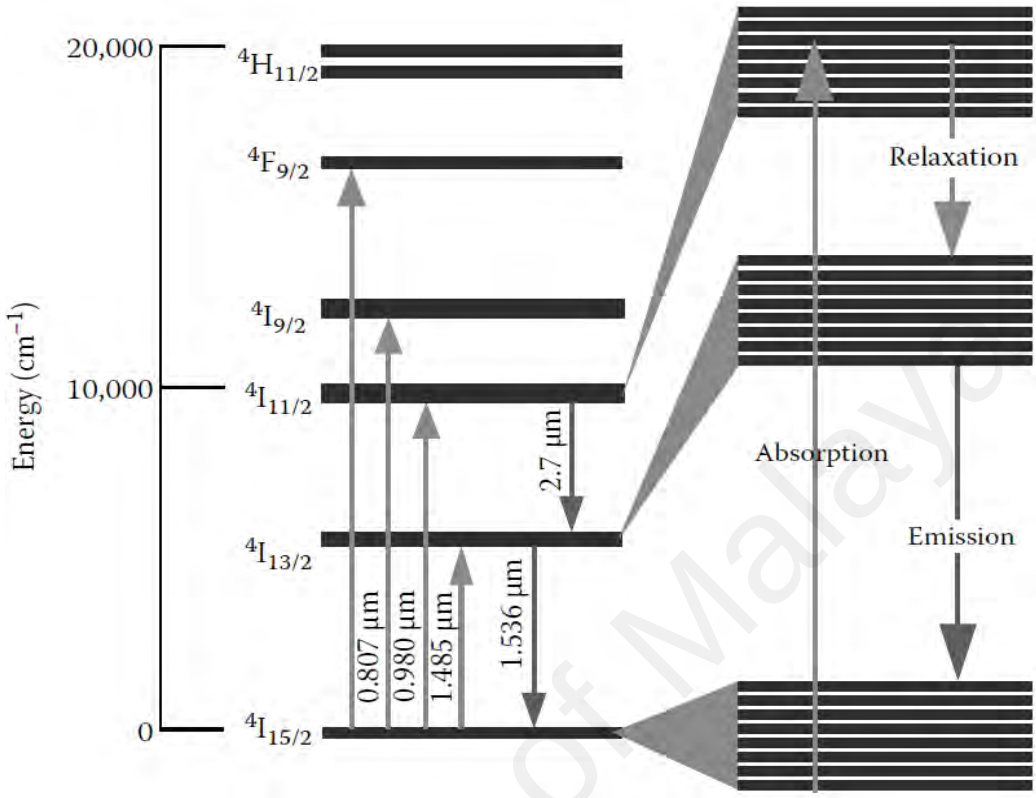

Figure 2.3: Energy level diagram of Erbium (Ngo, 2016)

2. 4 Pulsed Fiber Lasers

Fiber lasers will typically produce continuous wave (CW) operation, in which the light intensity is constant in time. CW operation is useful for application that requires precise frequency control, such as optical telecommunications and optical spectroscopy (Quimby, 2006). However, there are many practical applications in which pulsed lasers are more desirable such as laser ranging, laser cutting and laser surgery.

Fiber lasers can generate optical pulses by the techniques of Q-switching or mode-locking. Pulsed fiber lasers can be generated by active and passive techniques (Ursula Keller, 2003). The active technique utilizes a modulator to produce the pulses, while a passive technique is obtained through inserting a saturable absorber (SA) device inside a

laser cavity. The first SA was demonstrated in 1966 to generate pulses in Nd: glass laser (Stetser & DeMaria, 1966). Due to the simplicity of passive Q-switched and mode-locking techniques, they have been widely explored in the last few years (Grelu & Akhmediev, 2012). Passive Q-switching laser operation depends on the SA to modulate the Quality factor Q inside the laser cavity and produce pulses accordingly. While the passive mode-locking technique, on the other hand, uses SA in a laser cavity to act as a mode-locker and produce extremely short pulses, i.e. fixed-phase relationship is induced between the longitudinal modes of the laser's resonant cavity. In the remaining of section 2.4, we will address the fundamentals behind pulses generation.

2.4.1 Q-switching

The Q-switching is a well-known technique for generating pulses based on modulating the Q-factor of the laser cavity. The Q represents the quality of the laser resonator in terms of cavity losses in such a way that high Q indicates low intra-cavity loss and vice versa. The Q-switching phrase refers to the switching of the laser inter cavity loss from low to a high value to produce a short pulse width. The Q-switching produces pulse duration typically from microseconds to nanoseconds (N. N. Razak, Latiff, Zakaria, & Harun, 2017). There are many practical methods for producing Q-switched laser, each uses a different technique to modulate the Q of the cavity.

The use of a rotating mirror is the simplest method for producing Q-switching operation. One mirror in the laser is fixed, while the other mirror rotates at high speed on the vertical access, see Figure 2.4. When the two mirrors are in parallel (with some tolerance of $\Delta\theta$), then the Q of the cavity will be high. The cavity Q will switch from high to low in a time of $\Delta\theta/\omega$, where ω is the angular rotating speed of the mirror. This method was used in early solid-state lasers as it simple to be implemented, and recently in fiber lasers.

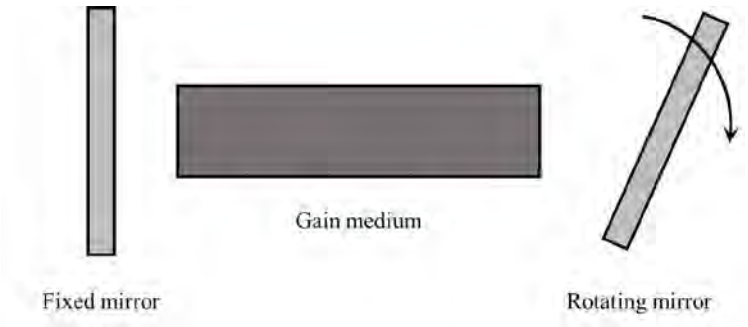

Figure 2.4: Pulsed laser based on rotating mirror

Another way for producing Q-switching operation is by inserting an electro-optic shutter inside the cavity, see Figure 2.5. The shutter is made by placing a polarizer (which is oriented to pass only one polarization of light) and Pockels cell both in the path of the beam inside the cavity. When a high voltage is applied to a Pockels cell, the polarization of the light will be rotated, and the light will be blocked by the polarizer.

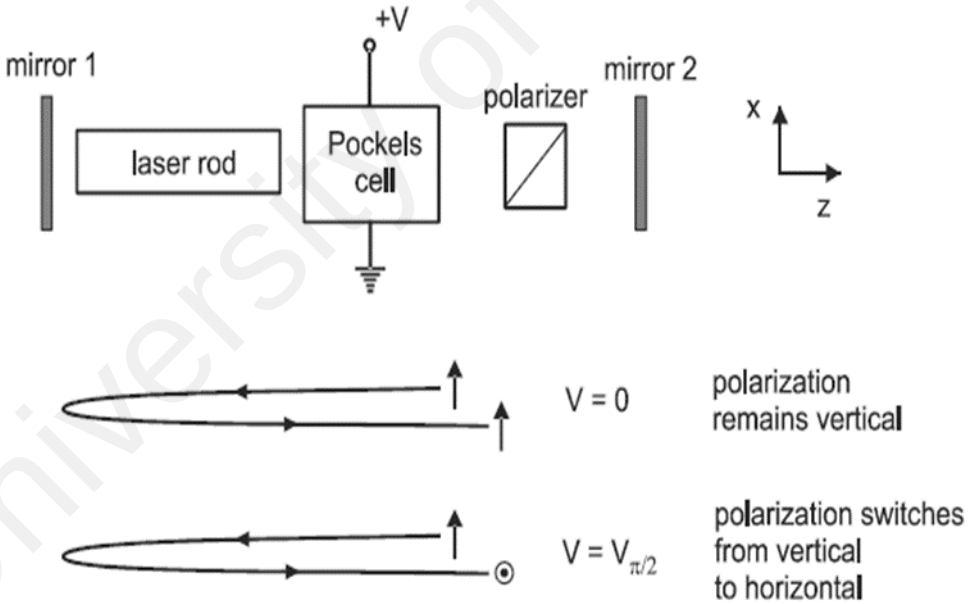

Figure 2.5: Pulsed laser based on the electro-optic shutter (Quimby, 2006)

When no voltage is applied, the light will efficiently be transmitted through the polarizer and Pockels cell. When the voltage is applied and removed rapidly, the Q factor of the cavity will be switched accordingly and, hence producing pulses. The switching

time in this technique can be about 20 ns in which a voltage of few kV is required by the Pockels cell. This technique is in common use but requires safety measures due to the high voltages involved.

The acousto-optic shutter can also be used to modulate loss inside a laser cavity. In this method, a transparent crystal is inserted the path of the light in the cavity. Then piezoelectric transducer (PZT) is used to generate acoustic waves with high intensity in the transparent crystal. Correspondingly, these crystals will have periodic variation in the refractive index, which will form a volume-phase grating. This will diffract the light and decreases the Q factor of the cavity and prevent lasing. If the acoustic waves are not applied to crystals, the Q factor is increased and the lasing is enabled, see Figure 2.6. These types of Q-switched lasers have the advantages very low optical insertion loss, relatively simple circuitry and ease of use for kHz's Q-switched repetition rate. However, they have slow switching times and low hold of ratio.

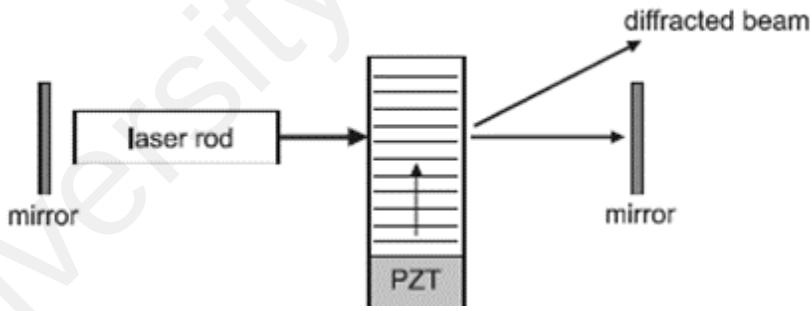

Figure 2.6: Pulsed laser by using Acousto-optic shutter, (Quimby, 2006)

In the active Q-switching, the duration and time of the change in Q are under active control, i.e. the timing and repetition rate are determined by the user. Alternatively, the laser cavity can also be Q-switched by itself. This method is termed as passive Q-switching. A passive Q-switching operation can be developed by using an SA inside the laser cavity. An SA can be used to modulate the intra-cavity loss and produce pulses. The

process begins as Q-factor is kept at a low level and prevent oscillation (i.e. high losses). That will lead the gain to build up inside the cavity through accumulating the spontaneous emission. When the Q-factor is suddenly switched to a high level, the lasing will start to build up and a pulse is formed. When the gain is depleted completely and pulse peak power is reached, the laser oscillation stops. The Q factor will be low again and the process starts from the beginning, see Figure 2.7. Passive Q-switching laser operation is normally more efficient in term of implementation cost and operation as it requires less control of cavity parameter. Passive Q-switching is generally convenient, simple and does not require and external driving circuitry.

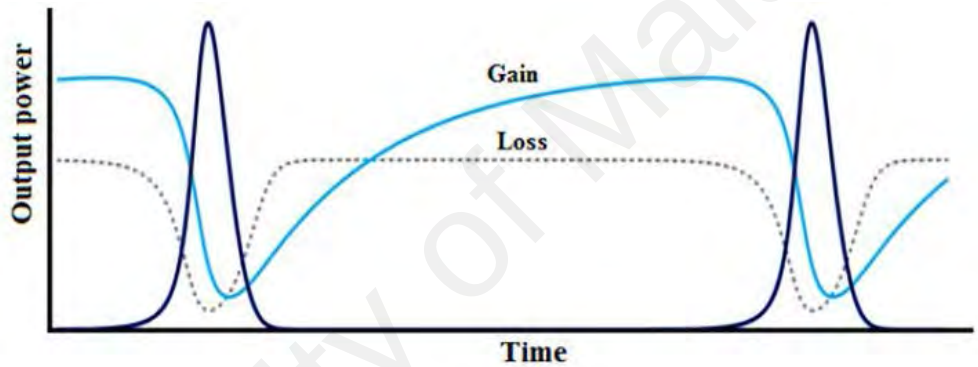

Figure 2.7: Passive Q-switched pulse formation

2.4.2 Mode-Locking

In mode-locking operation, the oscillated longitudinal modes are in synchronism, i.e. the phase of the different modes are locked and added constructively. Correspondingly, the laser will produce a train of pulses (Siegman, 1986). The frequency separation between modes, group velocity (Δvg) and the gain bandwidth are all responsible for determining the numbers of modes that can lase. The process for producing an ultrashort pulse in a mode-locked laser is much more complicated than Q-switched as it involves non-linearities, dispersion, cross-phase modulation (XPM) and self-phase modulation (SPM). The repetition rate (f_{rep}) (for

ring cavity) for pulse mode-locked fiber laser is determined by the cavity length, and it is given by the equation.

$$f_{rep} = c / nL \qquad (2.1)$$

where c is the speed of light, n refractive index and L is the length of the cavity. The repetition rate is inversely proportional to the round-trip time, T_R then

$$T_R = nL / c \qquad (2.2)$$

Figure 2.8 shows the difference between normal operation, CW operation, and mode-locking operation. Figure 2.8 (a) shows mode at random phases, while in Figure 2.8 (b) the modes are locked and mode-locked pulses are generated.

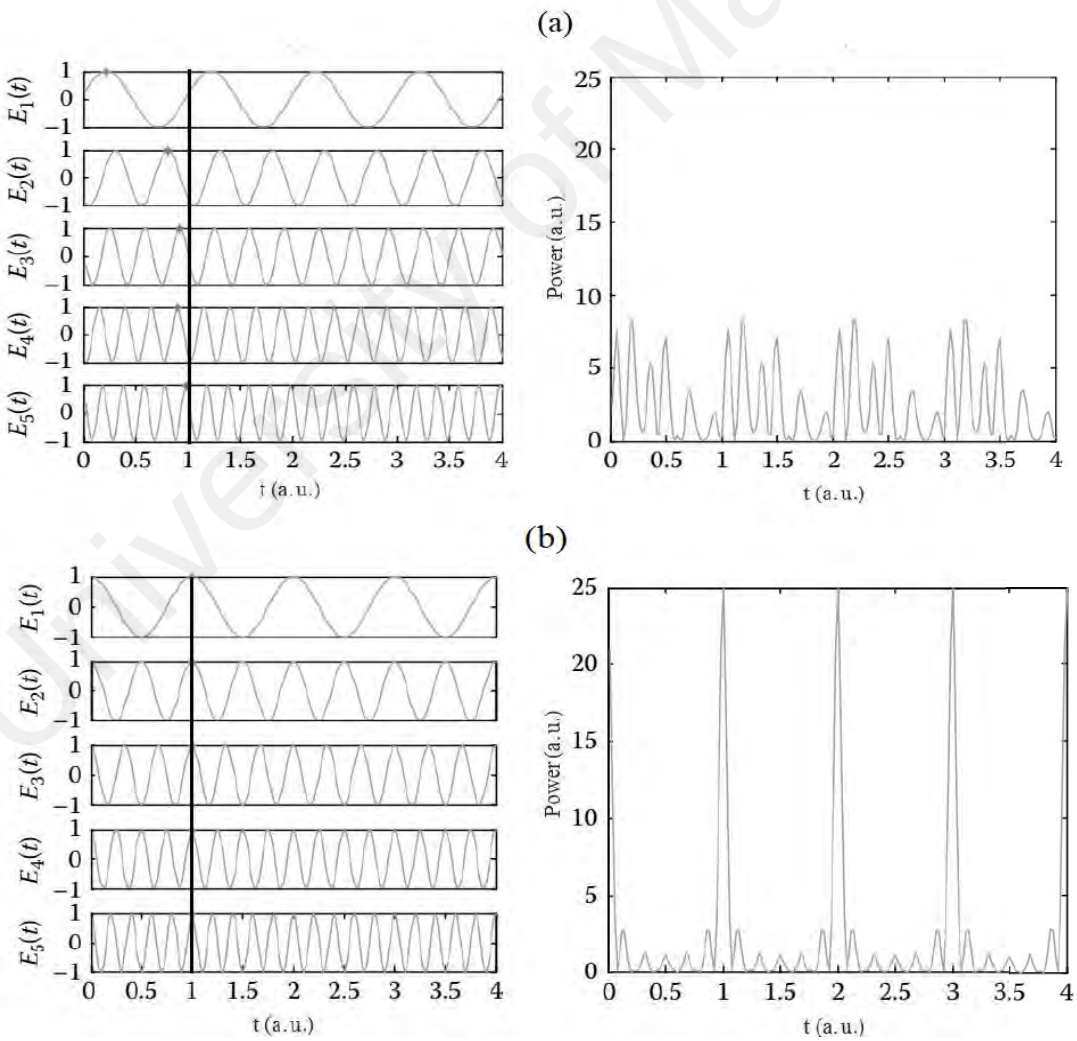

Figure 2.8: Electric field amplitudes versus time for (a) CW, (b) mode-locking (Ngo, 2016)

The mode-locked laser produces the pulse width in the range from nanoseconds to femtoseconds, which is depending on the SAs and cavity characteristics. There are two ways to achieve mode-locking: active and passive methods. Active mode-locking operation is like active Q-switching in terms of an external electronic device is used to modulate the signal, see Figure 2.9. Generally, there are two techniques to produce the active mode-locking pulses, that is amplitude modulation (AM) and frequency modulation (FM). AM technique is about using lose cavity to modulate the signal periodically, the pulses are then built up where there is minimum loss inside the laser cavity (Gupta, Onodera, Abedin, & Hyodo, 2002). The FM technique, on the other hand, is achieved through frequency chirping. The pulse is shortened and built up after several round trips due to the chirped light is swept out of the laser cavity (Nakazawa, Kubota, Sahara, & Tamura, 1998). However, active mode-locking has the disadvantages of low stability and low availability of fast external modulators. The passive mode-locking, on the other hand, can generate much shorter pulse width by utilizing SAs (Ursula Keller, 2003). Passive mode-locking is more effective and has more practical importance than active technique. It was demonstrated in 1968 by De Maria et al., in which Nd:glass was used as SA (W. Schmidt & Schäfer, 1968). But the fiber laser did not measure a regular pulse train and it remained a problem for passive techniques for more than two decades. The problem was only solved by utilizing semiconductor saturable absorber mirrors (SESAMs) in 1992 (U Keller et al., 1992).

The SA act as a mode-locker by putting some loss to the intra-cavity. The loss is relatively low for high intensities and high for low intensities pulses. I.e. a short pulse will induce a loss modulation as the high intensity (peak of the pulse) will saturate the SA, while low intensity (leading and trailing edges) would be absorbed by the SA. On the other hand, the gain will increase the intensity of the pulse, while other low-intensity will have their losses more than their gain, and they will die out (Duling III & Duling, 1995;

Ursula Keller, 2004), see Figure 2.9. The SA can produce very short pulses as the loss modulation of SA can be very fast due to the fast recovery time of the SA. Currently, the passive mode-locked laser based on SAs can produce ultrafast pulses in the range between picoseconds to femtoseconds depending on the SA parameters (M. Ahmed et al., 2014; Jung et al., 2014). Soliton mode-locking is one of the techniques that is frequently used to generate sub-picosecond and femtosecond pulse width in a fiber laser. Solitons are of great interest, as they maintain their velocity and shape through time. The soliton operation results from an interplay between the dispersion and nonlinear effects. The pulses obtained typically have a high pulse quality and hardly any chirp with a nice hyperbolic secant ($sech^2$) shape. In this thesis, the focus will be on developing passive soliton mode-locking fiber lasers.

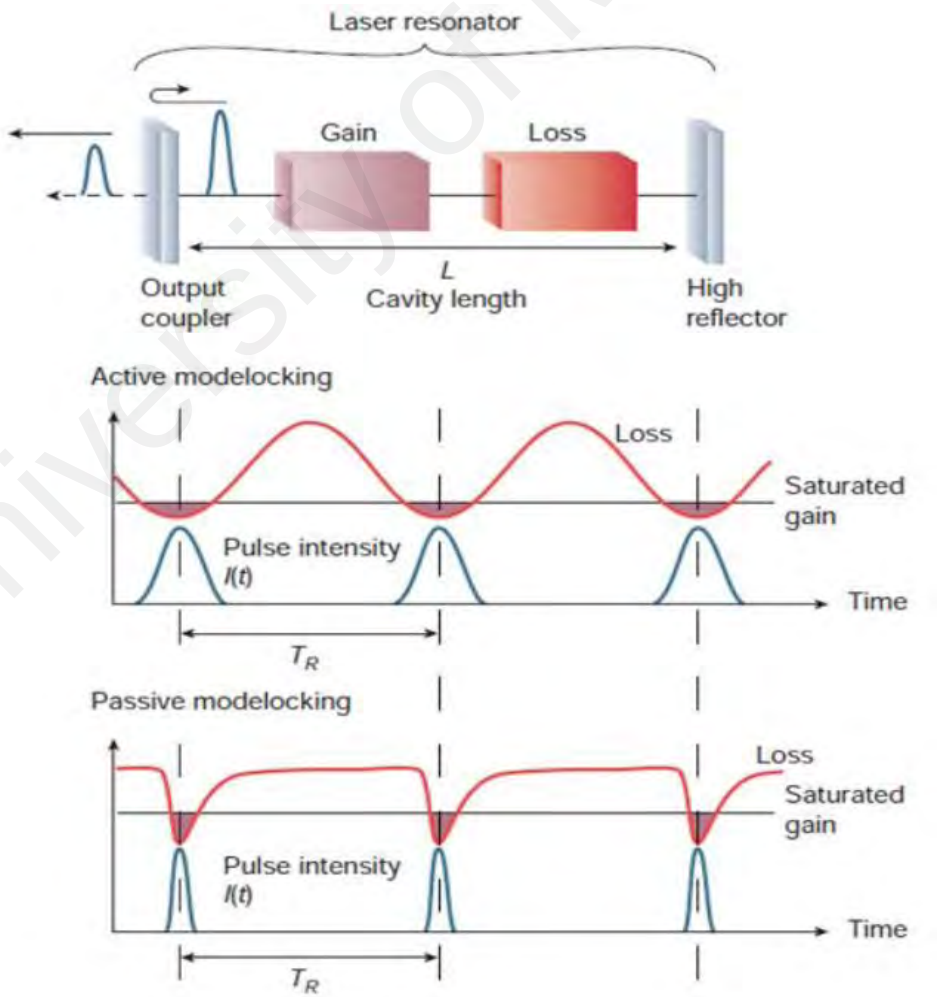

Figure 2.9: Schematic laser cavity setup for active and passive mode-locking (Ursula Keller, 2003)

2. 5 Saturable Absorbers (SAs)

SAs are nonlinear optical devices which have an intensity-dependent transmission. The SAs are widely utilized as a passive modulator in both Q-switched and mode-locked lasers. The parameters of choosing an SA are damage threshold, wavelength range, saturation intensity, recovery time and modulation depth (H Zhang et al., 2014). The damage threshold is defined as the maximum input light intensity that SA can absorb before it been damaged. The wavelength range is the region of operation that the SA must be synchronized with the gain of the corresponding lasing medium. The saturation intensity is known as the required light intensity to saturate the absorption of the SA. While the speed limit on the switching device (which affect the duration of the pulses) is known as recovery time. The modulation depth is the value for the maximum possible change of absorption the SA can have. Other parameters such as cost of fabrication and environmental stability are also important in choosing a SA.

These mentioned parameters are governed by the atomic arrangement and chemical composition of the SA material. These parameters can be described in the equation of saturable absorption and as shown below (Bao et al., 2011) :

$$a(I) = \frac{a_0}{1+\frac{I}{Is}} + a_{ns} \qquad (2.3)$$

where a_0 is modulation depth, a_{ns} is nonsaturable absorption, I is the light intensity I_S is the saturation intensity. While the saturable absorption can be expressed as,

$$a_s = N\beta \qquad (2.4)$$

where the N and β represent the concentration of the material and absorption ground cross-section respectively. The saturable absorption indicates that a certain number of photons are absorbed per unit distance from the SA device. In case that the saturable absorption coefficient was large, then photons will be absorbed over a short distance into

the SA. The non-saturable absorption, on the other hand, is the loss that cannot be saturated by the SA because of the nonsaturable defect in absorption and scattering loss.

2. 6 Saturable Absorber Materials

SAs can be divided into two categories: artificial and real SA. The nonlinear polarization rotation effect can be used inside a laser cavity to mimic the behaviour of a real SA by inducing an intensity-dependent transmission. This technique is simple, but the stability of the generated pulses is difficult to be maintained since the operation is strongly dependent on the oscillating light polarization. Real SA uses materials that show an intrinsic nonlinear decrease in absorption as the light intensity increase. To date, several types of SAs have been intensively investigated for developing Q-switched and mode-locked fiber lasers. In this part, we restrict the focus to real SAs.

2.6.1 Carbon Nanotubes

Carbon Nanotubes (CNT) was found by Iijima in 1991 during the arc discharge method (Ando & Iijima, 1993). CNTs can be produced from graphene through rolling the graphene on the cylindrical nanostructure. The atomic structure of graphitic materials of 0D Fullerene, 1D CNT, 2D graphene and 3D graphite is shown in Figure 2.10 (Geim & Novoselov, 2010). Several methods have been proposed to utilize CNT as SA in fiber lasers, for example, optical deposition, free space arrangement and sandwiching the SA between two fiber ferrules (Z Sun, Hasan, & Ferrari, 2012). CNTs can be single-walled nanotubes (SWCNTs) or multi-walled nanotubes (MWCNTs) (that is according to the number of walls that form the CNT). SWCNTs have been considered as a promising SA device due to their intrinsic saturable wide absorption wavelength bandwidth, ultrafast recovery time and absorption properties (Harun et al., 2012). However, SWCNTs suffer from a low damage threshold (M. H. M. Ahmed et al., 2014).

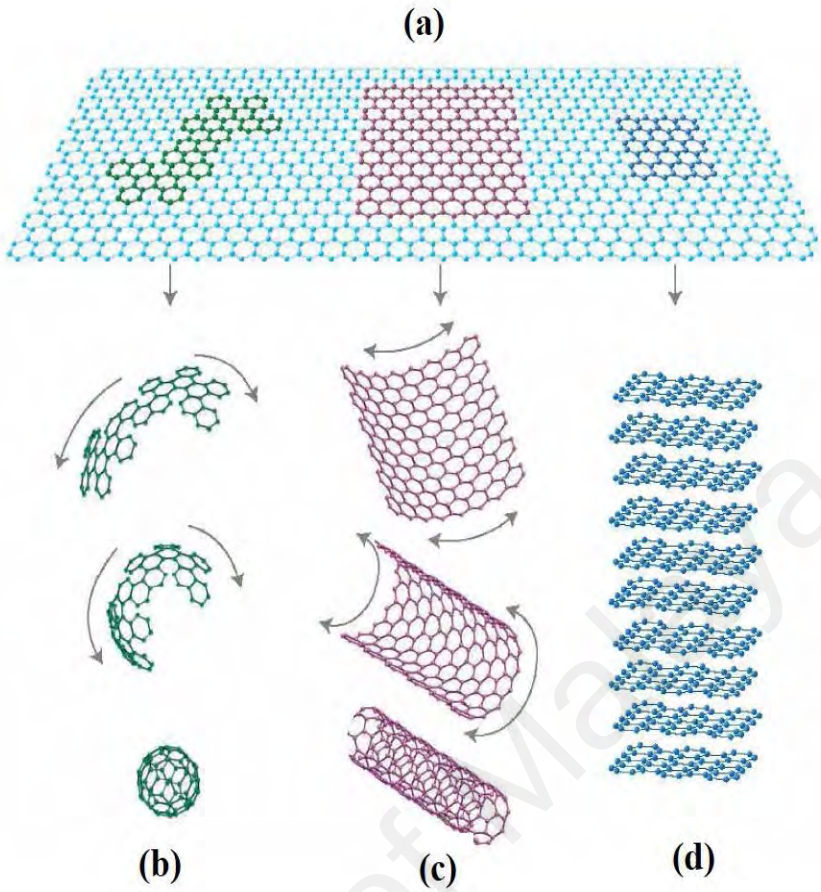

Figure 2.10: (a) 2D graphene (b) 0D Fullerene, (c) 1D CNT and (d) 3D Graphite (Geim & Novoselov, 2010)

On the other hand, MWCNTs have attracted much attention due to their advantages such as the fabrication cost of MWCNT material is about 50%–20% of that of SWCNT (L. Zhang et al., 2011). Additionally, the damage threshold of MWCNTs is higher than that of SWCNTs (Ramadurai et al., 2008) as the outer walls can protect the inner walls from damage. However, the MWCNTs has a high saturation intensity which it is not a very attractive feature for mode-locking operation as this would require high irradiation intensity to reach absorption saturation (Lim et al., 2006). Therefore, there are only a few demonstrations for MWCNTs as a SA. Generally, CNTs often demand band gap engineering or charity control which limits its operation at certain wavelengths (Q. Bao et al., 2009). Table 2.1 review the works that have been demonstrated by using CNT as SA.

Table 2.1: CNT as a saturable absorber in fiber laser cavities

Laser Type	SA	Wave-length (nm)	Pulse width	Repetition rate	Maxi-mum Output power (mW)	SNR (dB)	Reference
Q-switched laser	SWCNT	1533.6	16.9 to 8 µs	9.52 to 33.33 kHz	9.5	50	(Ahmed et al., 2015)
		1073	6.45 to 3.11 µs	17.1 to 23.6 kHz	14.65		(Al-Masoodi et al., 2014)
	MWCNT	1534.5	11.7 to 8.3 µs	38.11 to 48.22 kHz	4.8	27	(Azooz et al., 2015)
		1533.6	9.5 to 4.2 µs	6.12 to 33.62 kHz	12.4	40	(Ahmed et al., 2015)
		1055–1063	17 to 8.87 µs	10.41 to 29 kHz	1	36	(AHH Al-Masoodi, Ahmed, Arof, & Harun, 2018)
Mode-locked laser	SWCNT	1533.6	1.8 ps	15.3 MHz	4.3	-	(M. Ahmed et al., 2014)
		1564.2	0.77 ps	17.7 MHz	0.91	37.4	(Markom, Sen-Winson, Paul, & Harun, 2017)
	MWCN	1550	1.28 ps	4.54 MHz	-	-	(Cheng, Lin, & Lin, 2013)

2.6.2 2D Nanomaterials Saturable Absorber

2D nanomaterials have different optical, thermal, electronic and mechanical properties from its 3D form (Novoselov et al., 2004). 2D material can be used in the field of optoelectronics particularly in photovoltaics, photo-detection, and photoluminescence. Additionally, the 2D materials can be used as SA to generate Q-switched and mode-locked pulse lasers (Huang & Luo, 2014; Zhang et al., 2014). The usage of 2D nanomaterials has

started since the 1960s, as 2D nanomaterials provide greater benefits due to their extraordinary properties (Savage, 2012). The 2D nanomaterials provide enhanced biological functionality, chemical and physical due to their high surface-to-volume ratios, uniform shapes, and surface charge. Over the years, several materials have been extracted from 2D nanomaterials families such as graphene, topological insulators (TIs),TMDs and black phosphorus (BP) (Kambe et al., 2014; Xia, Wang, & Jia, 2014), see Figure 2.11 below. These materials will be reviewed in detail in the following paragraphs.

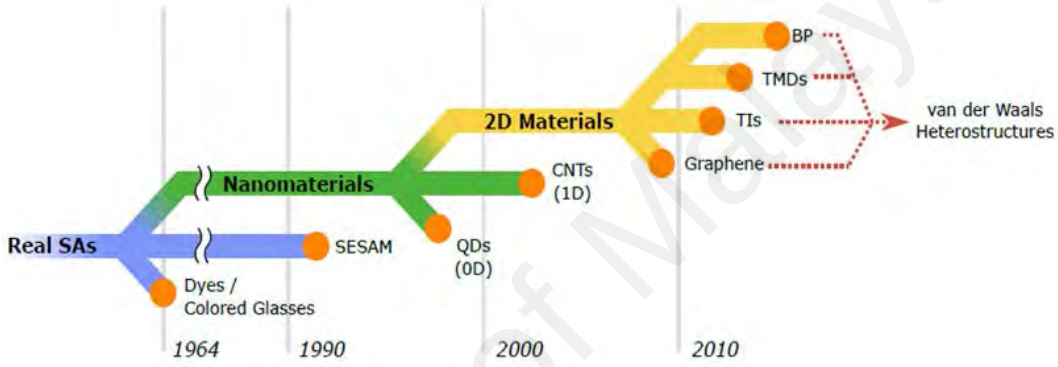

Figure 2.11: The evolution of real saturable absorbers (Robert Woodward & Kelleher, 2015)

2.6.2.1 Graphene

Geim and Novoselov have discovered single-layer graphene in 2004 and found that the graphene does not exist in a free-state (Geim & Novoselov, 2010). Single-layer graphene and few-layer graphene can be produced from graphite by using scotch-tape method (Geim & Novoselov, 2010) and also by chemical vapour deposition (CVD) method (Obraztsov, Obraztsova, Tyurnina, & Zolotukhin, 2007). Graphene has become the interest of researchers as it has valuable and unique electronic properties (Geim & Novoselov, 2010). Single-layer graphene has an optical transmittance of about 97.7% which enables the materials to be used in the broadband application (Bonaccorso, Sun, Hasan, & Ferrari, 2010). Graphene has been addressed in several fields, as its nonlinear

optical properties have enabled the material to be utilized in photonic applications (Hasan et al., 2009). Graphene has been widely explored as SA in Q-switched and mode-locked fiber lasers, as it has an ultrafast saturable absorption. The first usage of graphene as SA in mode-locked fiber laser was in 2009 (Zhipei Sun et al., 2010). It should be mentioned that graphene has the drawback of zero band gaps which limited its capability in several applications. Several works had demonstrated graphene as SA for mode-locked and Q-switched fiber laser, as illustrated in Table 2.2.

Table 2.2: Graphene as an SA for both Q-switch and mode-lock laser

Laser Type	Wavelength (nm)	Pulse width	Repetition Rate	SNR (dB)	Output power (mW)	References
Q-switched laser	1558.28	9.58 to 6	47.94 to 67.8 kHz	62	-	(Zuikafly, Khalifa, Ahmad, Shafie, & Harun, 2018)
	~1550	2.8 to 0.2 µs	31.7 to 236.3 kHz	-	7.8	(Wei, Zhou, Fan, & Liu, 2012)
	1027.03	3.2 to 1.3 µs	28.9- 110 kHz	-	15.6	(L. Zhang et al., 2012)
Mode-locked laser	1069.8	0.58 ps	0.9 MHz	-	0.37	(Zhao, Tang, Wu, Bao, & Loh, 2010)
	1565	0.756 ps	1.79 MHz	65	2	(Q. Bao et al., 2009)
	1561.6	1.3 ps	6.99 MHz	-	10.7	(Song, Jang, Han, & Bae, 2010)
	1568.1	58.8 ps	7.29 MHz		1.68	(G. Liu, Feng, Zhang, Jiang, & Zhang, 2015)

2.6.2.2 Topological Insulator

TIs have attracted much of the research focus due to the efficient saturable absorption, large modulation depth and high nonlinear susceptibility. The most two important compounds of TI are Bismuth (III) Telluride (Bi_2Te_3) and Bismuth (III) Selenide (Bi_2Se_3). The Bi_2Te_3 and Bi_2Se_3 have complex layer structures, and they react with the elements at 500-900° C. These materials can be used in different fields, such as optoelectronics, television cameras, and switching devices as they have the properties of thermoelectric. However, the constructing process of TI materials are complicated, and thus they have limited applications. Table 2.3 review the utilization of TI in fiber laser technology.

Table 2.3: TI as an SA for both Q-switch and mode-lock laser

Laser Type	Wavelength (nm)	Pulse width	Repetition Rate	SNR (dB)	Output power (mW)	References
Q-switched laser	1070	252.6 to 6.6 µs	24.4 to 55 kHz	-	18.6	(A. H. H. Al-Masoodi et al., 2018)
	1560	62.72 to 5.1 µs	20.99 to 89.29 kHz	71.4	5.6	(Ismail et al., 2018)
	974	39.8 to 4.9 µs	40.1 to 6.2	50	6.1	(L. Sun et al., 2014)
	1493.6 - 1508.9	6.1 to 7.64 µs	36.6 to 26.1	58	0.21	(H Ahmad, Soltanian, et al., 2015)
Mode-locked laser	1935	0.795 ps	27.9 MHz	-	-	(Jung et al., 2014)
	1557	1.08	8.635	60	-	(Mao et al., 2015)
	~1031	46 ps	44.6 MHz	58	33.7	(Dou et al., 2014)

2.6.2.3 Transition Metal Dichalcogenides

Semiconducting TMDs such as MoS_2, $MoSe_2$ and WS_2 are having renewed interest for photonic and optoelectronic applications, expanding upon studies made in the 1960s. (Frindt, 1965; Wilson & Yoffe, 1969), with the use of modern processing techniques allowing new insight. The properties of TMDs based SA depends on the number of layers in the material (Q. H. Wang, Kalantar-Zadeh, Kis, Coleman, & Strano, 2012). For example, MoS_2 has an indirect band gap around 1.29 eV band gap, which increases because of stronger quantum confinement as the number of layers is reduced, resulting in a direct band gap of 1.80 eV (Mak, Lee, Hone, Shan, & Heinz, 2010). MoS_2 is widely used in microelectronics devices due to its good absorption coefficient (Wen, Xu, Liu, Lai, & Tang, 2017). However, TMDs suffer from a low optical damage threshold (Horiguchi, Honda, Kato, Nakashima, & Niidome, 2008; Latiff et al., 2017). Table 2.4 reviews the demonstration of TMDs in fiber laser technology.

Table 2.4: TMD as a SA for pulsed lasers

Laser Type	Wavelength (nm)	Pulse width	Repetition Rate	SNR (dB)	Output power (mW)	Reference
Q-switched laser	1551.4	10.7 to 5 µs	14.25 to 38.43 kHz	37	5.2	(M. H. M. Ahmed, A. H. H. Al-Masoodi, A. A. Latiff, H. Arof, & S. W. Harun, 2017)
	1086& 1093	21.3 to 10 µs	4.8 to 17.2 kHz	-	60	(Tey et al., 2017)
	1559.8	14.28 to 9.6 µs	70 to 104.1 kHz	-	12.82	(N. Razak, Yasin, Zakaria, Abdul Latiff, & Harun, 2017)
Mode-locked laser	1598.94	0.83 ps	17.1 MHz	41	1.26	(Ahmed, Latiff, Arof, Ahmad, & Harun, 2016)

Table 2.4, continued

Laser Type	Wavelength (nm)	Pulse width	Repetition Rate	SNR (dB)	Output power (mW)	Reference
Mode-locked laser	1073.86	28.3 ps	18.8 MHz	30	1.82	(A. H. H. Al-Masoodi, Ahmed, et al., 2017)
	1559	2.46 ps	1.8 MHz	62	-	(G. Wang, 2017)

2.6.2.4 Black Phosphorous

Black Phosphorous (BP) has recently joined the family of 2D materials (Churchill & Jarillo-Herrero, 2014). BP is widely used in optoelectronic and electronic applications as it has the properties of excellent conductivity and direct band gap (Han et al., 2017). BP has a direct band gap and can be tuned from ~0.3 to ~2 eV which correspond to the wavelength between ~4 to ~0.6 μm (Tran, Soklaski, Liang, & Yang, 2014). This feature makes it an interesting SA for fiber laser application. The research on BP has made steady progress in last few decades, including the study of crystal structures (Jamieson, 1963), superconducting properties (Wittig & Matthias, 1968), optical properties (Warschauer, 1963), and optical phonon (Ikezawa, Kondo, & Shirotani, 1983). However, these works did not attract much attention from the semiconductor research community. BP was only rediscovered from the perspective of 2D nanomaterials only when successful studies of graphene and few-layer TMDs were made. However, it should be mentioned that BP suffers from low damage threshold (Latiff et al., 2017), additionally, BP is a hydrophilic material (J. Li et al., 2016) which is easily damaged when exposed to water or oxygen. The table below review the work achieved by using BP as SA.

Table 2.5: BP as a SA for passive pulsed lasers

Laser Type	Wavelength (nm)	Pulse width	Repetition Rate	SNR (dBm)	Output power (mW)	Reference
Q-switched laser	1550.9	22.34 to 5.35 µs	7.46 to 28.57 kHz	-	0.18	(Fauziah, Rosol, Latiff, & Harun, 2017)
	1552.9	20.5 to 7.04 µs	9.1 to 44.33 kHz	50	5.7	(M. H. M. Ahmed et al., 2017)
	1562	40 to 9.84 µs	9.6 to 44.72 kHz	67	3.54	(Huanhuan Liu et al., 2019)
	1069.4	7.9 To 10.8 µs	8.2 to 32.9 kHz	30	10	(Ahmed Al-Masoodi, Ahmed, Abdul Latiff, Arof, & Harun, 2016)
Mode-locked laser	1560.7	0.57 ps	6.88 MHz	59	0.3	(Ahmed, Latiff, Arof, & Harun, 2016)
	1033.76	3.27 ps	10 MHz	39	4.8	(A. H. H. Al-Masoodi, Yasin, et al., 2017)
	1085.58	7.54 ps	13.5 MHz	45	10	(Hisyam, Rusdi, Latiff, & Harun, 2017)
	1571.45	0.946 ps	5.96 MHz	70	-	(Y. Chen, G. Jiang, S. Chen, Z. Guo, X. Yu, C. Zhao, H. Zhang, Q. Bao, S. Wen, D. Tang, et al., 2015)

CHAPTER 3: PREPARATION AND CHARACTERIZATION OF ORGANIC SATURABLE ABSORBERS

3. 1 Introduction

Organic materials have received considerable attention in the literature recently due to their many advantages. For instance, their excellent mechanical and chemical properties allow them to be processed by highly scalable industrial approaches. The ability of these materials of creating an interface with living tissues and cells has also received significant attention during the last few years. One of the main reasons that made organic materials successful is their ability to form close contact with the biological material (Šafaříková et al., 2018). The advance development of these materials has led to the demonstration of plastic bioelectronic devices that can be utilized as an efficient substitute for conventional devices based on inorganic materials and precious metals. They have been used in the application of cell cultures for modulating or sensing the electrical activity of cells (Martin, 2015; Owens & Malliaras, 2011; Rivnay, Owens, & Malliaras, 2014). Additionally, organic materials can also be processed so that they can be implanted into the human body for applications in drug delivery, neural recording and sensing (Kaltenbrunner et al., 2013; Khodagholy et al., 2014; Someya, Bao, & Malliaras, 2016). These materials can be used to develop ultralight, weight ultra-flexible and stretchable sensor arrays.

Organic materials might have the potential to be used as a bio-compatible, environmentally-friendly and high performance saturable absorbers (SAs). This is attributed to their ability to provide a large and ultrafast nonlinear response and broad spectral tunability (Boulet, Mohammadpour, & Shankar, 2015; Clark & Lanzani, 2010; Williams, 1983). They also offer mechanical flexibility, light-weight and low production cost (Someya et al., 2004) and thus they might increase the potential for applications in

biomedical laser processing and sensing (Khazaeinezhad et al., 2017). These materials, in comparison to inorganic materials, require simple fabrication and offer versatile molecular design (Clark & Lanzani, 2010; C. W. Lee, Kim, & Lee, 2014). Due to their customized properties for optoelectronics, organic materials have been utilized in various applications including organic solar cells (OSCs) (J. Y. Kim et al., 2007; Peumans, Uchida, & Forrest, 2011; Tang, 1986; Xue, Uchida, Rand, & Forrest, 2004), organic light-emitting diodes (OLEDs) (Adachi, Baldo, Thompson, & Forrest, 2001; Holmes et al., 2003; O. Y. Kim & Lee, 2012; Yook & Lee, 2012), organic bistable memory devices (Briseno et al., 2006; Muccini, 2006) and organic thin-film transistor (C. Kim, Facchetti, & Marks, 2007; J.-M. Kim et al., 2012).

Up to date, many works have been devoted to the demonstration of pulsed fiber laser by using a passive SA. Therefore, finding a new material to be used as a high-performance SA is of great interest, since the current SAs still suffer from many drawbacks as discussed in the previous chapters. Besides, there have been increasing concerns about the usage of the nano-materials as SAs as they might be dangerous on human health (Khazaeinezhad et al., 2017). Therefore, a non-hazardous biocompatible alternative SA would be highly favourable, especially for developing environmentally-friendly photonic devices which could find increasing applications in in-situ or in-vivo sensing and biomedical laser processing. Additionally, most of the developed SAs still have the issues of wavelength dependency, high manufacturing cost, difficulty in processing and difficulty in controlling the physical properties. A new SA that can overcome the above drawbacks will have a great research impact and could find many practical applications.

In this research work, three organic materials; Bis[2-(4,6-difluorophenyl)pyridinato-C^2,N](picolinato)iridium(III) (FIrpic), bis(8-hydroxyquinoline)zinc (Znq_2) and Tris(8-hydroxyquinoline)aluminum (Alq_3) were proposed and demonstrated as SAs for both Q-switched and mode-locked pulse generations. This chapter discusses the fabrication and

characterization of these SAs. These materials, FIrpic, Znq_2 and Alq_3, have previously attracted much attention as biological labels and probes as they have a higher resistance to photobleaching and intense and long-lived emission (Lo, 2007). Compared with the conventional inorganic materials, they have comparable high optical damage threshold (higher than 350 mW) and high output pulses energy. Furthermore, they have a low-cost and straightforward fabrication process, which could make them very useful and attractive in pulsed fiber laser technology.

3. 2 Fabrication and Characterization of FIrpic as SA

FIrpic is a blue phosphorescent bis-cyclometallated iridium complex. It can be produced by a straightforward synthesis process and has excellent stability and desirable electrochemical properties. FIrpic also has a suitable energy level and high emission efficiency (E. Baranoff & B. F. E. Curchod, 2015). It remains stable on the substrate during deposition regardless of the surface morphology. FIrpic also remains stable without any compositional or surface morphological damage after being exposed to an atmospheric environment or X-ray irradiation (Park et al., 2012). For these qualities, FIrpic is expected to become an ideal material for use as an organic SA. In this work, FIrpic was embedded into polyvinyl alcohol (PVA) to form a thin-film so that it can be easily integrated into a laser cavity to function as SA. PVA is reported to be an excellent host for producing a high-performance SA (Mao et al., 2015). Additionally, PVA has been intensively used in many applications due to its favourable physical properties such as biocompatibility, hydrophilicity and good chemical resistance (X. Chen, 2002; K. Wu, Zhang, Wang, Li, & Chen, 2015). Figures 3.1(a) and (b) show the molecule structure for FIrpic and PVA, respectively.

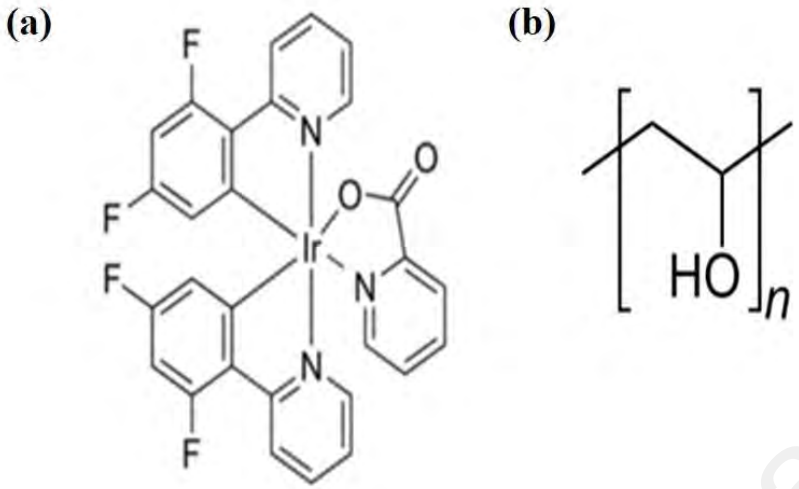

Figure 3.1: Molecular structures of (a) FIrpic and (b) PVA

FIrpic material used in this study was purchased from Sigma Aldrich. The FIrpic-PVA thin-film was prepared by a solvent casting technique and the preparation process is summarized in Figure 3.2. At first, 1 ml of deionized (DI) water was added to 10 mg of FIrpic material. The solution was stirred at 50° C for one hour then 2 drops of acetone were added to the solution to help in solving the FIrpic so that it could be distributed equally inside the solution. On the other side, PVA solution was prepared by adding of 1 g of PVA into 100 ml of DI water following by ultra-sonication for one hour at room temperature. Next, 5 ml of PVA solution was mixed with the prepared FIrpic solution. The mixture was then stirred for about three hours. After that, the mixture was poured to a borosilicate glass petri dish and dried at room temperature for 3 days. A thin-film with a diameter of 60 mm was obtained. The thickness of the produced films is about 50 µm and the mass fraction of FIrpic is about 16.7 wt%. The mass fraction of FIrpic is calculated by $\frac{w_{FIpric}}{(w_{PVA}+w_{FIpric})} \times 100$, where w_{PVA} and w_{FIpric} are the weights of PVA and FIrpic, respectively (Hamdalla & Hanafy, 2016). Finally, a small piece of the thin-film was attached to the fiber ferrule for use as SA device. The pristine PVA thin-film was also prepared in this work from the PVA solution for comparison purpose. It was obtained by

pouring the prepared PVA solution onto a borosilicate glass petri dish and dried it at room temperature for about 3 days.

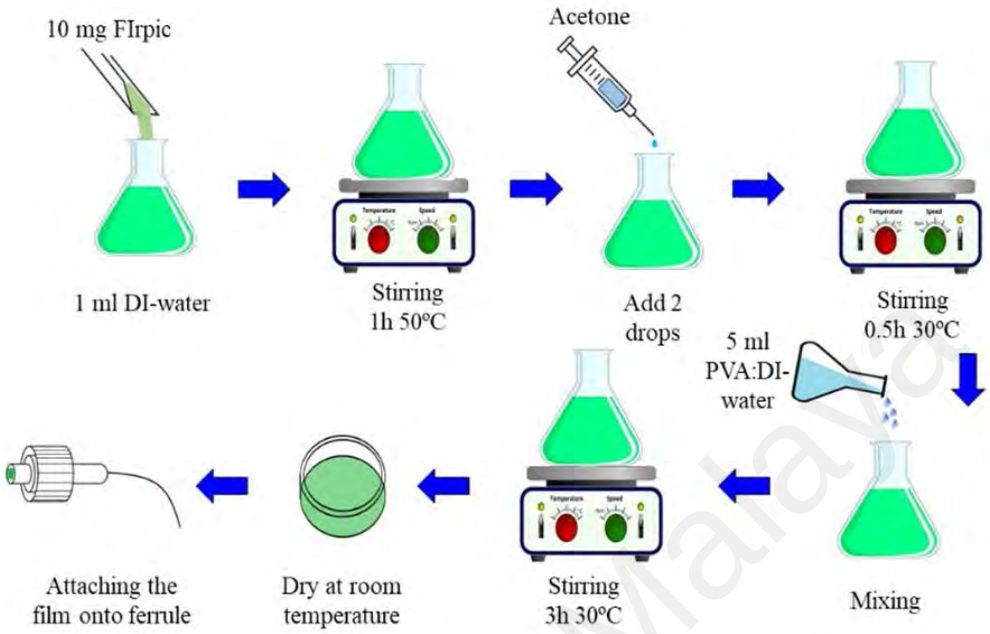

Figure 3.2: Fabrication process of FIrpic-PVA thin-film

The chemical groups in the PVA and FIrpic-PVA thin-films were investigated using Perkin Elmer Spectrum 400 Fourier Transform Infrared Spectroscopy (FTIR) Spectrometer. FTIR spectra were obtained for both PVA and FIrpic-PVA thin-films based on transmittance mode in the range of wavenumber from 4000 to 450 cm^{-1} with a resolution of 2 cm^{-1}. Figure 3.3 (a) compares the plotted spectrum of the FIrpic-PVA with the pristine PVA film. Most of the characteristic bands correspond to PVA could be observed in a pristine PVA film. In the spectrum of PVA, there is a broad and strong absorption at 3000–3600 cm^{-1}, peaking at 3298 cm^{-1}, which is due to the symmetrical stretching vibration of O–H from the intermolecular and intramolecular hydrogen bonds. The PVA stretching vibration peaks of CH_2, CH, C=O, C–O–C, C–O and C–C were observed at 2925, 2852, 1729, 1089, 1023 and 839 cm^{-1}, respectively, while the CH_2 bending, (CH+OH) bending, CH wagging and CH_2 rocking and (OH) wagging of PVA appear at 1437, 1370, 1242, 946 and 605 cm^{-1}, respectively. Two peaks significantly

appear at 1641 and 1602 cm^{-1} in the FIrpic-PVA thin-film which belong to the stretching vibration of C=C and C=N in the FIpric molecules, respectively (Hammer, Baker, Lenardi, & Gissler, 1997; Y. C. Kong, Yang, Li, & Chen, 2015; Lei et al., 2017). Figure 3.3 (b) shows the vibration peaks of small intensities at the fingerprint region of the FTIR spectrum (1500-500 cm^{-1}) after adding FIrpic into PVA. The appearance of these peaks is due to the small fraction of the organic material. These peaks refer to C-F, C-N and C-O stretching vibration bonds at the range of 1400-1000 cm^{-1}, while the peaks at the range between 1000-500 cm^{-1} correspond to the bending vibration of C-H and O-H bonds (DeCoste & Peterson, 2013; Mehta et al., 2016; Yap, Kida, Aoyama, Mori, & Sasaki, 1998).

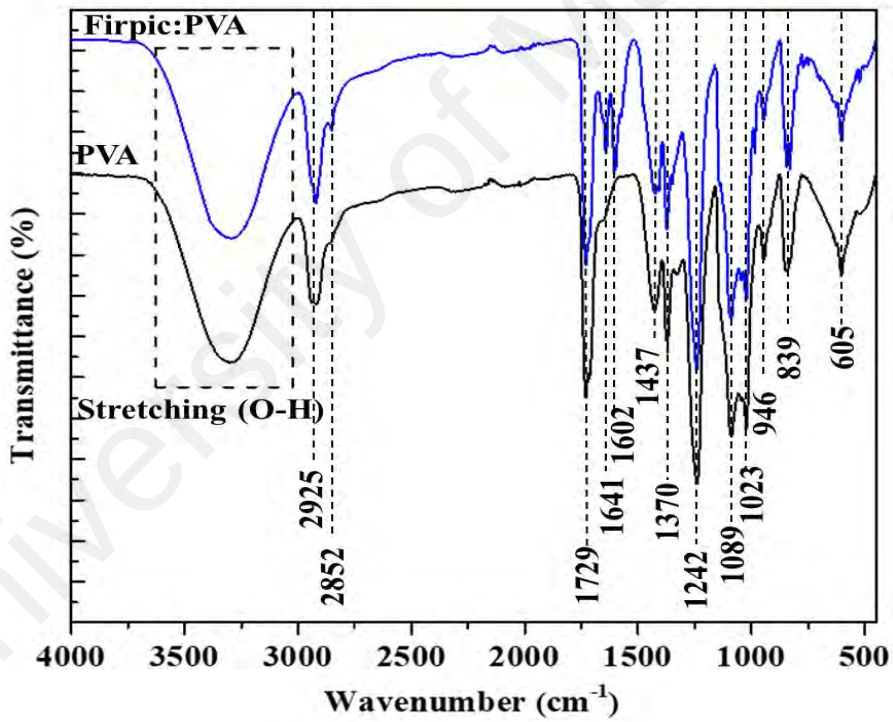

(a)

Figure 3.3: (a) FTIR spectra (b) FTIR fingerprint region of PVA and FIrpic-PVA thin-films

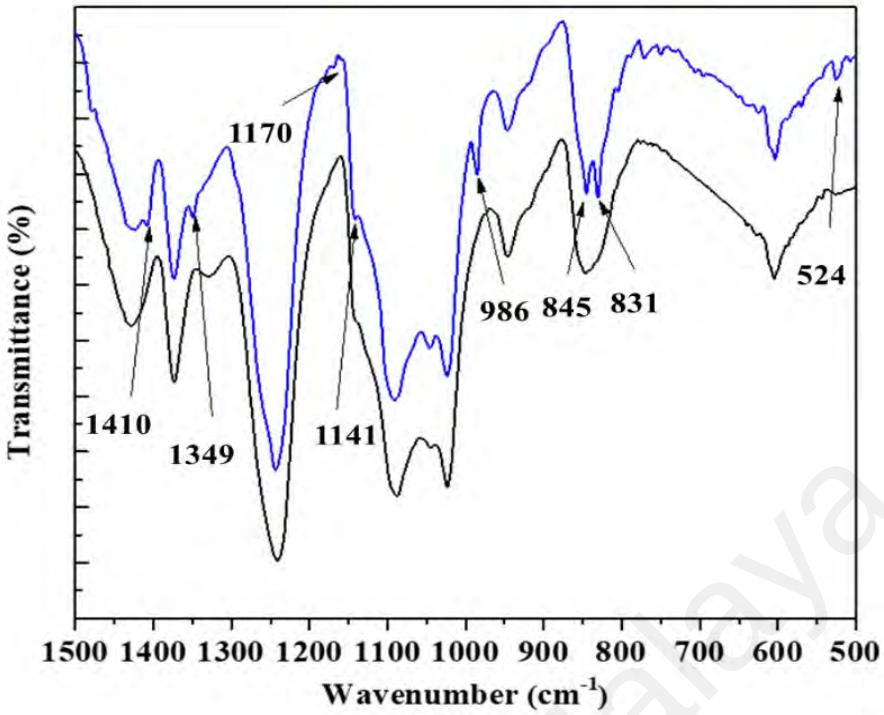

(b)

Figure 3.3, continued

SEM image of FIrpic-PVA thin-film, which is presented in Figure 3.4 (a), shows a homogenous surface with the appearance of some micron-sized particles in the range of 2-13 µm. These particles could belong to FIrpic agglomeration powder and the homogenous surface reveals the uniform distribution of FIrpic molecules along with the polymer. Figure 3.4 (b) shows the optical absorbance spectrum of FIrpic-PVA thin-film. Two asymmetric and broaden peaks centred at 388 and 1047 nm, respectively, can be clearly detected. These peaks could belong to the absorption band of FIrpic and PVA doped with FIrpic molecules, respectively. Baranoff and Curchod reported the absorption band of FIrpic in CH_2Cl_2 solution at 256 nm (E. Baranoff & B. F. Curchod, 2015). The redshift of the FIrpic absorption band is due to the formation of the micro-particles during fabrication and it is embedded in PVA polymer. The PVA absorption band comes from the doped material. The optical band gap, E_g, of the composited thin-film can be calculated from the following equation $(\alpha hv)^n = B(hv - E_g)$, where hv is the photon

energy, B is a constant relative to the material and n equals to 2 for direct transition and α is the absorption coefficient which can be calculated by Beer-Lambert's law as $\alpha(v) = 2.303 \times Abs(\lambda)/d$, where d is the thin-film thickness.

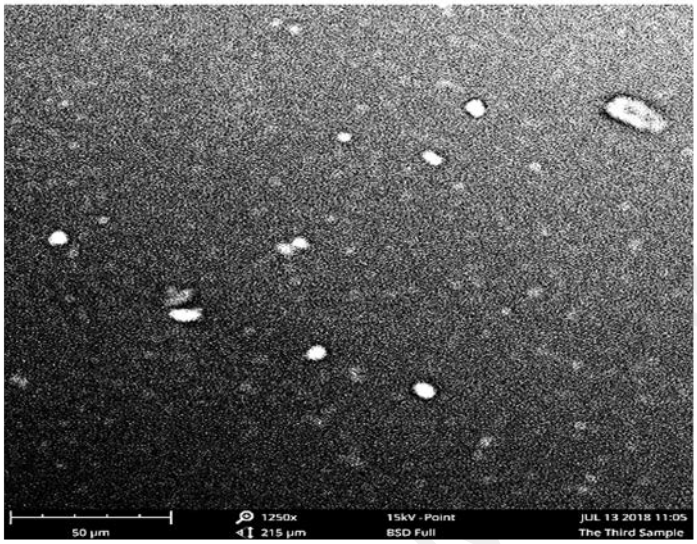

(a)

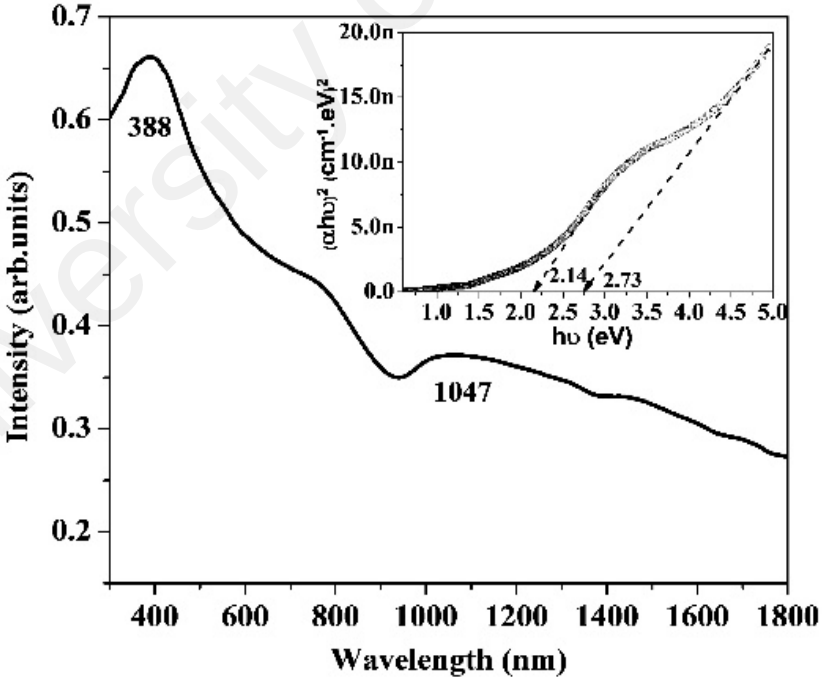

(b)

Figure 3.4: (a) SEM image of FIrpic-PVA thin-film, (b) optical absorption spectrum of FIrpic-PVA thin-film. (An inset Figure is the calculated optical band gap obtained by extrapolation to α = 0)

By linear extrapolation at the horizontal axis of $(\alpha h\nu)^2$ against $h\nu$, we can obtain the optical band gap which is equal to $h\nu$. Two band gaps of FIpric:PVA thin-film can be observed at about 2.14 and 2.73 eV, as can be seen in the inset of Figure 3.4 (b). These band gaps correspond to the PVA doped by FIrpic and micro-particles of FIrpic. Doping PVA by material modifies the band gap of PVA (6.28 eV) (Abdullah, Aziz, Omer, & Salih, 2015). So, 16.7 wt% of FIrpic significantly decreases the band gap of the PVA. It should be mentioned that the energy band gap of FIrpic is 2.65 eV (Adamovich et al., 2003; Ren et al., 2004).

To investigate the saturable absorption of the FIrpic-PVA thin-film, the nonlinear transmission property was characterized using a standard 2-arm transmission measurement scheme. Figure 3.5 (a) shows the measurement set-up, which consists of a home-made mode-locked laser as a pulsed source. The laser used has a pulse width, repetition rate and centre wavelength of 2.83 ps, ~1 MHz and 1572 nm, respectively. An erbium-doped fiber amplifier (EDFA) was used to amplify the mode-locked pulse train and a variable optical attenuator was utilized to vary the output power of the source. The output of attenuator was split equally into the test part (R1) (in which Alq_3: PVA SA was incorporated) and reference part (R2) by a 3-dB coupler. The output powers of R1 and R2 were measured by an optical power meter. By varying the attenuation, the transmission of the SA was determined by computing the difference between the average output powers of R1 and R2. The experimental data for transmission was fitted according to a simple two-level SA model (Zhen et al., 2015)

$$T(I) = 1 - \alpha_s * \exp\left(-I/I_{sat}\right) - a_{ns} \qquad (3.1)$$

where $T(I)$ is the transmission, $\alpha_s$is the modulation depth, I_{sat} is the saturation intensity, I is the input intensity, and a_{ns} is the non-saturable absorption. Figure 3.5 (b) shows the plotted nonlinear transmission characteristic of the FIrpic-PVA thin-film. As shown in the figure, it has a modulation depth of ~12.8% with a saturation intensity of 5.5 MW/cm^2.

The linear optical absorption of FIrpic PVA is also measured by transmitting a broadband light from the white light source through the thin-film, then the output intensity was measured by an optical spectrum analyzer (OSA). The result is shown in Figure 3.5 (c). The SA shows a flat absorption of about 2 dB in the range of 1500–1600 nm.

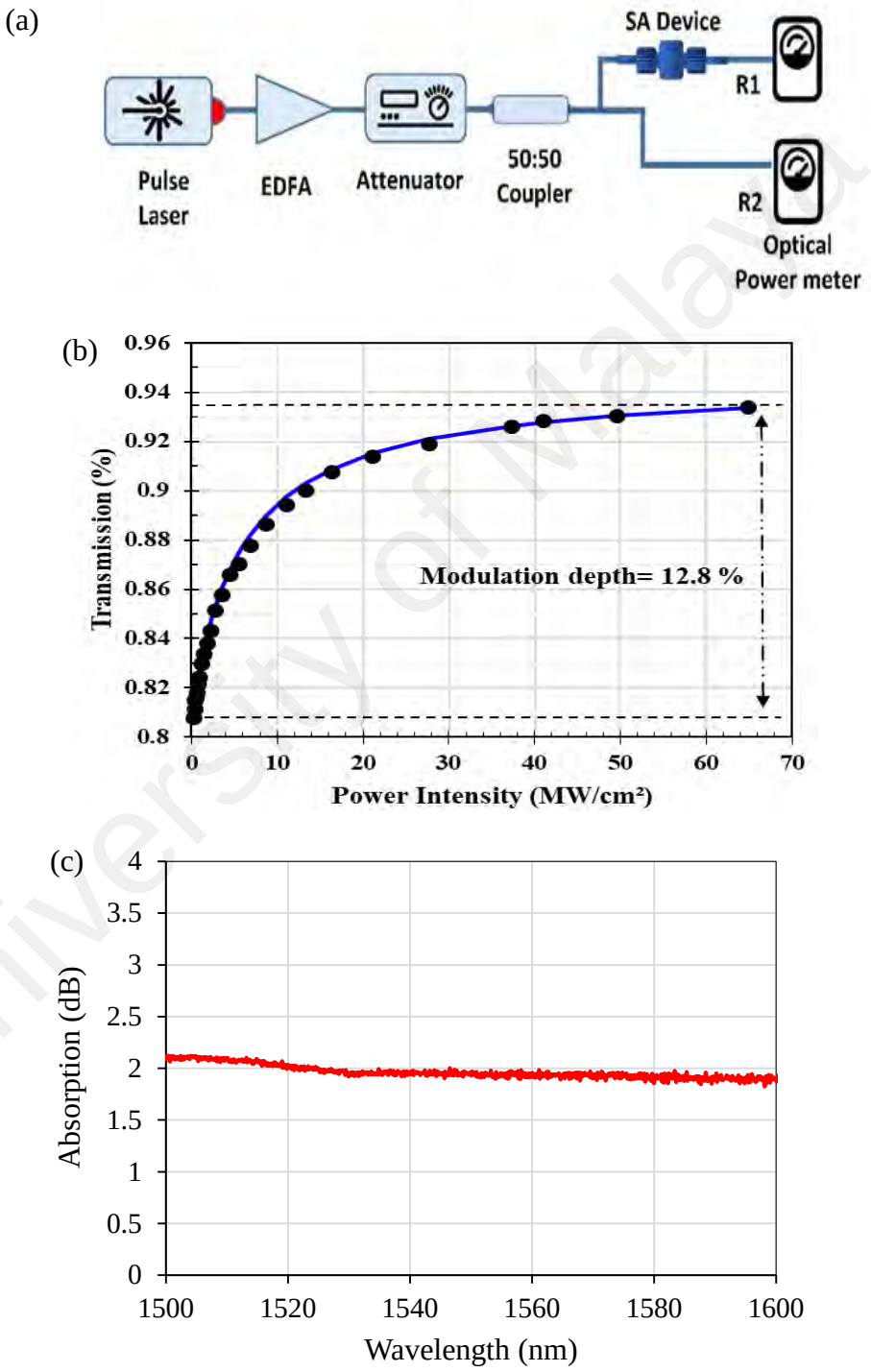

Figure 3.5: (a) Non-linear transmission measurement (b) Non-linear transmission profile and (c) linear absorption of FIrpic: PVA

3. 3 Fabrication and Characterization of Znq_2 as SA

Znq_2 has excellent electron transport and high electroluminescence at room temperature (Yin et al., 2000). It also has high quantum yields, low operating voltage and good injection efficiency. Znq_2 could produce an efficient fluorescence with high stability and this made it one of the most famous and most important light emitter and electron transport material candidates for OLED. In this study, the optical property of the Znq_2 film is further investigated for SA application. The SA was fabricated by the drop-casting technique in which Znq_2 was embedded into PVA to form a thin-film. Znq_2 powder was purchased from Sigma Aldrich, it has a weight of 353.69 g/mol and purity of 99%. First, 100 mg of Znq_2 powder was dissolved into 10 ml of (Isopropyl alcohol) IPA, then the solution was stirred at 50° C for 180 minutes. On the other hand, 1 g of PVA powder was dissolved into 120 ml of distilled water, followed by stirring for 30 minutes. Then, 20 ml of PVA solution was added to Znq_2 solution. The mixture was then stirred for 24 hours at room temperature. The mixture was then poured into a petri dish to form a thin-film. The produced thin-film had a thickness of ~50 µm. The fabrication process is summarized in Figure 3.6.

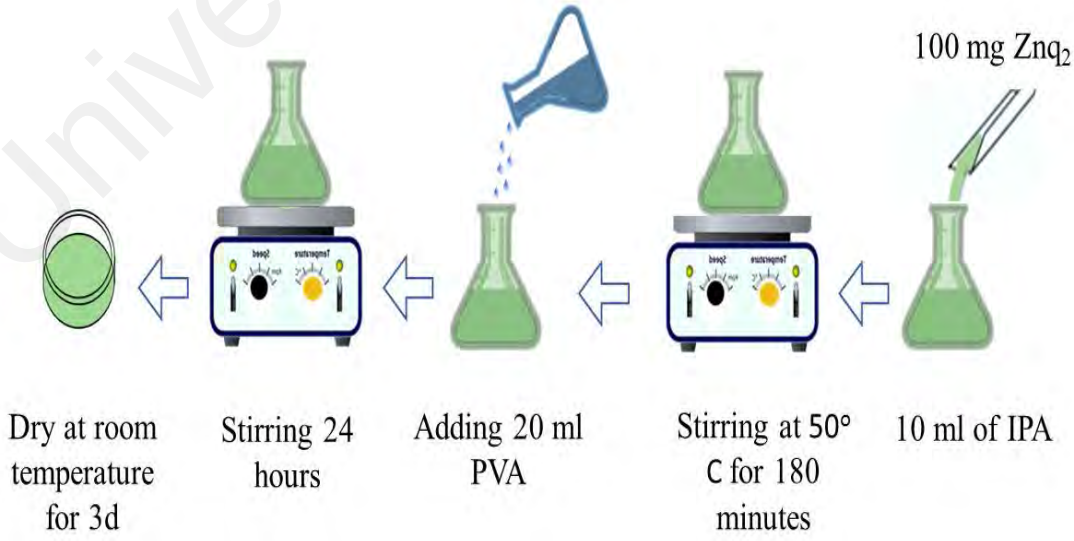

Figure 3.6: Fabrication process of Znq_2: PVA SA

An FTIR spectrometer was then used to analyses the chemical groups in the SA thin-film. Figure 3.7 (a) shows the FTIR transmission spectra obtained in the range between 4000 to 500 cm^{-1} with a resolution of 2 cm^{-1} for both PVA and Znq_2: PVA thin-films. The Znq_2: PVA curve shows similar FTIR spectrum as PVA except for two peaks at 1577 and 1327 cm^{-1}, which are assigned to the quinoline group of Znq_2, additionally, the pyridyl and phenyl groups in Znq_2 are observed 1499 cm^{-1}. While, the peak at 743 cm^{-1} is attributed to the in-plane ring deformation (Bharathi Devi, Arulmozhichelvan, & Murugakoothan, 2017; Pan, Liang, Mao, Zhu, & Chen, 2007; Shao, Wang, Wang, & Chen, 2011). Figure 3.7 (b) shows the SEM image of Znq_2: PVA. It shows a homogeneous distribution of the Znq_2 within the PVA. The linear absorption of the SA was investigated in the wavelength range between 900 nm to 1650 nm.

The SA had an absorption of ~ 1.2 dB at the region of 1550 nm, see Figure 3.7 (c). The linear absorption was measured by comparing the optical spectrum of the light before and after it penetrates the SA thin-film. To check the non-linear transmission of the SA, a mode-locked fiber with a pulse width, repetition rate, and central wavelength of 1.2 ps, 2 MHz and 1562 nm, respectively, was used as pulse source as described in the previous section. An EDFA and variable optical attenuator were used to amplify and to vary the output power of the pulsed laser, respectively. The output of attenuator was split equally into two points, R1 and R2. R1 represents the output power as it went through the SA while R2 is the reference point (i.e. the output power). The transmission of the SA was determined by computing the difference between R1 and R2. Znq_2 has a modulation depth and saturation intensity of 17.6% and 103.6 MW/cm^2, see Figure 3.7 (d)

(a)

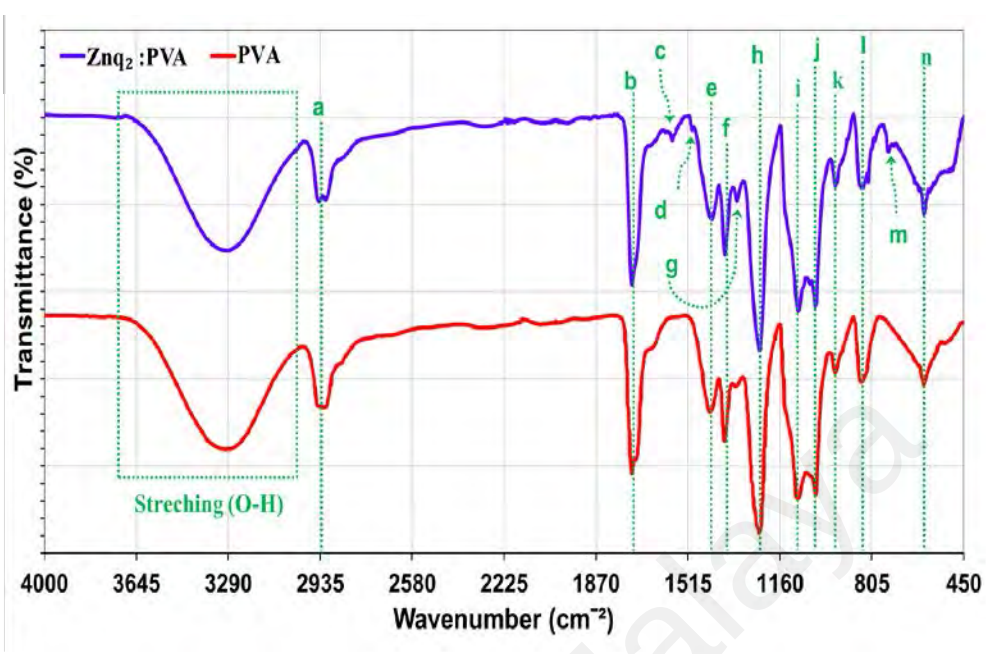

(b)

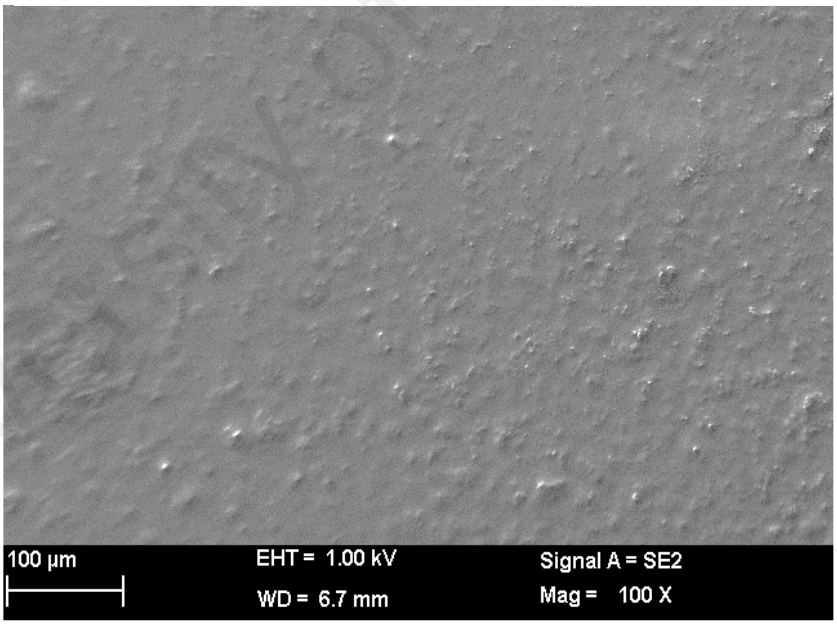

Figure 3.7: (a) FTIR of Znq_2: PVA and PVA thin-films (a=2925, b=1729, c=1577, d=1499, e=1428, f=1374, g=1327, h=1242, i=1089, j=1023, k=946, l=845, m=743 and n=604 cm^{-1}) (b) SEM image, (c) linear absorption spectrum of Znq_2: PVA thin-film and (d) modulation depth of Znq_2: PVA thin-film

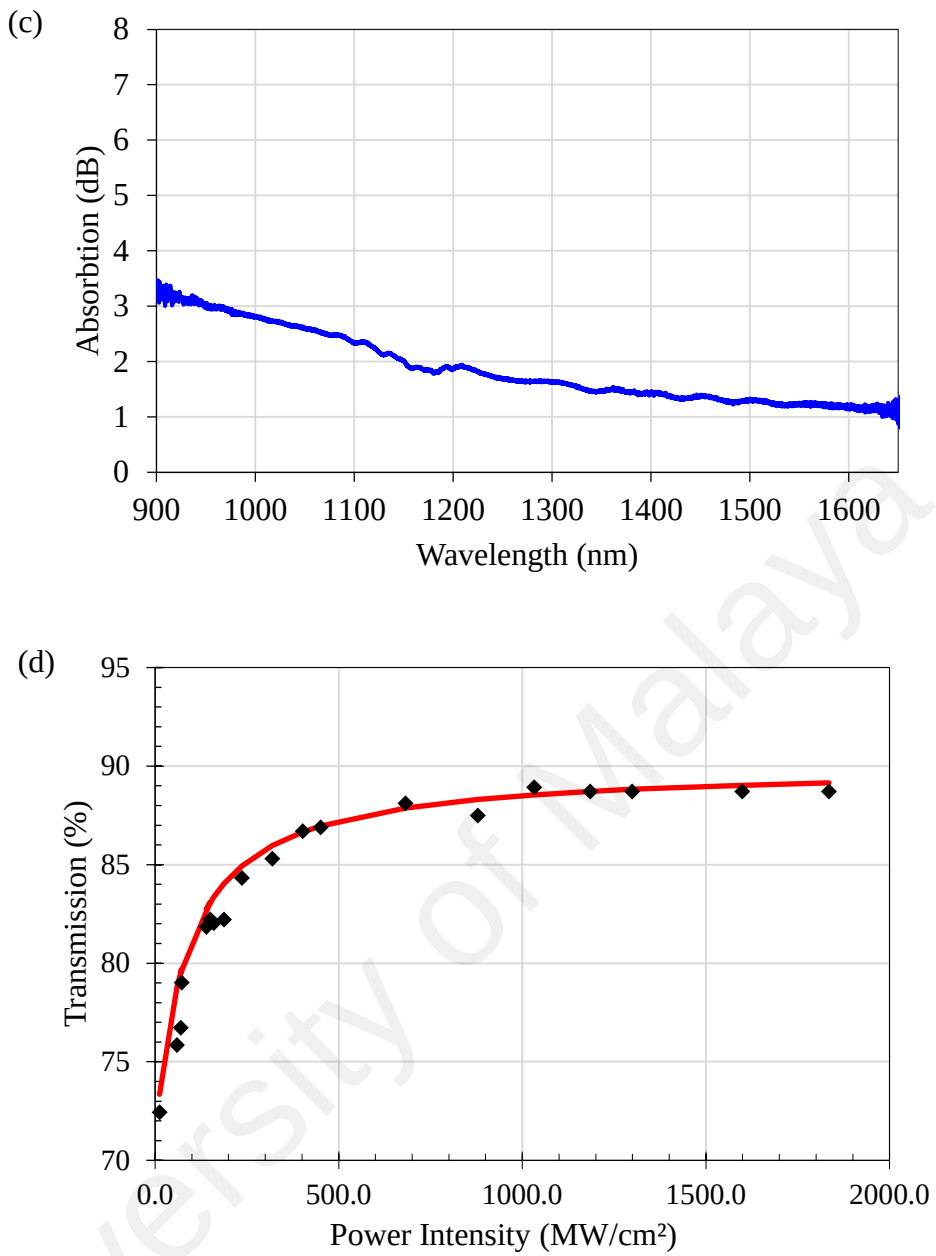

Figure 3.7, continued

3. 4 Fabrication and Characterization of Alq_3 as SA

Alq_3 is considered the most rigorously studied small-molecule organic semiconductor (Xie et al., 2016); thus it became the choice for organic SA in this research work. Alq_3 which has superior thermal stability, can be easily synthesized and purified (Hairong Li, Zhang, Wang, & Zheng, 2003). Alq_3 also has high photoconductivity and long operational lifetimes (Fukuda, Wei, Ichikawa, & Taniguchi, 2007). Furthermore, Alq_3 has the

advantages of highly stable thin-film formation and excellent heat resistance (Yawalkar, Dhoble, Thejo Kalyani, Atram, & Kokode, 2013). Alq_3 powder used was purchased from Sigma Aldrich (product no. 697737-1G) (Sigm-Aaldrich, 2019) and it has a purity of 99.995% and molecular weight of 459.43 g/mol. Figure 3.8 shows the molecular structure of the Alq_3, which was embedded into the PVA polymer by a drop-casting technique at room temperature.

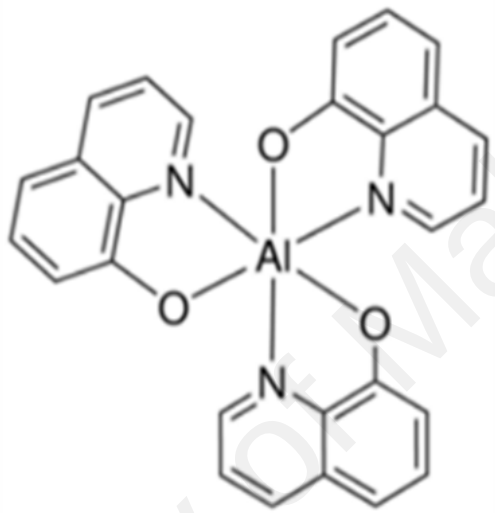

Figure 3.8: Molecular structure of Alq_3

The fabrication process of the Alq_3: PVA thin-film is illustrated in Figure 3.9. Firstly, 1 ml of distilled water was added to 10 mg of purchased Alq_3 powder. Subsequently, the solution was stirred at 50° C for one hour and then 2 drops of acetone were added to the solution for equal distribution of Alq_3 along with the solution. On the other side, 1 g of PVA was dissolved in 100 ml distilled water followed by ultra-sonication for one hour at room temperature. Next, 5 ml of PVA solution was mixed with the Alq_3 solution. The mixture solution was then stirred for about three hours at room temperature. After that, the mixture was poured into a borosilicate glass petri dish with a diameter of 60 mm to form a thin-film, which can be easily separated after drying for three days at room temperature. The thickness of the thin-film was measured using Mitutoyo micrometer

screw gauge and it was about 50 µm. Finally, the fabricated film was cut into a tiny piece and attached to a fiber ferrule.

Figure 3.9: The fabrication process of Alq_3: PVA thin-film

The fabricated film was characterized to analyze the chemical groups in the materials by using Perkin Elmer Spectrum 400 FTIR Spectrometer. In the experiment both pure PVA and Alq_3: PVA thin-films were analyzed based on transmittance mode with a resolution of 2 cm^{-1}. Figure 3.10 (a) shows the FTIR transmission spectra for both PVA and Alq_3: PVA thin-films, which were obtained in the range of wavenumber from 4000 to 500 cm^{-1}. As shown in the figure, various FTIR absorption peaks were obtained for PVA, which are related to the hydroxyl and acetate groups. On the other hand, the Alq_3 embedded into PVA thin-film shows similar FTIR spectrum as PVA thin-film except for the appearance of three peaks at 2176, 1580 and 750 cm^{-1}. 2176, 1580 and 750 cm^{-1} peaks correspond to Al-O-H, C=N and Al-N modes for Alq_3 chemical bonding (Correia, Santos, Garcia, Peres, & Wang, 2015; Laukamp, Salama, & González-Álvarez, 2016; Quintero et al., 2013), respectively.

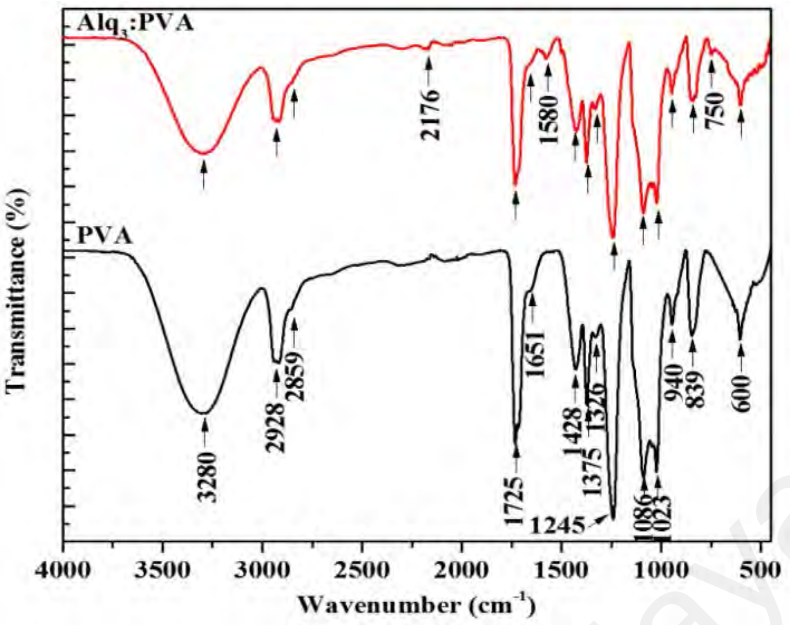

(a)

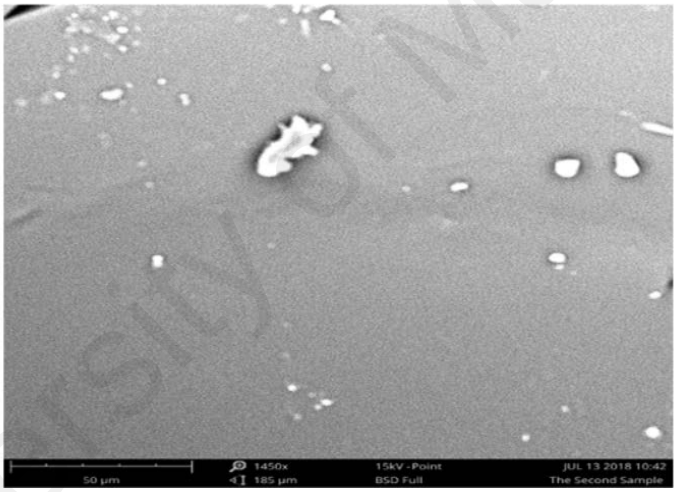

(b)

Figure 3.10: (a) FTIR spectra of PVA and Alq_3: PVA thin-films and (b) SEM of Alq_3: PVA thin-film

The SEM image of Alq_3:PVA thin-film was also obtained as shown in Figure 3.10 (b). It indicates a soft surface with a uniform distribution of Alq_3 in the PVA polymer. The dots shown on the surface is contamination, which could be formed from the aggregated particles of the large molecules of Alq_3 which are difficult to be dispersed among the PVA molecules. The absorbance characteristic of the prepared Alq_3: PVA polymer thin-film was also measured using a spectrophotometer (Perkin Elmer, Lambda

750), which operates in a wavelength range between 250 and 2000 nm. The optical absorbance spectrum of the Alq_3:PVA thin-film is depicted in Figure 3.11 (a). The appearance of two peaks is seen at around 300 and 385 nm which are assigned to the $\pi \rightarrow \pi^*$ transition of PVA and Alq_3 materials, respectively due to unsaturated bonds (Aziz, Rasheed, Saeed, & Abdullah, 2017; Cuba & Muralidharan, 2015; Elashmawi, Hakeem, & Selim, 2009). The absorption coefficient (α) can be obtained by Beer-Lambert's law as $(v)=2.303\times Abs(\lambda)/d$, where d is the thin-film thickness and it is around 50 µm. Alq_3 is an organic semiconductor and thus the optical band gap, E_g, can be estimated from the absorption coefficient in equation $(\alpha hv)^n=B(hv-E_g)$ by extrapolating hv to $\alpha=0$, where B is a constant relative to the material, hv is the photon energy, and n = 2 for direct transition. The observed band gaps of the Alq_3: PVA thin-film are about 2.5 and 2.4 eV, as can be seen from the Tauc plot in Figure 3.11 (b), which belong to Alq_3 and modified PVA thin-film (Abdullah et al., 2015; Divayana et al., 2007), respectively. The optical band gap of Alq_3 can be recognized due to the large particles of Alq_3 on the Alq_3: PVA thin-film, as can be observed in the SEM image. Moreover, doping PVA by 10 mg of Alq_3 modified the optical band gap of PVA from 6.28 to 2.4 eV due to the uniform distribution of the Alq_3 molecules along with the PVA polymer (Abdullah et al., 2015).

It should be noted that even though the band gap of Alq_3 is about 2.5 and 2.4 eV (which means that absorption peaks of Alq_3 are located near 500 nm), the saturable absorption was observed near 1000 nm which is sub-band gap absorption. The sub-band gap absorption is attributed to some defects in the material. The evidence of these defects and their physical origin in Alq_3 is addressed in ref. (Grecu, Mirea, Ghica, Cölle, & Schwoerer, 2005). These defects create new states in the band gap. These states absorb sub-band gap photons and affect the absorption spectra, causing artefacts and features that interpreted as lower band gap than the actual non-defected value. These defects lead to decreasing the optical energy gap and shifting the absorption edge towards the higher

wavelength of the incident (S. Wang et al., 2014). A similar case has been reported in ref. (K. Wu et al., 2015). The authors used WS_2 as SA in which it has a direct band gap of ~2.0 eV (~630 nm) and the indirect band gap is ~1.4 eV (~886 nm) (Chhowalla et al., 2013), but they still produced a mode-lock operation in 1.5 µm region. The authors attributed the sub-band gap absorption to some defects as well as absorption of edge modes and two-photon absorption (TPA). MoS_2 also has a direct band gap of ~1.8 eV (688 nm) and the indirect band gap is 0.86 - 1.29 eV (1443 -962 nm) (S. Wang et al., 2014), but the sub-band gap absorption was observed in which the saturable absorption property was observed in a wide band beyond this limitation. Further investigation is still required to understand the sub-band gap absorption in Alq_3, as this is beyond the scope of this thesis. That investigation would help to address the absorption mechanism in Alq_3 in 1 µm and 1.5 µm region in further details.

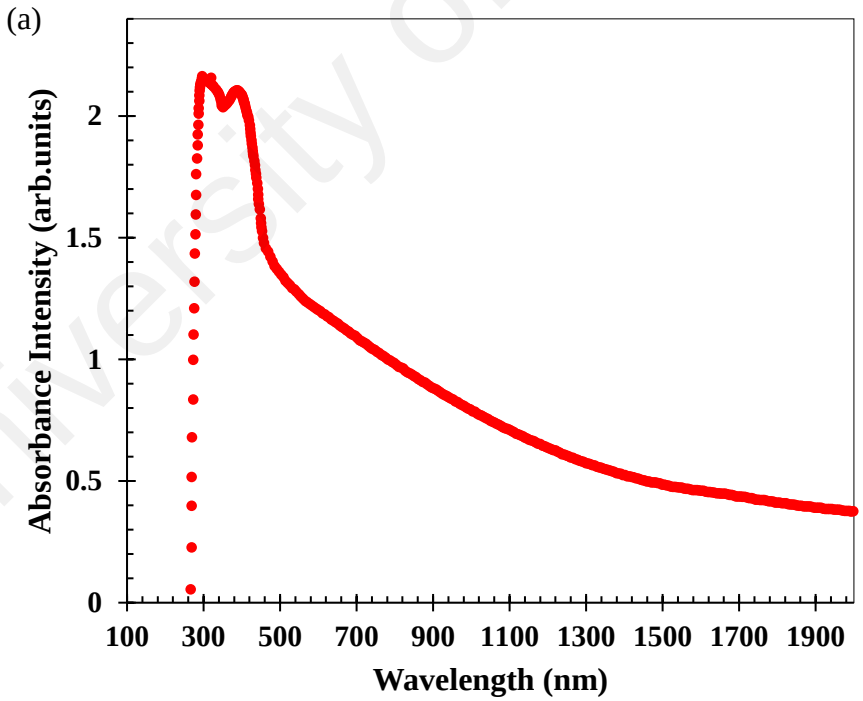

Figure 3.11: (a) The measured absorption spectrum for the Alq_3: PVA thin-film and (b) the Tauc's plot

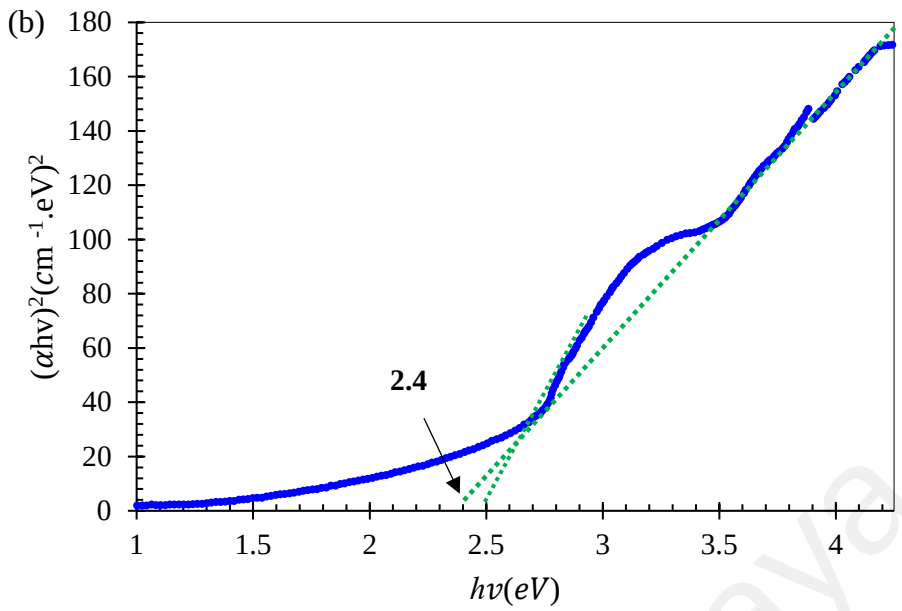

Figure 3.11, continued

The proposed Alq_3: PVA thin-film has a broadband absorption region covering the visible to 2000 nm as shown in Figure 3.11 (a). This shows the material can be used as SA to generate Q-switched and mode-locked pulses with broad spectral tunability. Besides the linear absorption, the modulation depth of the Alq_3 SA is also important to determine the recovery and response time of the material whether it is fast enough to support both Q-switching and mode-locking pulses generation. For instance, the recovery time should be between the pulse duration (of the Q-switching operation) and the upper-state lifetime of the gain medium. This SA could also be used to produce a mode-locking operation by balancing the dispersion and nonlinearity characteristics of the laser cavity. The non-linear transmission of the Alq_3: PVA was characterized by using the setup shown in Figure 3.5 (a). Figure 3.12 (a) shows the nonlinear transmission characterization of Alq_3: PVA film in which a saturation intensity and modulation depth of 3 MW/cm^2 and~ 8.1% were obtained, respectively. Figure 3.12 (b) presents that Alq_3:PVA has a flat absorption of about 2 dB in the range from 900–1600 nm.

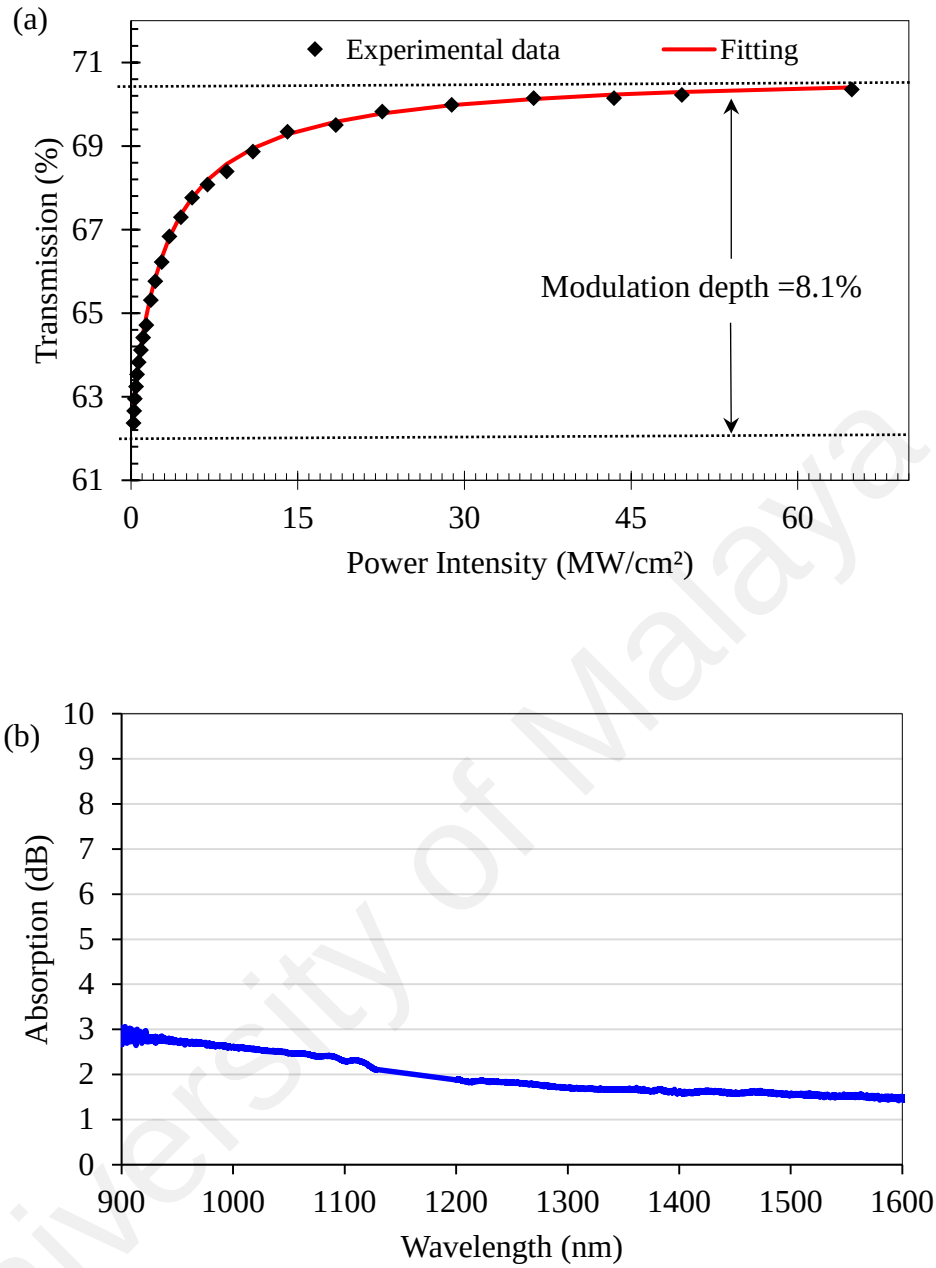

Figure 3.12: (a) Nonlinear transmission and (b) linear absorption of the fabricated Alq_3: PVA film

3. 5 Summary

Three SA thin-films were successfully developed based on three different organic materials; FIrpic, Znq_2 and Alq_3. Each of these materials was embedded into PVA to form a thin-film by solvent casting technique. The fabricated films were successfully characterized in terms of FTIR spectra, linear absorption and nonlinear transmission. The

characteristics of these films were summarized in Table 3.1. It is obtained that the modulation depth of the three organic materials was above 6%, which should be sufficient to make the developed SAs function as Q-switchers or mode-lockers.

Table 3.1: Comparison of the modulation depth, saturation intensity and non-Saturable absorbance between FIrpic, Znq_2 and Alq_3

SA material	Modulation depth (%)	Saturation intensity (MW/cm^2)	Non-Saturable absorbance
FIrpic	12.8	5.5	93.5
Znq_2	17.6	103.6	88.7
Alq_3	8.1	3	70

CHAPTER 4: Q-SWITCHED PULSE GENERATION BY USING ORGANIC MATERIALS

4. 1 Introduction

The search of new techniques for generation of a short pulse laser is always at the centre of research, as pulsed lasers have many applications in medicine, remote sensing, long-range optical communication and fiber sensor. Passive Q-switching is the typical technique and one of the most effective ways of producing short and high-energy laser pulses. Since they are advantageous in terms of simplicity, compactness and design flexibility (Petropoulos, Offerhaus, Richardson, Dhanjal, & Zheludev, 1999). Q-switched lasers can be produced by modulating the Q-parameter (quality factor) such that a series of short and intense pulses are generated (Kurkov, 2011; Morkel, Jedrzejewski, Taylor, & Payne, 1992; Svelto & Hanna, 2013). Here Q is defined as the ratio of the energy stored in the cavity to the losses per oscillation cycle. The pulse width of the Q-switched laser is usually in a range of μs to few ns while the repetition rate is normally in the kHz region. Q-switched pulses train can be generated from either active or passive methods. Active methods are normally obtained by using electro-optic modulator, which is driven by an external electrical generator to generate pulses (Alvarez-Chavez et al., 2000; Kee et al., 1998). Passive Q-switching, on the other hand, can be realized by incorporating a saturable absorber (SA) device in the laser cavity. Although active Q-switching can address long term stability and controllable repetition rate, it has the disadvantages of low damage threshold and low peak power. On the contrary, passive techniques are more useful due to their advantages of low cost, compactness, simplicity and flexibility as compared to the active Q-switching, which requires additional electronic components (Svelto & Hanna, 2013).

Semiconductor saturable absorber mirror (SESAM) was among the earliest types and the most popular SA used to passively generate Q-switching pulses in a fiber laser cavity

(S. X. Xu, Li, Hao, Zhai, & Zeng, 2008). However, they are costly and have a relatively small operation wavelength range. SESAMs dominance was suppressed with the introduction of carbon nanotubes (CNTs) (Y. Gao et al., 2013). CNT based SA offered significant advantages in terms of a simpler fabrication and easier packaging. Furthermore, the operating wavelength range in CNT is much wider than SESAM (A. Schmidt et al., 2008). However, CNT has restricted practical applications due to the dependence of response spectral range on the nanotube sizes. Graphene, on the other hand, (J. Zhao et al., 2012) and topological insulators such as bismuth telluride (Bi_2Te_3) (Zakaria et al., 2018), bismuth selenide (Bi_2Se_3) (H Ahmad, Salim, Azzuhri, Soltanian, & Harun, 2015) and antimony telluride (Sb_2Te_3) (J Sotor, Sobon, Grodecki, & Abramski, 2014), have been successfully employed in various fiber lasers setup to produce Q-switching pulses. However, graphene has the drawbacks of wavelength-dependent, low modulation depth (between 0.5% and 1.8% per layer (Sobon, 2015)) as well as a small optical absorption range which pose a limitation in many applications, while TIs have complex fabrication processes that allow the flow of electrons on their surface (M. H. M. Ahmed et al., 2017). Black Phosphorous (BP) (L. Kong et al., 2016) and Transition Metal Dichalcogenides (TMD) materials such as Tungsten disulfide (WS_2) (J. Lin, Hu, Chen, Gu, & Xu, 2015), Tungsten diselenide (WSe_2) (B. Chen et al., 2015), Molybdenum diselenide ($MoSe_2$) (RI Woodward et al., 2015), and Molybdenum Sulfide (MoS_2) (S. Wang et al., 2014) have also gained many interests. They have good potential for pulse laser applications due to their thickness-dependent band gap and unique absorption properties (B. Chen et al., 2015; M Zhang et al., 2015). However, the process of fabricating these materials as SAs are slightly complicated.

To date, there are many new approaches in research to develop new high-performance SAs for generating a Q-switched laser operation (Hisyam, Rusdi, Latiff, & Harun, 2016). Finding a new material to be used as high-performance SAs for Q-switching pulse

generation is of great interest. In that regards, organics materials are a promising candidate for developing new SAs, as they may have broad spectral tunability, large and ultrafast nonlinear response and they can be solution-processed at low cost. Additionally, organic materials would be highly desirable as a bio-compatible alternative for developing non-hazardous and environmentally-friendly photonic devices which could find increasing applications in biomedical laser processing and sensing. In comparison to traditional inorganic materials, organic materials have the advantages of versatile molecular design, simple fabrication, low-cost processing and easy control of physical properties of materials. Hence, organic materials have been utilized in different areas, which include solar cells (Peumans et al., 2011), bi-stable memory devices (Briseno et al., 2006), light-emitting diodes (OLEDs) (Holmes et al., 2003) and organic thin-film transistor (Choi, Jin, Park, Kim, & Gal, 2012).

In this chapter, various Q-switched Erbium-doped fiber lasers (EDFLs) are demonstrated using the newly developed organic material-based SA devices. Here, three organic materials; Bis[2-(4,6-difluorophenyl)pyridinato-C^2,N](picolinato)iridium(III) (FIrpic), bis(8-hydroxyquinoline)zinc (Znq_2) and Tris(8-hydroxyquinoline)aluminum (Alq_3) are used for the generation of stable Q-switched laser pulses. A small piece of the developed SA thin-film was sandwiched between two ferrule connectors and incorporated into the laser setup. The Q-switching pulses were successfully generated as the pump power was increased above the threshold. The pulse width reduced, and the repetition rate increased as the pump power was further increased, which confirmed the Q-switching operation.

4. 2 Q-switched Pulse Generation with FIrpic Based SA

4.2.1 Experimental Setup

The proposed setup of the fiber laser cavity is shown in Figure 4.1. A 980 nm laser diode (LD) was utilized to pump the laser cavity and it was integrated into the laser cavity via the 980 port of 980/1550 nm wavelength division multiplexer (WDM). The output port of the WDM was connected to an erbium-doped fiber (EDF) which works as a gain medium. The cavity length was about 8 m that is 5.5 m single-mode fiber (SMF-28), 2 m EDF and 0.5 m WDM. The EDF has an erbium ions absorption of 23 dB/m at 980 nm with numerical aperture, core and a cladding diameter of 0.16, 4 µm and 125 µm, respectively. The other end of EDF was connected to a polarization-independent isolator (ISO) to maintain unidirectional laser propagation before being connected to the SA device while the other end of the SA device was connected to a 50/50-output coupler (OC). The FIrpic thin-film SA was cut into 1 × 1 mm^2 and sandwiched between two fiber ferrules to form a SA device. An index matching gel was pre-applied with a very small quantity to hold the film between the fiber ferrules as well as to prevent spurious reflection.

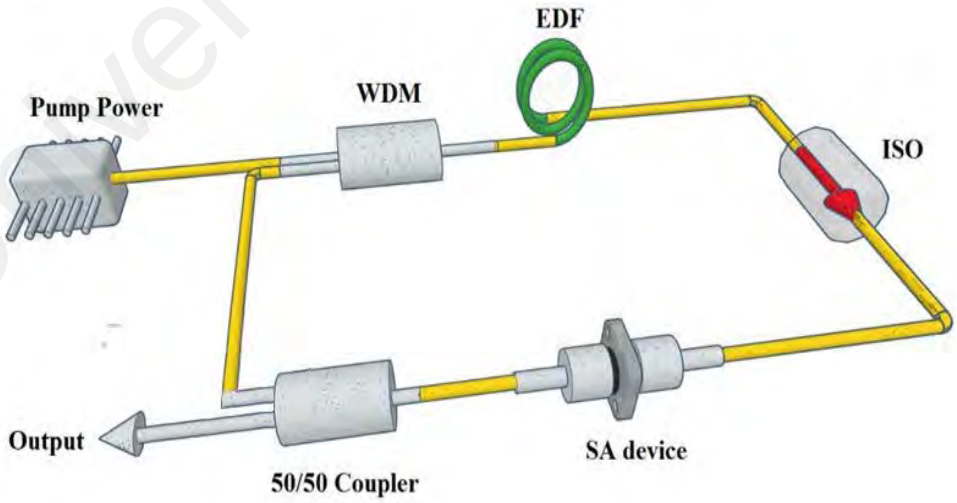

Figure 4.1: Experimental setup of Q-switched EDFL with FIpric thin-film SA in a ring cavity

One of the 50% output coupler port was connected to the 1550 nm port of the WDM, thus completing the fiber laser cavity. The other 50% output of the OC was utilized for testing purposes. The output spectrum, temporal characteristic in the time domain, output power and radio frequency (RF) spectrum were measured by using an optical spectrum analyzer, 500 MHz oscilloscope through 7 GHz photodetector, optical power meter and RF spectrum analyzer, respectively.

4.2.2 Q-switching Performance

At the initial phase of the experiment, the laser operated in continuous wave (CW) regime as the pump power was increased above the threshold of 20 mW. A self-starting and stable passively Q-switched EDFL oscillation using FIpric was observed when the pump power exceeded the threshold at 30 mW. Figure 4.2 depicts the output spectrum of the Q-switching pulse in EDFL at the threshold pump power, which centers at a wavelength of 1560.4 nm with 2.2 nm 3-dB bandwidth. The Q-switching pulse train operation remained stable as the pump power was raised to 208 mW.

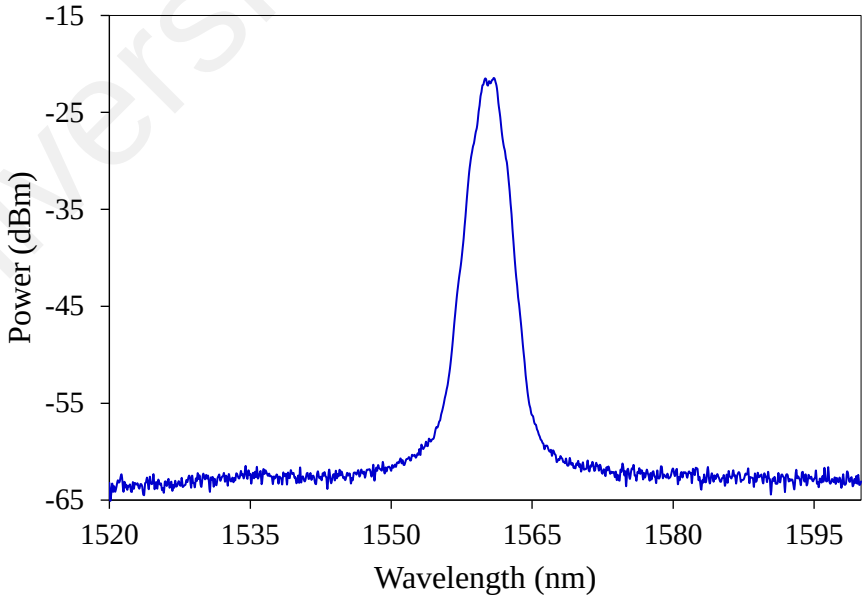

Figure 4.2: Optical spectrum of FIpric based Q-switched EDFL

To prove that the FIrpic based SA triggered the Q-switched operation, the cavity was launched with no SA inside. In this case, no Q-switched operation was observed even when the incident pump power was tuned over a wide range. Figure 4.3 shows the oscilloscope pulse train at a pump power of 208 mW. The pulse train maintained a uniform intensity distribution without observable fluctuation, nor amplitude modulation in a laboratory condition for 2 hours. This confirms the stability of the regime and its capability to operate with various repetition rates and pulse widths. By increasing the pump power up to the maximum available input of 270 mW, the pulses became unstable as FIpric SA was over-saturated without thermal damage. The thermal damage threshold of the SA is higher than 270 mW.

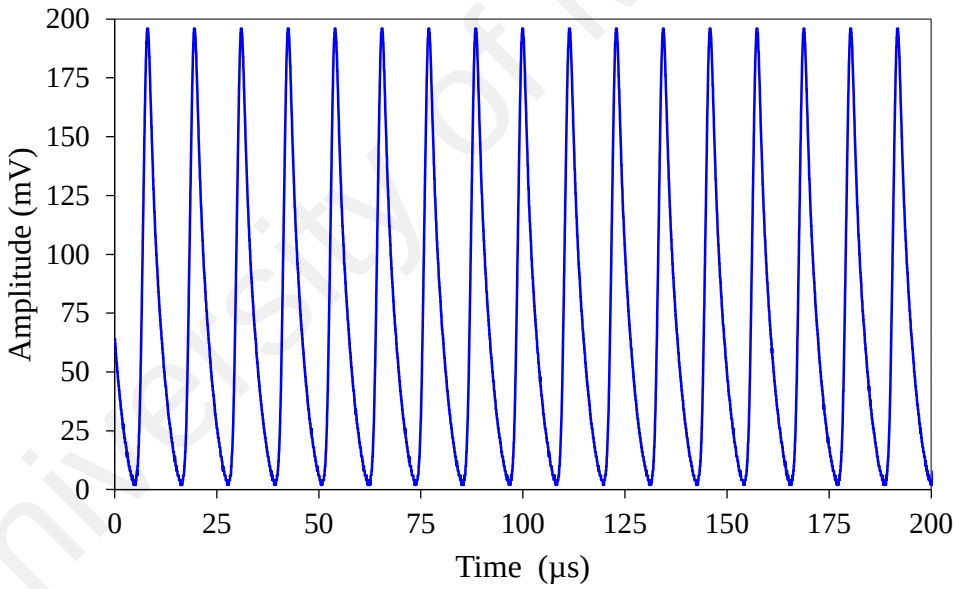

Figure 4.3: Typical pulse train of the Q-switched EDFL at LD power of 208 mW

Figure 4.4 (a) shows a monotonic increment of repetition rate from 39.22 to 87.4 kHz as the pump power was increased from 30 to 208 mW. The pulse-width decreased from 9.5 to 3.4 µs at the same pump power range, which agrees to the typical characteristic of a Q-switched laser. The shortest pulse width of 3.4 µs is obtained at 208 mW pump power. This long pulse duration is attributed to the long cavity length (Dong, Hao, Hu, & Liaw,

2011; M. Wu, Chen, Zhang, & Wen, 2014). We expect that a short pulse duration and enhanced overall Q-switching operation would be achieved by shortening the cavity length, enhancing the cavity birefringence and reducing the cavity losses (Degnan, 1995; Herda, Kivistö, & Okhotnikov, 2008). Raising the incident pump power resulted in more gain feed to saturate the SA. Consequently, the threshold energy stored in the gain medium was reached earlier, leading to an increase in the repetition rate and a decrease in the pulse width.

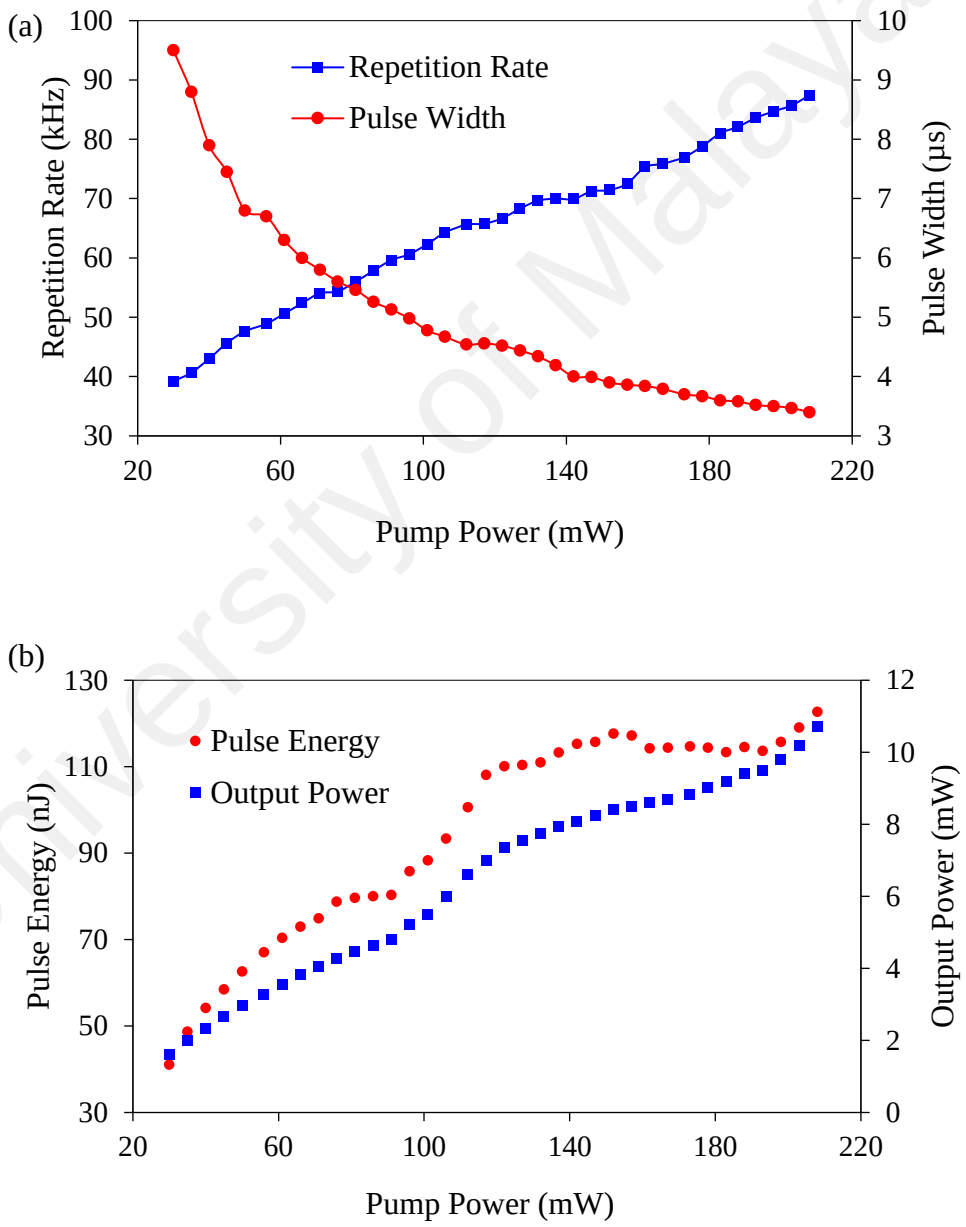

Figure 4.4: (a) Repetition rate and pulse width versus input pump power and (b) pulse energy and output power versus input pump power

As the pump power was increased from 30 to 208 mW, the pulse energy increased from 41 to 122.6 nJ and the output power linearly increased from 1.61 to 10.72 mW with an efficiency of 4.89%, as shown in Figure 4.4 (b). To check the stability of the Q-switching operation, we measured the RF of the output spectrum with a span of 900 kHz. Figure 4.5 (a) and (b) shows the fundamental RF peaks at 87.4 kHz with a span of 900 kHz and 90 kHz, respectively. The signal-to-noise ratio (SNR) is 58.36 dB at the fundamental frequency, which depicts excellent Q-switching stability (H. Ahmad, Zulkifli, Thambiratnam, & Harun, 2013). In comparison with other works that addressed a similar cavity setup with SAs like CNT, Bi_2Se_3, BP, $MoSe_2$ and TiO_2 in ref (Harith Ahmad et al., 2017; Harith Ahmad, Siti Aisyah Reduan, et al., 2016; M. H. M. Ahmed, A. H. H. Al-Masoodi, A. A. Latiff, H. Arof, & S. W. J. I. J. o. P. Harun, 2017; HH Liu, Chow, Yamashita, Set, & Technology, 2013; L. Sun et al., 2014), respectively, FIrpic showed a very high SNR, a very high output power, high pulse energy and wide input pump power range (i.e. from 30 mW to 208 mW).

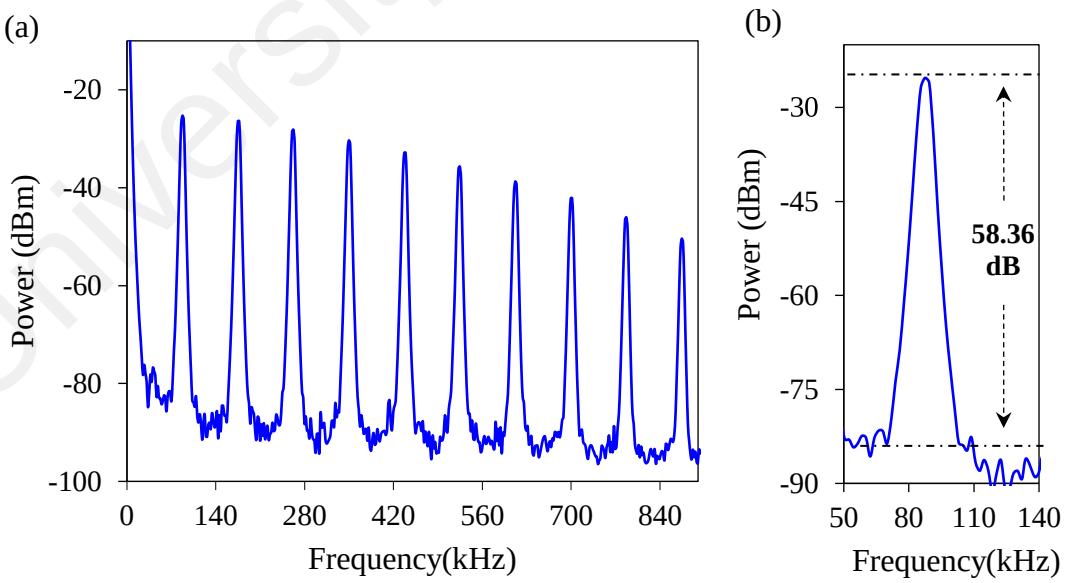

Figure 4.5: (a) RF spectrum of Q-switched EDFL at a pump power of 208 mW with a span of 900 kHz and (b) with a span of 90 kHz

4. 3 Dual-Wavelength Q-switched EDFL with Microfiber Filter and FIrpic SA

4.3.1 Experimental Arrangement

The proposed setup of the dual-wavelength Q-switched EDFL cavity is shown in Figure 4.6 (a). A 2 m long EDF was used as a gain medium, it has an erbium ions absorption of 23 dB/m at 980 nm ps^2/km. A laser diode (LD) operating at 980 nm was used to pump the EDF via the 980/1550 WDM. The EDF was also connected to the isolator (ISO) device, which was used to prevent light reflection and thus allow a unidirectional operation of the laser. The cavity length was about 8 m that is 5.5 m single-mode fiber (SMF-28), 2 m EDF and 0.5 m WDM. The SA device was made by inserting 1 mm^2 piece of FIrpic thin-film between two fiber ferrules. A non-adiabatic microfiber was used in the cavity to produce dual-wavelength output. Finally, 3-dB output coupler was used to extract 50% of the light from the cavity. The output spectrum, pulse train, and RF spectrum were measured by using OSA, 500 MHz oscilloscope with 7 GHz photodetector, and RF spectrum analyzer, respectively.

A flame brushing technique fabricated the microfiber, see Figure 4.6 (b). A coating-removed SMF was held horizontally by two motorized fiber holders. The fiber holders have a sliding section in which they can be pulled apart. During the tapering process, an oxy-butane torch flame was used to heat the fiber to its softening temperature, and at the same time, the ends of the SMF were pulled apart to reduce the diameter. The torch had 10 mm long flame, and it was perpendicular and had a constant distance (a pinpoint tip) to the clamped fiber. To ensure an optimal flame performance, we carefully controlled the oxygen gas supply pressure. The temperature and flame level are vital parameters to manage to produce the non-adiabatic microfiber (Harith Ahmad, Rahman, Sakeh, Razak, & Zulkifli, 2016; B. Wang, Zhang, Pang, Wang, & Yang, 2011; Zheng et al., 2013). The insertion loss and the inter-modal interference of the fiber were both monitored during the fabrication process by launching amplified spontaneous emission (ASE) in one end

and observing the output by OSA on the other end of the SMF. The produced microfiber had a diameter of 8 µm and a tapering length of 11 mm.

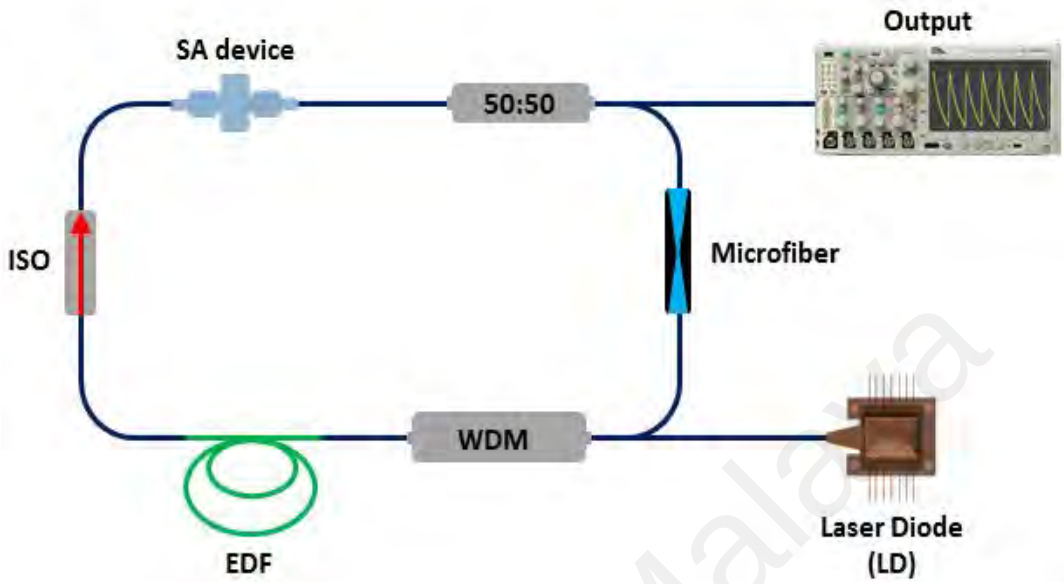

(a)

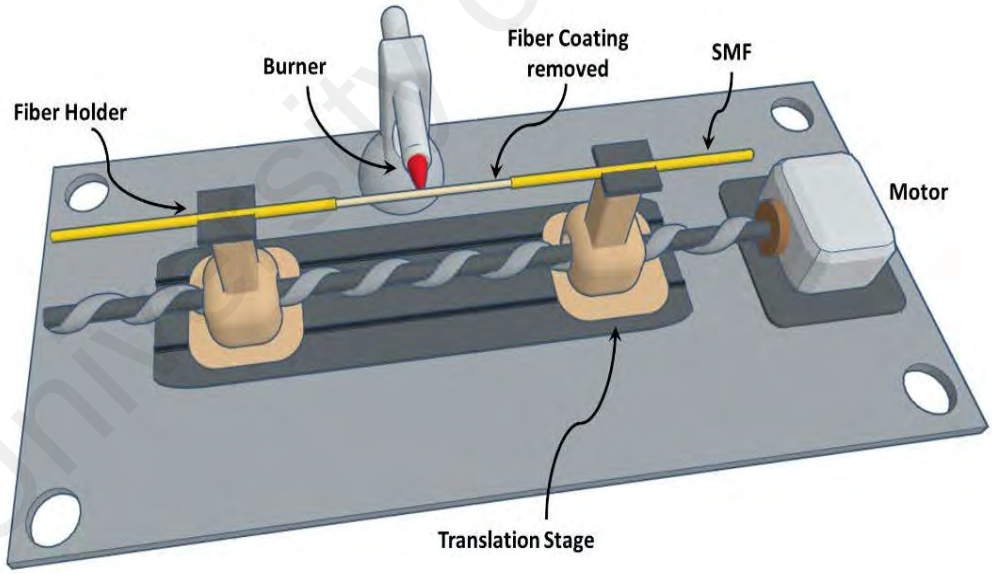

(b)

Figure 4.6 : (a) Cavity setup for dual-wavelength Q-switched EDFL and (b) experimental setup for the fabrication process of microfiber via the flame brushing technique.

4.3.2 Dual-Wavelength Q-switched EDFL Performance

In the proposed laser, the FIrpic based SA was used as a Q-switcher to transform the CW operation into a pulse train, while the microfiber was used to generate the dual-wavelength output. The laser cavity starts to generate a CW laser at a threshold pump power of 25 mW. A stable dual-wavelength Q-switch (DWQS) pulse train was obtained as the pump power was further increased within 35 mW to 213 mW. Figure 4.7 shows the dual-wavelength output spectrum at 213 mW, the peaks were located at 1558.1 nm and 1562.6 nm giving a spacing of about 4.5 nm with almost the same intensity of 12.61 dBm and 12.69 dBm and 3-dB bandwidth of 0.3 nm and 0.1 nm, respectively.

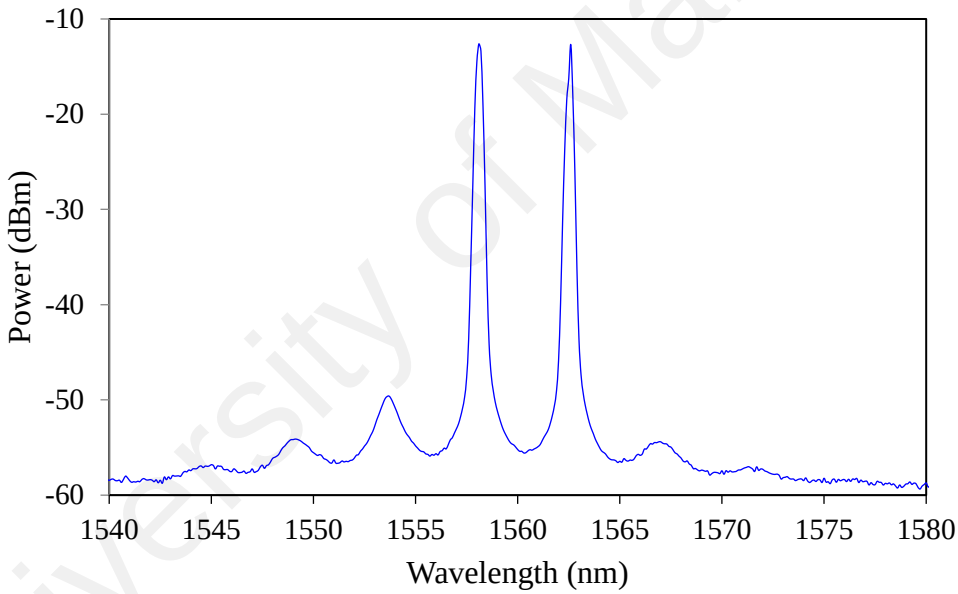

Figure 4.7: Optical spectrum of the DWQS laser

The produced dual-wavelength output was stable throughout the experiment. To check the stability of the proposed laser, the spectrum was sampled every ~25 minutes for the total duration of 500 minutes. The time-based output spectrum is given in Figure 4.8. From this figure, the DWQS is highly stable and provided excellent performance, in which the peaks maintained the same wavelengths and intensities with only minimal fluctuations. Changing the pump power did not affect the obtained spectrum. To make

sure that both peaks have the same pulse width, repetition rate and SNR, we used a tunable bandpass filter (TBF) at the output of the DWQS laser. During the experiment, the TBF was tuned to 1558.1 nm and 1562.6 nm and it was found that there was a negligible difference between the two peaks. However, the TBF was then set to 1562.6 when the data was collected.

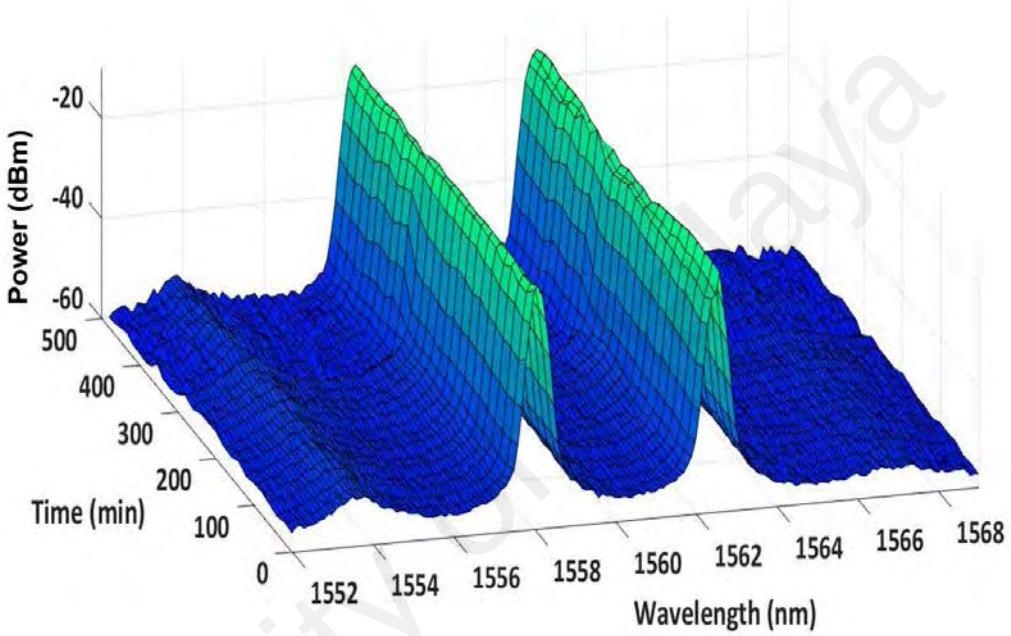

Figure 4.8: Output laser spectrum sampled for 500 minutes

The pulsing was produced as the LD power was increased from 35 mW to 213 mW. The pulse width was decreased from 8.4 µs to 3.6 µs as the input power increased, see Figure 4.9 (a). While, the repetition rate, output power and pulse energy were correlated linearly with the input LD power, they increased from 32.15 kHz to 78 kHz, 1.8 mW to 8.7 mW and 58.48 nJ to 110.13 nJ, respectively, see Figure 4.9 (b). Both the repetition rate and the pulse duration behave as expected, the pulse duration reduced in an almost exponential manner, while the pulse repetition rate increased linearly to the rising LD power.

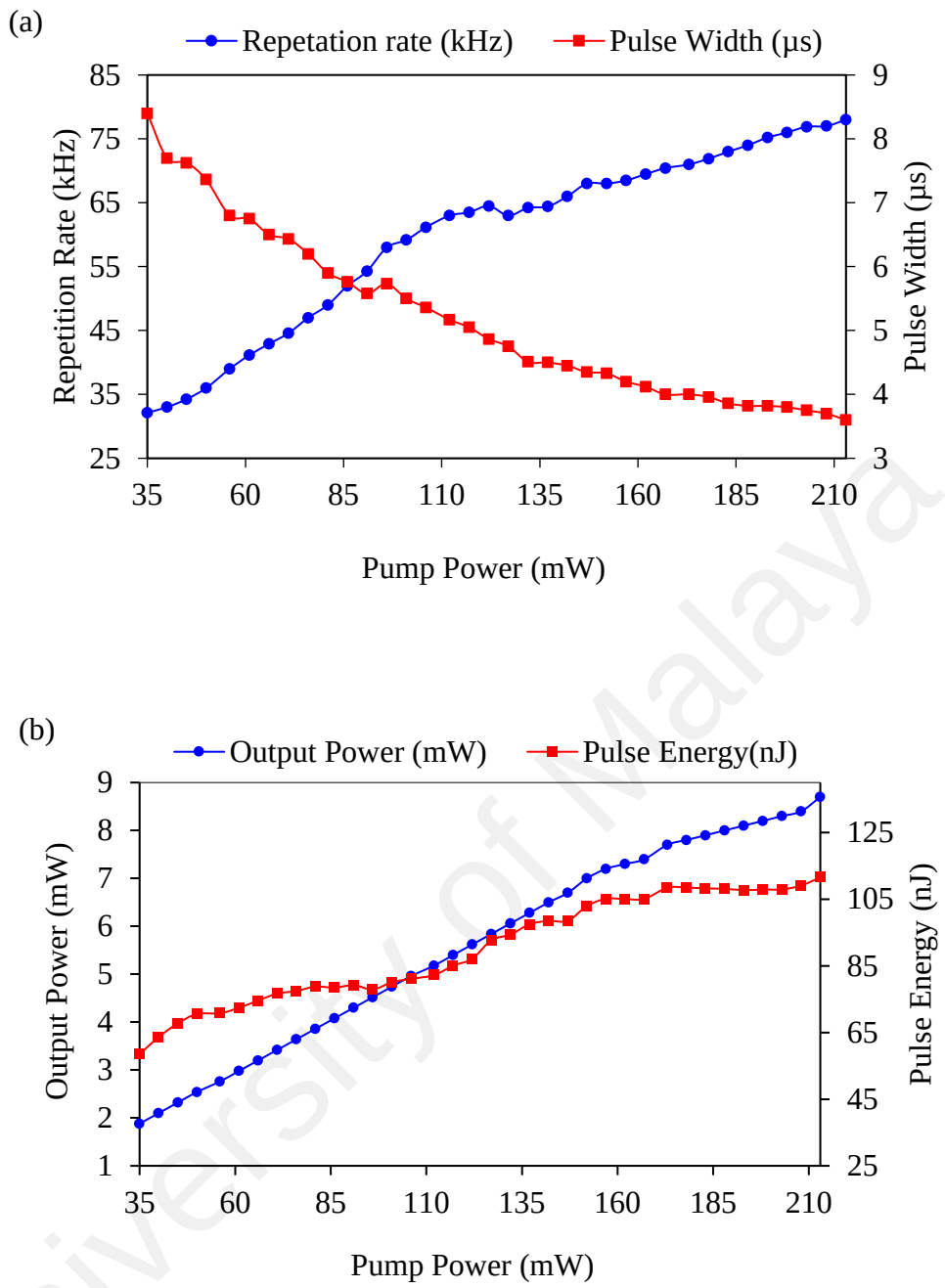

Figure 4.9: LD power vs (a) Repetition rate and pulse width and (b) output power and pulse energy

Figure 4.10 (a) shows the output pulse train at the maximum input LD power, the pulse train was very stable with no modulation of instabilities, which indicates a stable performance. The inset Figure shows the pulse period of about ~ 12.8 µs which is coincident with the fundamental frequency observed on the RF spectrum. The RF spectrum of DWQS laser with span and resolution bandwidth of 300 kHz and 350 kHz,

respectively, is given in Figure 4.10 (b). The fundamental frequency has an SNR of 55.36 dB, which reveals the excellent stability of the system.

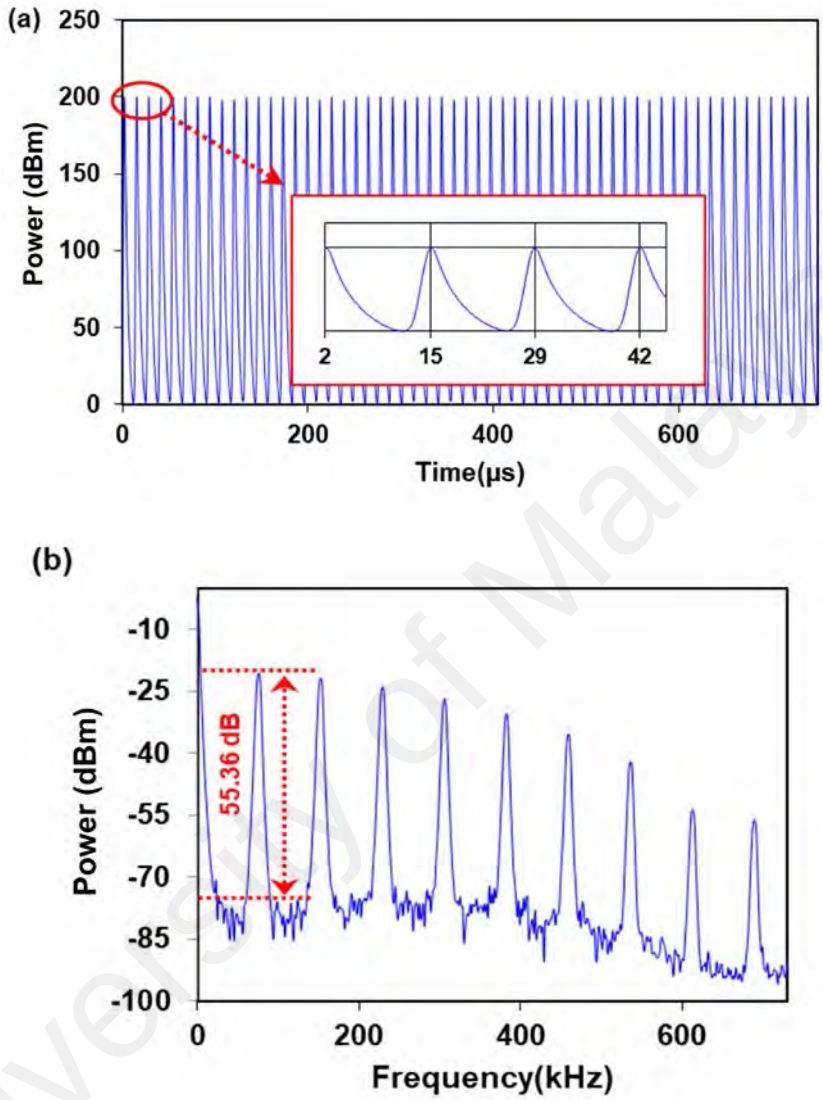

Figure 4.10: (a) Pulse train at maximum input LD power and (b) RF spectrum with a span of 700 kHz.

4. 4 Q-switched Pulse Generation by Using Znq_2 as SA

4.4.1 Fixed Wavelength Operation

The setup used in this experiment is similar to the previous Q-switched laser based on FIrpic SA as described in section 4.2.1 (Figure 4.1). However, the cavity length of the proposed new laser was slightly shorter, about 6 m comprises of 3.5 m long SMF-28, 2

m long EDF and 0.5 m long WDM fiber. The FIrpic SA device was replaced with Znq_2 SA, which was prepared by a similar fashion using the fabricated Znq_2 thin-film. At first, the laser operation was investigated without the incorporation of the SA thin-film in the cavity. As the pump power was gradually increased to reach a threshold of 30 mW, CW laser was generated at a peak wavelength of ~1560 nm. No pulsing operation was observed as the LD power was tuned up to 350 mW. As the SA thin-film was incorporated into the cavity, a stable pulsing operation was observed at LD power was varied from the threshold of 38 mW to 198 mW. At a pump power of 38 mW, the repetition rate was 45 kHz and it increased linearly to 86 kHz as the pump power was increased to 198 mW, see Figure 4.11. The Figure also shows that the average output power increased linearly 1.9 mW to 8.2 mW.

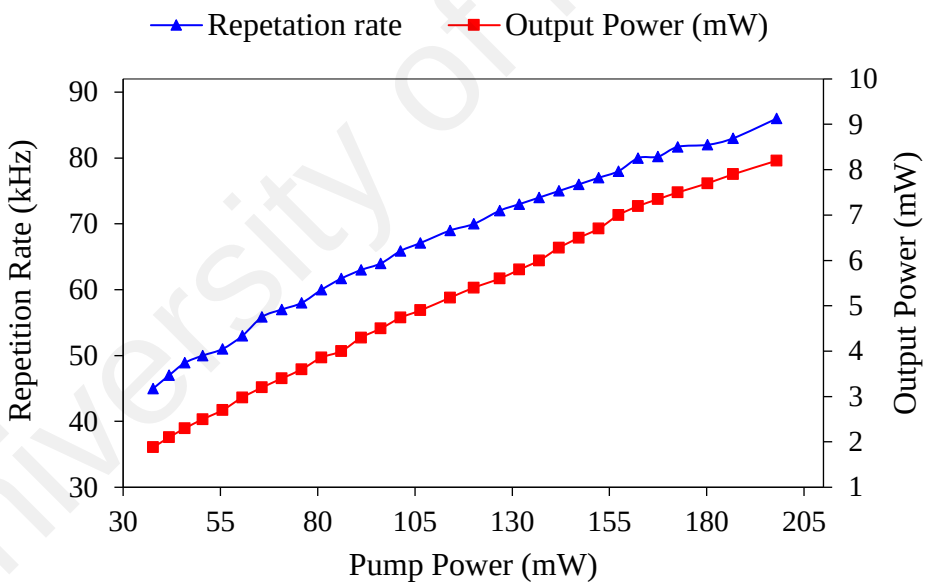

Figure 4.11: Output power and repetition rate as a function of pump power

The produced pulse width was decreased from 6.6 µs to 2.8 µs as the LD power increased, as shown in Figure 4.12 (a). The behaviors of repetition rate and pulse width with the LD power are the typical characteristic of the Q-switching operation. The more power delivered by the LD, the shorter time for the SA to be saturated. This reduces the

rising and falling times of pulses, and hence reduce the pulse period and pulse duration. On the other hand, the peak power increased linearly from 41.8 mW to 96.5 mW. The linear increment of pulse energy and peak power indicates a stable performance of the laser operation. Figure 4.12 (b) shows the pulse energy increasing almost linearly from 41.78 nJ to 95.35 nJ, that indicates a stable performance of the Q-switched laser.

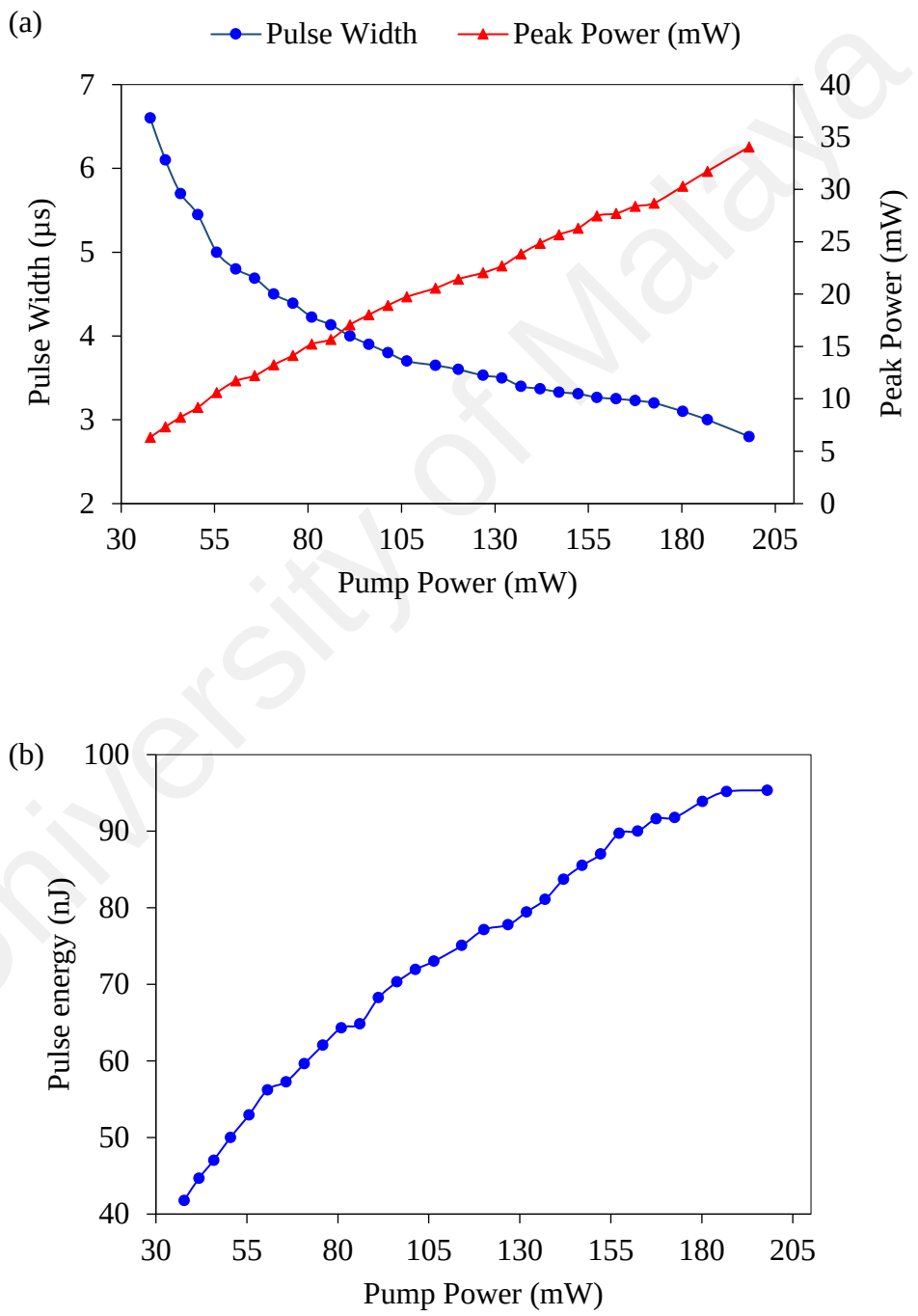

Figure 4.12: (a) Peak power and pulse width as a function of pump power and (b) pulse energy as a function of pump power

Figure 4.13 (a) shows the output optical spectrum of the laser, the spectrum is centred at 1560 nm with 3-dB bandwidth of 1.5 nm. Figure 4.13 (b) shows the output pulse train at the maximum LD power. The pulse train is very stable and uniform with no instabilities or modulation. All the pulses had an intensity of 264 mV (± 2 mV). The inset Figure shows the pulse train period of ~11.55 µs for a duration of 40 µs.

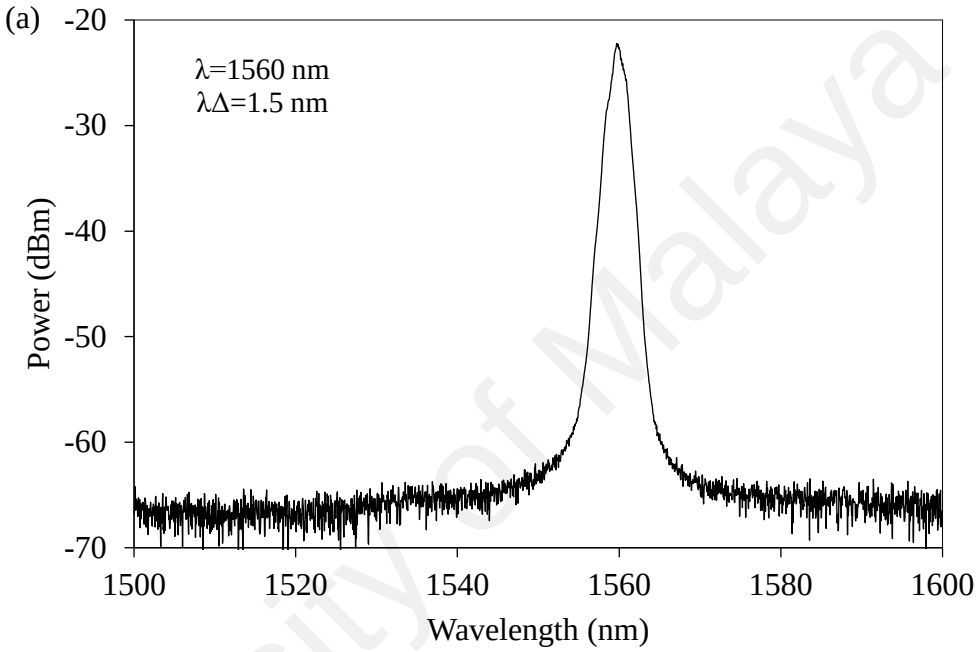

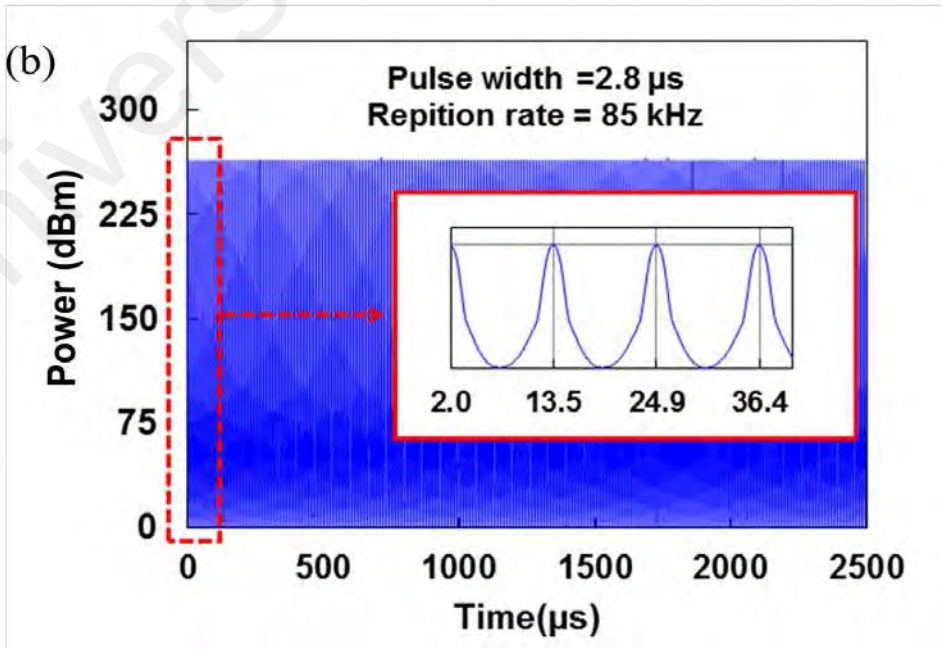

Figure 4.13: (a) Optical spectrum of the Znq_2 based Q-switched EDFL and (b) typical pulse train of the Znq_2 based Q-switched EDFL, Inset shows the pulse period

The RF spectrum with a span of 500 kHz is given in Figure 4.14. The figure shows the fundamental frequency is located at 86 kHz with an SNR of 57.4 dB. This high SNR further indicates a stable and good performing Q-switching operation. We believe that the performance of the laser operation can be enhanced given that cavity parameters are enhanced by shortening the cavity length or employing an EDF with a higher gain.

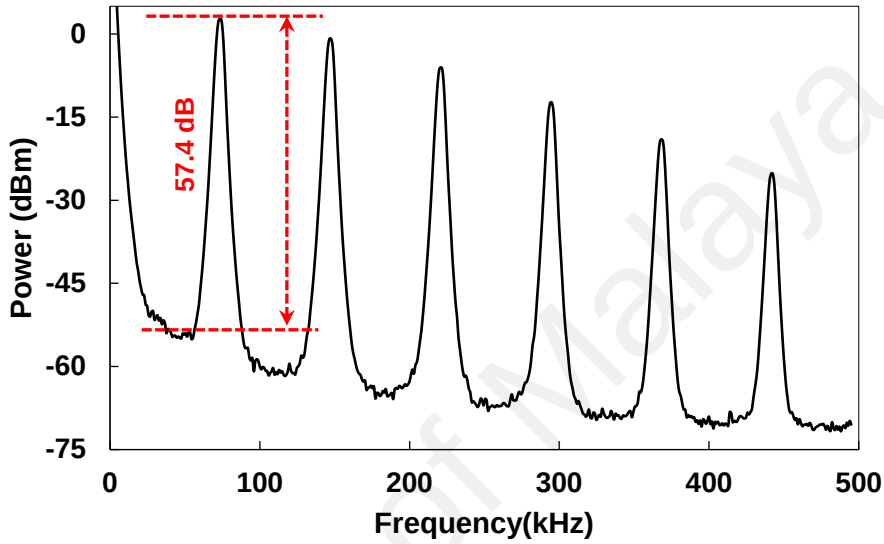

Figure 4.14: RF spectrum showing the SNR of 57.4 dB

4.4.2 Tunable Wavelength Operation

In this experiment, we used the same cavity as the one in the previous experiment, except that a TBF was incorporated into the cavity. The TBF was inserted between OC and WDM. Through tuning the TBF at the maximum input pump power, the central wavelength was shifted continuously from 1520.0 nm to 1563.3 nm, giving a range of 43.3 nm and covering almost all C-band region. The TBF allows a minimum increment of 0.1 nm, as it is the smallest granularity provided by the micrometer head of the TBF. Figure 4.15 shows the output spectra of the laser, which was tuned at the step of ~ 1 nm (to ensure clarity) when the LD power was fixed at 206 mW. The peak power of the spectra was maintained at almost the same level of −3.23 dBm ± 1.2 dBm with the same pattern and shape, which suggests that the pulsing operation was very stable.

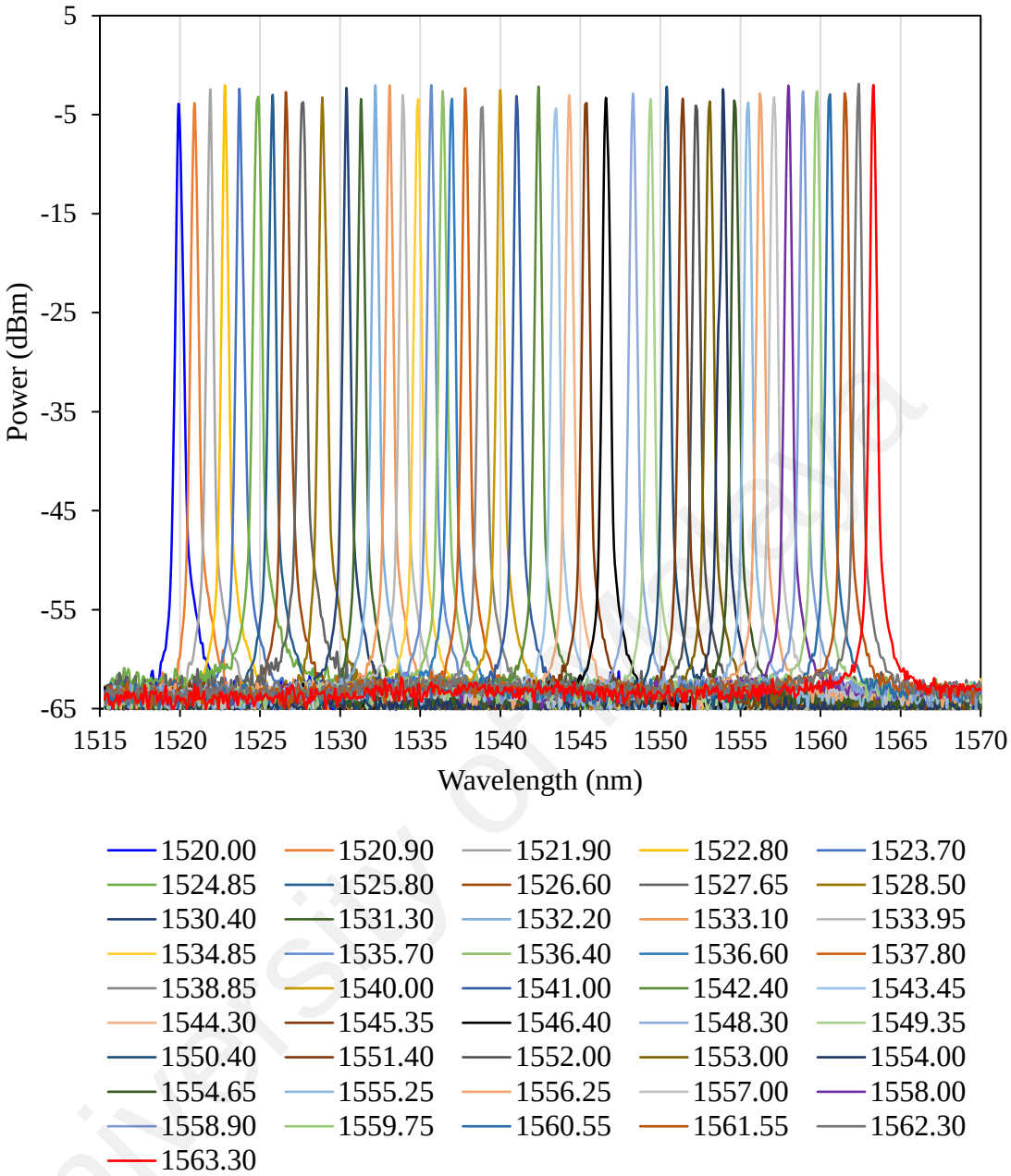

Figure 4.15: Output spectra of the tunable laser at different wavelength operation between 1520.0 nm and 1563.3 nm

Figure 4.16 illustrates the effect of tunable wavelength operation on the pulse duration and pulse repetition rate. The pulses produced were wavelength dependent. As the TBF was shifted from 1520.0 nm to 1529.65 nm, the pulse duration shortened from 3 µs to 2.12 µs. Then it was increased gradually to 3 µs again as the TBF was tuned to 1563.3 nm. The pulse repetition rate (which behaved inversely to the pulse width) reached its

highest value of 111.6 kHz at 1529.65 nm. This is attributed to the EDF gain is much higher at 1529.65 nm than other wavelengths. A higher gain will result in a shorter time for the SA to be saturated, which will lead to shortening the pulse width and increasing the pulse repetition rate. The effects of wavelength tuning were also investigated on the pulse energy and average output power, see Figure 4.17 (a). The figure shows that the average output power decreased as the operating wavelength shifted to a shorter wavelength even though the LD is kept at the same power of 206 mW.

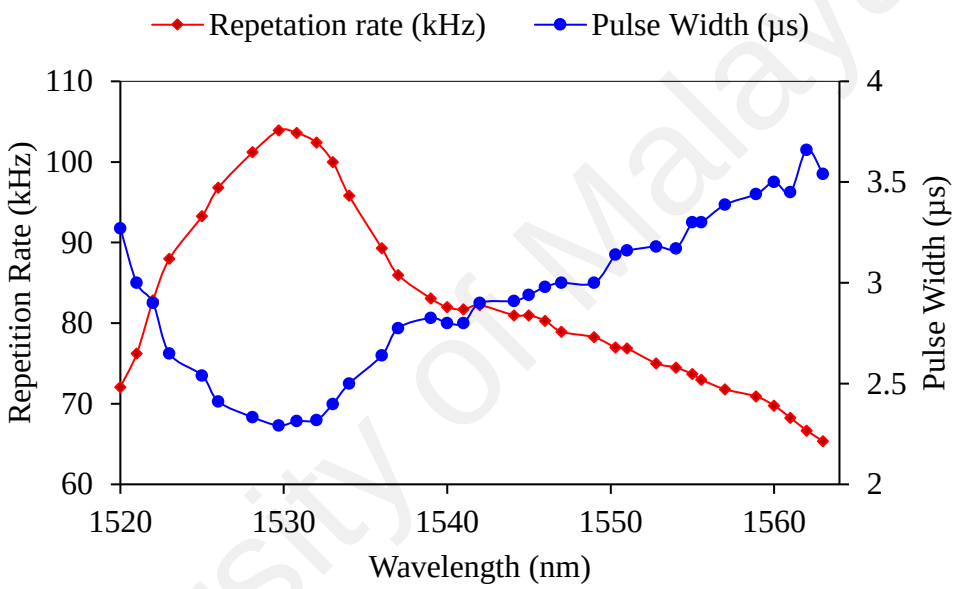

Figure 4.16: Pulse repetition rate and pulse width duration vs wavelength

This is due to the loss of TBF, which is higher at shorter wavelength region. The pulse energy, as it is inversely correlated with the repetition rate, increased from 15 nJ at 1530.4 nm to 37.3 nJ at 1563.3 nm. Figure 4.17 (b) shows the output RF spectrum at a span of 810 kHz at maximum LD power and as the TBF was tuned to 1551.4 nm. Anritsu-MS2683A device recorded the data with a resolution bandwidth (RBW) of 300 Hz. The figure reveals a high SNR value of 53.2 dB.

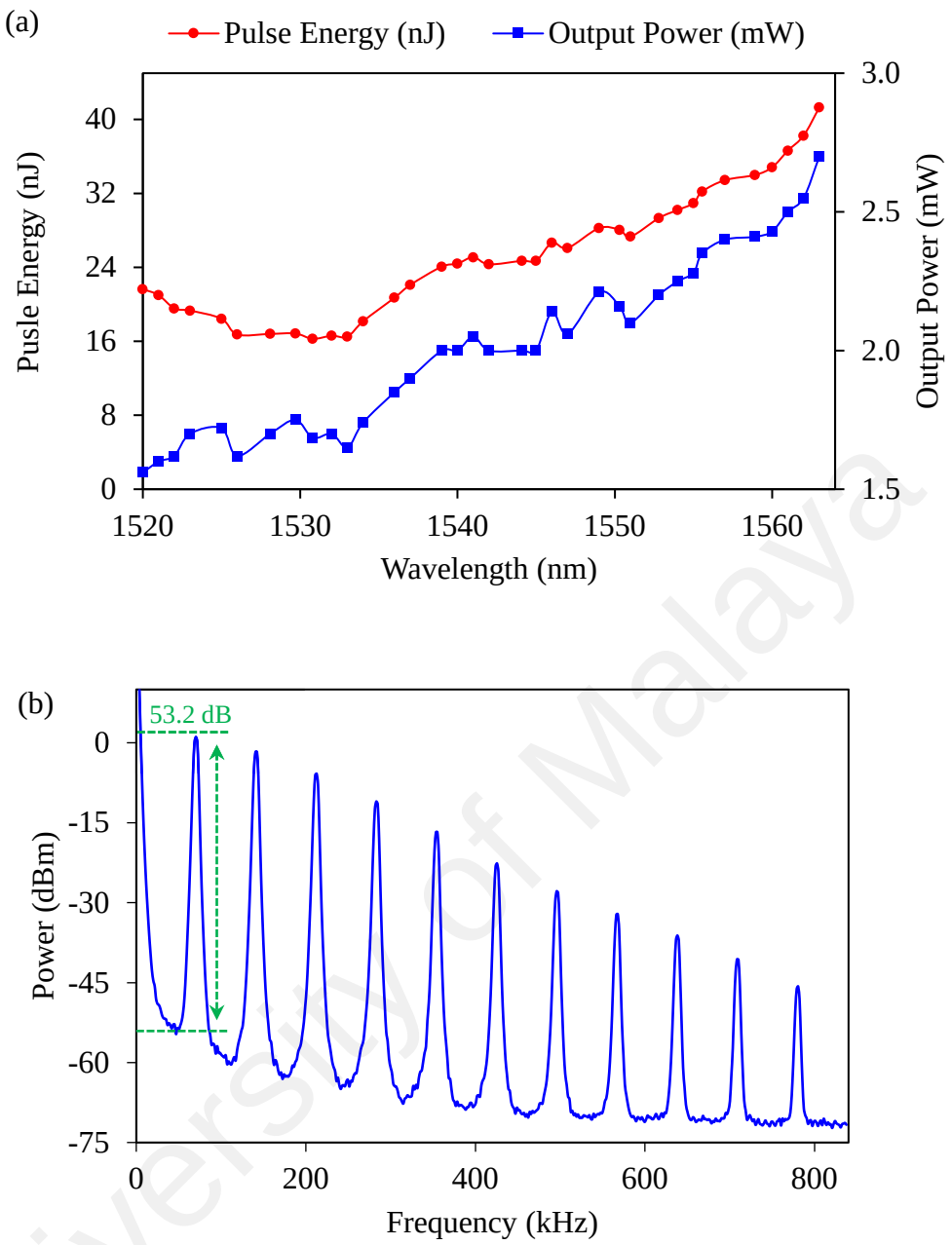

Figure 4.17: (a) Output power and pulse energy at different operating wavelengths and (b) RF spectrum with a span of 840 kHz

It should be noted that recording the long-term operation for a single wavelength will not reflect the performance at other wavelengths. Additionally, the TBF will filter any distortion or fluctuation that output spectrum might have. It should be noted that this experiment took around 4 hours to record all the required data. During the experiment, the laser-produced the same performance in which the output pulse train and SNR were

both very stable. The wider pulse width obtained in this experiment in comparison with the previous work is due to the length and the insertion loss induced to the cavity by the TBF. It is believed that a shorter pulse width can be achieved by using a shorter cavity length of less than 1 meter. By further increasing the LD power up to 350 mW, the output pulse trains showed some fluctuation, then disappeared. This is due to the SA was fully saturated. The pulsing operation was obtained again as the LD power reduced below 206 mW. We concluded that the optical damage threshold value is above 350 mW as if the SA was damaged, no Q-switching operation can be produced again. Additionally, we did not observe any deformation of the SA during and after the experiment.

This experiment demonstrates that Znq_2 could operate as a broadband passive Q-switcher and showed that the Q-switching pulsing was easily tuned to a different wavelength, which is the goal of this work. Broadband absorption of the SA is the key feature to obtain a widely-tunable fiber laser (Y. Huang et al., 2014b). Znq_2 is a promising broadband SA as it showed very comparable performance with other SAs such as SnO_2, TiO_2, MoS_2 and MWCNT reported in (H. Ahmad, Hassan, Ahmad, Zulkifli, & Harun, 2016; H. Ahmad et al., 2019; Y. Huang et al., 2014a; Siddiq, Chong, Pramono, Muntini, & Ahmad, 2019) in terms of the wavelength tuning range, SNR, pulse energy, and pulse width. This experiment is suitable for practical applications that require a wide tunable wavelength range with highly stable performance such as environmental sensing, biomedical diagnostics and metrology. The tuning range in this experiment was limited by the TBF and not by SA. Thus, we believe that a wider tuning range can be developed given that a TBF with a wider tuning range is addressed. Additionally, higher pulse energy and higher average output power can be developed by addressing a high-gain fiber (Z. Luo et al., 2014), and enhancing the cavity parameters (Spühler et al., 1999). It should be mentioned that by removing the TBF and adding 52 m SMF a mode-lock operation was observed with pulse-duration and repetition rate of 1.6 ps and 1.8 MHz, respectively.

4. 5 Q-switched Fiber Laser with Alq_3 SA

4.5.1 1.5 µm Operation

In this subsection, a Q-switched EDFL is demonstrated by using the newly developed Alq_3 PVA thin-film as a SA. The SA device was constructed by sandwiching a piece of ~1×1 mm^2 of the prepared Alq_3 thin-film in between two optical fiber ferrules. The insertion loss of the SA was measured to be around 0.8 dB. The SA device was incorporated in an EDFL cavity. The cavity length was estimated to be approximately 6 m. At first, the spectrum of the EDFL was measured (before inserting the SA device into the cavity) and CW operation was obtained at a threshold pump power of 15 mW.

As the Alq_3: PVA SA was incorporated into the cavity, the Q-switching pulses train was observed at the threshold pump power of 20 mW. The pulses train was held stable and robust as the pump power was raised to the maximum input pump power of 122 mW. This low threshold pump power of Q-switched pulse is attributed to a low intra-cavity loss of the Alq_3:PVA thin-film based SA due to the use of high gain fiber and optimal feedback from the output optical coupler**.**

Figure 4.18 illustrates the optical spectrum output of the CW and the proposed Q-switched EDFL based on Alq_3: PVA SA at an input pump power of 20 mW. The laser operation with Alq_3:PVA SA was obtained at a shorter wavelength regime compared to that of the CW laser without SA. The insertion of the SA increased the cavity loss and thus the lasing wavelength was shifted to a shorter wavelength to acquire more gain to compensate for the loss. As depicted in Figure 4.18, the spectrum is centred at a wavelength of 1564 nm and 1559 nm with 3-dB bandwidth of 0.22 nm and 1 nm for CW and Q-switching pulse, respectively. The spectral broadening of the Q-switched laser was observed because of self-phase modulation inside the cavity. Alq_3 has a band gap of 2.5 eV - 2.7 eV, which corresponds to wavelengths in the visible range. Due to quantum defects in the material, the band gap may reduce and thus the material can function as a Q-

switcher in the C-band wavelength region. This is due to the absorption characteristic, which depends on the crystal form and particle size, as explained in ref. (Satoh, Nakashima, Kamikura, & Yamamoto, 2008). Figure 4.19 (a), (b) and (c) show the typical pulse trains at incident pump powers of 20, 76, and 122 mW, respectively. Inset figures show a single pulse profile at each input pump power.

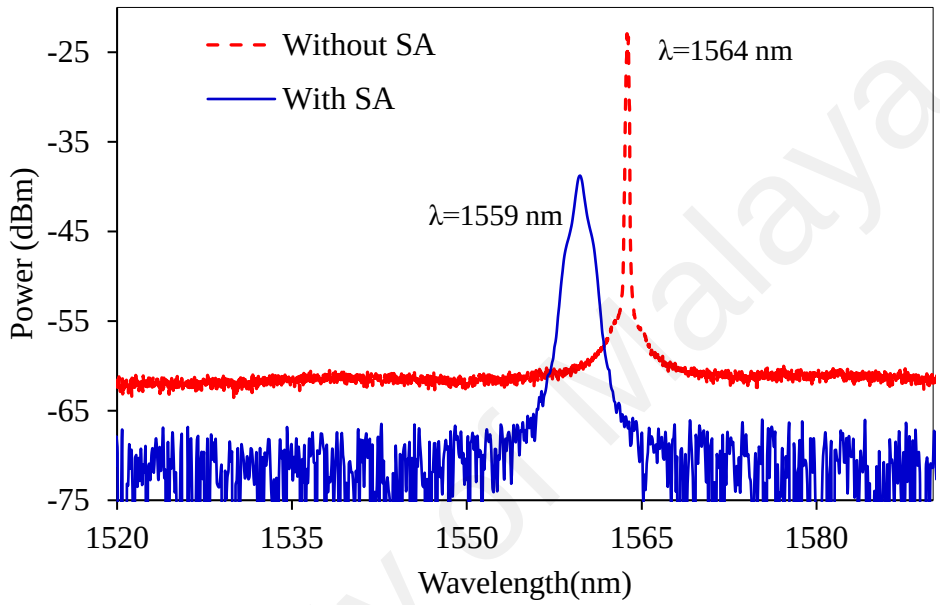

Figure 4.18: The output spectra of the fiber laser cavity with and without Alq_3: PVA SA for Q-switched and CW, respectively, at 20 mW pump power

At pump power threshold of 20 mW, the Q-switched laser operates at a repetition rate and a pulse width of 31.65 kHz and 6.65 µs, respectively, as shown in Figure 4.19 (a). By increasing the pump power to 76 mW, the pulse repetition rate was increased to 85.65 kHz, while the pulse width was reduced to 1.71 µs (see Figure 4.19 (b)). The maximum repetition rate of 144.5 kHz and the shortest pulse width of 1.2 µs were achieved at the maximum pump power of 122 mW as shown in Figure 4.19 (c). It is found that the pulse width shrinks and the repetition rate increases as the pump power increase. The Q-switching pulse trains are stable and have a uniform distribution with no fluctuation, which indicates that the fiber laser can operate in stable Q-switched operation with variable repetition rates. However, as the input pump power is raised above 122 mW, an amplitude

fluctuation was observed, and the pulse train became unstable, and finally, the Q-switching pulses train disappeared. That might be attributed to SA being bleached under high input pump power. Similar behaviour has been reported with different kinds of SAs (H. Ahmad et al., 2017; Q. Wang et al., 2015).

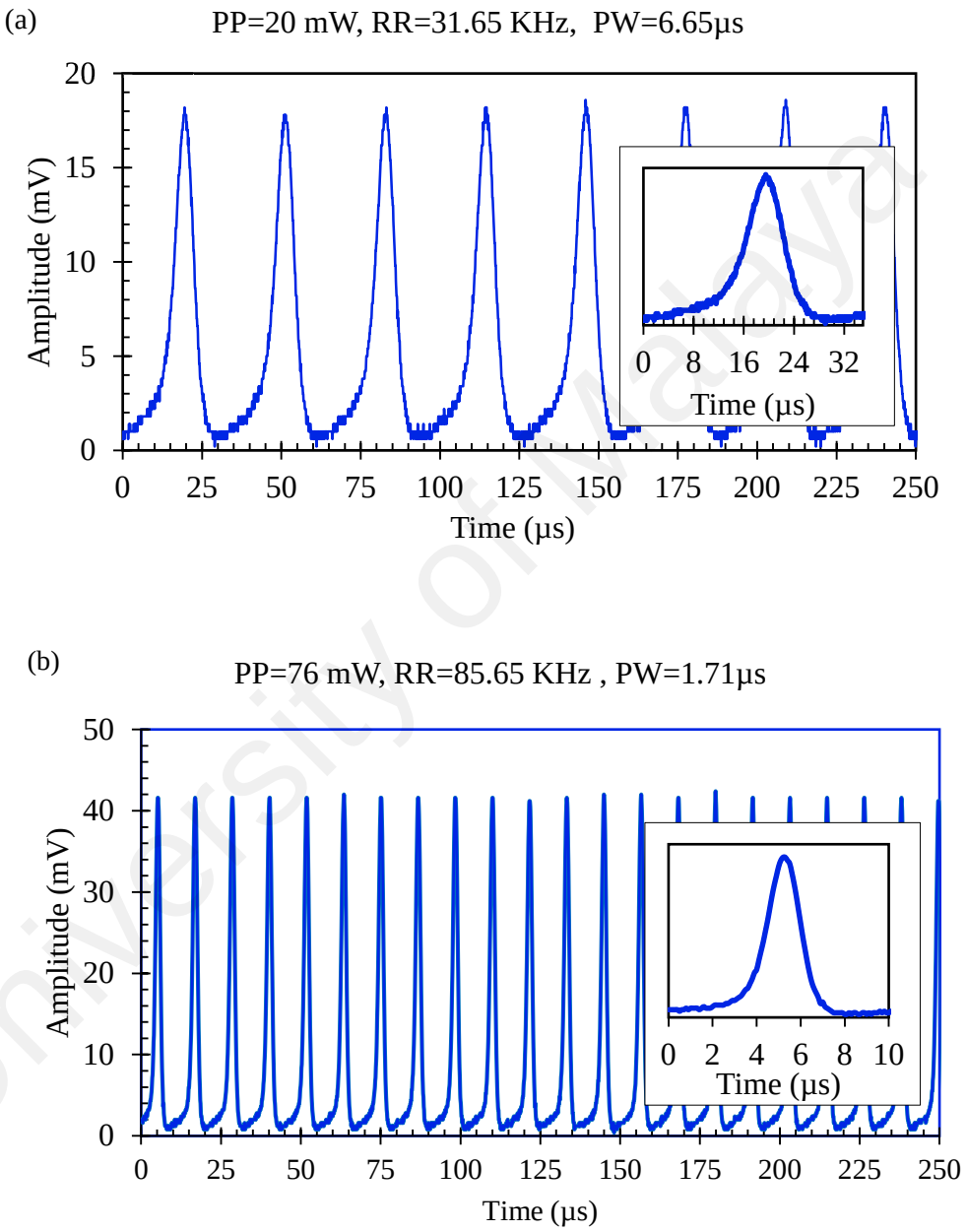

Figure 4.19: Q-switched output pulse train with inserting of single envelope pulse in EDFL using Alq_3 SA at incident pump powers of (a) 20 mW, (b) 76 mW, and (c) 122 mW. PP: pump power, RR: repetition rate and PW: pulse width

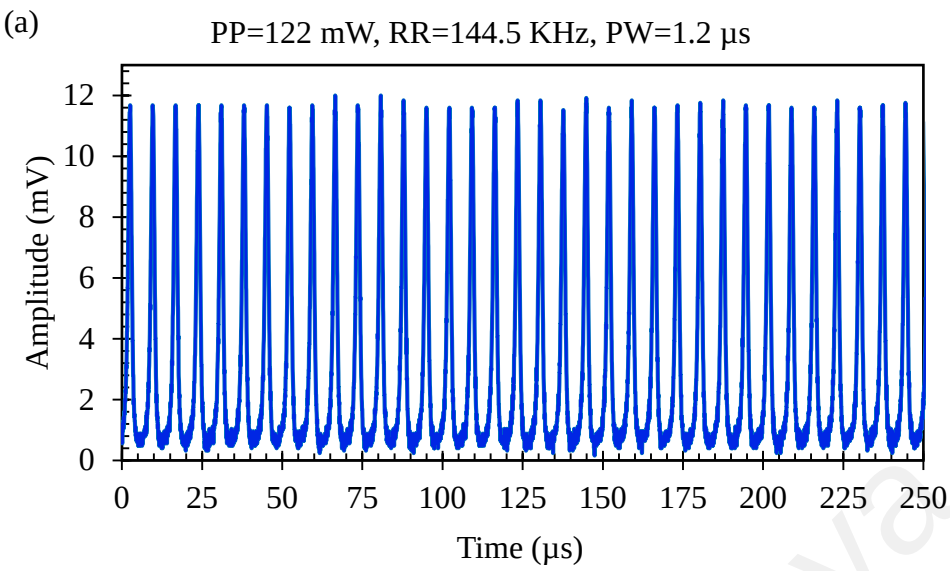

Figure 4.19, continued

When the input pump power was decreased to the range between 20 mW to 122 mW, a stable Q-switching pulses train was produced again, proving that the Alq_3 based SA was not damaged. To check the stability of Q-switching pulse operation, we recorded the corresponding RF spectrum at a maximum input pump power of 122 mW as revealed in Figure 4.20 (a). The spectrum depicts the fundamental frequency at 144.5 kHz with SNR of ~46 dB, as shown in Figure 4.20 (b).

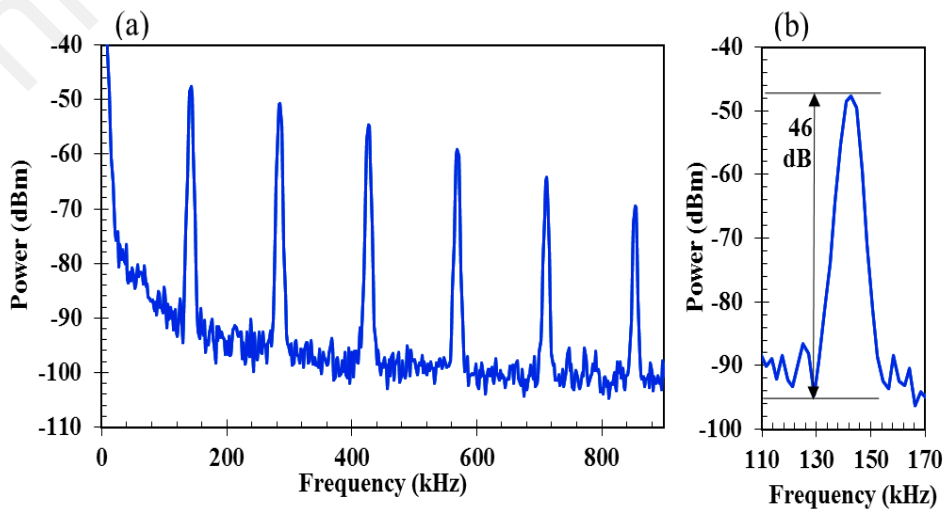

Figure 4.20: Radio-frequency spectrum at a pump power of 122 mW with a span of (a) 900 kHz (b) 60 kHz

When the pump power was increased from 20 to 122 mW, the repetition rate increased from 31.65 to144.5 kHz and the pulse width reduced from 6.6 to 1.2 µs as shown in Figure 4.21 (a). The high repetition rate and short pulse width might be attributed to the recovery time of the SA. When the SA's recovery time is much shorter than the time duration between the Q-switching pulses, the pulse repetition rate will increase with the volumetric input pump power rate (Degnan, 1995). However, further research is required to improve the performance of Alq_3 SA and to determine its recovery time. Figure 4.21 (b) illustrates the output power and pulse energy against the pump power. As the pump power increased, the output power raised from 1.4 to 8.19 mW and the pulse energy also increased from 44.23 nJ to 56.67 nJ. The pulse energy reached its maximum value of 63.89 nJ at a pump power of 101 mW.

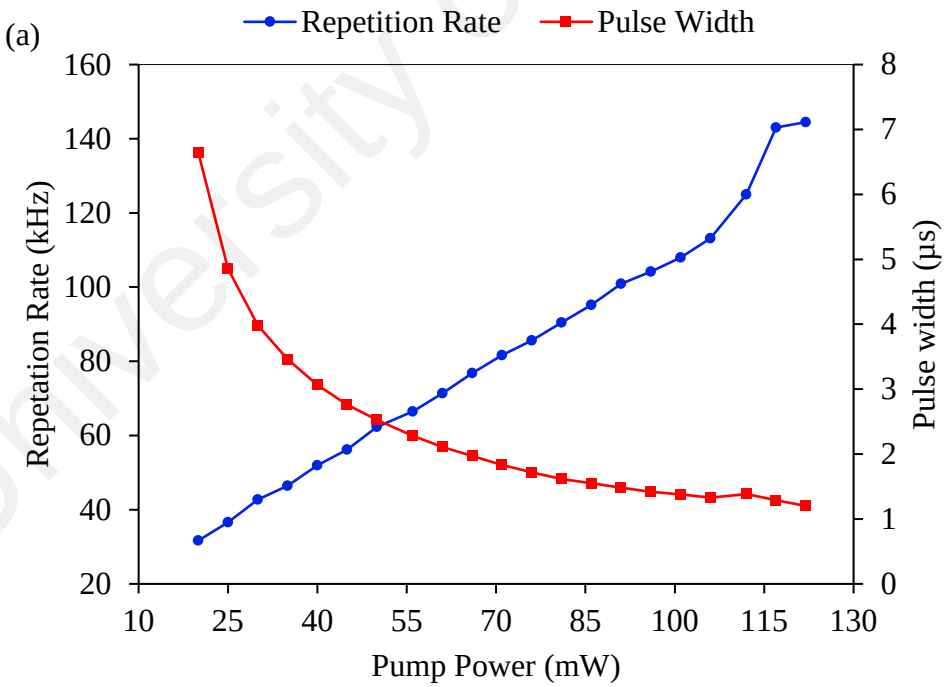

Figure 4.21: (a) Pulse width and pulse repetition rate versus incident pump power and (b) Output power and pulse energy versus incident pump power

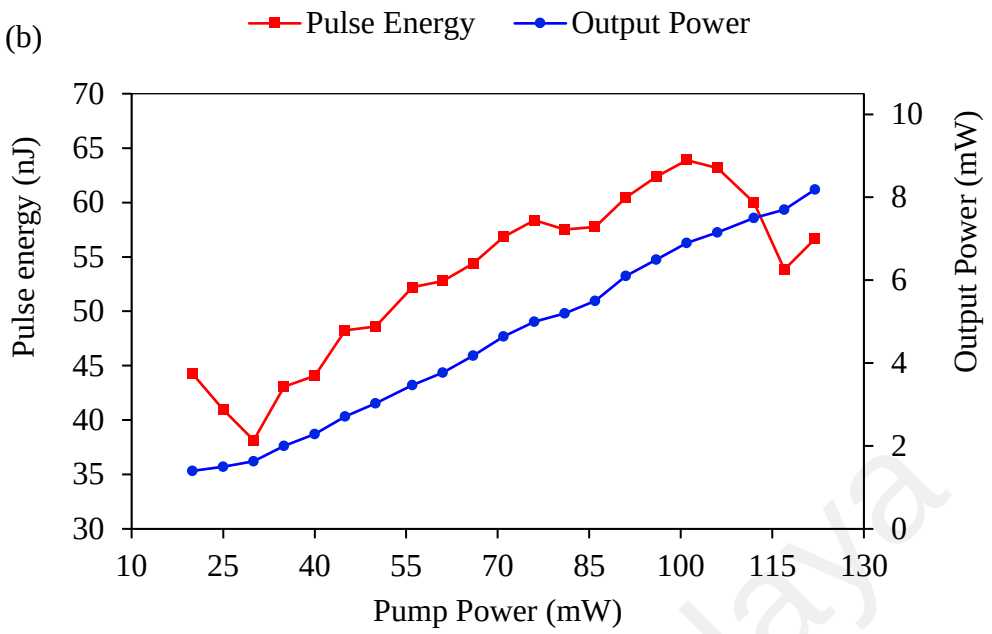

Figure 4.21, continued

Figure 4.22 depicts the output spectrum of the Q-switched operation at 122 mW pump power. The spectrum was sampled at an interval of 10 min for a total duration of 1 hour to examine the consistency of the output spectra. As shown in the figure, all spectra have an almost similar pattern, shape and spectral intensity (all the samples have a spectral intensity of about −42.8 dBm) which indicates that the Q-switched fiber laser is reliable and stable over time. It was confirmed that the Alq_3: PVA thin-film based organic SA had no sign of damage or melting and was still in good shape after the Q-switched operation lasted for more than 60 minutes. The fiber laser showed a stable performance without observable fluctuation in the output spectra.

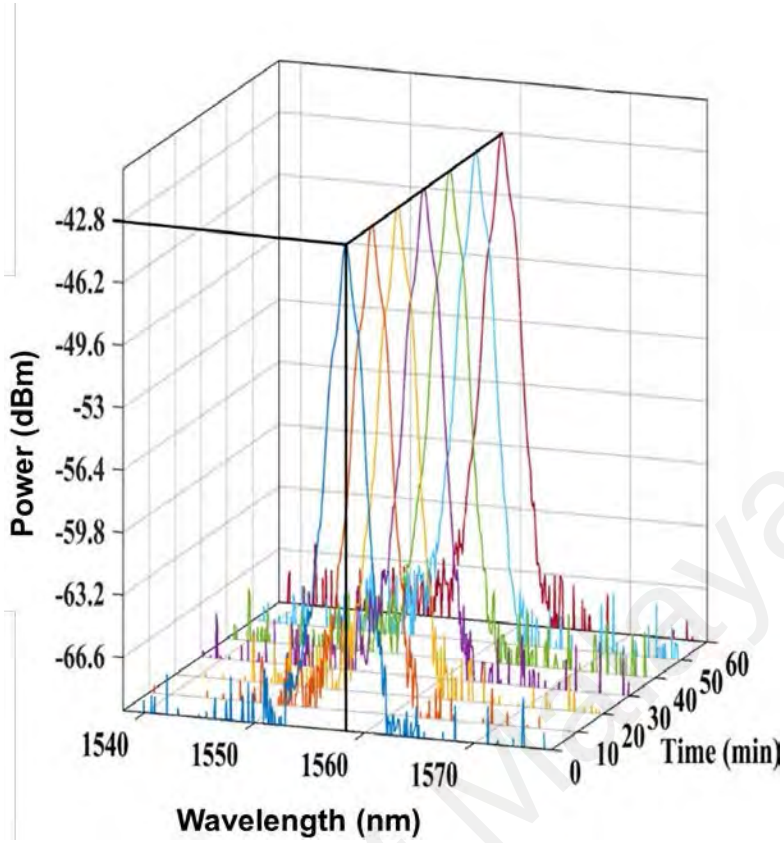

Figure 4.22: Laser spectrum sampled at 10 min intervals for 1 h duration

4.5.2 High Pulse Energy Q-Switched Fiber Laser Operating at 1.0 µm Operation

In this subsection, a Q-switched fiber laser operating in 1.0 µm region is demonstrated by using Alq_3 PVA thin-film as a SA. The SA device was incorporated into an ytterbium-doped fiber laser (YDFL) cavity. The cavity setup is presented in Figure 4.23. A 1.4 m long Ytterbium-doped fiber (YDF) was used as a gain medium. The YDF has Yb ions concentration of 1500 ppm, a core diameter of 4 µm and a numerical aperture of 0.20. The cavity length was approximately 25 m. The ring cavity was coupled with a 980 nm LD through a 980/1064 nm WDM. A 50:50 optical coupler (OC) was spliced to another end of the YDF to allow half of the output to be extracted for performance monitoring. The remaining output was directed to the Alq_3: PVA thin-film which was sandwiched between two fiber ferrules. An optical isolator was used to eliminate back-reflection. The

characteristics of the laser were analyzed using a digital oscilloscope with 2 GHz photodetector, an optical spectrum analyzer and a 7.8 GHz RF spectrum analyzer.

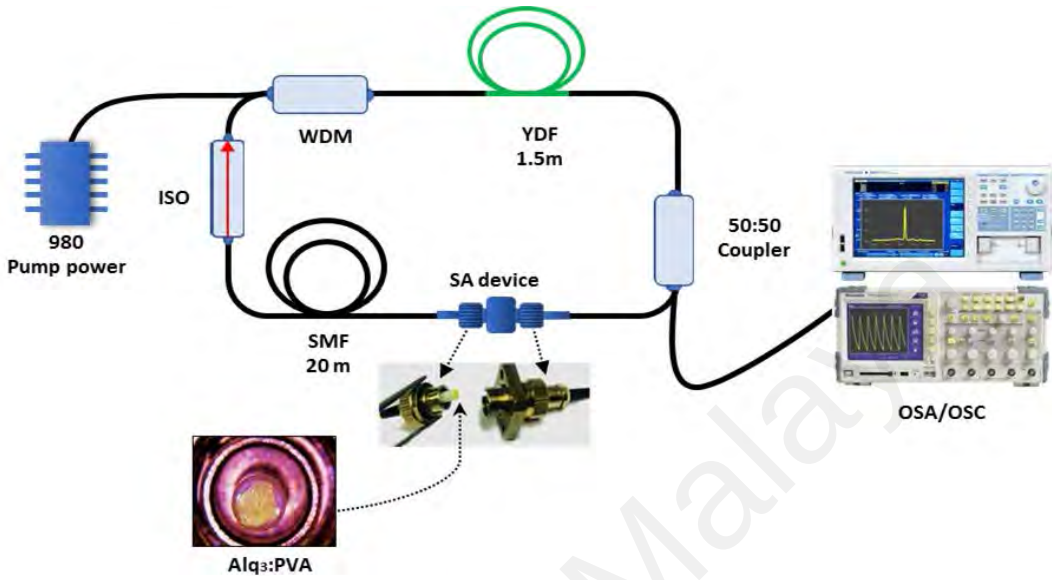

Figure 4.23: Configuration of the proposed Alq_3 based Q-switched YDFL

At first, a CW laser emission was produced at input LD power of 60 mW. A self-starting and stable Q-switched YDFL operation was recorded as the pump power was increased above the threshold of 84 mW. The Q-switching operation was maintained up to pump power of 147 mW where the relatively high energy and high output power were achieved. Figure 4.24 (a) shows the output spectrum of the Q-switched YDFL, which operated at a centre wavelength of 1066.7 nm with a 3-dB bandwidth of 0.2 nm. Figure 4.24 (b) shows the temporal characteristic of the Q-switched pulse train at the maximum input pump power; the inset Figure shows the pulse train in the time scale of 3.5 ms. The inset figure shows a uniform intensity distribution without amplitude modulation nor fluctuation (as almost all the pulses had an amplitude of 168 mV ∓ 0.05 mV when they were recorded at a sampling period of 0.7 μs), which indicates the fiber laser has stable performance.

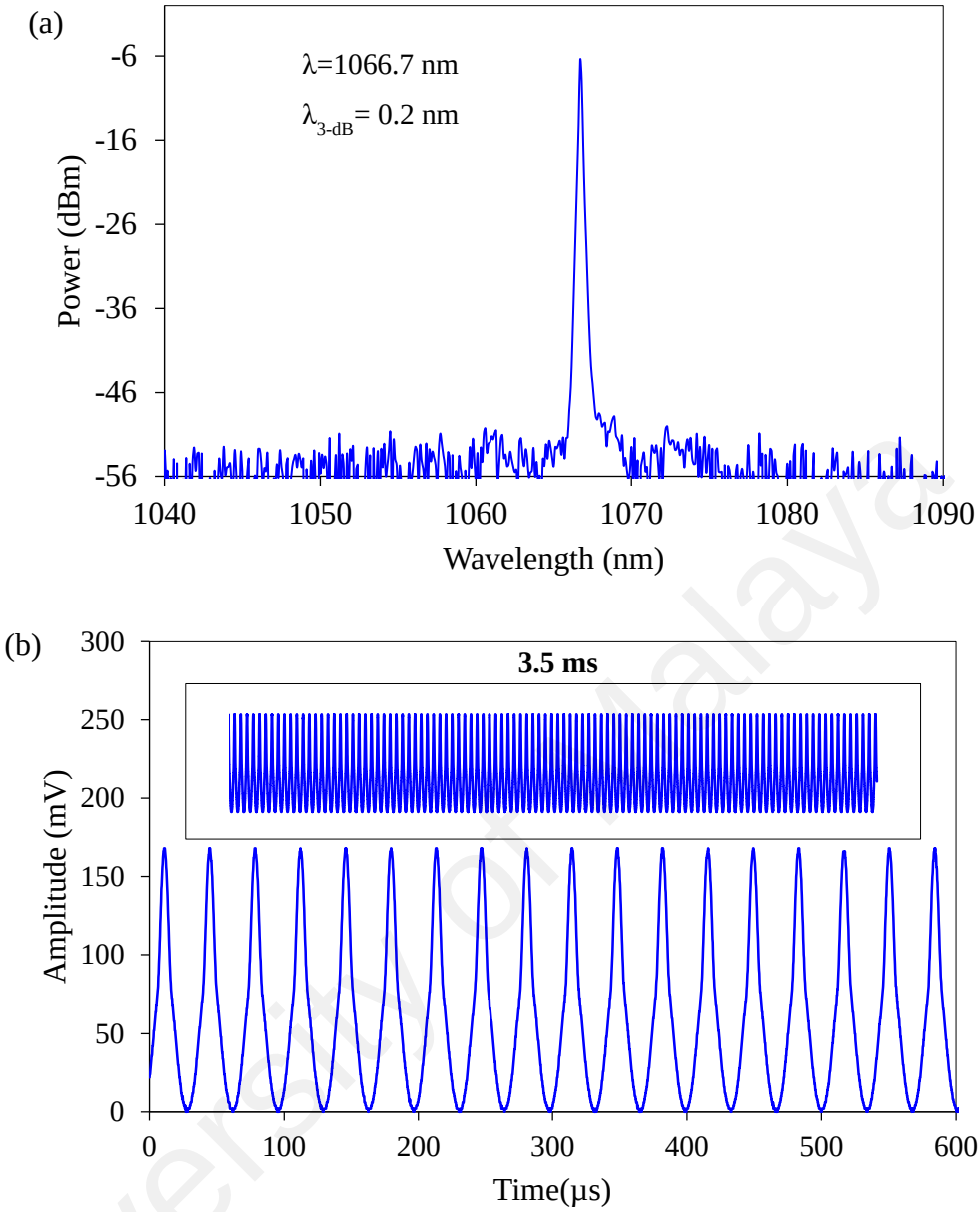

Figure 4.24: (a) Output spectrum of the Q-switched YDFL operating at 1066.7 nm and (b) typical pulse train at the maximum input LD power of 147 mW

Figure 4.25 shows the repetition rate and pulse width of the YDFL versus pump power. It is obtained that the pulse repetition rate increased from 12.95 kHz to 29.62 kHz while the pulse width shortened from 24 µs to 9 µs as the input LD power was tuned from threshold to maximum value, i.e. from 84 mW to 147 mW. Increasing the input pump power (up to 249 mW) caused the pulse train to be unstable and then disappeared. That might be attributed to the SA being over-saturated, as similar behaviour has been reported previously (H Ahmad et al., 2017; Y. Chen et al., 2014; Q. Wang et al., 2015). The LD

power was increased up to the maximum power of 350 mW to investigate the damage threshold for the SA. As the LD power was gradually reduced within 84 mW to 147 mW, the Q-switched operation was observed again. Hence, we concluded that the thermal damage of the SA is higher than 350 mW.

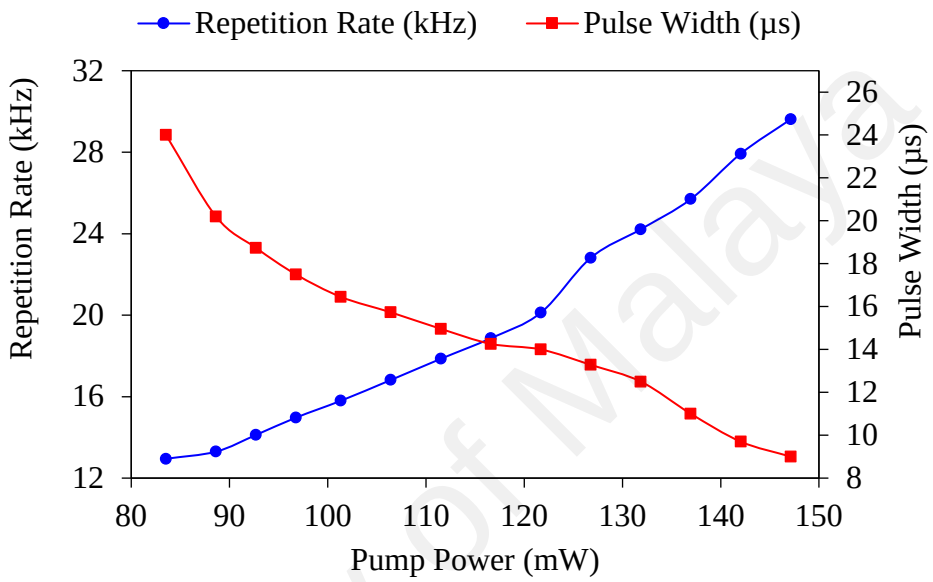

Figure 4.25: Pulse repetition rate and pulse width as a function of input LD power

Figure 4.26 shows the average output power and pulse energy against pump power. It is observed that the output power increased almost linearly from 4 mW to 24 mW with an increase in the input pump power from 84 to 147 mW. The average output power of the cavity was relatively high, that is due to the high performance and low insertion loss of the SA and low inter-cavity loss (Herda et al., 2008). Additionally, a large portion of signal power was extracted from the cavity due to the high taping ratio of the OC. The slope efficiency of the YDFL was obtained at around 30%. The proposed YDFL also produced high pulse energy ranging from 0.3 to 0.81 µJ as the pump power was increased from 84 mW to 147 mW. The high pulse energy is attributed to the high average output power and low repetition rate.

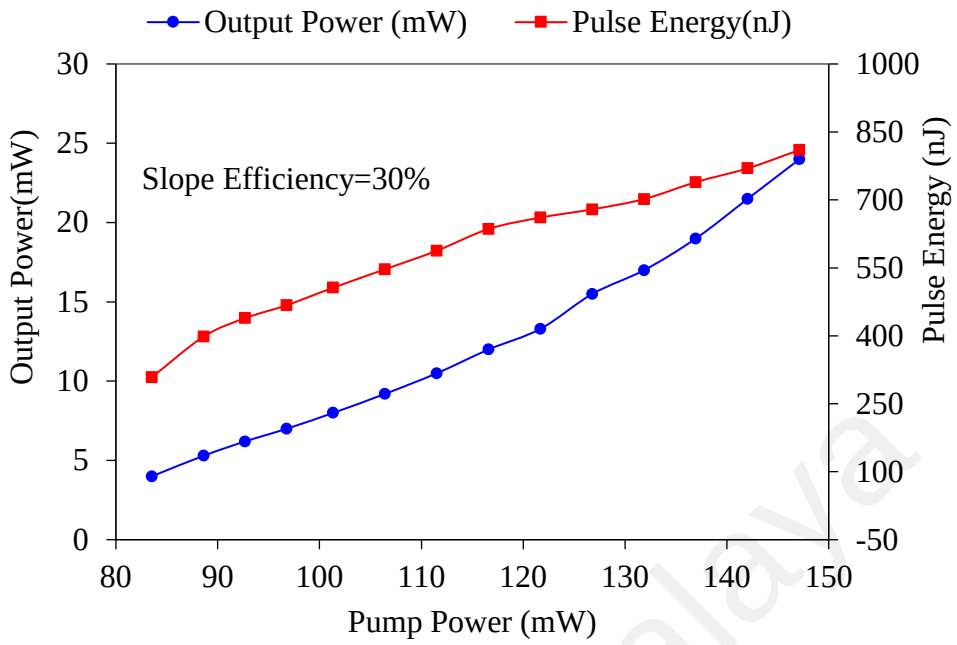

Figure 4.26: Average output power and pulse energy versus input LD power for Alq_3 based Q-switched YDFL

The maximum pulse energy is 0.81 µJ, which is the highest compared to other passively Q-switched fiber lasers reported so far that operating in in 1 µm region (Hou et al., 2018; K.-X. Huang et al., 2017; Rahman, Latiff, Rusdi, Dimyati, & Harun, 2018; J. Wang et al., 2018). As shown in Figure 4.27 (a), the peak power also increased almost linearly from 12.9 to 90 mW within the given pump power range. To check the stability of Q-switched laser operation, the RF spectrum was measured with a span of 300 kHz, see Figure 4.27 (b). The inset Figure shows the fundamental RF peaks at 29.62 kHz with an SNR of about 50 dB, which indicates excellent Q-switching stability.

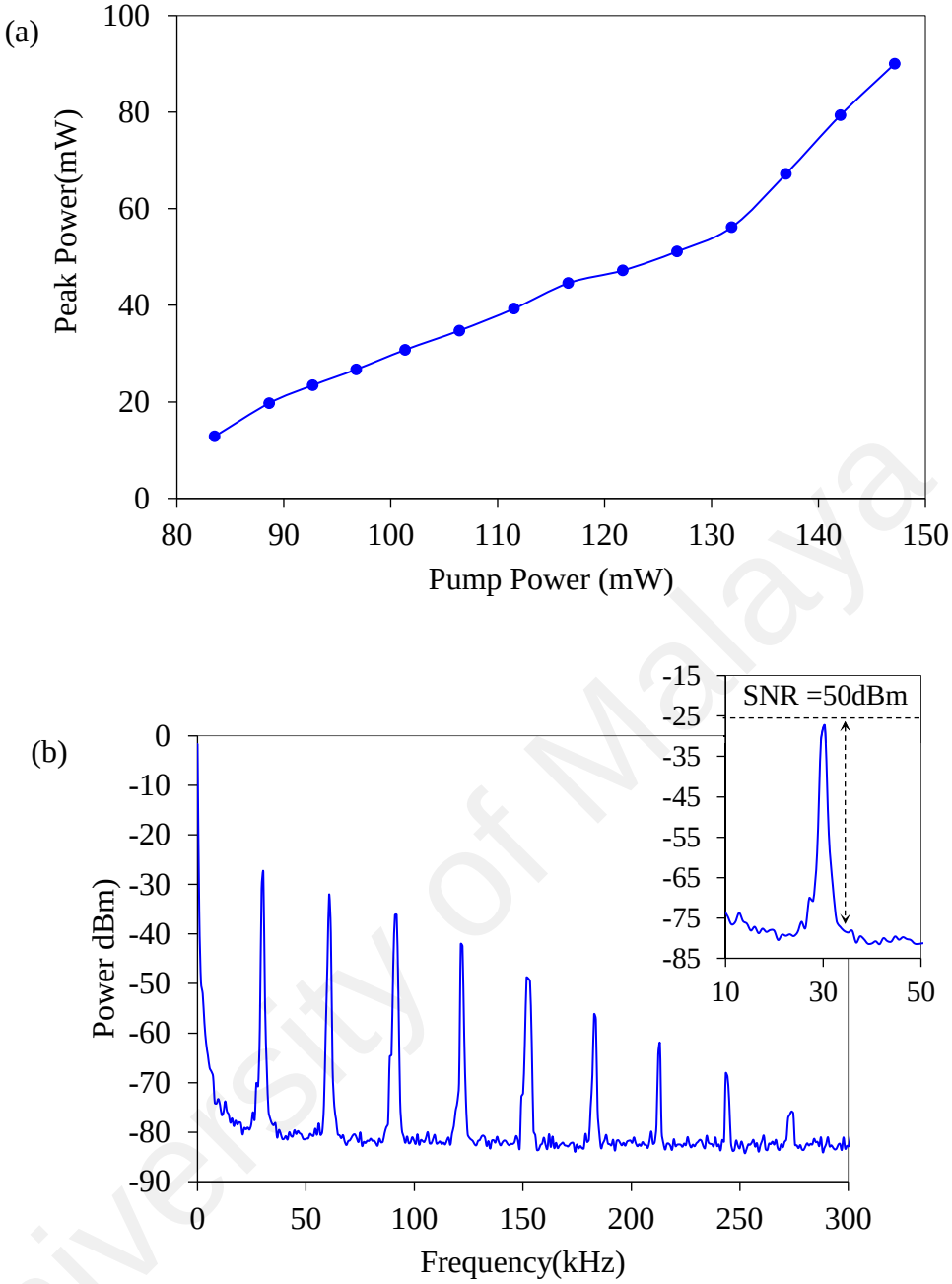

Figure 4.27: Peak power against LD power for Alq_3 based Q-switched YDFL, and (b) RF spectrum of the Q-switched YDFL. Inset shows the fundamental frequency with SNR 50 dB at a span of 40 kHz.

4.5.3 Short pulse width Q-switched YDFL

In this subsection, a Q-switched YDFL with a shorter pulse width is demonstrated by reducing the cavity length (as given in Figure 4.23) to 5 m. The proposed YDFL successfully produced a Q-switched pulse train with reduced pulse width and higher

repetition rate. Both pulse energy and peak power performances were also changed with this modification. In the new cavity, the CW YDFL emission was observed at the input LD power of 50 mW, while the threshold and maximum LD power for generating the Q-switched pulses were 87 mW and 147 mW, respectively. The optical spectrum showed almost similar shape in comparison with the previous cavity setup with slightly broader 3-dB bandwidth of about 0.4 nm, as can be seen in Figure 4.28.

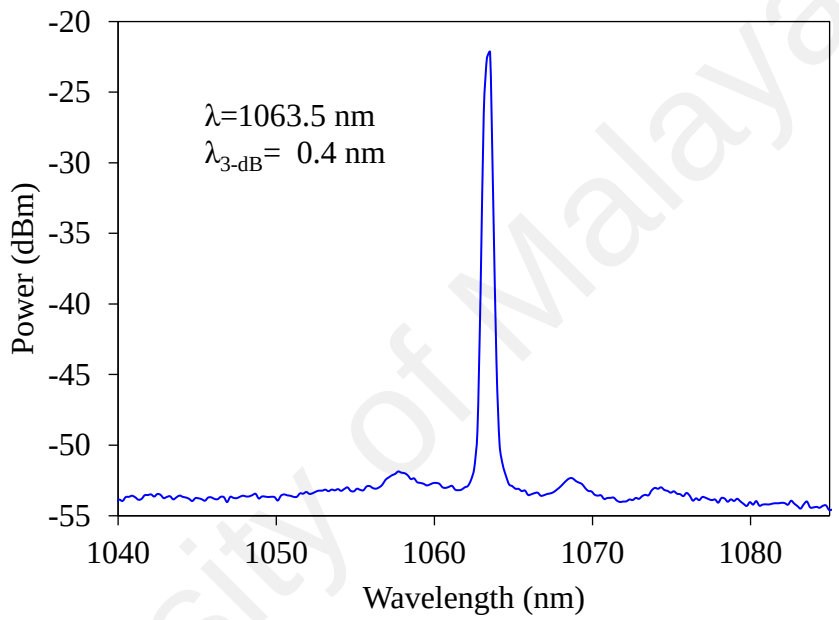

Figure 4.28: Optical spectrum of the Q-switched YDFL with 5 m cavity length

The centre wavelength slightly shifted to a shorter wavelength to compensate for the round-trip time difference due to the change in physical cavity length. Figure 4.29 shows the temporal characteristics at the maximum input LD power. The pulse train is more stable and uniform than the one in the previous setup which indicates the performance and stability of the fiber laser is enhanced. The inset presents the pulse train at a time scale of 2.5 ms.

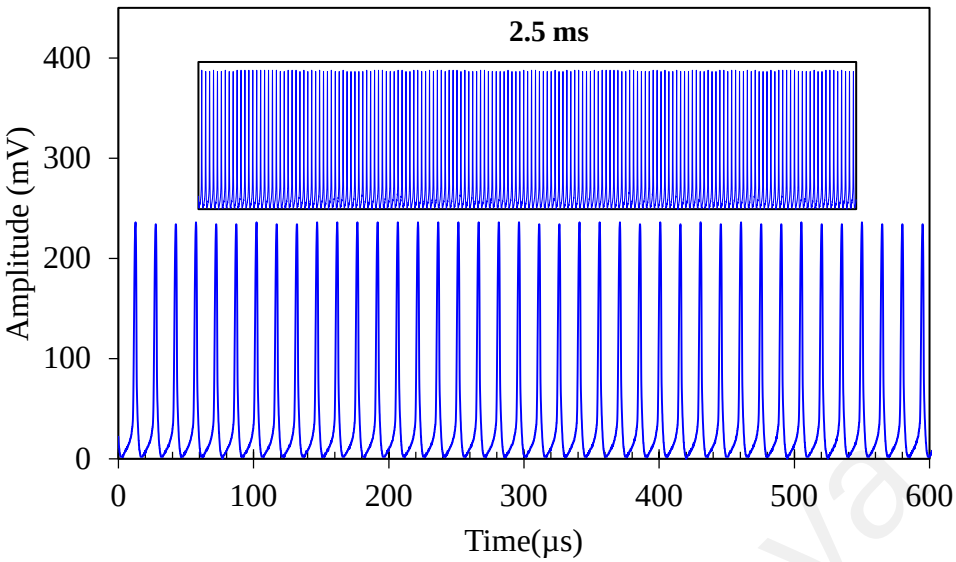

Figure 4.29: Pulse train at the maximum LD power

The repetition rate was raised from 25.2 kHz to 66.3 kHz and the pulse duration was shortened from 9.9 µs to 1.9 µs as the input LD power was raised from threshold to the maximum value, see Figure 4.30. The pulse repetition rate was increased as compared to the previous setup, as the decrease in the cavity length resulted in a shorter time for a pulse to travel through the cavity. Besides, the saturation of the SA is more rapid as compared to the 25 m cavity, resulting in a shorter pulse width and larger repetition rate.

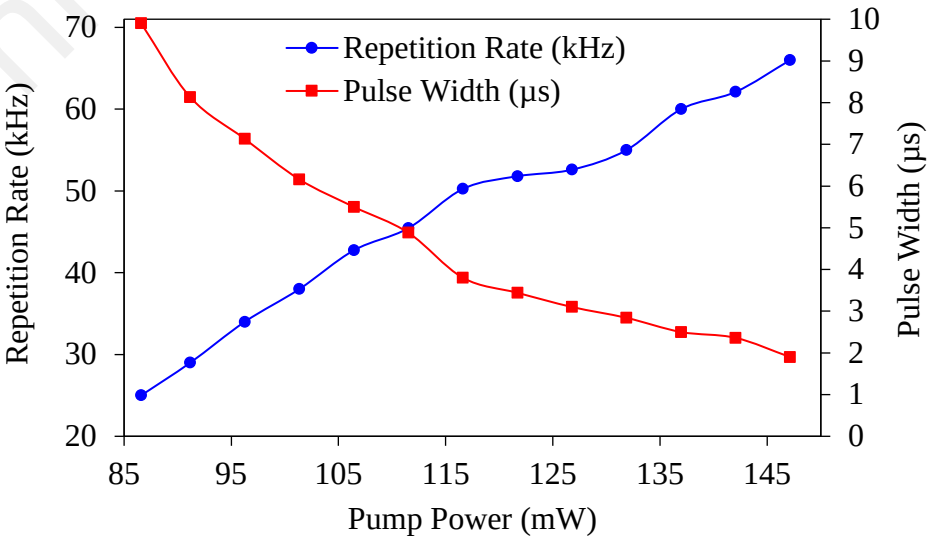

Figure 4.30: Pulse repetition rate and pulse width duration versus input LD power

The output power was enhanced in comparison to the previous setup due to lower optical loss with shorted cavity length. This setup produced an output power of 8.62 mW which is about twice the power produced in the previous experiment at the same input LD power. At the same time, higher slope efficiency was obtained, which is 33%. As can be seen from Figure 4.31, the output power reached the maximum value of about 30 mW at maximum input LD power. The maximum pulse energy achieved in this setup is 451.5 nJ which is about half of the value in the previous setup. That can be attributed to the pulse energy being inversely proportional to the pulse repetition rate. The increment in the pulse repetition rate resulted in a drop in the pulse energy.

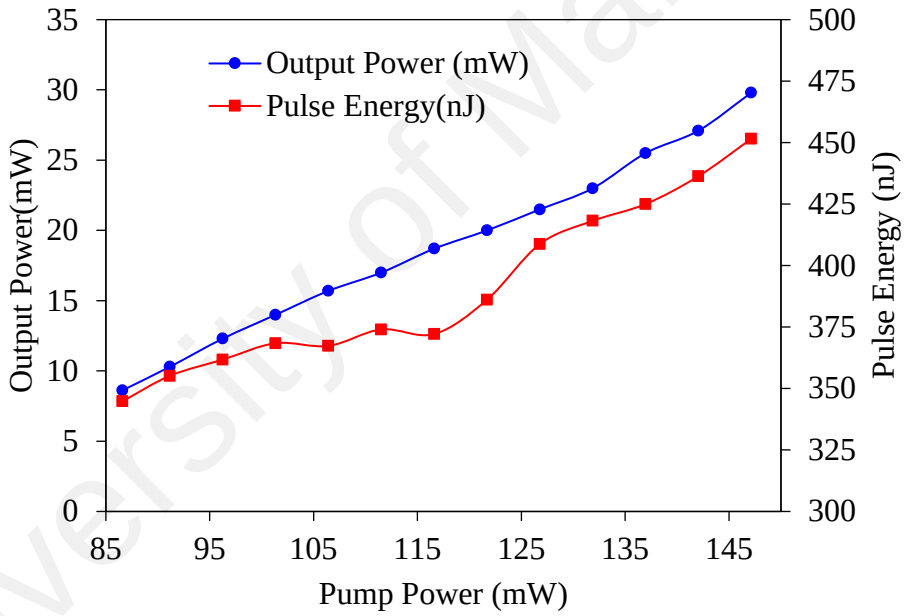

Figure 4.31: Output power and pulse energy as a function of input LD power

The peak power was enhanced tremendously in this setup reaching linearly to a maximum value of 237.62 mW at maximum input LD power of 147 mW, see Figure 4.32. That can be attributed to the peak power being correlated inversely with the pulse width and proportionally with the pulse energy.

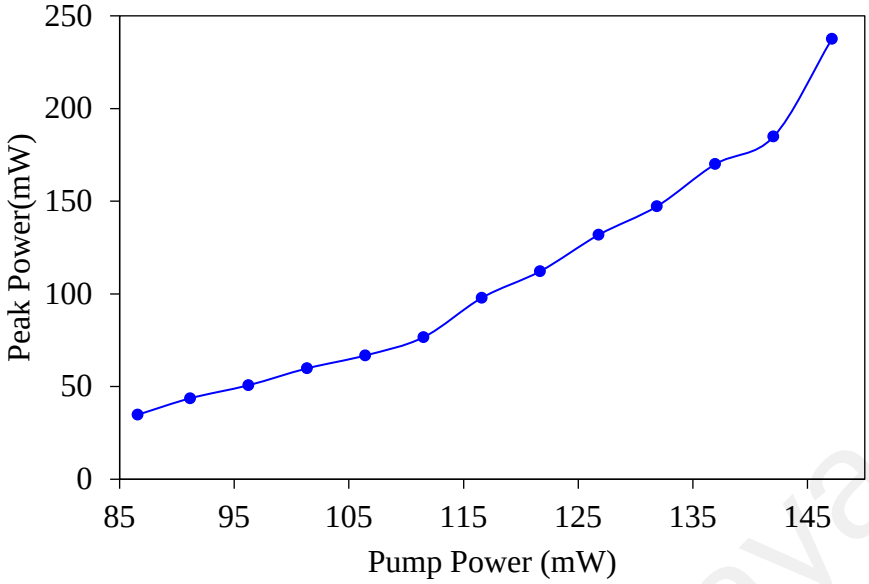

Figure 4.32: Peak power versus input LD power

In this setup, the pulse width was decreased by about eight times while the pulse energy was reduced only to the half as compared with the previous setup under similar considerations. Figure 4.33 shows an improvement in Q-switching stability. The SNR was recorded to be 52.78 dB, see the inset Figure. Additionally, the RF spectrum shows more harmonics up to 3 MHz which further indicates better stability of fiber laser.

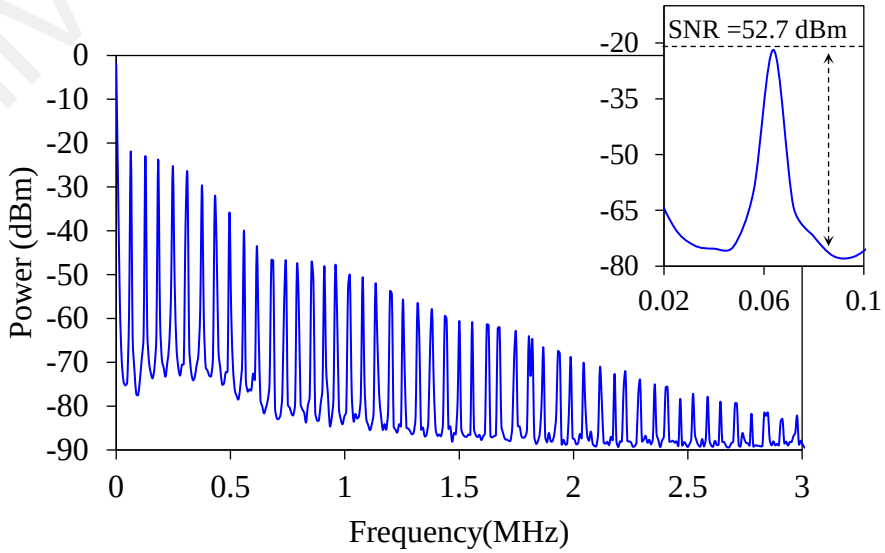

Figure 4.33: RF spectrum, inset Figure shows SNR at a span of 40 kHz

The reduction in RF intensities (in Figure 4.27 (b) and Figure 4.33) confirms the Q-switching operation, which has a relatively bigger pulses width than the mode-locking. To check the long-term stability of the fiber laser, we sampled the output spectrum every ~ 12 minutes for the total duration of 138 minutes, see Figure 4.34. The samples were almost identical, as the peaks were located at 1063 nm with an optical power intensity of −22 dBm ∓ 0.4 dBm. This further confirms the stability of the pulsed laser and shows that the SA can withstand long term operation. An optimized Q-switching operation can be obtained by further reducing the cavity length and/or enhancing the cavity design (Degnan, 1995; Herda et al., 2008). To the best of our knowledge, this work has achieved (by using SA based compact all-fiber ring cavity and through two different setups) very high pulse energy and very high peak power at 1 µm region. Additionally, this is the first demonstration of passive Q-switched fiber laser using an organic material as SA operating in 1 µm region.

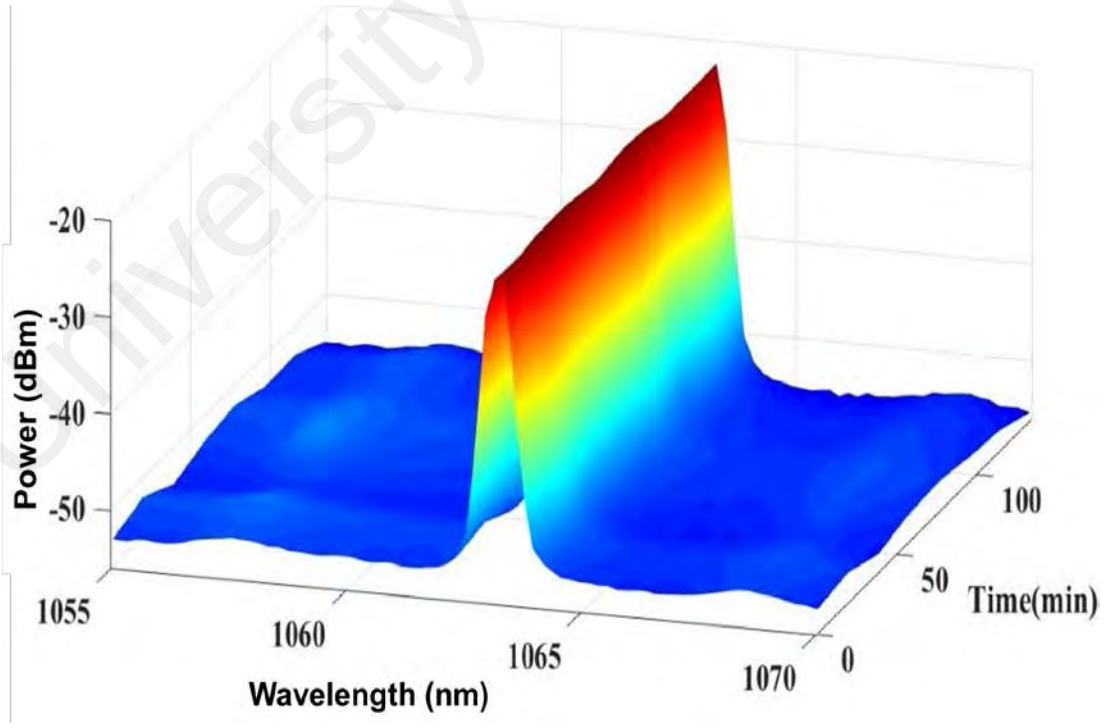

Figure 4.34: Output optical spectrum evolution for the total duration of 135 minutes

4. 6 Summary

Q-switched fiber lasers have been successfully demonstrated using the newly developed organic material based SAs operating in both 1.5 and 1.0 µm wavelength regions. At first, FIrpic SA was used to produce pulses train operating at a central wavelength of 1560.4 nm. The laser's pulse width reduces from 9.5 µs to 3.4 µs while the repetition rate increases from 39.22 to 87.4 kHz as the pump power was increased from 30 to 208 mW. The SA was also used to produce a dual-wavelength output operating at 1558.1 nm and 1562.6 nm by incorporating a microfiber device inside the cavity. Znq_2 was then used to produce Q-switching pulses. The laser produced pulse width and repetition rate in a range of 6.6- 2.8 µs and 45-86 kHz as the pump power was varied from 38 to 198 mW. Tunable Q-switched EDFL was also realized by using Znq_2 SA as a Q-switcher. The central wavelength of the tunable laser can be shifted continuously from 1520.0 nm to 1563.3 nm, covering almost all C-band region by tuning the band-pass filter inside the laser cavity. Finally, the developed Alq_3 SA was successfully used to produce Q-switched EDFL operating at 1559 nm, which the pulse width is tunable from 6.6 to 1.2 µs and the repetition rate is tunable from 31.65 to 144.5 kHz. The SA also used to produce Q-switching pulsing with high-output power and high pulse energy at 1.0 µm region. The Q-switched YDFL produced high pulse energy of 0.8 µJ and peak power of 90 mW at cavity length of 25 m. As the laser cavity was reduced to 5 m, the peak power increased to 237.62 mW, the pulse energy dropped to 451.5 nJ and the minimum pulse width was reduced from 9 µs to 1.9 µs. These results indicate that the proposed organic materials can be easily used to generate different types of Q-switched fiber lasers with a low-cost, simple and straightforward fabrication process. All the produced laser output had a very high SNR of around 56 dB and very stable performance in terms of long-term operation and stable pulse train output. Table 4.1 summarize the performance of the Q-switched fiber lasers developed by using Firpic, Znq_2 and Alq_3 as saturable absorbers. This work

presents the first demonstration of these materials in fiber laser technology to the best of our knowledge.

Table 4.1: Performance of Q-switched fiber lasers by using the developed SAs

Section in the thesis	Pulse width (µs)	Repetition rate (kHz)	Wavelength (nm)	Pulse energy (nJ)	SNR (dB)	SA
4.2.2	9.5 – 3.4	39.22 – 87.4	1560.4	122.6	58.36	FIrpic
4.3.2	8.4 – 3.6	32.15 – 78	1558.1 and 1562.6	110.13	55.36	
4.4.1	6.6 – 2.8	45 – 86	1560	95.35	57.4	Znq_2
4.4.2	–	-	1520 – 1563.3	-	53.2	
4.5.1	6.6 – 1.2	31.65 – 144.5	1559	63.8	46	Alq_3
4.5.2	24 – 9	12.95 – 29.62	1066.7	810	50	
	9.9 –1.9	25.2 – 66.3	1063.5	451.5	52.7	

CHAPTER 5: MODE-LOCKED PULSE GENERATION BY USING ORGANIC MATERIALS

5. 1 Introduction

Ultrafast mode-locked fiber lasers have gained a great research interest in recent years due to their unique advantages, such as low cost, flexibility and good reliability (X. Liu, 2011; L. Zhang et al., 2011). Additionally, they have widespread applications in telecommunications, supercontinuum generation, material processing, nonlinear microscopy and frequency comb generation (Fermann & Hartl, 2013; Nicholson, Yablon, Westbrook, Feder, & Yan, 2004; Smirnov, Kobtsev, & Kukarin, 2014). The mode-locked lasers are normally produced by a passive technique by utilizing many types of saturable absorbers (SAs), such as transition metal-doped bulk crystals (D. Lin et al., 2010) and semiconductor saturable absorber mirrors (SESAMs) (M. Wang, Chen, Li, Huang, & Chen, 2014). However, doped crystal SAs are mainly utilized in solid-state laser while SESAMs are costly and work only in a narrow wavelength range and also require a complex fabrication to improve their damage threshold (Saraceno et al., 2011). SA based mode-locked fiber lasers have also been demonstrated using carbon nanotubes (CNTs) and graphene (H. Zhang et al., 2010). CNTs have the advantages of easy and low-cost fabrication, while graphene has the advantage of ultrafast recovery time (Q. Bao et al., 2009), wide operation spectral range (B. Y. Zhang et al., 2013) and large absorption per layer (Nair et al., 2008). Yet, both have some limitations, as CNTs often require band gap engineering (Q. L. Bao et al., 2009), and graphene suffers from the absence of band gap. Recently, transition metal dichalcogenides (TMDs), such as tungsten disulfide (WS_2) (Yan et al., 2015) and molybdenum disulfide (MoS_2) (Hao Liu et al., 2014), have been extensively investigated and demonstrated as SAs, as they show unique absorption property (B. Chen et al., 2016). But, TMDs suffer also from a low optical damage threshold (Horiguchi et al., 2008; Latiff et al., 2017), and a complicated and costly

fabrication process. Recently, black phosphorus (BP) has been reported as a promising SA (Jaroslaw Sotor et al., 2015). BP has a broadband nonlinear optical response (Lu et al., 2015) and it can be easily fabricated as it consists of only one element (phosphorus). However, BP is a hydrophilic material (J. Li et al., 2016) which is easily damaged when exposed to water and oxygen.

Nevertheless, these nanomaterials might be dangerous on human health in the case of long-term exposure (Nel et al., 2006). Besides, there are several attempts more recently to develop SA from new material. In that respect, organic materials might have the potentials in fiber laser technology. They can be utilized as a high-performance, bio-compatible and environment-friendly SAs. organic materials have the advantages of ultrafast nonlinear response and broad spectral tunability (Boulet et al., 2015; Clark & Lanzani, 2010; Williams, 1983). Additionally, They could increase the applications in sensing and in-situ biomedical laser processing (Khazaeinezhad et al., 2017). Furthermore, they are mechanically flexible, light-weight, and can be produced at a low cost (Someya et al., 2004). Due to their unique characteristics, organic materials are used in several applications, such as an organic thin-film transistor (J.-M. Kim et al., 2012), organic light-emitting diodes (O. Y. Kim & Lee, 2012; Yook & Lee, 2012), organic solar cells (J. Y. Kim et al., 2007; Peumans et al., 2011), and organic bistable memory devices (Briseno et al., 2006).

In this chapter, various mode-locked erbium-doped fiber lasers (EDFLs) are demonstrated using the newly developed organic material-based SA devices. Three organic materials; Bis[2-(4,6-difluorophenyl)pyridinato-C^2,N](picolinato)iridium(III) (FIrpic), bis(8-hydroxyquinoline)zinc (Znq_2) and Tris(8-hydroxyquinoline)aluminum (Alq_3) are used in this work for the generation of stable mode-locked laser pulses. FIrpic was successfully used as mode-locker and produced a soliton wavelength. The produced pulsing was stable and showed long term operation. On the other hand, Znq_2 was

successfully used to produce ultrafast pulsing with dark pulsing, white pulsing and supercontinuum operations. Alq_3 was successful as well in generating mode-locking pulses in both regions of 1.0 µm and 1.5 µm regions. Different pulse widths were generated as the parameters of the cavity were changed. It should be mentioned that dark pulses are less affected by intra-pulse-stimulated Raman scatters and stable in the presence of fiber loss and noise (L.-Y. Wang et al., 2012; X. Wang, Zhou, Wang, Xiao, & Liu, 2014). That makes them very attractive in applications of optical-processing system and telecommunications.

5. 2 Mode-Locked Erbium-Doped Fiber Laser with FIrpic SA

In this section, a soliton mode-locked EDFL is demonstrated using FIrpic PVA film as a SA. Figure 5.1 shows the configuration of the proposed mode-locked laser, which is almost similar setup to the Q-switched laser (Figure 4.1) as described in section 4.2.1 of the previous chapter except that the output coupler (OC) used was 99:1 and a spool of single-mode fiber (SMF-28) was added between the SA device and isolator.

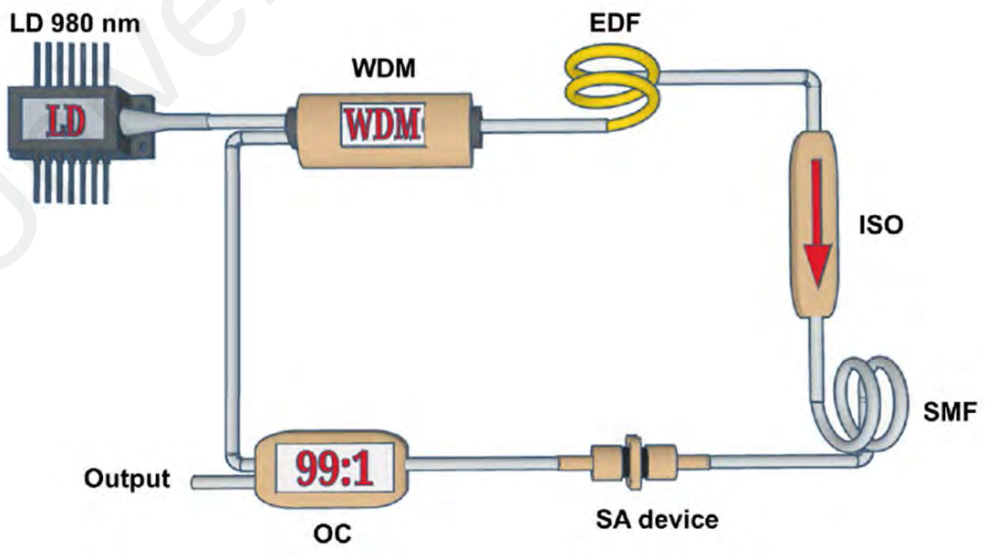

Figure 5.1: Configuration of the mode-locked EDFL

The balance between the nonlinearity effect and group velocity dispersion (GVD) inside the ring cavity was managed through the addition of SMF which allows the generation of a soliton mode-locking. The addition of 52 m SMF causes the cavity to operate in anomalous dispersion of about -1.216 ps^2, the total cavity length was about 60 m. The wavelength division multiplexer (WDM) coupler, SMF and EDF have GVD of -48.5, -21.7, and 27.6 ps^2/km. A 99:1 OC was also used to maintain a high-power oscillating inside the laser cavity. The laser self-started mode-locking pulses at the pump power of 35 mW and the mode-locking operation were maintained up to the maximum pump power of 188 mW. The laser has an optical spectrum centred at 1562.57 nm with a 3-dB bandwidth of 1.8 nm, as shown in Figure 5.2. The mode-locking pulses had a soliton shape spectrum with Kelly sidebands that can be easily observed due to the periodic perturbation in the cavity. The employment of SMF into the cavity led to the increase in the net dispersion, birefringence and nonlinearity of cavity which helps the mode-locking operation.

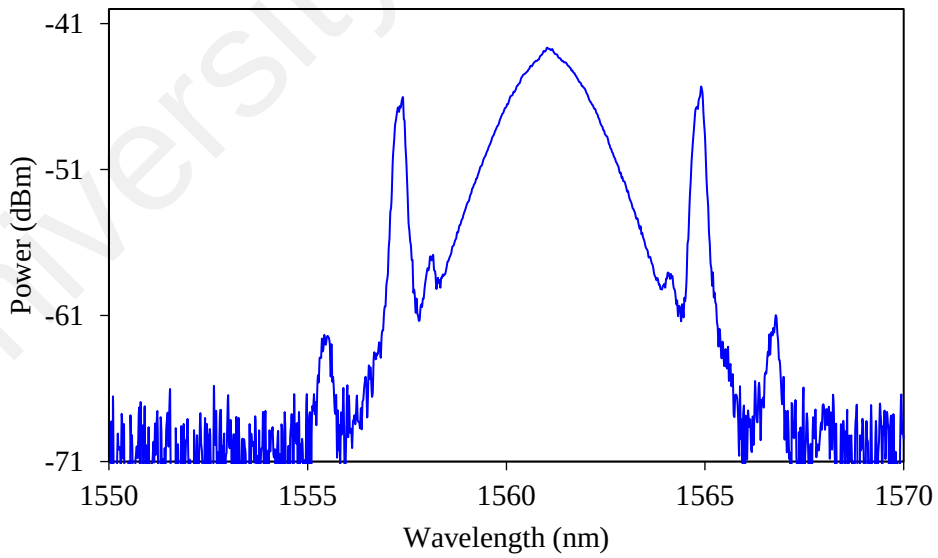

Figure 5.2: Optical spectrum of the soliton laser

Additionally, the saturation absorption effect from FIrpic based SA and the non-linearity of the EDF also contributed to the formation of soliton mode-locked pulses train.

Figure 5.3 shows the output pulse train of the soliton laser in the time domain at the maximum pump power of 188 mW. It shows a very uniform pulse amplitude with a pulse width of about~120 ns. An attempt was made to measure the pulse width with an autocorrelator, and it was unsuccessful due to the limited specifications of the autocorrelator as it could only detect a pulse width narrower than 50 ps. The interval between adjacent pulses is about 291.5 ns which represents a repetition rate of 3.43 MHz. The obtained repetition rate matches the fundamental frequency and the total cavity length of about 60 m.

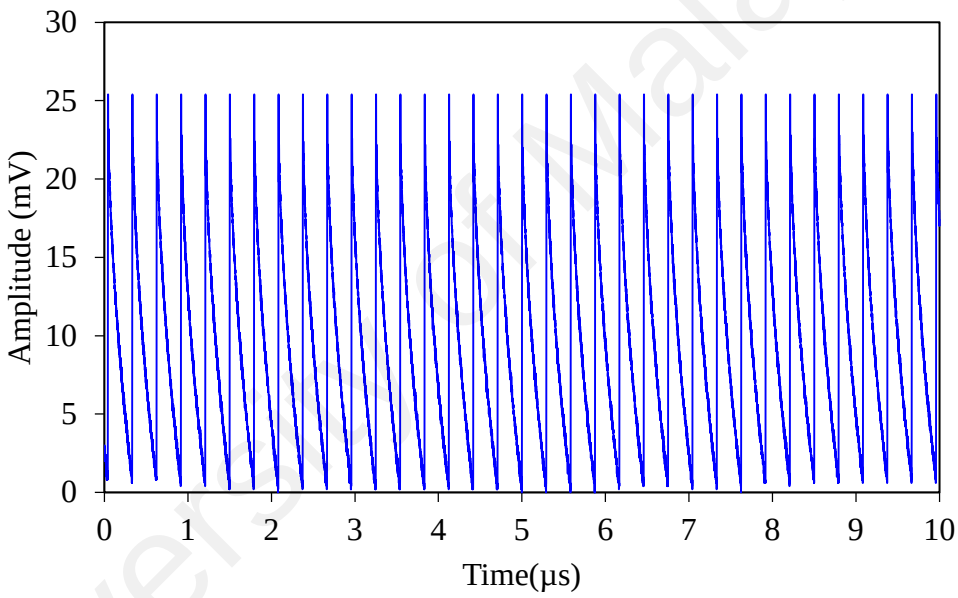

Figure 5.3: Optical pulse train in the time domain

The output power and pulse energy versus input pump power are also investigated in the proposed mode-locked EDFL and the results are shown in Figure 5.4. As the pump power was tuned from 35 mW to 188 mW, the output power and pulse energy increased from 0.19 to 1.1 mW and from 0.06 to 0.33 nJ, respectively. The RF spectrum was also measured to check the stability of the mode-locking operation in a span of 85 MHz with a resolution bandwidth (RBW) of 10 Hz, as shown in Figure 5.5. The figure shows the fundamental frequency with many harmonics. The fundamental frequency operates at

3.43 MHz with an SNR of 38.3 dB as shown in the inset figure. It is observed that the number of harmonics is limited, which further verifies that the mode-locked laser is operating in a nanosecond regime.

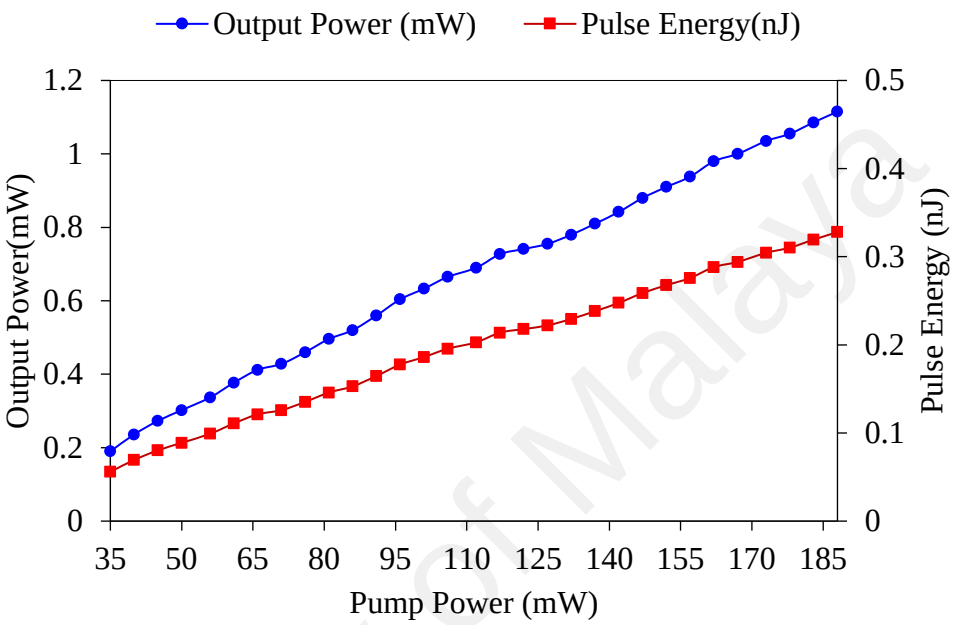

Figure 5.4: Output power and pulse energy versus input pump power

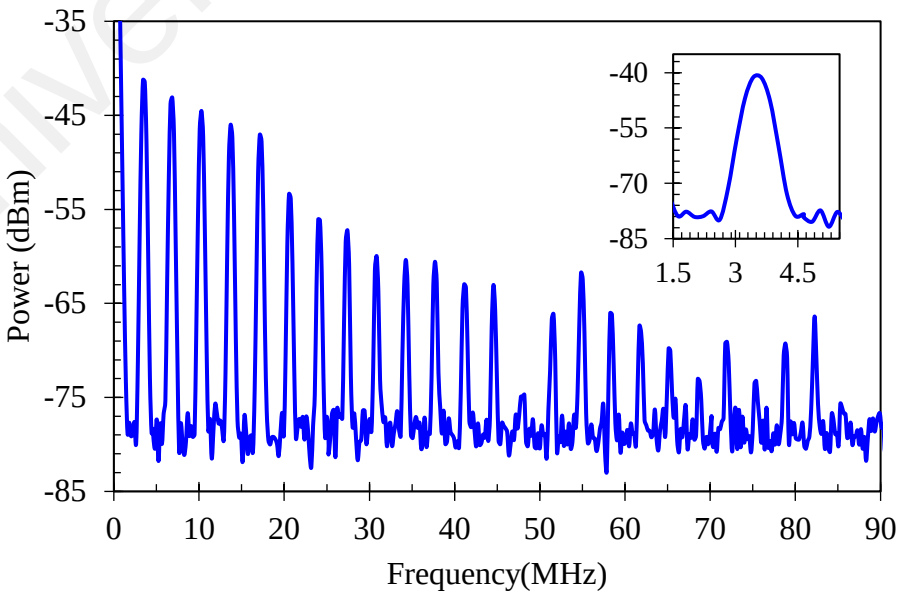

Figure 5.5: RF spectrum

Finally, the output optical spectrum was sampled at an interval of ~45 min for a total duration of 320 minutes, see Figure 5.6. The figure shows the samples have almost the same shape, pattern and optical power intensity (about −42.7 dB ± 0.17 dB) which reveals the very good performance of the SA device. In summary, a soliton mode-locked laser was successfully achieved in anomalous dispersion cavity through the addition of 52 m SMF. The mode-locked laser has a fixed repetition rate of 3.43 MHz and 120 ns pulse width. To the best of the authors' knowledge, this is the first report of the organic material being used as a SA in a fiber laser cavity. These results indicate that FIrpic is suitable for use in producing pulsed lasers operating in the 1.5 µm wavelength region. The generated pulses laser has comparable performance to those of other SA materials such as CNTs, graphene, TMDs, MoS_2, WS_2 and BP (Babar, Harun, Yasin, & Ahmad, 2017; Cheng et al., 2013; B. Gao et al., 2018; N. Razak et al., 2017; Rosol et al., 2017; Yang, Yang, Li, & Lin, 2019)

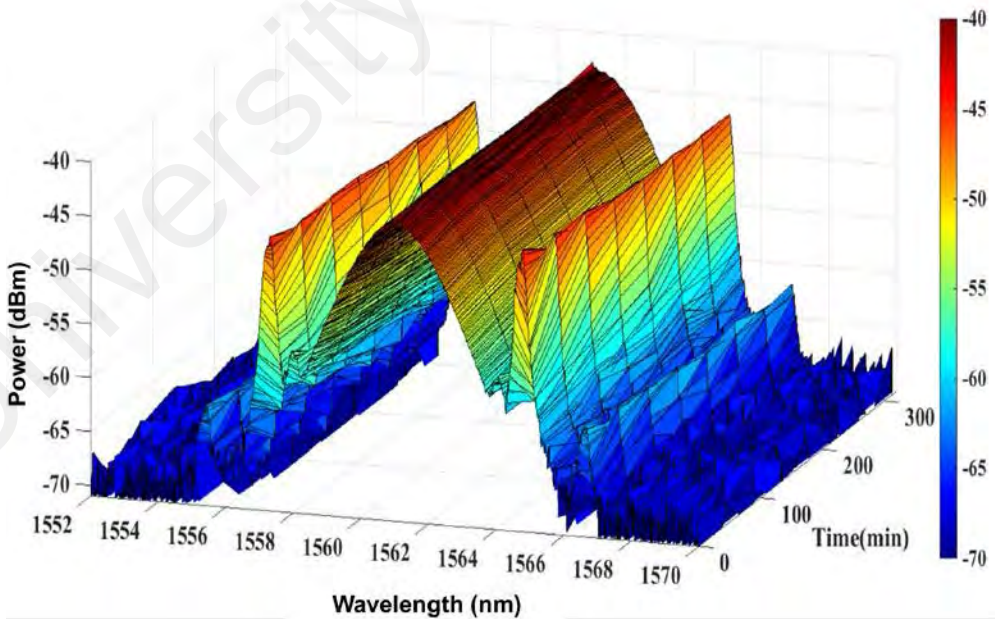

Figure 5.6: Output optical spectrum sampled at an interval of ~45 minutes for the total duration of 320 minutes. The colour-bar on the left is a reference for the intensity

5. 3 Mode-Locked Laser by Using Znq_2 as SA at 1.5 µm Region

5.3.1 White Pulse Operation

In this section, a mode-locked EDFL is demonstrated using Znq_2 as SA to operate at 1.5 µm region. A stable soliton mode-locked pulse train was produced as the LD intensity gradually increased to 15 mW. Figure 5.7 - Figure 5.13 summarize the performance of the mode-locked laser. The cavity configuration used in this experiment is similar to the one presented in Figure 5.1, expect the cavity length and optical coupler (OC) used in this experiment is 59.5 m and 90:10, respectively. The laser produced a soliton optical spectrum at a central wavelength 1560.6 nm with a 3-dB bandwidth of 2 nm, see figure 5.7. The soliton mode-locked operation is due to the interplay of self-phase modulation and group velocity dispersion, which is facilitated by the anomalous cavity dispersion.

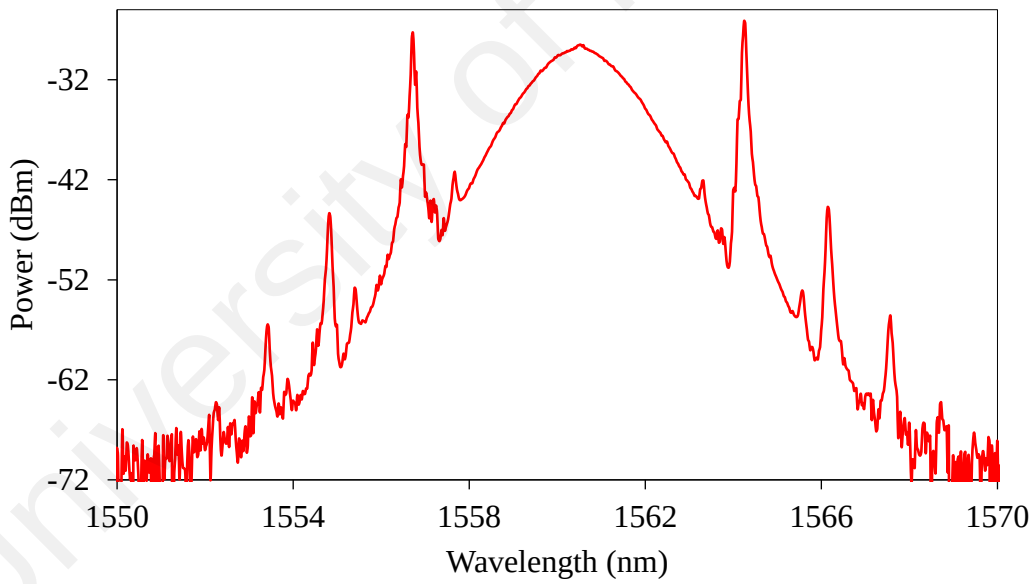

Figure 5.7: Optical spectrum of mode-locked operation based on Znq_2 SA

This is confirmed by the presence of Kelly sidebands on the spectrum (Lazaridis, Debarge, & Gallion, 1995). The spectrum presents symmetrical Kelly sidebands centred at 1560.6 nm. The measured distance (Δd) between the central wavelength and the 1st, 2nd and 3rd order Kelly sidebands are ± 3.65 nm ± 5.9 nm and ±6.97 nm, respectively

These values are very close to the theoretical values, which were obtained at 3.7 nm, 5.7 nm and 7 nm, respectively. They were calculated based on the relation between the (Δd), central wavelength, pulse duration and total net dispersion of the cavity as described in Ref. (Smith, Blow, & Andonovic, 1992). A highly-sensitive auto-correlator was used to accurately measure the pulse width. The autocorrelation trace with sech^2 fitting is given in Figure 5.8. The pulse has a T_{FWHM} of 1.46 ps, as the full width at half maximum (FWHM) duration of the autocorrelation trace (Tac) is 2.16 ps. The time-bandwidth product (TBP) is calculated to be 0.359, which is larger than the transform-limited value of 0.315, indicating that the generated pulses are slightly chirped. The calculated pulse width is 1.27 ps, which is very close to the measured value.

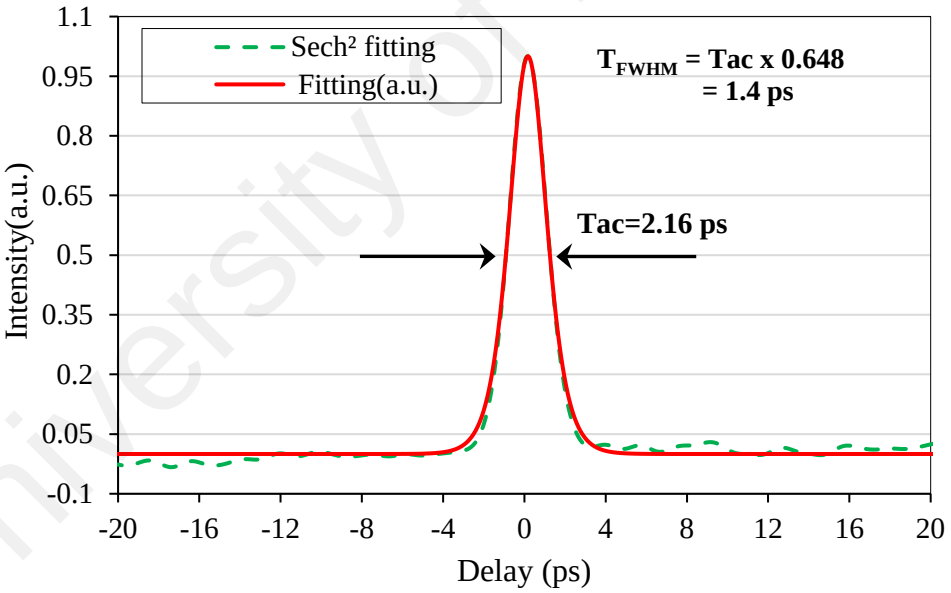

Figure 5.8: Autocorrelation trace of the mode-locking operation based on Znq_2 SA

The ultrafast pulsing was produced as the LD intensity was increased from 15 mW to 249 mW. As the LD intensity is lowered below 15 mW, the pulsing operation was disappeared and only continuous wave (CW) operation was produced as observed on the oscilloscope. Similarly, the pulsing operation was disappeared when we raised the LD

intensity above 249 mW and up to the maximum available of 350 m. That is attributed to the bleaching of the SA. When we reduced the LD intensity below 250 mW, the laser restored the mode-locking operation. Hence, we concluded that the SA damage threshold is higher than 350 mW. If the SA was damaged, no mode-locking operation could be produced. The average output intensity and pulse energy are increased linearly from 0.3 mW and 0.1 nJ to 2.6 mW and 0.74 nJ, respectively, see Figure 5.9.

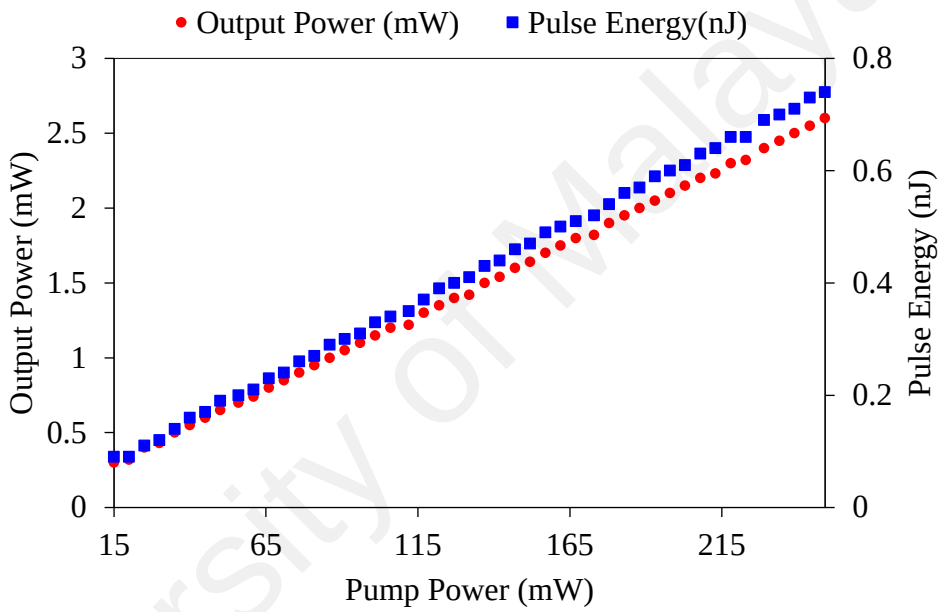

Figure 5.9: Output power and pulse energy as a function of LD power

The RF spectrum with a span of 250 MHz and 11 MHz is given in Figure 5.10. It indicates that the laser has a repetition rate of 3.5 MHz. The spectrum also shows a high number of cavity harmonics that the intensity decreased in relative to the fundamental frequency, which suggests a good and stable mode-locking operation with a small pulse width. Additionally, the laser has an excellent signal to noise ratio of 60.6 dB, while the short-span RF spectrum showed no Q-switching instabilities. This proves the stable mode-locking operation.

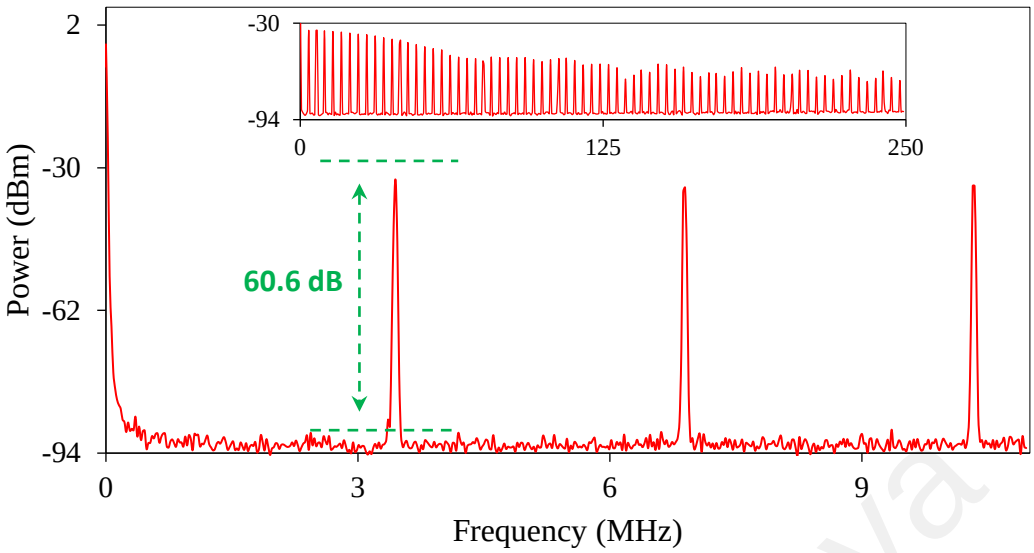

Figure 5.10: RF spectrum at a span of 11 MHz. The inset figure shows the spectrum in a span of 250 MHz

Figure 5.11 shows the typical pulse train of the mode-locked laser within 10 µs span. The pulse width measured by the oscilloscope is 102 ns, which is due to the limited resolution. The pulse train produced a stable operation in which no instabilities nor is distortion observed. The inset Figure shows the pulse train in a shorter span of 1 µs. As illustrated in the inset Figure, the pulses have a pulse period of ~ 288 ns, which it coincides with the repetition rate and the cavity length.

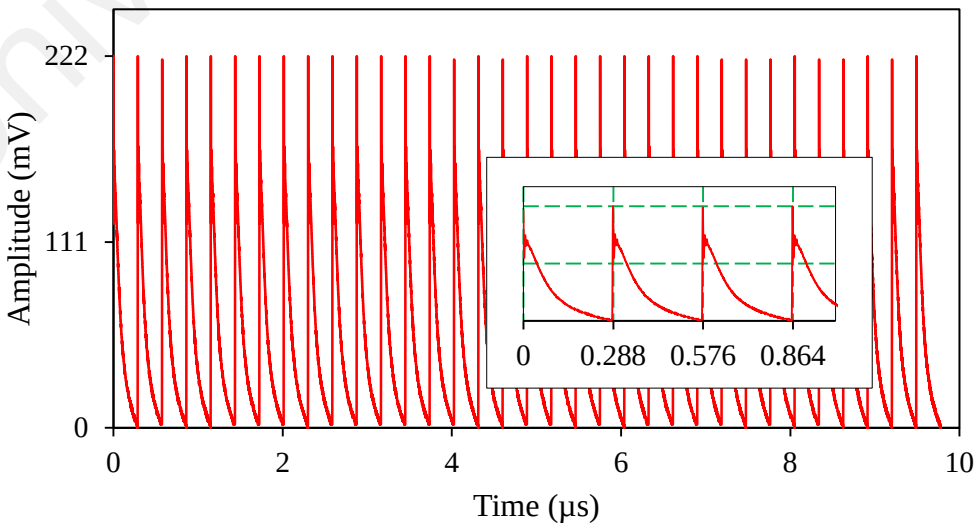

Figure 5.11: Output pulse train of the mode-locked laser based on Znq_2 SA

5.3.2 Dark Pulse Operation

In this experiment, the mode-locked fiber laser could generate not only the bright pulses but also dark pulses, by appropriately managing the polarization state of the cavity. The oscilloscope trace of the dark pulse train is given in Figure 5.12. Obvious dark pulses have appeared. The pulse period is 288 ns, which is the same as in the bright pulses, determined by the cavity length. No bright pulses are observed on the pulse train, on the other hand, the saw-tooth like pulse train is attributed to the noise produced by the photo-detector.

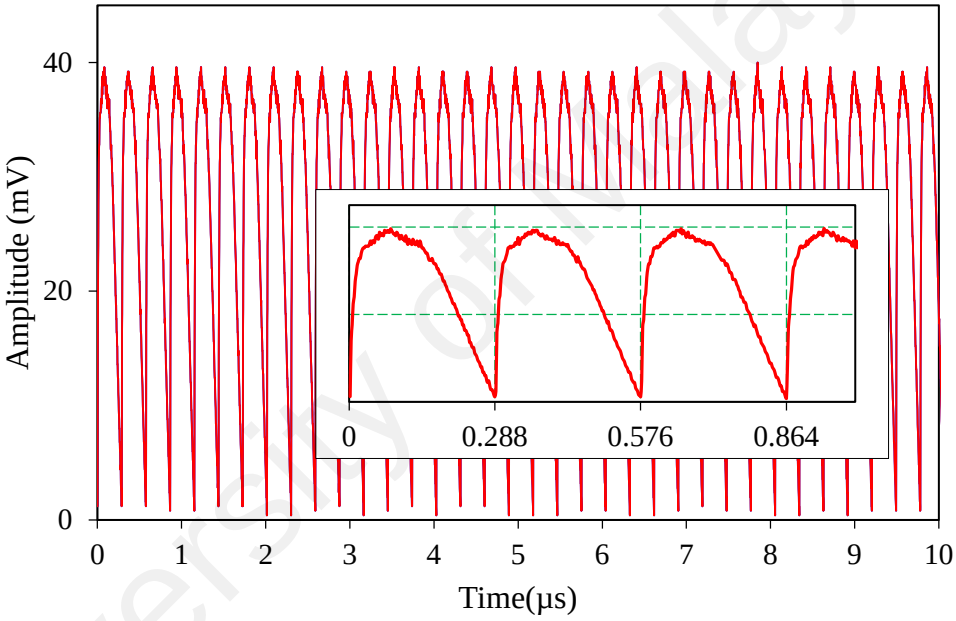

Figure 5.12: Output dark pulse train based on Znq_2 SA

The RF spectrum of the dark pulses is presented in Figure 5.13. The laser maintained an excellent SNR of 60.8 dB. The experiment shows that Znq_2-SA can act as a promising mode-locker, providing a bright and dark pulse operation. To confirm that the pulsing operation is attributed to the Znq_2-SA, the Znq_2-SA was removed from the cavity. In this case, no bright or dark pulsing operation was observed on the oscilloscope, no matter how the polarization of the cavity or LD intensity was changed. Further investigations of this

SA in ultrafast lasers are needed, as this is the first demonstration of bright and dark pulsing operation using Znq_2-SA.

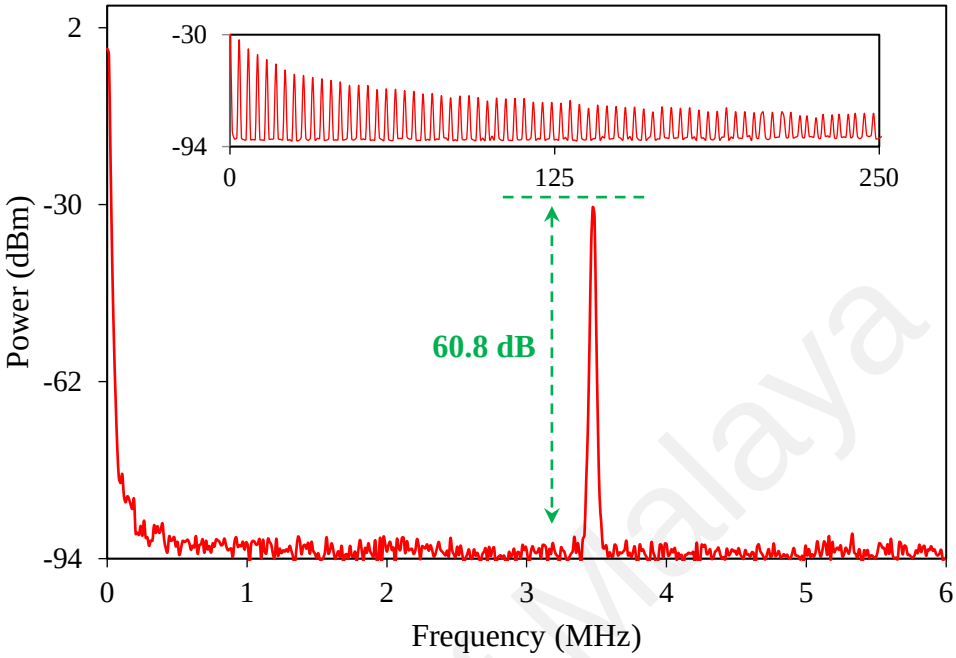

Figure 5.13: RF spectrum of dark mode-locked operation at a span of 6 MHz. The inset figure shows the spectrum at a span of 250 MHz

5.3.3 Supercontinuum Pulse Generation with Znq_2 Based EDFL

In this subsection, the developed Znq_2 based EDFL is used as a pump to generate a supercontinuum (SC) light. SC generation has attracted much of research interest in recent years due to its various applications, such as spectroscopy, optical communications, optical frequency metrology and mobile clockwork, (Keren, Brand, Levi, Levit, & Horowitz, 2002). SC can be generated by using noise-like pulses (NLPs) (A.-P. Luo et al., 2015), short pulses (Han Zhang, Tang, Zhao, Wu, & Tam, 2009) and ultra-short pulses (Sumimura, Genda, Ohta, Itoh, & Nishizawa, 2010), and nonlinear propagation media like standard fiber (SMF) (Zaytsev et al., 2013), zero-dispersion fiber, tapered fiber (Liao et al., 2012), highly nonlinear fiber (HNLF) (Liao et al., 2012) and photonic crystal fiber (PCF) (Travers, Rulkov, Cumberland, Popov, & Taylor, 2008).

In this work, output pulses from the developed Znq_2 based EDFL were launched into a 100 m long PCF to generate SC. Figure 5.14 (a1) shows the output spectrum of the pulses before and after the PCF at the maximum input pump power of 249 mW. It is observed that the output spectrum was significantly broadened after the PCF. Figure 5.14 (a2) and (a3) shows the autocorrelation trace of the laser, which was obtained before and after the PCF respectively. The T_{FWHM} was reduced to 640 fs after the supercontinuum generation as observed after the PCF. To improve the performance of supercontinuum, an erbium-doped fiber amplifier (EDFA) device is used to amplify the input mode-locked laser, which functioned as the pump. The average output power was increased to 32 mW after amplification. Figure 5.14 (b1) compares the output optical spectrum before and after amplification. It is observed that the output spectrum was also broadened after the amplification.

Figure 5.14 (b2) shows the output spectrum of the amplified pulses at a wider span, which indicates the spectral broadening has covered a wider range from 1200 nm to 1750 nm. The OSA used in this experiment had a wavelength range up to 1750 nm. Thus, it is believed that the spectrum is widened beyond 1750 nm. Figure 5.14 (b3) shows the auto-correlator trace of the pulses, which indicates T_{FWHM} of about 2.78 ps. The pulse width obtained was broadened as compared to unamplified input pulses and the previous SC generation after PCF (without amplification). To enhance the SC operation, the amplified pulses were injected into the PCF. The spectrum had an enhanced broadening, see Figure 5.14 (c1) and (c2). While the pulse width is reduced to 260 fs as shown in Figure 5.13(c3)

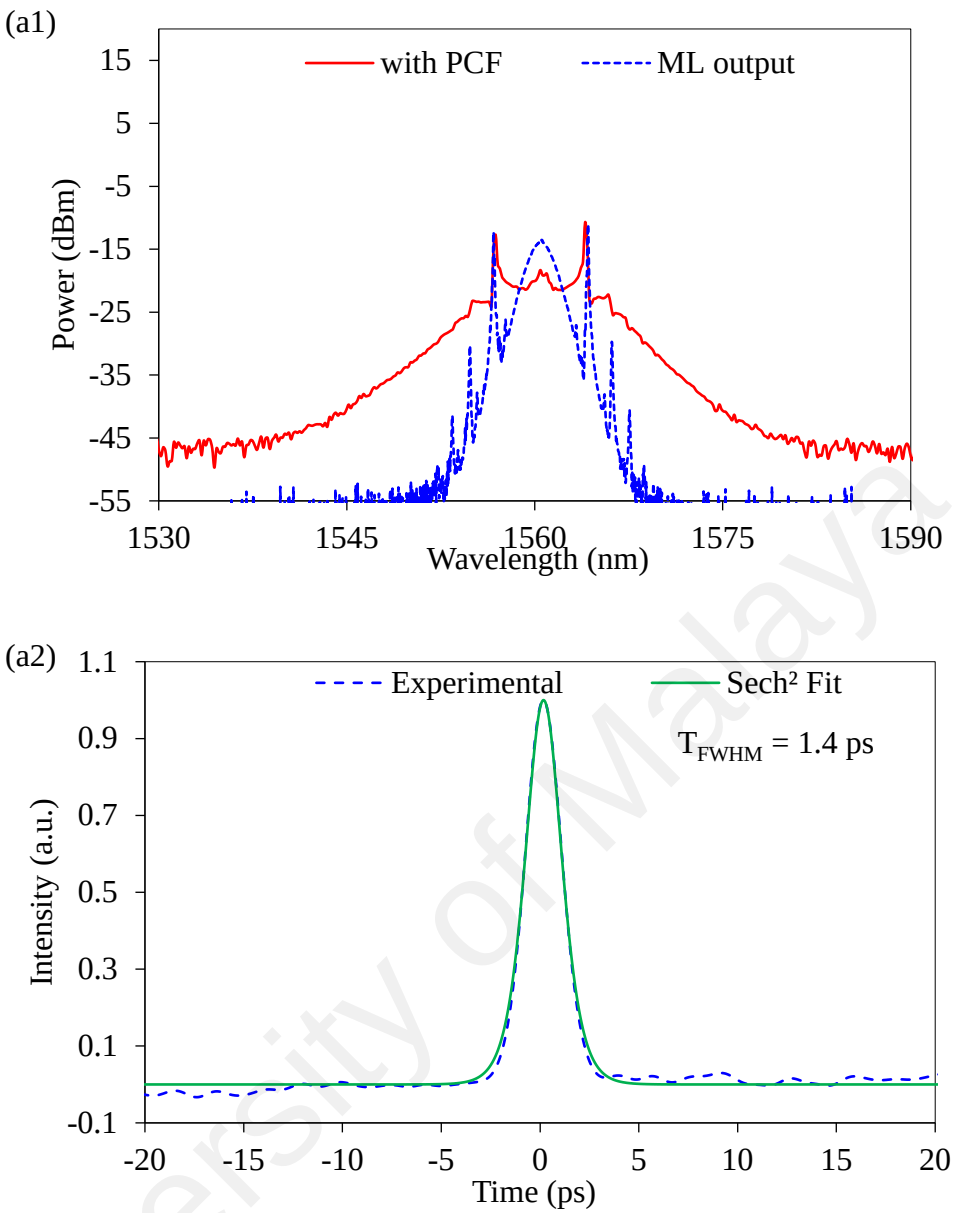

Figure 5.14 (a1) Output spectrum for normal mode-lock (ML) operation and when 100 m PCF attached to the output of the cavity, (a2) autocorrelation trace for normal ML operation, (a3) autocorrelation trace when the 100 PCF attached, (b1) output spectrum for normal ML operation and when EDFA attached to the output of the cavity at a span of 60 nm, (b2) output spectrum for normal ML operation and when EDFA attached to the output of the cavity at span 550 nm, (b3) autocorrelation trace for normal ML operation and when EDFA attached to the output of the cavity, (c1) output spectrum for normal ML operation and when EDFA and 100 PCF are attached to the output of the cavity at span of 60, (c2) output spectrum for normal ML operation and when EDFA and 100 PCF are attached to the output of the cavity at a span of 550 nm, and (c3) autocorrelation trace when EDFA and 100 PCF are attached to the output of the cavity

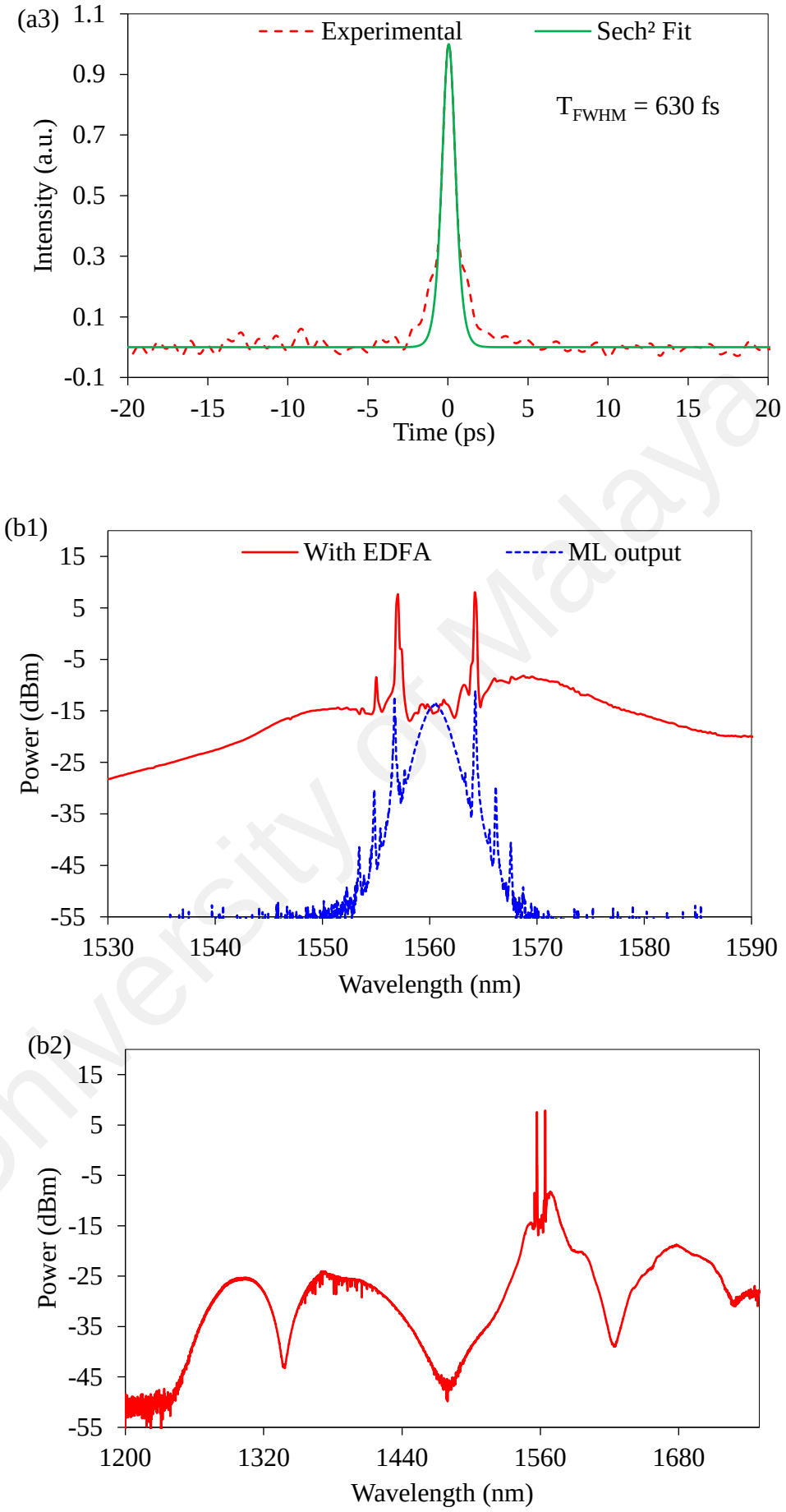

Figure 5.14, continued

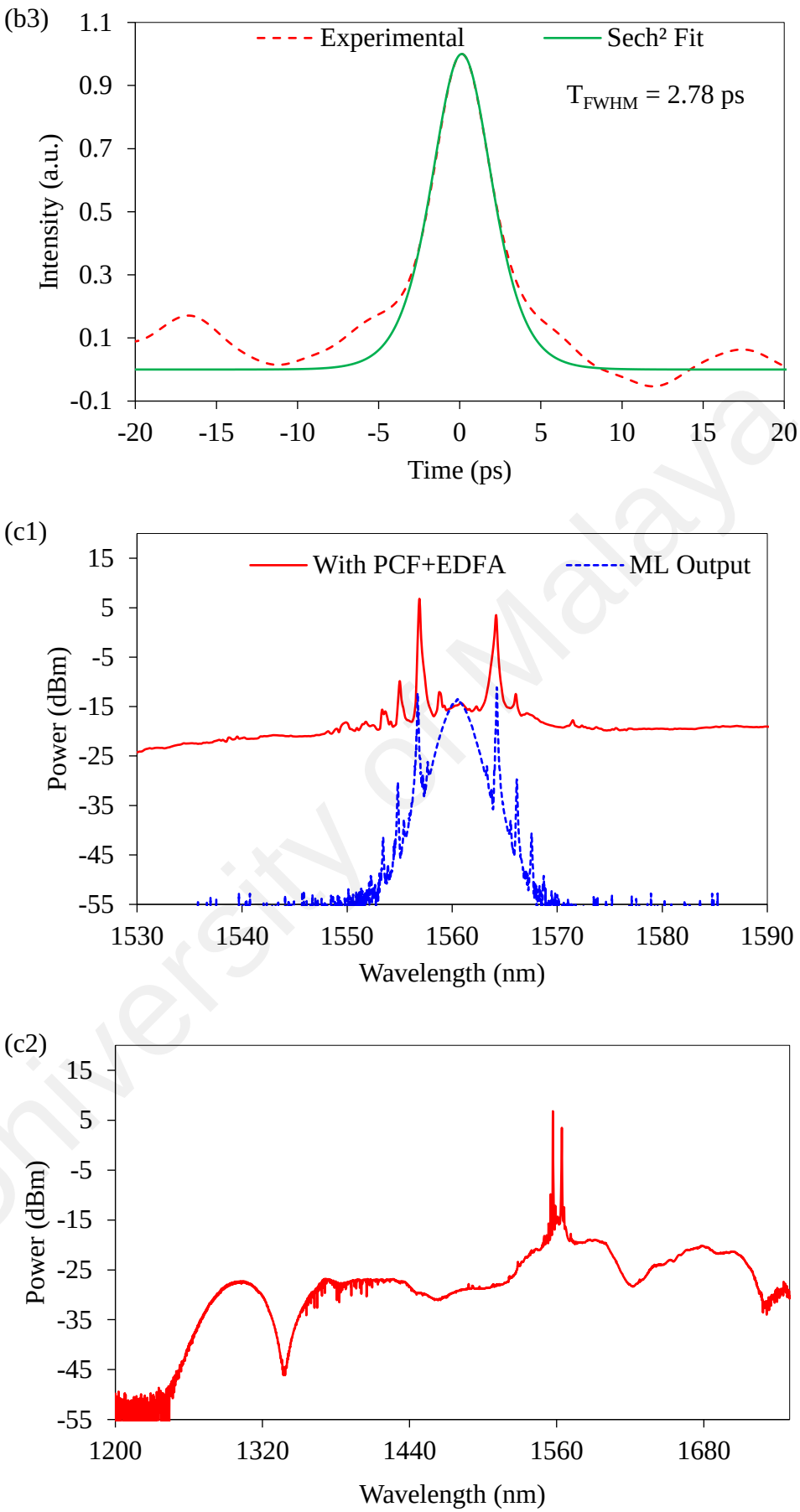

Figure 5.14, continued

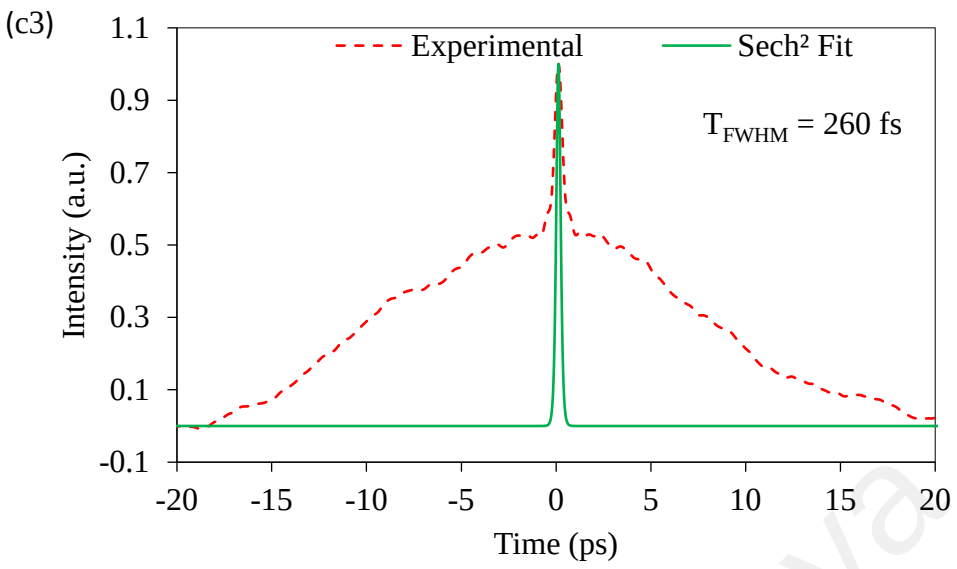

Figure 5.14, continued

5. 4 Mode-Locked EDFL with Alq_3 Saturable Absorber

5.4.1 Experimental Setup

The configuration of the proposed fiber laser is shown in Figure 5.15. The fiber laser cavity consists of a 2 m long Erbium-doped fiber (EDF) as a gain medium, 0.5 m long WDM fiber and 110 m long standard SMF. The EDF has a core diameter of 4 μm, NA of 0.16, and erbium ion absorption of 23 dB m^{-1} at 980 nm. The cavity length was 112.5 m with net cavity dispersion of - 2.356 ps^2. The group velocity dispersion of the EDF, WDM and SMF were 27.6, −48.5 and −21.7 ps^2/km, respectively. Pump light at 980 nm was injected from a laser diode (LD) into the cavity via the WDM. An isolator (ISO) was used to prevent light reflection, and an 80:20 optical coupler was used to couple out 20% of intra-cavity power. The output optical spectrum, RF spectrum, oscilloscope traces and pulse width were observed by optical spectrum analyzer (OSA) with a spectral resolution of 0.07 nm, RF spectrum analyzer (RFSA) (Anritsu MS2683A), real-time oscilloscope (OSC) (GW INSTEK GDS-3352, 350 MHz bandwidth with 1.2 GHz photodetector) and an autocorrelator, respectively.

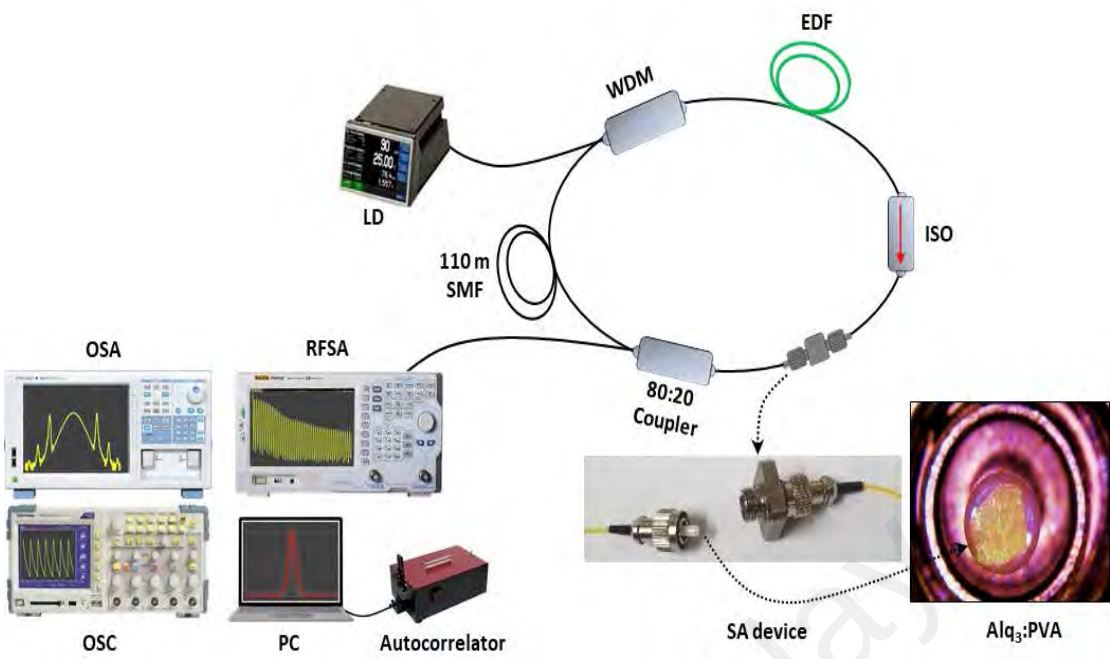

Figure 5.15: EDFL cavity setup with Alq_3 SA as a mode-locker

5.4.2 1.6 Picosecond Mode-Locked Pulse Generation

The proposed Alq_3 based EDFL produced a CW operation at an input LD power of 10 mW, while the mode-locked operation was obtained and sustained as the LD power increased from 25 mW to 274 mW. When the LD power raised to its maximum of 350 mW, the mode-locked operation was disappeared, i.e. the CW operation was observed again in which no pulsing was observed in the oscilloscope and the soliton shape turned into single peak centred at 1561.5 nm wavelength. As we reduced the LD power below 274 mW, the mode-locked pulsing was produced again. Hence, the damage threshold of the proposed soliton laser was confirmed to be above 350 mW. It is believed that if the LD power has damaged the SA, there is no mode-locking operation can be produced when the LD power was reduced back in the range between 25 mW to 274 mW. However, this is not the case in our observation. The reason for the switching in the laser regime is attributed to the SA was fully saturated. In another experiment, the Alq_3: PVA film has been removed from the cavity to verify that Alq_3 caused the pulsing operation. In this case, no pulsing was observed despite tuning the LD power over a wide range and

changing the polarization inside the cavity by twisting and bending optical fibers. By inserting the Alq_3: PVA back into the fiber laser cavity, the mode-locking pulses was observed again. It is concluded that Alq_3 was purely responsible for the mode-locking operation rather than other components. The output optical spectrum of the pulsing operation showed that the fiber laser produced a soliton mode-locking regime, see Figure 5.16. The spectrum shows a typical soliton-like shape with symmetrical Kelly sidebands centred at 1561.5 nm. The separation between the central wavelength and the 1st, 2nd and 3rd order Kelly sidebands are ± 2.55 nm, ± 3.95 nm and ± 4.94 nm, respectively. The autocorrelation trace of the mode-locking operation is given in Figure 5.17. The pulse width has T_{FWHM} of 1. 6 with an estimated TBP of 0.350. The TBP is higher than the transform-limited prediction of 0.313, showing that the pulses were chirped. The minimum possible pulse width duration (calculated mathematically) is ~ 1.43 ps.

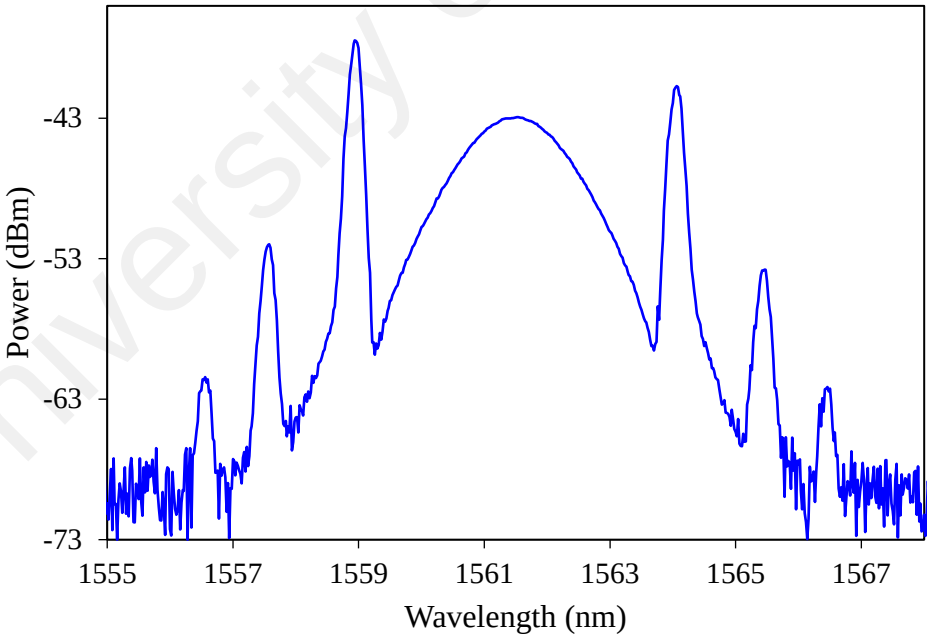

Figure 5.16: Output spectrum from the proposed Alq_3 based mode-locked EDFL

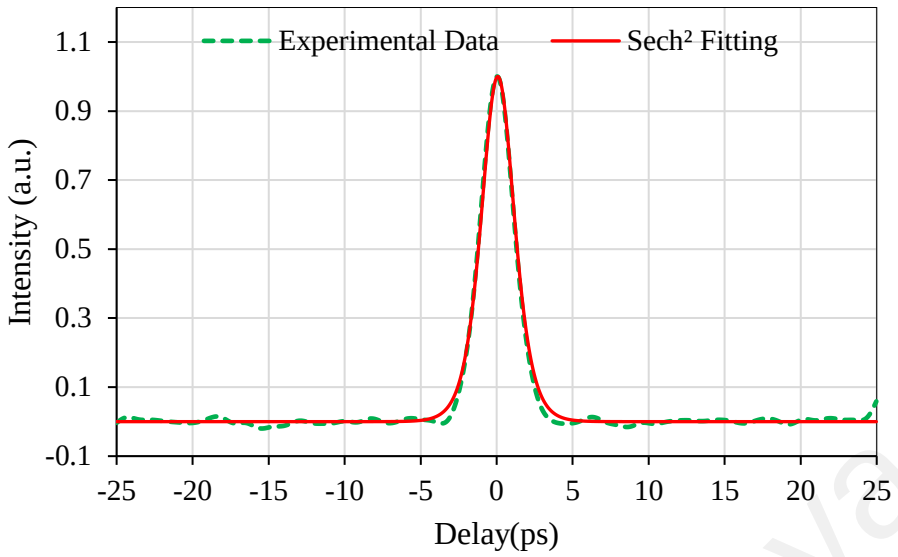

Figure 5.17: Autocorrelator trace of the mode-locked pulses from the Alq_3 based EDFL

Figure 5.18 (a) shows the measured RF spectrum within a span of 80 MHz, which indicates the fundamental frequency operates at a repetition rate of 1.8 MHz with a signal to background noise ratio (SNR) of 41.5 dB. The spectrum also shows a high cavity harmonic as well as a high spectral purity without significant spectra modulation, which proves the stability of the mode-locking operation. The output pulse energy and output power against the input LD power are given in Figure 5.18 (b).

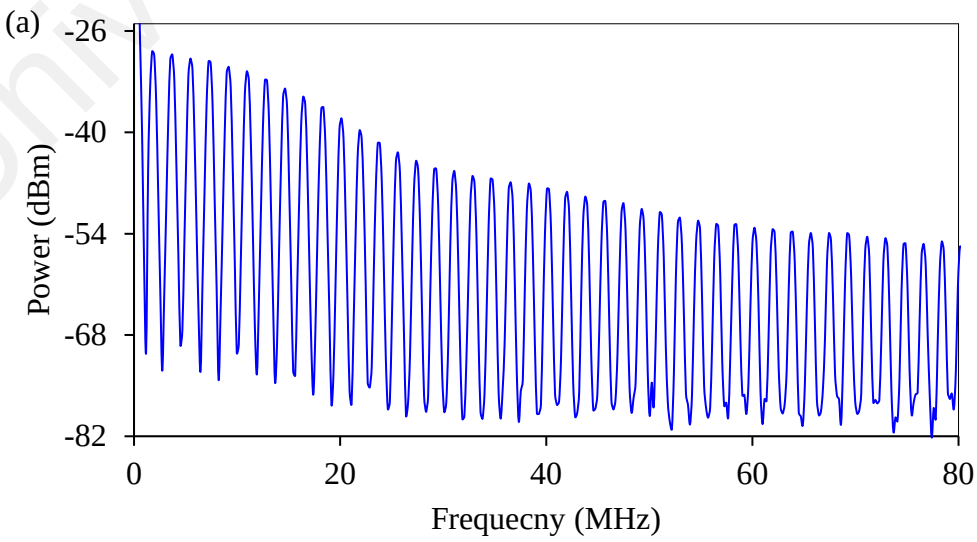

Figure 5.18: (a) RF spectrum of the proposed Alq_3 based mode-locked EDFL and (b) pulse energy and output power as a function of input LD power

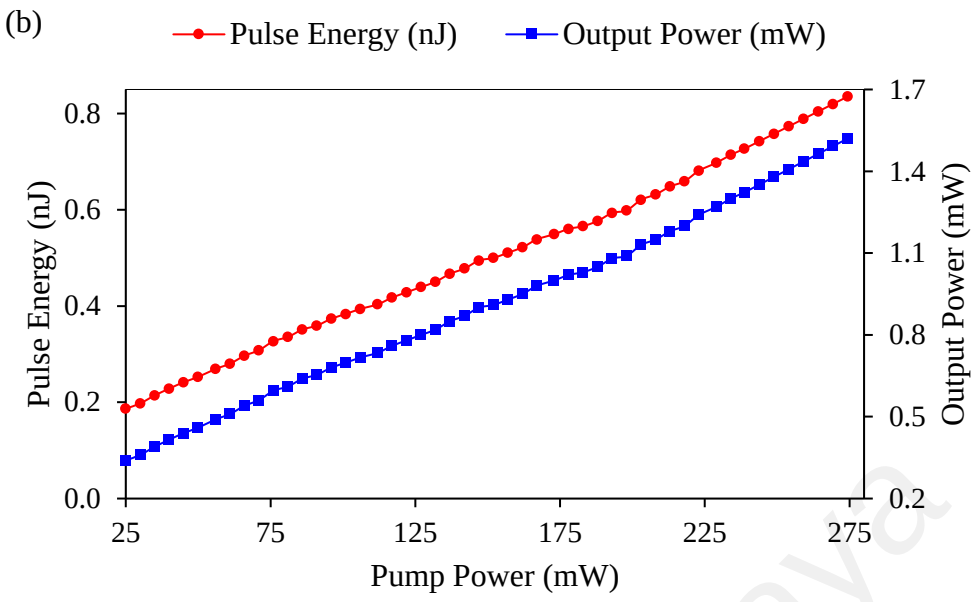

Figure 5.18, continued

As the LD power was tuned from 25 mW to 274 mW, the pulse energy can be raised linearly from 0.19 nJ to 0.84 nJ and the output power increased from 0.34 mW to 1.52 mW. The oscilloscope was used to check the temporal pulse train as shown in Figure 5.19. The pulse train has a very uniform distribution, which indicates that the laser operation was very stable. The pulse period was measured to be 545 ns, which it is in coincident with the pulse repetition rate and cavity length.

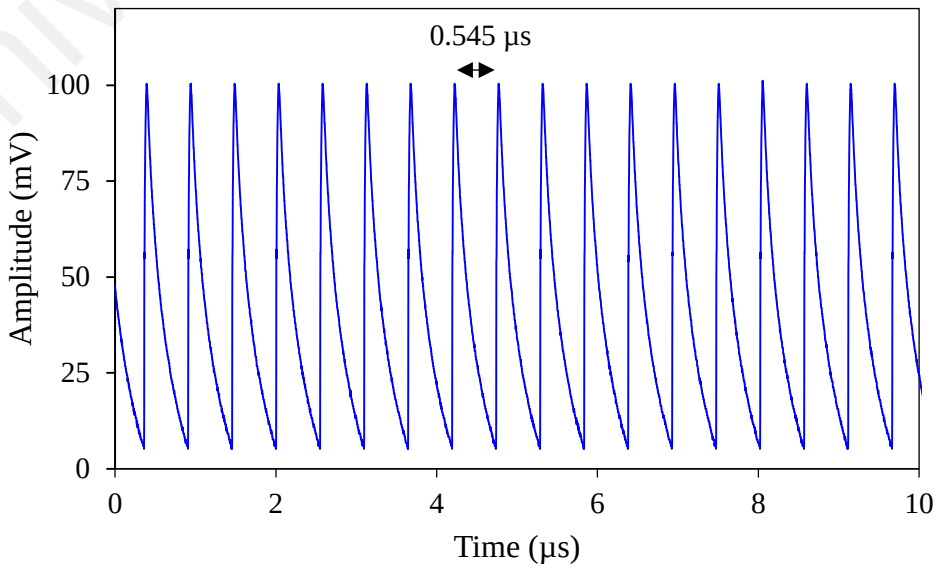

Figure 5.19: Output pulse train of mode-locked laser based on Alq_3 as SA

The pulse train showed a sawtooth-like aspect, this is attributed to the noise produced by photo-detector attached to the oscilloscope. This assumption agrees with the high SNR and the short pulse width produced by the fiber laser. To check the long-term operation of Alq_3: PVA SA, the optical spectrum was sampled every ~ 42 minutes for 420 minutes, as shown in Figure 5.20. The figure depicts a very stable operation in which all the samples had the same central wavelength and the amplitude of 1561.5 nm −42.9 dBm, respectively. Additionally, the samples show that the Kelly sidebands kept the same optical intensity and wavelengths throughout the sampling process, in which the 1st order had intensities of −37.6 dBm and −40.83 dBm (at 1558.95 nm and 1564.05 nm), the 2nd order had intensities of −52.0 dBm and −53.83 dBm (at 1557.55 nm and 1565.45 nm) and 3rd order had intensities of −61.6 dBm and −62.26 dBm (at 1556.56 nm and 1566.44 nm), respectively. This further proves the stability of the mode-locking operation and indicates that Alq_3: PVA can provide the same performance and can also withstand a long-term illumination. It should be mentioned that a mode-locked operation with a wider pulse width duration and lower repetition rate was achieved with a longer cavity length. It is believed that by further decreasing the cavity length, an enhanced fiber laser operation can be obtained.

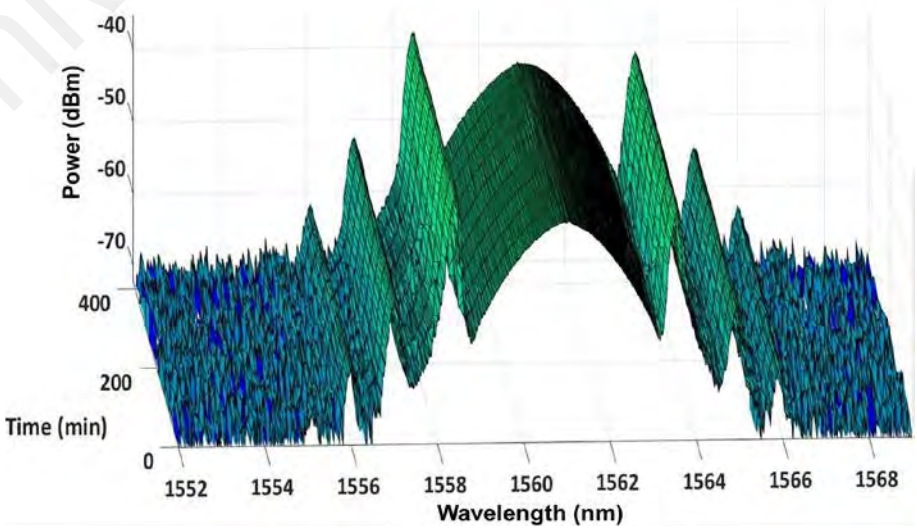

Figure 5.20: Output optical spectrum sampled for 420 minutes

5.4.3 1.26 Picosecond Mode-Locked Pulse Generation

In this subsection, the performance of the Alq_3 based mode-locked EDFL is investigated by reducing the cavity length from 112.5 m to 61.5 m. It was obtained by removing 50 m long SMF from the previous experimental setup. A self-starting soliton mode-locking was produced at 61 mW and the operation was sustained as the input power is increased up to 183 mW. Figure 5.21 (a) illustrates the output pulse train of the fiber laser. The peak to peak spacing is about 297.5 ns, which is equivalent to the cavity round-trip time and pulse repetition rate of 3.36 MHz and coincides with the estimated fundamental frequency of the cavity. The oscilloscope gave a much wider pulse duration (107.1 ns) than the actual value, which is due to the limited resolution of the oscilloscope. It can be observed that the pulse train has a very uniform pulse amplitude which indicates a stable mode-locking operation. To measure the pulse duration accurately, we used a highly-sensitive auto-correlator to measure the autocorrelation trace, see Figure 5.21 (b). The pulse width has T_{FWHM} of 1.26 ps as estimated from the FWHM duration of the autocorrelation trace (Tac) of 1.95 ps and assuming $sech^2$ curve fitting. The TBP is calculated to be 0.324, which is slightly deviated from the transform-limited TBP of 0.315, suggesting that the pulse was slightly chirped in which the theoretical pulse-width was calculated to be 1.22 ps. Figure 5.21 (c) illustrates the relation between LD power versus average output power and output pulse energy. The result depicts that as the LD power increases, the average output power raises linearly from 0.98 to 1.87 mW. The figure also shows the linear increment of pulse energy; it was raised from 0.29 to 0.56 nJ as the input power was increased. As the LD power was increased to exceed 183 mW up to the maximum available power of 350 mW, the mode-locked EDFL became unstable and disappeared. This is due to the over-saturation of the Alq_3: PVA film. When the pump power was decreased within 61 mW to 183 mW, the mode-locked pulsing was re-produced again, indicating that thin-film was not damaged.

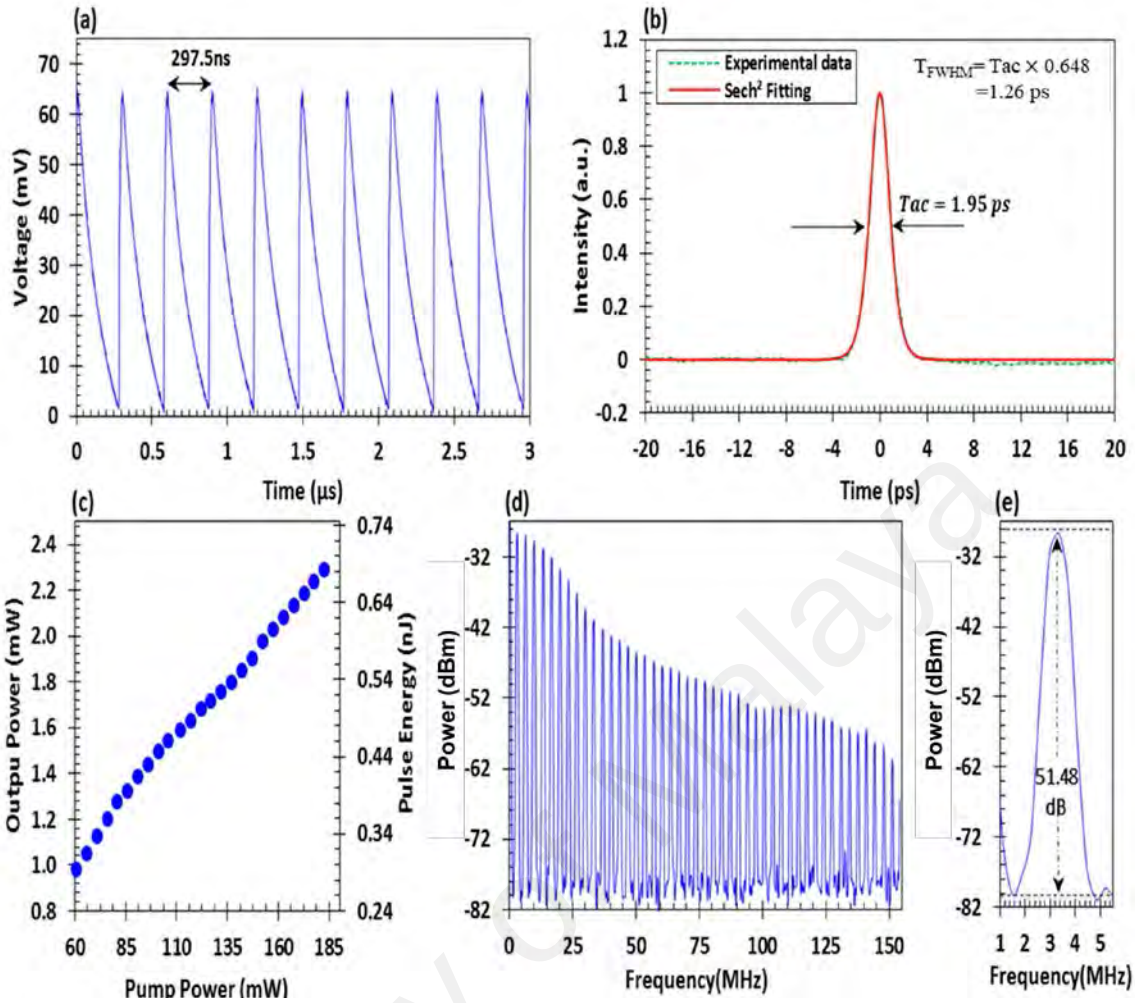

Figure 5.21: Picosecond pulsing laser in 61.5 m cavity length with 80:20 OC: (a) oscilloscope trace of the soliton laser; (b) autocorrelator trace showing a pulse duration of 1.26 ps ; (c) pulse energy and average output power against LD power; RF spectrum with a span of (d) 148 MHz, and (e) 4.5 MHz

To further check the stability of the laser, the RF spectrum was recorded over a span of 148 MHz, as shown in Figure 5.21 (d). The Figure depicts high cavity harmonics without any noticeable instabilities. Additionally, the harmonics decreased relative to the fundamental frequency, proving good mode-locking performance. Figure 5.21 (e) shows the fundamental frequency of 3.36 MHz has a very good SNR of 51.48 dB which further indicates a stable and excellent pulsing operation. The net cavity dispersion in this experiment is anomalous, resulting in soliton mode-locked pulses generation through the interplay of self-phase modulation and group velocity dispersion. This is confirmed by the presence of Kelly sidebands on the spectrum (Lazaridis et al., 1995), see Figure 5.22

(a). The spectrum has a central wavelength of 1561 nm with a 3-dB bandwidth of 2.09 nm. The distance between the centre wavelength and the 1st order Kelly sideband (Δd) is 3.7 nm. The theoretical value for the distance was calculated to be 3.653 nm. This value was obtained or calculated by using the relation between the central wavelength and mth order of the Kelly sideband position as described in the following equation (Smith et al., 1992);

$$\Delta d = \frac{(1.7627)\lambda^2}{2\pi C\,\tau}\sqrt{\frac{4m\pi}{|\beta|}\left(\frac{\tau}{1.7627}\right)^2 - 1} \qquad (5.1)$$

where λ, τ and β are central wavelength, pulse duration and total net dispersion of the cavity, respectively. Figure 5.22 (b) shows the Δd as a function of the pulse duration for 1st, 2nd and 3rd Kelly sideband orders. There is a slight difference between the measured and calculated values of Δλ for the 1st order of the Kelly sideband.

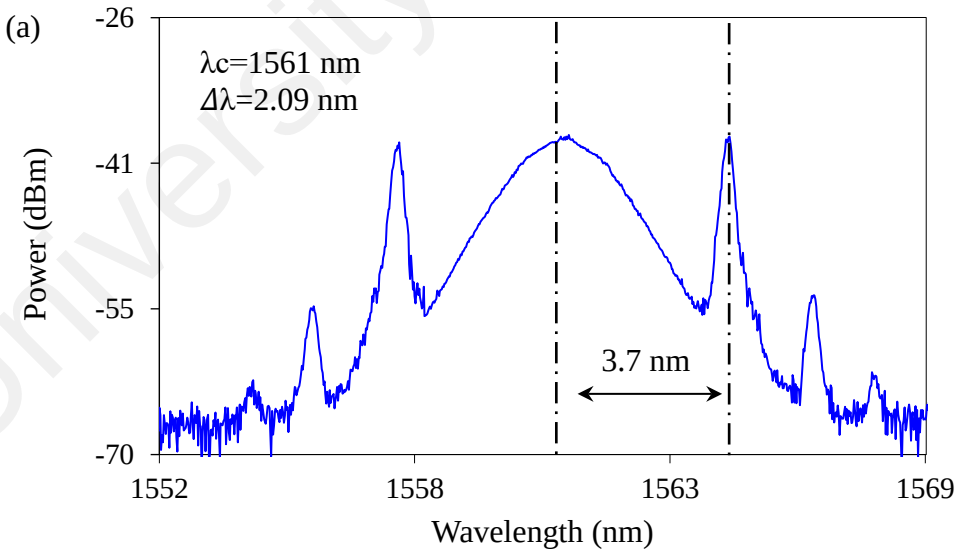

Figure 5.22: Picosecond pulsing laser in 61.5 m cavity length with 80:20 OC: (a) output spectrum; (b) *m*th order Kelly sidebands distance to the centre wavelength versus pulse width at a central wavelength of 1561 nm; and (c) optical spectrum sampled for 220 minutes

(b)

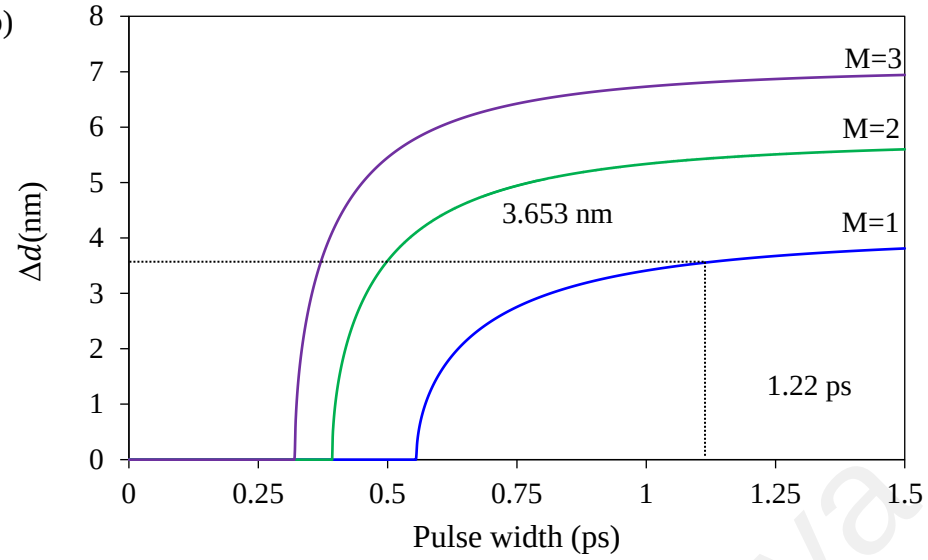

(c)

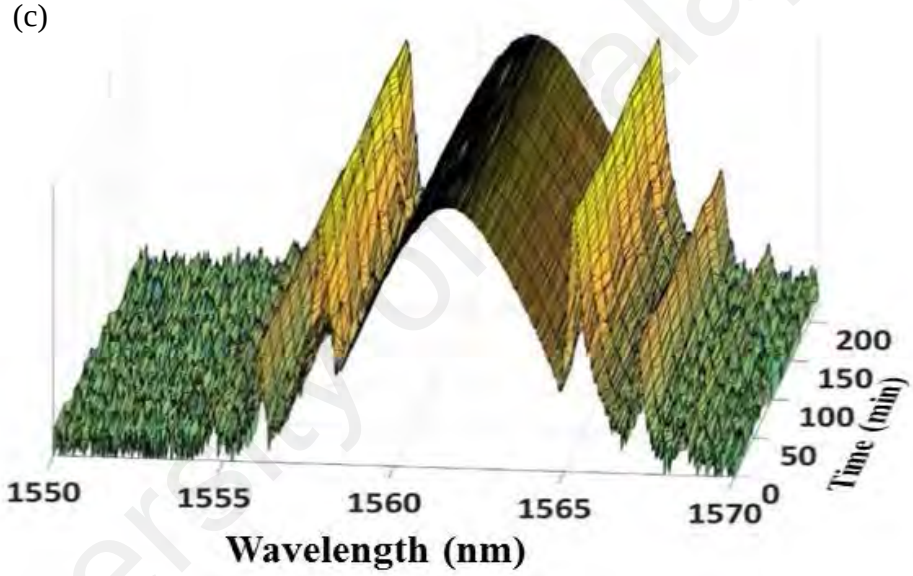

Figure 5.22, continued

The calculated and measured 3-dB values are 2.033 nm and 2.09 nm, which are almost equal. The 3-dB is calculated through

$$\Delta\lambda = \frac{0.315\,\lambda^2}{C\,\tau} \qquad (5.2)$$

Figure 5.22 (c) shows the long-term performance over 220 minutes at input LD power of 183 mW. The shapes of the plotted spectra are almost like one another, further indicating a very stable mode-locked operation.

It should be noted that no mode-locking was generated when we extracted the SA from the cavity or when we replaced the SA with pure PVA film, even though the LD power was tuned over a wide range and the fiber was twisted and bent accordingly in both cases. We conclude that Alq_3 is responsible for the passive mode-locking operation.

5.4.4 970 Femtosecond Mode-Locked Laser Operation

In this experiment, only 80:20 OC was replaced with 95:5 OC, while the rest of the cavity configurations were as the previous setup. The system maintained almost the same performance except that the pulse width and SNR are reduced to 970 fs and 43.3 dB, respectively, see Figure 5.23. The pulse train maintained the same performance, in which no instabilities are observed, as shown in Figure 5.23 (a).In comparison with the previous experiment, the pulse train revealed by oscilloscope had the same pulse width of about 106 ns and the same pulse period of 297 ns. The pulse period also coincides with the fundamental frequency of 3.36 MHz and equivalent to the cavity round-trip, as the cavity length was the same as in the previous experiment.

The pulse width T_{FWHM} was reduced to 970 fs; this reduction in the pulse width is attributed to the utilization of the 95:5 OC. The calculated pulse width is 966 fs, which is almost the same as the measured value as the TBP in this cavity is 0.316. The 95:5 OC extracted a small portion of the signal and increased the oscillating power within the cavity. Correspondingly, the number of modes that can pass through the intensity-dependent transmission mode-locker (the SA) were increased. Hence, the pulse width was reduced, as it is inversely correlated the number of modes that are locked together inside the cavity. Figure 5.23 (b) shows the autocorrelation trace. Like the previous setup, the experimental result is perfectly matched with $sech^2$ fitting, which indicates excellent and stable performance.

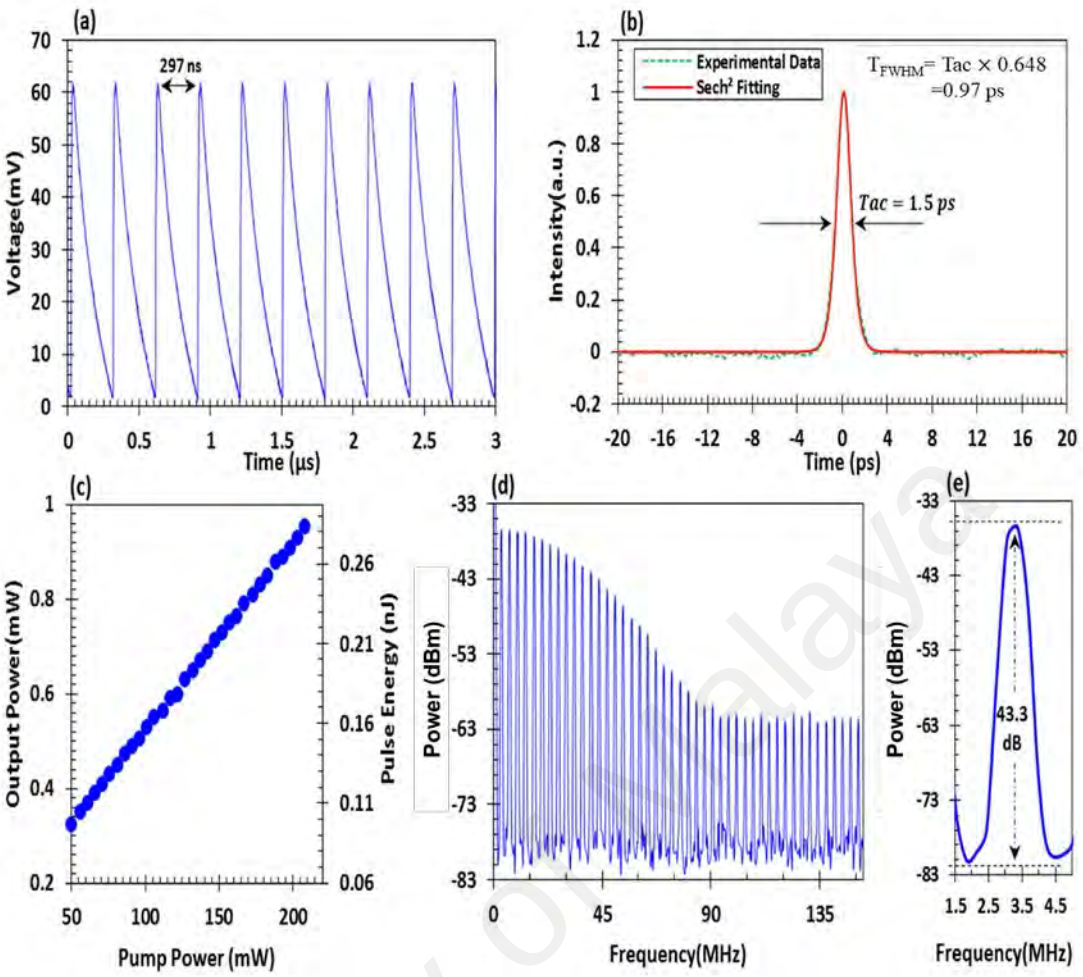

Figure 5.23: Femtosecond pulsing laser in 61.5 m cavity length with 95:5 OC: (a) output pulse train; (b) autocorrelator trace showing a pulse duration of 970 fs ; (c) average output power and pulse energy versus LD power; RF spectrum with a span of (d) 153 MHz, and (e) 3.5 MHz

The output power was reduced as compared with the previous setup since this OC allowed a small portion of the signal to be extracted from the cavity. Correspondingly, the pulse energy was also reduced, as the pulse energy is correlated with average output power. The maximum average output power and maximum pulse energy are about 0.95 mW and 0.28 nJ, respectively, see Figure 5.23 (c). On the other hand, the SNR is reduced to 43.4 dB, which might be attributed to the increase in the non-linearity that is introduced by the 95:5 OC. However, the cavity still produced high harmonics up to 153 MHz, see Figure 5.23 (d). Figure 5.23 (e) shows the fundamental frequency with a span of 3.5 MHz. The output optical spectrum is given in Figure 5.24 (a). In comparison with the previous

experiment, the spectrum is centred at the same wavelength of 1561.1 nm but with a wider 3-dB bandwidth of 2.65 nm. The pulse width is inversely correlated with the 3-dB bandwidth, as indicated by Equ (5.2). As expected, the spectrum showed a reduction in the Δd for the 1st order Kelly sideband, since the pulse width was reduced while the cavity dispersion and central wavelength were maintained as in the previous experiment, see Figure 5.24 (b). The measured and calculated values of Δd were 3.42 nm and 3.357 nm. Figure 5.24 (c) shows the long-term stability of the mode-locking operation. The spectrum was sampled every ~18 minutes for the total duration of 176 minutes. The samples also show a very stable operation.

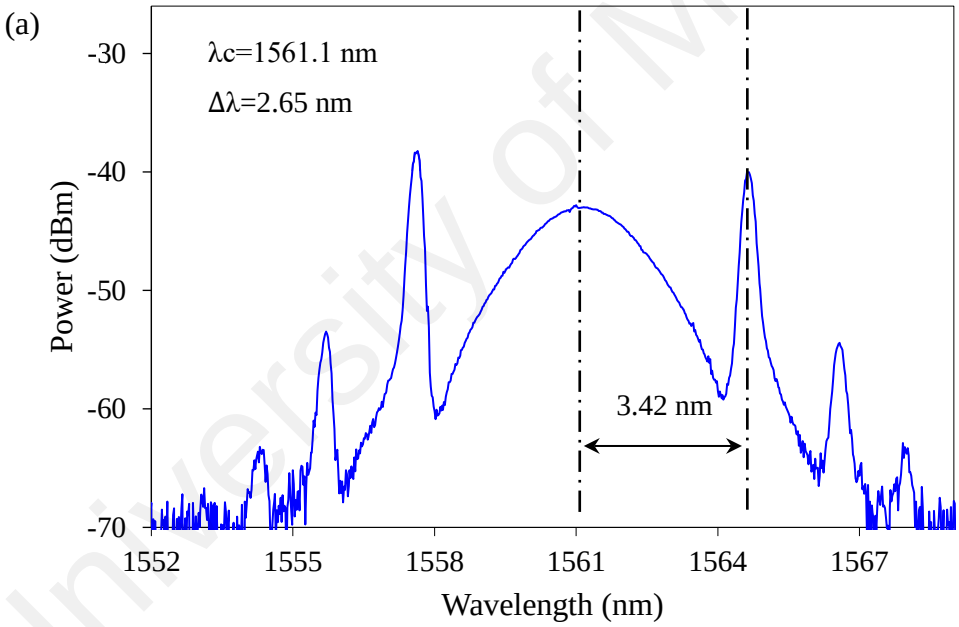

Figure 5.24: Femtosecond pulsing laser in 61.5 m cavity length with 95:5 OC: (a) output spectrum; (b) mth order Kelly sidebands distance to the centre wavelength versus pulse width at a central wavelength of 1561 nm; and (c) optical spectrum sampled for 176 minutes

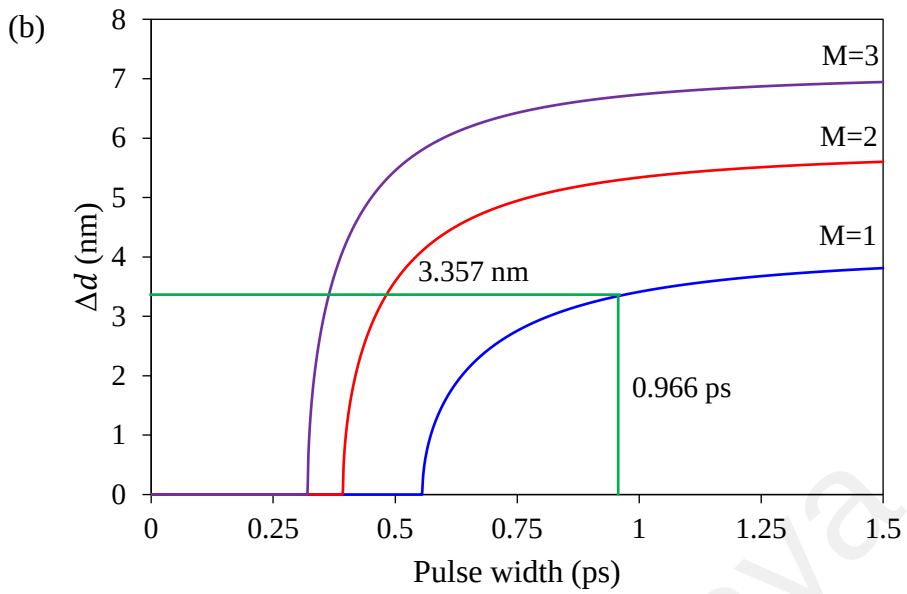

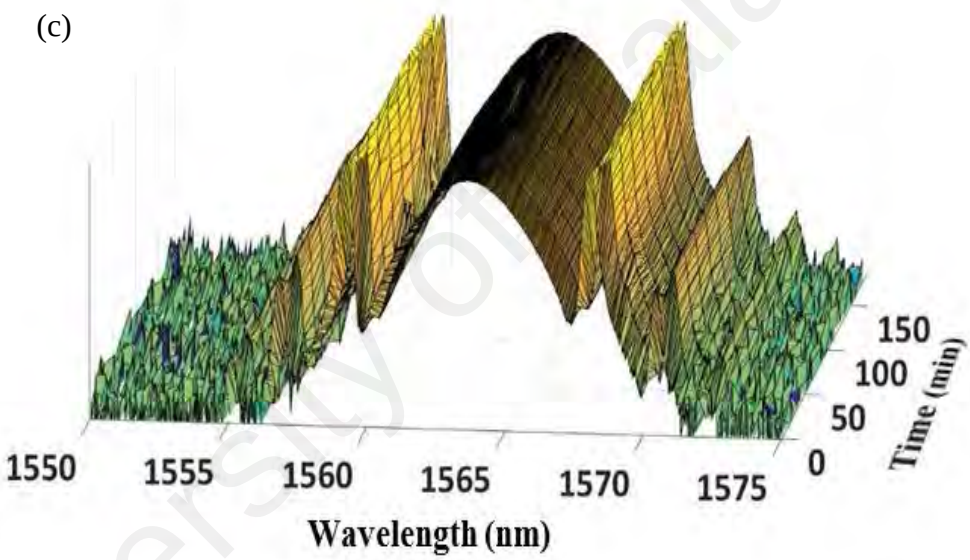

Figure 5.24, continued

5.4.5 820 Femtosecond Mode-Locked Laser Operation

In this experiment, a shorter round trip was facilitated by further reducing the length of SMF spool from 52 m to 32.5 m, and by using 80:20 OC. The total cavity length was 42 m with an estimated dispersion of -0.8262 ps^2. Correspondingly, a soliton mode-locked laser with a wider spectrum, shorter pulse width and higher repetition rate was produced. The mode-locked operation was generated at a pump power range from 71 to 198 mW. Figure 5.25 (a) shows a typical pulse train with uniform pulse shape and period.

The oscilloscope recorded pulse width of 102 ns due to the limited resolution. It should be mentioned that the sawtooth-like pulse train produced by the oscilloscope is attributed to the noise produced by photo-detector. The pulse period is reduced to 205 ns, which correspond to a repetition rate of 4.9 MHz. The pulse width in this experiment has T_{FWHM} of 820 fs, as depicted in Figure 5.25 (b). The output pulse energy and average output power of this laser are presented in Figure 5.25 (c). At LD power of 198 mW, the pulse energy and average output power are 0.46 nJ and 2.27 mW, respectively. The RF spectrum within a span of 148 MHz is given in Figure 5.25 (d), the spectrum reveals a high cavity harmonic. The fundamental frequency of 4.9 MHz is presented in Figure 5.25 (e) with a span of 4.5 MHz. The figure shows a very high SNR value of 51.58 dB.

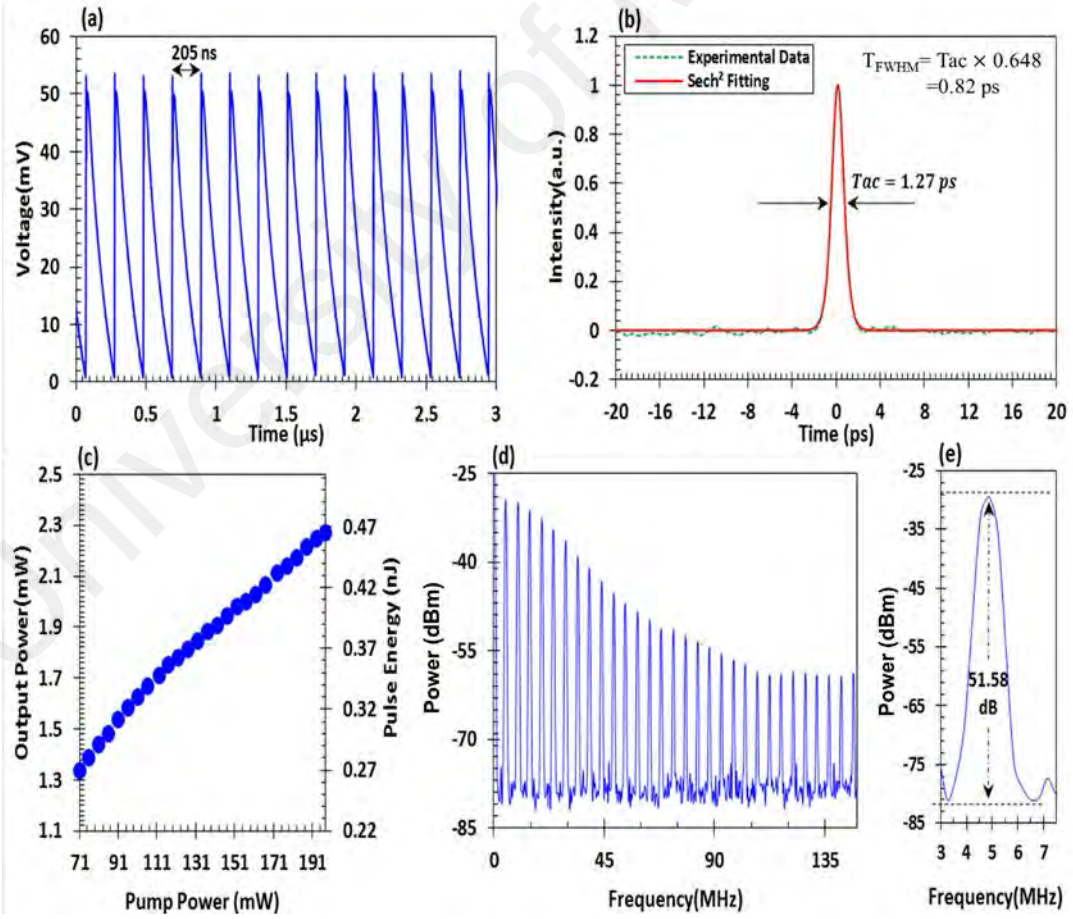

Figure 5.25: Femtosecond pulsing laser in 42 m cavity length with 80:20 OC: (a) oscilloscope trace of the soliton laser, (b) autocorrelator trace, (c) LD power against average output power and pulse energy, (d) RF spectrum with a span of 148 MHz and (e) RF spectrum with a span of 4.5 MHz

Figure 5.26 (a) shows the optical spectrum of the femtosecond mode-locked laser centred at 1560.8 nm, which is almost the same central wavelength as in the previous experiments. The TBP in this experiment is 0.328 which indicates that the output pulses were chirped in which the theoretical pulse duration is calculated to be 0.787 ps, this chirping also results in a difference between the theoretical and measured values of Δd and 3-dB bandwidth (Ausschnitt, Jain, & Heritage, 1979). The Δd value for the 1st order Kelly sideband position was calculated to be 4.129 nm, which differs compared to that of the measured value of 5.28 nm, see Figure 5.26 (b). A wider Δd is obtained in this experiment (even though the pulse duration was reduced), that is due to the increment in the cavity dispersion as compared to the previous experiments. The measured 3-dB bandwidth in this experiment is 3.25 nm, while the calculated value is 3.122 nm. The slight discrepancy is probably due to a small error in the autocorrelation measurement. The optical spectrum was sampled every ~ 30 minutes for 270 minutes, see Figure 5.26 (c).

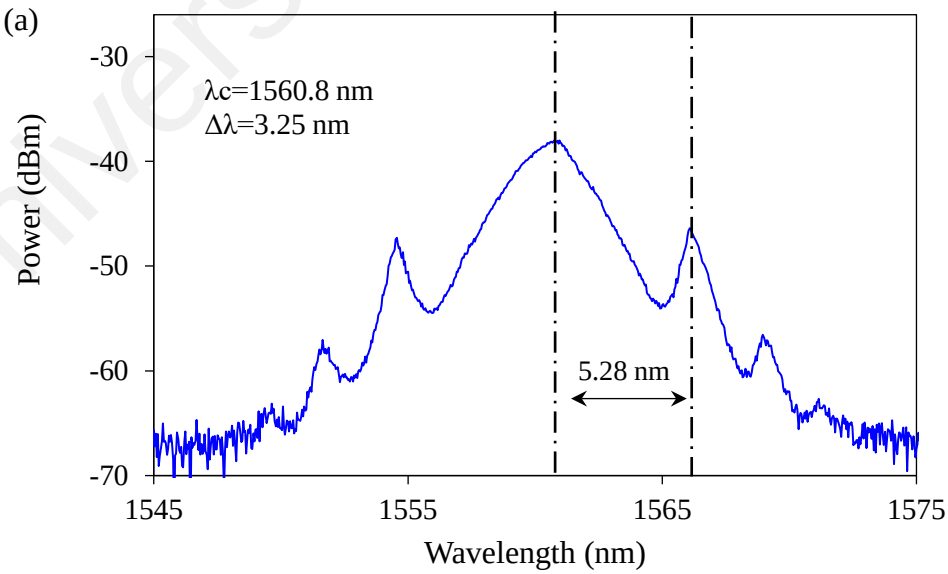

Figure 5.26: Femtosecond pulsing laser in 42 m cavity length with 80:20 OC: (a) output spectrum, (b) mth order Kelly sidebands distance to the centre wavelength versus pulse duration at a central wavelength of 1560.8 nm, and (c) optical spectrum sampled for 270 minutes.

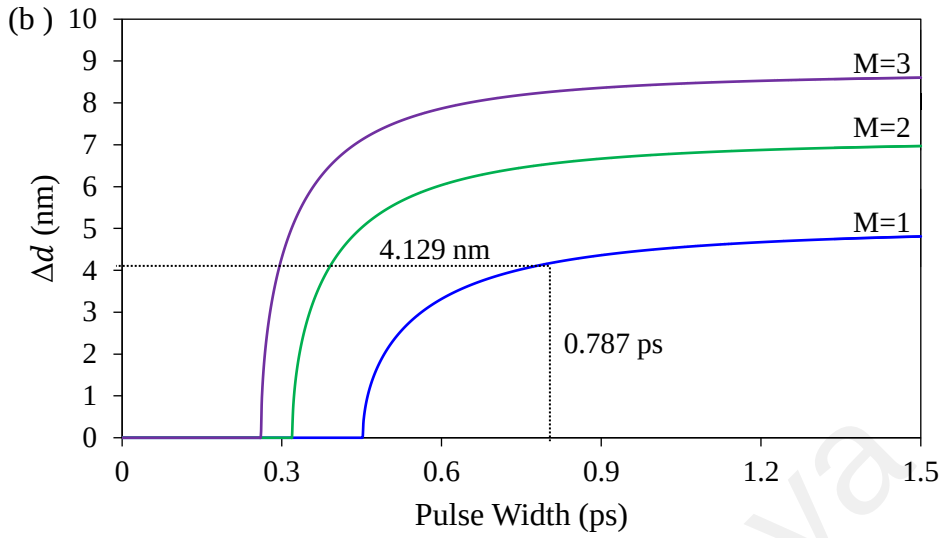

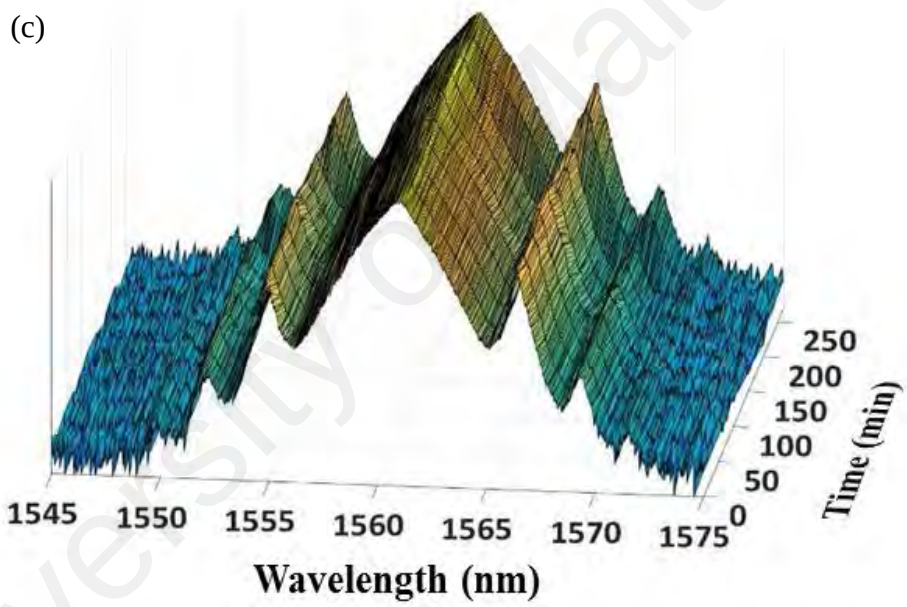

Figure 5.26, continued

Like the previous experiments, the mode-locked laser showed a very stable performance in which the intensity, peak locations and spectral bandwidth were very stable. It is believed that shorter pulse duration, higher repetition rate and higher pulse energy can be delivered if shorter cavity length is addressed along with a higher gain medium. This work demonstrated that Alq_3 has great potentials in ultrafast fiber lasers.

5. 5 Mode-Locked Laser at 1066 nm by Using Alq_3 as SA in a YDFL Cavity

As explained in chapter 3, the SA was synthesized through the drop-casting method, in which the Alq_3 powder was embedded into PVA. The produced SA thin-film had modulation depth, saturation intensity, linear transmission and thickness of 8.1%, 3 MW/cm^2, 98% (in the range from 900–1600 nm) and 50 μm, respectively. A small piece of the thin-film was then inserted between two FC/PC to form the mode-locker device. The experimental setup of the proposed Alq_3 based ytterbium-doped fiber laser (YDFL) is shown in Figure 5.27. The SEM image of the SA is shown in the inset of Figure 5.27. A 980 nm LD was used to lunch power to the cavity through a 980/1064 WDM coupler. A 1.5 m long single-mode ytterbium-doped fiber (YDF) (with an ion-absorption of 280 dB/m at 920 nm and cut-off wavelength of 1010 nm) was used as a gain medium. A 20-meter SMF was added to the cavity to manage the dispersion regime. The total length of the cavity was around ~28 m. A 50:50 optical coupler was used to extract 50% of the signal from the cavity, and an optical isolator (ISO) was addressed to prevent light reflection. Additionally, a polarization controller (PC) was used in the cavity. The optical spectrum, RF spectrum and optical pulse train were monitored using the OSA, RF spectrum analyzer, and digital oscilloscope, respectively.

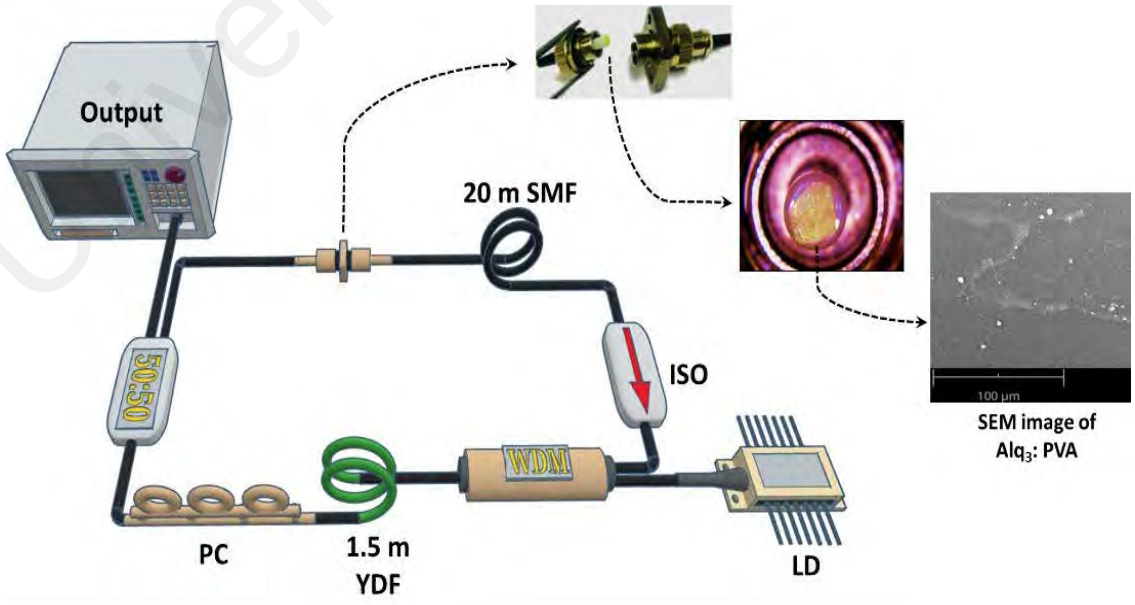

Figure 5.27 Fiber laser cavity

The mode-locked operation was easily achieved when the SA was incorporated into the cavity. At first, a continuous lasing was produced at a threshold power of 50 mW. Then by increasing the power to range between 133 mW - 249 mW, a stable and self-started mode-locked operation was observed with a pulse repetition rate, central wavelength and 3-dB bandwidth of 6.84 MHz, 1066.2 nm and 0.2 nm, respectively. Figure 5.28 (a) shows the output pulse train at maximum power, the pulse width given by the oscilloscope is ~ 62 ns. Which is much wider than what we expect, this is attributed to the limited resolution of the oscilloscope. The pulse train indicates a very stable performance, in which there is no instabilities, nor distortion on the pulse train. The inset figure shows a pulse train with a shorter span of 0.57 µs. As shown in Figure 5.28, the period is ~146.5 ns, which is in coincident with the pulse repetition rate and cavity length. The pulse-width can be found by using the TBP formula. The calculated pulse width is 5.96 ps with TBP of 0.315 for $Sech^2$ pulse profile. Figure 5.28 (b) presents the RF spectrum with span up to 377 MHz and a resolution bandwidth of 300 kHz. The fundamental frequency is located at 6.84 MHz with an SNR of 74 dB, which indicated excellent stability of the fiber laser. The output power and pulse energy of the fiber laser were relatively high, see Figure 5.28 (c).

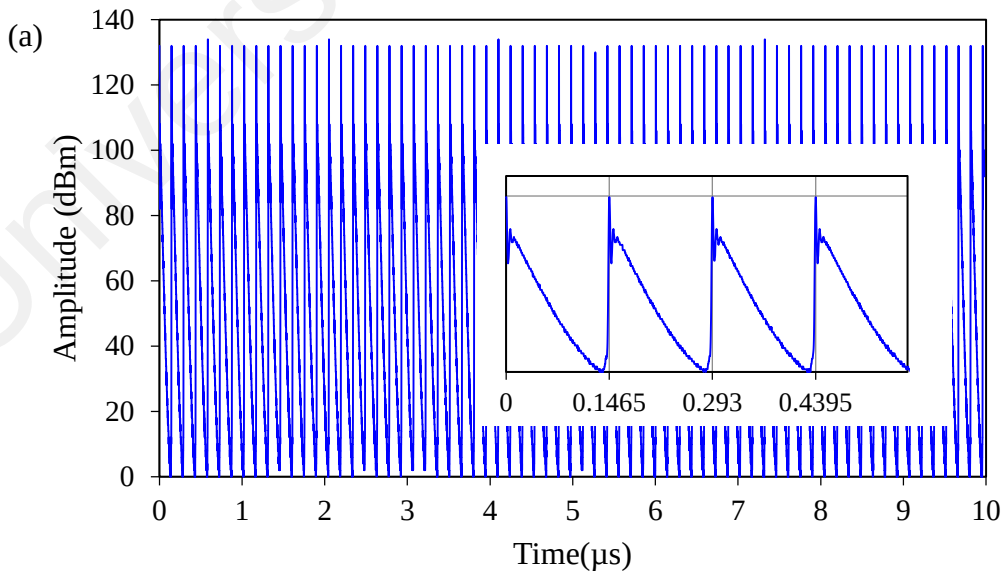

Figure 5.28: (a) Typical pulse train and (b) RF spectrum of the laser and (c) output pulse energy and average output power versus LD power

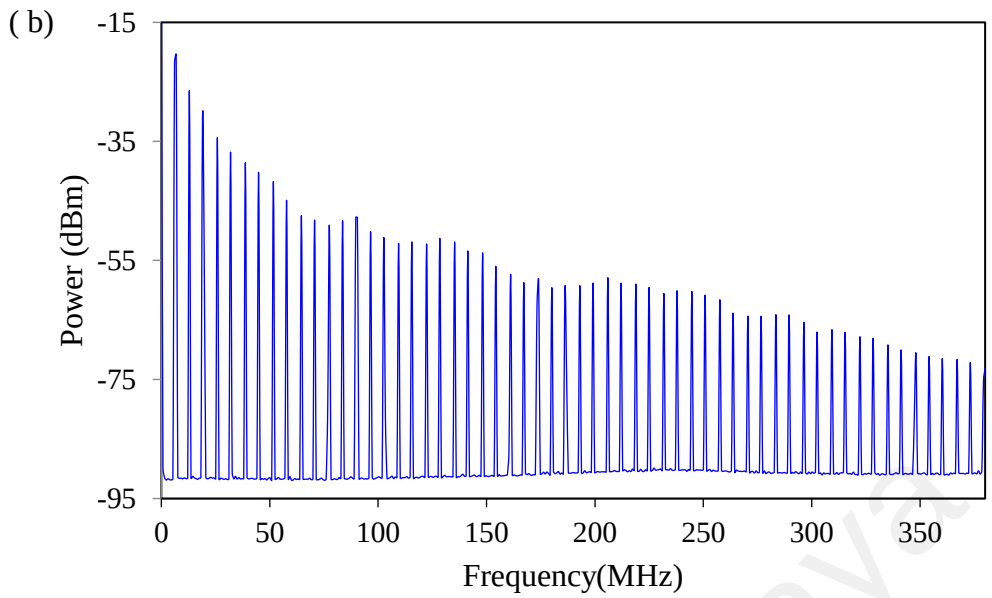

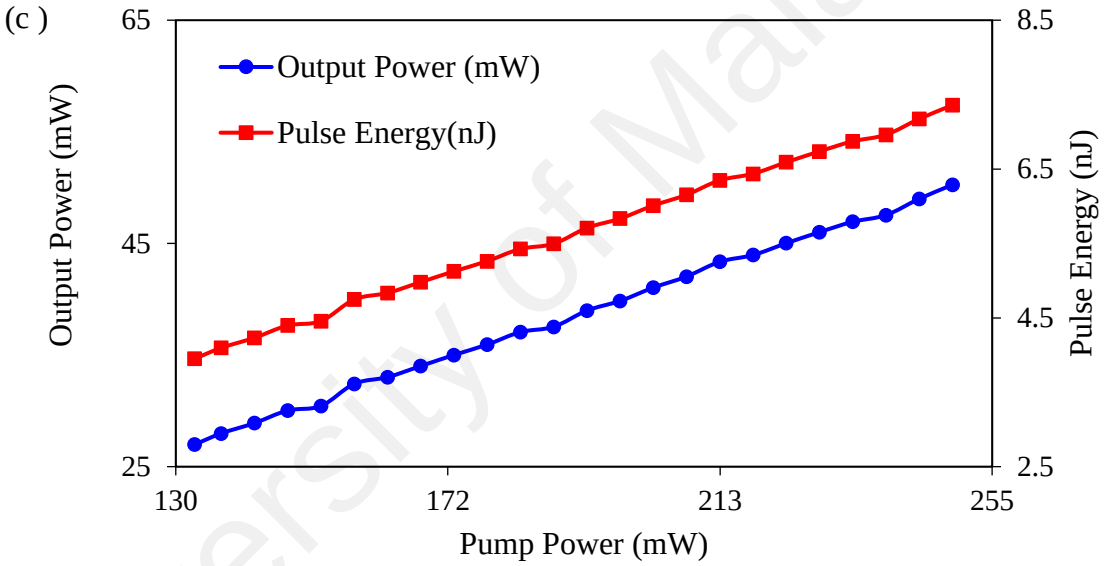

Figure 5.28, continued

The average output power raised linearly from 27mW to 50.2mW with a slope efficiency of 19.7 %. While the highest pulse energy was 7.35 nJ. The output spectrum of a single wavelength mode-locking operation is shown in Figure 5.29 (a). The figure shows the optical spectrum has a peak at 1066.2 nm with a 3-dB spectral bandwidth of 0.2 nm. The system produced the same performance during ~6 hours experiment, which further indicates the stability of the system. A polarization-dependent loss could be generated by squeezing and tuning the PC. Combining that with that cavity birefringence,

a spectral filter could be developed, which could be used to achieve a multi-wavelength pulsing operation (H. Zhang, Tang, Wu, & Zhao, 2009). Therefore, a multi-wavelength operation was obtained by carefully tuning the PC. Figure 5.29 (b) shows the spectrum of a multi-wavelength mode-locked laser. The peaks are located at ~1060.9 nm, 1063.6 nm, 1066.3 nm, 1069 nm, 1071.7 nm, 1074.4 nm and 1077.1 nm with intensities of −27.7 dBm, −12.1 dBm, 6.7 dBm,4.9 dBm, −6.7 dBm, −17.64 dBm and −30.5 dBm, respectively. The peaks are 2.7 nm (∓.05 nm) apart. The operation can be sustained for a long time, given that no environment perturbations applied to the laser. The output pulse train maintained the same performance on the oscilloscope in terms of pulse width and pulse period. The motivation of this work is to draw attention to the potentials that organic materials have as mode-locker in 1.0 µm region. As this is first-time, to the best of our knowledge, that Alq_3 is used as mode-locker in 1.0 µm region. The all-fiber based ring cavity produced a very high output power and high peak power of 57 mW and 1.4 kW, respectively. The RF spectrum showed the laser had a very high SNR of 74 dB, which shows an excellent performance by the laser.

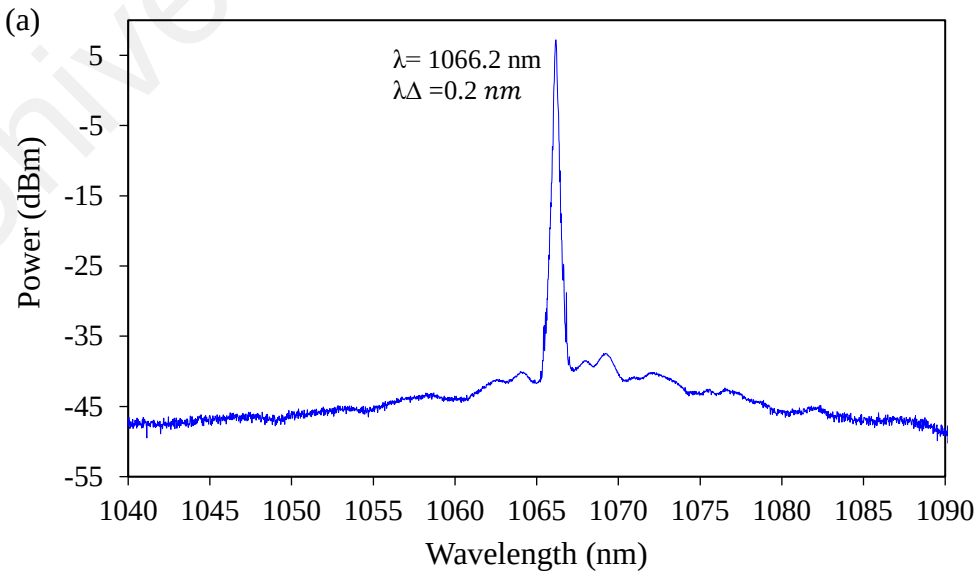

Figure 5.29: Laser output spectrum (a) narrow spectrum and (b) broadened spectrum.

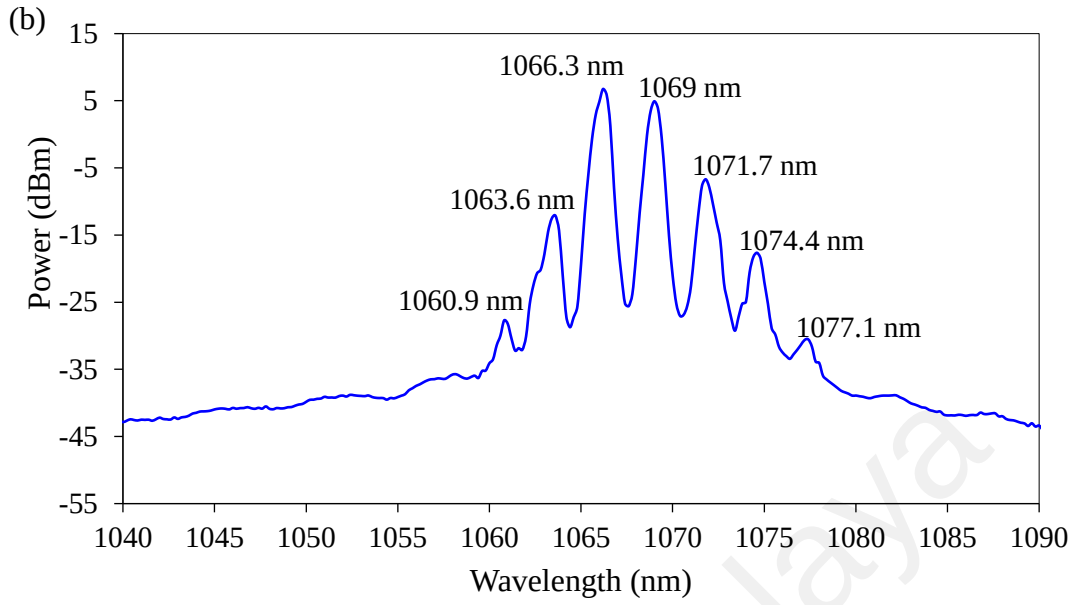

Figure 5.29, continued

5. 6 Summary

Different types of mode-locked lasers were successfully demonstrated by using organic materials as the SA. In the first part, a mode-locked laser was produced by using FIrpic as SA. The repetition rate and pulse width are 3.43 MHz and 120 ns. Then Znq_2 was used to produce another mode-locked laser with enhanced performance. In this case, the pulse width and repetition rate were 1.46 ps and 3.5 MHz. A dark pulses mode-locking operation was also realized by appropriately managing the polarization state of the cavity. Furthermore, a supercontinuum light generation was also successfully demonstrated by launching the output pulses from the Znq_2 based mode-locked EDFL into a 100 m long PCF. This process resulted in reducing the pulse width to 640 fs. Ultrafast lasers were also demonstrated by using Alq_3 SA in four different configurations. These lasers produced pulse width/ repetition rate of 1.6 ps / 1.8 MHz, 1.26 ps / 3.36 MHz, 970 fs / 3.36 MHz and 820 fs / 4.9 MHz by using cavity length /optical coupler (OC) of 112.5 m / 80:20 OC 61.5 m / 80:20 OC, 61.5 m / 95:5 OC and 42 m / 80:20 OC, respectively. All

configurations produced a soliton laser with a very stable mode-locking operation operating at a central wavelength of ~1561 nm. The results presented in this chapter show that the developed organic materials based SAs have a very high potential to be used in fiber laser technology. In the last part of this chapter, high output power mode-locked YDFL was also demonstrated to operate at 1066.2 nm with a pulse width and repetition rate of 5.96 ps and 6.84 MHz, respectively. The SNR produced by this laser is very high (74 dB). In short, different types of mode-locked fiber lasers were successfully produced in this chapter with a simple and straightforward fabrication process as this work is attended to draw the attention of organic materials in fiber laser technology. This is the first time that FIrpic, Znq_2 and Alq_3 have been used in fiber laser technology, to the best of our knowledge. Table 5.1 presents the performance of different mode-locked lasers by using the developed SAs.

Table 5.1: Performance of mode-locked fiber lasers by using the developed SAs

Section in the thesis	Cavity length (m)/ coupler	3-dB (nm)	Wave-length (nm)	Pulse Width (ps)	Repetition rate (MHz)	SNR (dB)	SA
5.2	60/99:1	1.8	1562.57	120 ns	3.43	38.3	FIrpic
5.3.1	59.5/90:10	2	1560.6	1.46	3.5	60.6	Znq_2
5.4.2	112.5/ 80:20	1.6	1561.5	1.6	1.8	41.5	Alq_3
5.4.3	61.5/ 80:20	2.09	1561.5	1.26	3.36	51.48	
5.4.4	61.5/ 95:05	2.65	1561.1	0.97	3.36	43.3	
5.4.5	42/ 80:20	3.25	1560.8	0.82	4.9	51.58	
5.5	28/50:50	0.2	1066.2	5.96 ps	6.84	74	

CHAPTER 6: CONCLUSION AND FUTURE WORK

6. 1 Conclusion

There is strong motivation to find new materials to be used as a high-performance SAs, as the rapid development of SAs has provided several new opportunities for nonlinear optics. In that regard, organic materials have the advantages of large and ultrafast nonlinear response and broad spectral tunability. Moreover, they offer mechanical flexibility, light-weight and low production cost, additionally, organic materials could increase the applications in biomedical laser processing and sensing as they are (in general) non-hazardous and environmentally-friendly materials. These materials, in comparison to inorganic materials, require simple fabrication and offer versatile molecular design. Despite numerous works reported on the use of organic materials in the linear regimes and in a relatively low power domain, the applications of organic materials in nonlinear optics, especially in the fiber lasers pulse generation, have yet to be fully explored.

The goal of this research work is to draw attention to the potentials that organic materials have in fiber laser technology. Organic materials used in this work produced very interesting results for different types of pulsed fiber lasers. This work involved the fabrication and characterization of newly developed passive SAs based on organic materials, these materials are FIrpic, Znq_2 and Alq_3. In chapter 3, the fabrication and characterization of these materials have been thoroughly described. The fabrication process was straight forward, simple and low-cost where PVA was used to form thin-films. PVA is a suitable host to produce high-performance SA due to its favourable physical properties such as biocompatibility and good chemical resistance. Additionally, PVA has excellent film-forming, mechanical and adhesive properties. Then these SAs thin-films were characterized in terms of FTIR, SEM image, linear and non-linear absorptions. The FIrpic, Znq_2 and Alq_3 have a saturation intensity of 5.5 MW/cm^2, 103.6 MW/cm^2, 3 MW/cm^2 and modulation

depth of 12.8%, 17.6% and 8.1% and linear absorption of ~ 2 dB, 1.2 dB and 2 dB at the region of 1550 nm, respectively.

Different types of passive Q-switched fiber laser were successfully developed at 1.5 µm region. FIrpic based SA was used to generate Q-switched pulsing operation with a single and dual-wavelength operation. A stable Q-switched laser operating at 1560.4 nm was achieved at a threshold pump power of 30 mW. The pulse repetition rate increased from 39.22 to 87.4 kHz and the pulse width decreased from 9.5 to 3.4 µs as the pump power was gradually increased from 30 to 208 mW. Znq_2 were used to demonstrate Q-switched pulsing operation covering almost all the C-band region. The produced pulse width was decreased from 6.6 µs to 2.8 µs as the LD power increased, while the repetition rate was increased from 45 kHz to 86 kHz as the pump power was increased to 198 from 38 mW. Then a tunable bandpass filter was used to induce a tunability on the output wavelength. Correspondingly, the wavelength was shifted continuously and covered almost all the C-band region from ~1520 nm to ~1563 nm. Furthermore, Alq_3 was used to generate a Q-switched laser operating at 1559 nm. The generated pulse train was stable and has a pulse width decreased from 6.65 to 1.2 µs and the pulse repetition rate increased from 31.65 to 144.5 kHz as the pump power increased from 20 to 122 mW. The potential of organic materials for generating Q-switching at 1067 nm was also confirmed. Alq_3 was used in an ytterbium-doped fiber laser cavity and produced high pulse energy of 0.8 µJ and high peak power of 90 mW. When the laser cavity was reduced from 25 m to 5 m, the peak power increased and the pulse energy dropped to 237.62 mW and 451.5 nJ, respectively. Additionally, the minimum pulse width was reduced from 9 µs to 1.9 µs.

Chapter 5 was set to address the potentials of the proposed organic materials in generating ultrafast mode-locked fiber lasers. FIrpic based SA has successfully produced a soliton mode-locking pulses at a wavelength of 1562.57 nm. The mode-locked laser had a repetition rate of 3.43 MHz and a pulse width of 120 ns within the pump power of 35–

188 mW. On the other hand, Znq_2 was used as a mode-locker to generate a dark and white mode-locking operation. The pulse width and the repetition rate in the white mode-locked laser were 1.2 ps and 3.5 MHz, respectively. Furthermore, Znq_2 were used to generate a supercontinuum light by incorporating 100 m long PCF at the output of the cavity. Finally, several mode-locking operations were demonstrated by using Alq_3 as SA. By incorporating Alq_3 into the fiber laser cavity, a stable pulsing was achieved. The laser pulses have a pulse width of 1.6 ps with a soliton spectrum centred at 1561.5 nm. The pulses train exhibits a very stable output with a high signal to noise ratio (SNR) of 41.5 dB in 112.5 m cavity with 80:20 optical coupler. The pulse width / repetition rate changed to 1.26 ps/3.36 MHz, 970 fs/3.36 MHz and 820 fs/4.9 MHz by changing the cavity length /OC to 61.5 m/80:20 OC, 61.5 m /95:5 OC and 42 m/ 80:20 OC, respectively. The Alq_3 was used to develop ultrafast fiber laser at 1066.2 nm with a pulse width and repetition rate of 5.96 ps and 6.84 MHz, respectively. The SNR produced by this laser is significantly high of 74 dB which proves the stability of the developed fiber laser.

6. 2 Future Work

All the proposed objectives have been successfully implemented. However, the demonstration of the organic materials in pulsed fiber laser technology can be further explored. Further work should be devoted to enhancing the performance of the proposed fiber laser in terms of shorting the pulse width, increasing the repetition rate and the output power and pulse energy. This can be achieved by addressing a shorter cavity length and enhanced gain medium. Additionally, future work should focus on exploring the developed SAs in other wavelength regions such as 2 µm and 3.5 µm using a different gain medium, this will be a very interesting area to investigate. As to the best of our knowledge, there is no research addressing organic materials-based SA in these wavelength regions. On the other hand, developing a new set of organic material for fiber

laser application will be very interesting research work. As through this thesis, we found that these materials have very attractive performance in fiber laser technology.

REFERENCES

Abdullah, O. G., Aziz, S. B., Omer, K. M., & Salih, Y. M. (2015). Reducing the optical band gap of polyvinyl alcohol (PVA) based nanocomposite. *Journal of Materials Science: Materials in Electronics, 26*(7), 5303-5309.

Adachi, C., Baldo, M. A., Thompson, M. E., & Forrest, S. R. (2001). Nearly 100% internal phosphorescence efficiency in an organic light-emitting device. *Journal of Applied Physics, 90*(10), 5048-5051.

Adachi, C., Kwong, R. C., Djurovich, P., Adamovich, V., Baldo, M. A., Thompson, M. E., & Forrest, S. R. (2001). Endothermic energy transfer: A mechanism for generating very efficient high-energy phosphorescent emission in organic materials. *Applied Physics Letters, 79*(13), 2082-2084.

Adamovich, V. I., Cordero, S. R., Djurovich, P. I., Tamayo, A., Thompson, M. E., D'Andrade, B. W., & Forrest, S. R. (2003). New charge-carrier blocking materials for high efficiency OLEDs. *Organic electronics, 4*(2-3), 77-87.

Ahmad, H., Hassan, S. N. M., Ahmad, F., Zulkifli, M. Z., & Harun, S. W. (2016). Broadband tuning in a passively Q-switched erbium doped fiber laser (EDFL) via multiwall carbon nanotubes/polyvinyl alcohol (MWCNT/PVA) saturable absorber. *Optics Communications, 365*, 54-60. doi:https://doi.org/10.1016/j.optcom.2015.12.004

Ahmad, H., Ismail, M. A., Sathiyan, S., Reduan, S. A., Ruslan, N., Lee, C. S. J., . . . Harun, S. W. J. O. C. (2017). S-band Q-switched fiber laser using MoSe2 saturable absorber. *382*, 93-98.

Ahmad, H., Rahman, M., Sakeh, S., Razak, M., & Zulkifli, M. (2016). Humidity sensor based on microfiber resonator with reduced graphene oxide. *Optik-International Journal for Light and Electron Optics, 127*(5), 3158-3161.

Ahmad, H., Reduan, S. A., Ali, Z. A., Ismail, M., Ruslan, N., Lee, C., . . . Harun, S. W. J. I. P. J. (2016). C-band Q-switched fiber laser using titanium dioxide (TiO_2) as saturable absorber. *8*(1), 1-7.

Ahmad, H., Reduan, S. A., Ruslan, N. E., Lee, C. S. J., Zulkifli, M. Z., & Thambiratnam, K. (2019). Tunable Q-switched erbium-doped fiber laser in the C-band region using nanoparticles (TiO_2). *Optics Communications, 435*, 283-288. doi:https://doi.org/10.1016/j.optcom.2018.11.035

Ahmad, H., Salim, M., Azzuhri, S. R., Soltanian, M., & Harun, S. (2015). A passively Q-switched ytterbium-doped fiber laser based on a few-layer Bi_2Se_3 saturable absorber. *Laser Physics, 25*(6), 065102.

Ahmad, H., Samion, M., Muhamad, A., Sharbirin, A. S., Shaharuddin, R., Thambiratnam, K., . . . Ismail, M. F. (2017). Tunable 2.0 µm Q-switched fiber laser using a silver nanoparticle based saturable absorber. *Laser Physics, 27*(6), 065110.

Ahmad, H., Samion, M. Z., Muhamad, A., Sharbirin, A. S., Shaharuddin, R. A., Thambiratnam, K., . . . Ismail, M. F. (2017). Tunable 2.0 µ m Q-switched fiber

laser using a silver nanoparticle based saturable absorber. *Laser Physics, 27*(6), 065110. Retrieved from http://stacks.iop.org/1555-6611/27/i=6/a=065110

Ahmad, H., Soltanian, M., Narimani, L., Amiri, I., Khodaei, A., & Harun, S. (2015). Tunable S-band Q-switched fiber laser using Bi 2 Se 3 as the saturable absorber. *IEEE Photonics Journal, 7*(3), 1-8.

Ahmad, H., Zulkifli, A. Z., Thambiratnam, K., & Harun, S. W. (2013). 2.0- m Q-Switched Thulium-Doped Fiber Laser With Graphene Oxide Saturable Absorber. *IEEE Photonics Journal, 5*(4), 1501108-1501108. doi:10.1109/JPHOT.2013.2273733

Ahmed, M., Ali, N., Salleh, Z., Rahman, A., Harun, S., Manaf, M., & Arof, H. (2014). All fiber mode-locked Erbium-doped fiber laser using single-walled carbon nanotubes embedded into polyvinyl alcohol film as saturable absorber. *Optics & Laser Technology, 62*, 40-43.

Ahmed, M. H. M., Al-Masoodi, A. H. H., Latiff, A. A., Arof, H., & Harun, S. W. (2017). Mechanically exfoliated 2D nanomaterials as saturable absorber for Q-switched erbium doped fiber laser. *Indian Journal of Physics, 91*(10), 1259-1264. doi:10.1007/s12648-017-1045-8

Ahmed, M. H. M., Al-Masoodi, A. H. H., Latiff, A. A., Arof, H., & Harun, S. W. J. I. J. o. P. (2017). Mechanically exfoliated 2D nanomaterials as saturable absorber for Q-switched erbium doped fiber laser. *91*(10), 1259-1264.

Ahmed, M. H. M., Ali, N. M., Salleh, Z. S., Rahman, A. A., Harun, S. W., Manaf, M., & Arof, H. (2014). All fiber mode-locked Erbium-doped fiber laser using single-walled carbon nanotubes embedded into polyvinyl alcohol film as saturable absorber. *Optics & Laser Technology, 62*, 40-43. doi:https://doi.org/10.1016/j.optlastec.2014.02.012

Ahmed, M. H. M., Ali, N. M., Salleh, Z. S., Rahman, A. A., Harun, S. W., Manaf, M., & Arof, H. (2015). Q-switched erbium doped fiber laser based on single and multiple walled carbon nanotubes embedded in polyethylene oxide film as saturable absorber. *Optics & Laser Technology, 65*, 25-28. doi:https://doi.org/10.1016/j.optlastec.2014.07.001

Ahmed, M. H. M., Latiff, A. A., Arof, H., Ahmad, H., & Harun, S. W. (2016). Soliton mode-locked erbium-doped fibre laser with mechanically exfoliated molybdenum disulphide saturable absorber. *Iet Optoelectronics, 10*(5), 169-173. doi:10.1049/iet-opt.2015.0097

Ahmed, M. H. M., Latiff, A. A., Arof, H., & Harun, S. W. (2016). Ultrafast erbium-doped fiber laser mode-locked with a black phosphorus saturable absorber. *Laser Physics Letters, 13*(9), 095104. doi:10.1088/1612-2011/13/9/095104

Al-Masoodi, A., Ahmed, M., Abdul Latiff, A., Arof, H., & Harun, S. W. (2016). Q-Switched Ytterbium-Doped Fiber Laser Using Black Phosphorus as Saturable Absorber. *Chinese Physics Letters, 33*, 054206. doi:10.1088/0256-307X/33/5/054206

Al-Masoodi, A., Ahmed, M., Arof, H., & Harun, S. (2018). Multi-wavelength Q-switched ytterbium-doped fiber laser with multi-walled carbon nanotubes. *Fiber and Integrated Optics, 37*(2), 92-102.

Al-Masoodi, A. H. H., Ahmad, F., Ahmed, M. H. M., Al-Masoodi, A. H. H., Alani, I. A. M., Arof, H., & Harun, S. W. (2018). Q-switched and mode-locked ytterbium-doped fibre lasers with Sb2Te3topological insulator saturable absorber. *Iet Optoelectronics, 12*(4), 180-184. doi:10.1049/iet-opt.2017.0134

Al-Masoodi, A. H. H., Ahmed, M. H. M., Latiff, A. A., Azzuhri, S. R., Arof, H., & Harun, S. W. (2017). Passively mode-locked ytterbium-doped fiber laser operation with few layer MoS2 PVA saturable absorber. *Optik, 145*, 543-548. doi:https://doi.org/10.1016/j.ijleo.2017.08.011

Al-Masoodi, A. H. H., Yasin, M., Ahmed, M. H. M., Latiff, A. A., Arof, H., & Harun, S. W. (2017). Mode-locked ytterbium-doped fiber laser using mechanically exfoliated black phosphorus as saturable absorber. *Optik, 147*, 52-58. doi:https://doi.org/10.1016/j.ijleo.2017.08.038

Al-Masoodi, A., Ismail, M., Ahmad, F., Kasim, N., Munajat, Y., Ahmad, H., & Wadi Harun, S. (2014). Q-switched Yb-doped fiber laser operating at 1073 nm using a carbon nanotubes saturable absorber. *Microwave and Optical Technology Letters, 56*(8), 1770-1773.

Alvarez-Chavez, J. A., Offerhaus, H. L., Nilsson, J., Turner, P., Clarkson, W., & Richardson, D. (2000). High-energy, high-power ytterbium-doped Q-switched fiber laser. *Optics Letters, 25*(1), 37-39.

Ando, Y., & Iijima, S. (1993). Preparation of carbon nanotubes by arc-discharge evaporation. *Japanese Journal of Applied Physics Part 2 Letters, 32*, L107-L107.

Ausschnitt, C. P., Jain, R. K., & Heritage, J. P. (1979). Cavity length detuning characteristics of the synchronously mode-locked CW dye laser. *Quantum Electronics, IEEE Journal of, 15*, 912-917. doi:10.1109/JQE.1979.1070118

Aziz, S. B., Rasheed, M. A., Saeed, S. R., & Abdullah, O. G. (2017). Synthesis and characterization of CdS nanoparticles grown in a polymer solution using in-situ chemical reduction technique. *Int J Electrochem Sci, 12*, 3263-3274.

Azooz, S. M., Ahmed, M. H. M., Ahmad, F., Hamida, B. A., Khan, S., Ahmad, H., & Harun, S. W. (2015). Passively Q-switched fiber lasers using a multi-walled carbon nanotube polymer composite based saturable absorber. *Optik, 126*(21), 2950-2954. doi:https://doi.org/10.1016/j.ijleo.2015.07.065

Babar, I. M., Harun, S. W., Yasin, M., & Ahmad, H. (2017). Mode-locking pulse generation in cladding pumped Erbium-Ytterbium co-doped fiber laser with graphene PVA film. *Optik, 136*, 531-535. doi:https://doi.org/10.1016/j.ijleo.2017.02.062

Bao, Q., Zhang, H., Ni, Z., Wang, Y., Polavarapu, L., Shen, Z., . . . Loh, K. P. (2011). Monolayer graphene as a saturable absorber in a mode-locked laser. *Nano Research, 4*(3), 297-307.

Bao, Q., Zhang, H., Wang, Y., Ni, Z., Yan, Y., Shen, Z. X., . . . Tang, D. Y. (2009). Atomic-layer graphene as a saturable absorber for ultrafast pulsed lasers. *Advanced Functional Materials, 19*(19), 3077-3083.

Bao, Q. L., Zhang, H., Wang, Y., Ni, Z. H., Yan, Y. L., Shen, Z. X., . . . Tang, D. Y. (2009). Atomic-Layer Graphene as a Saturable Absorber for Ultrafast Pulsed Lasers. *Advanced Functional Materials, 19*(19), 3077-3083. doi:10.1002/adfm.200901007

Baranoff, E., & Curchod, B. F. (2015). FIrpic: archetypal blue phosphorescent emitter for electroluminescence. *Dalton Transactions, 44*(18), 8318-8329.

Baranoff, E., & Curchod, B. F. E. (2015). FIrpic: archetypal blue phosphorescent emitter for electroluminescence. *Dalton Transactions, 44*(18), 8318-8329. doi:10.1039/C4DT02991G

Bharathi Devi, V., Arulmozhichelvan, P., & Murugakoothan, P. (2017). Synthesis and characterization of Znq2 and Znq2:CTAB particles for optical applications. *Bulletin of Materials Science, 40*(6), 1049-1053. doi:10.1007/s12034-017-1460-7

Bloom, B., Nicholson, T., Williams, J., Campbell, S., Bishof, M., Zhang, X., . . . Ye, J. (2014). An optical lattice clock with accuracy and stability at the 10− 18 level. *Nature, 506*(7486), 71.

Bonaccorso, F., Sun, Z., Hasan, T., & Ferrari, A. (2010). Graphene photonics and optoelectronics. *Nature Photonics, 4*(9), 611.

Boulet, J., Mohammadpour, A., & Shankar, K. (2015). Insights into the solution crystallization of oriented Alq3 and Znq2 microprisms and nanorods. *Journal of nanoscience and nanotechnology, 15*(9), 6680-6689.

Briseno, A. L., Mannsfeld, S. C. B., Ling, M. M., Liu, S., Tseng, R. J., Reese, C., . . . Bao, Z. (2006). Patterning organic single-crystal transistor arrays. *Nature, 444*, 913. doi:10.1038/nature05427

Cai, J.-H., Chen, H., Chen, S.-P., & Hou, J. (2018). Compressibility of dissipative solitons in mode-locked all-normal-dispersion fiber lasers. *Journal of Lightwave Technology, 36*(11), 2142-2151.

Cao, W., Wang, H., Luo, A., Luo, Z., & Xu, W. (2011). Graphene-based, 50 nm wide-band tunable passively Q-switched fiber laser. *Laser Physics Letters, 9*(1), 54.

Chen, B., Zhang, X., Guo, C., Wu, K., Chen, J., & Wang, J. (2016). Tungsten diselenide Q-switched erbium-doped fiber laser. *Optical Engineering, 55*(8), 1-5, 5. Retrieved from https://doi.org/10.1117/1.OE.55.8.081306

Chen, B., Zhang, X., Wu, K., Wang, H., Wang, J., & Chen, J. (2015). Q-switched fiber laser based on transition metal dichalcogenides MoS 2, MoSe 2, WS 2, and WSe 2. *Optics Express, 23*(20), 26723-26737.

Chen, X. (2002). Preparation and property of TiO 2 nanoparticle dispersed polyvinyl alcohol composite materials. *Journal of materials science letters, 21*(21), 1637-1639.

Chen, Y., Jiang, G., Chen, S., Guo, Z., Yu, X., Zhao, C., . . . Tang, D. (2015). Mechanically exfoliated black phosphorus as a new saturable absorber for both Q-switching and mode-locking laser operation. *Optics Express, 23*(10), 12823-12833.

Chen, Y., Jiang, G., Chen, S., Guo, Z., Yu, X., Zhao, C., . . . Fan, D. (2015). Mechanically exfoliated black phosphorus as a new saturable absorber for both Q-switching and Mode-locking laser operation. *Optics Express, 23*(10), 12823-12833. doi:10.1364/OE.23.012823

Chen, Y., Zhao, C., Chen, S., Du, J., Tang, P., Jiang, G., . . . Tang, D. (2014). Large energy, wavelength widely tunable, topological insulator Q-switched erbium-doped fiber laser. *IEEE Journal of Selected Topics in Quantum Electronics, 20*(5), 315-322.

Cheng, K.-N., Lin, Y.-H., & Lin, G.-R. (2013). Single- and double-walled carbon nanotube based saturable absorbers for passive mode-locking of an erbium-doped fiber laser. *Laser Physics, 23*(4), 045105. doi:10.1088/1054-660x/23/4/045105

Chhowalla, M., Shin, H. S., Eda, G., Li, L.-J., Loh, K. P., & Zhang, H. (2013). The chemistry of two-dimensional layered transition metal dichalcogenide nanosheets. *Nature Chemistry, 5*, 263. doi:10.1038/nchem.1589

Choi, H.-K., Jin, S.-H., Park, J.-W., Kim, S. Y., & Gal, Y.-S. (2012). Electro-optical and electrochemical properties of poly(2-ethynylthiophene). *Journal of Industrial and Engineering Chemistry, 18*(2), 814-817. doi:https://doi.org/10.1016/j.jiec.2011.10.005

Chong, C. Y. (2008). Femtosecond fiber lasers and amplifiers based on the pulse propagation at normal dispersion. *Cornell University*. doi:https://ecommons.cornell.edu/handle/1813/10833

Churchill, H. O., & Jarillo-Herrero, P. (2014). Two-dimensional crystals: Phosphorus joins the family. *Nature Nanotechnology, 9*(5), 330.

Clark, J., & Lanzani, G. (2010). Organic photonics for communications. *Nature Photonics, 4*(7), 438.

Coddington, I., Swann, W. C., Nenadovic, L., & Newbury, N. R. (2009). Rapid and precise absolute distance measurements at long range. *Nature Photonics, 3*(6), 351-356. doi:10.1038/nphoton.2009.94

Correia, F. C., Santos, T. C., Garcia, J. R., Peres, L. O., & Wang, S. H. (2015). Synthesis and characterization of a new semiconductor oligomer having quinoline and fluorene units. *Journal of the Brazilian Chemical Society, 26*(1), 84-91.

Cuba, M., & Muralidharan, G. (2015). Improved luminescence intensity and stability of thermal annealed ZnO incorporated Alq 3 composite films. *Journal of fluorescence, 25*(6), 1629-1635.

DeCoste, J. B., & Peterson, G. W. (2013). Preparation of hydrophobic metal-organic frameworks via plasma enhanced chemical vapor deposition of perfluoroalkanes for the removal of ammonia. *JoVE (Journal of Visualized Experiments)*(80), 51175.

Degnan, J. J. (1995). Optimization of passively Q-switched lasers. *IEEE Journal of Quantum Electronics, 31*(11), 1890-1901.

Digonnet, M. J. (2001). *Rare-earth-doped fiber lasers and amplifiers, revised and expanded*: CRC press.

Divayana, Y., Sun, X., Chen, B., Lo, G., Sarma, K., & Kwong, D. (2007). Bandgap engineering in Alq3-and NPB-based organic light-emitting diodes for efficient green, blue and white emission. *Solid-State Electronics, 51*(11-12), 1618-1623.

Dong, B., Hao, J., Hu, J., & Liaw, C.-y. (2011). Short linear-cavity Q-switched fiber laser with a compact short carbon nanotube based saturable absorber. *Optical Fiber Technology, 17*(2), 105-107. doi:https://doi.org/10.1016/j.yofte.2010.12.001

Dou, Z., Song, Y., Tian, J., Liu, J., Yu, Z., & Fang, X. (2014). Mode-locked ytterbium-doped fiber laser based on topological insulator: Bi2Se3. *Optics Express, 22*(20), 24055-24061. doi:10.1364/OE.22.024055

Du, J., Wang, Q., Jiang, G., Xu, C., Zhao, C., Xiang, Y., . . . Zhang, H. (2014). Ytterbium-doped fiber laser passively mode locked by few-layer Molybdenum Disulfide (MoS 2) saturable absorber functioned with evanescent field interaction. *Scientific reports, 4*, 6346.

Duling III, I. N., & Duling, I. N. (1995). *Compact sources of ultrashort pulses* (Vol. 18): Cambridge University Press.

Elashmawi, I., Hakeem, N., & Selim, M. S. (2009). Optimization and spectroscopic studies of CdS/poly (vinyl alcohol) nanocomposites. *Materials chemistry and physics, 115*(1), 132-135.

Fauziah, C. M., Rosol, A. H. A., Latiff, A. A., & Harun, S. W. (2017). The generation of Q-switched erbium-doped fiber laser using black phosphorus saturable absorber with 8% modulation depth. *IOP Conference Series: Materials Science and Engineering, 210*, 012043. doi:10.1088/1757-899x/210/1/012043

Feng, T., Mao, D., Cui, X., Li, M., Song, K., Jiang, B., . . . Quan, W. (2016). A Filmy Black-Phosphorus Polyimide Saturable Absorber for Q-Switched Operation in an Erbium-Doped Fiber Laser. *Materials (Basel, Switzerland), 9*(11), 917. doi:10.3390/ma9110917

Fermann, M. E., & Hartl, I. (2013). Ultrafast fibre lasers. *Nature Photonics, 7*, 868. doi:10.1038/nphoton.2013.280

Frindt, R. (1965). Optical Absorption of a Few Unit-Cell Layers of MoS_2. *Physical review, 140*(2A), A536.

Fukuda, T., Wei, B., Ichikawa, M., & Taniguchi, Y. (2007). Enhanced modulation speed of tris (8-hydroxyquinoline) aluminum-based organic light source with low-work-function electrode. *Japanese Journal of Applied Physics, 46*(12R), 7880.

Gao, B., Ma, C., Huo, J., Guo, Y., Sun, T., & Wu, G. (2018). Influence of gain fiber on dissipative soliton pairs in passively mode-locked fiber laser based on BP as a saturable absorber. *Optics Communications, 410*, 191-196. doi:https://doi.org/10.1016/j.optcom.2017.10.014

Gao, Y., Zhao, T. Z., Li, C. Y., Ge, W. Q., Wu, Q., Shi, Z. H., . . . Wang, Y. G. (2013). Diode-side-pumped passively Q-switched Nd:YAG laser at 1123 nm with reflective single walled carbon nanotube saturable absorber. *Optics Communications, 286*, 261-264. doi:10.1016/j.optcom.2012.08.045

Geim, A. K., & Novoselov, K. S. (2010). The rise of graphene. In *Nanoscience and Technology: A Collection of Reviews from Nature Journals* (pp. 11-19): World Scientific.

Ghelfi, P., Laghezza, F., Scotti, F., Serafino, G., Capria, A., Pinna, S., . . . Bogoni, A. (2014). A fully photonics-based coherent radar system. *Nature, 507*, 341-345. doi:10.1038/nature13078

Grecu, M. N., Mirea, A., Ghica, C., Cölle, M., & Schwoerer, M. (2005). Paramagnetic defect centres in crystalline Alq3. *Journal of Physics: Condensed Matter, 17*(39), 6271-6283. doi:10.1088/0953-8984/17/39/012

Grelu, P., & Akhmediev, N. (2012). Dissipative solitons for mode-locked lasers. *Nature Photonics, 6*, 84. doi:10.1038/nphoton.2011.345

Gupta, K. K., Onodera, N., Abedin, K. S., & Hyodo, M. (2002). Pulse repetition frequency multiplication via intracavity optical filtering in AM mode-locked fiber ring lasers. *IEEE Photonics Technology Letters, 14*(3), 284-286.

Hamdalla, T. A., & Hanafy, T. A. (2016). Optical properties studies for PVA/Gd, La, Er or Y chlorides based on structural modification. *Optik-International Journal for Light and Electron Optics, 127*(2), 878-882.

Hammer, P., Baker, M., Lenardi, C., & Gissler, W. (1997). Synthesis of carbon nitride films at low temperatures. *Journal of Vacuum Science & Technology A: Vacuum, Surfaces, and Films, 15*(1), 107-112.

Han, S., Zhang, F., Wang, M., Wang, L., Zhou, Y., Wang, Z., & Xu, X. (2017). Black phosphorus based saturable absorber for Nd-ion doped pulsed solid state laser operation. *Indian Journal of Physics, 91*(4), 439-443.

Harun, S. W., Ismail, M., Ahmad, F., Ismail, M., Nor, R. M., Zulkepely, N., & Ahmad, H. (2012). A Q-switched erbium-doped fiber laser with a carbon nanotube based saturable absorber. *Chinese Physics Letters, 29*(11), 114202.

Hasan, T., Sun, Z., Wang, F., Bonaccorso, F., Tan, P. H., Rozhin, A. G., & Ferrari, A. C. (2009). Nanotube–polymer composites for ultrafast photonics. *Advanced materials, 21*(38-39), 3874-3899.

Herda, R., Kivistö, S., & Okhotnikov, O. G. (2008). Dynamic gain induced pulse shortening in Q-switched lasers. *Optics Letters, 33*(9), 1011-1013. doi:10.1364/OL.33.001011

Hisyam, M. B., Rusdi, M. F., Latiff, A. A., & Harun, a. S. W. (2016). PMMA-doped CdSe quantum dots as saturable absorber in a Q-switched all-fiber laser. *Chin. Opt. Lett., 14*(8), 081404. doi:1671-7694

Hisyam, M. B., Rusdi, M. F. M., Latiff, A. A., & Harun, S. W. (2017). Generation of Mode-Locked Ytterbium Doped Fiber Ring Laser Using Few-Layer Black Phosphorus as a Saturable Absorber. *IEEE Journal of Selected Topics in Quantum Electronics, 23*(1), 39-43. doi:10.1109/JSTQE.2016.2532270

Holmes, R., Forrest, S., Tung, Y.-J., Kwong, R., Brown, J., Garon, S., & Thompson, M. (2003). Blue organic electrophosphorescence using exothermic host–guest energy transfer. *Applied Physics Letters, 82*(15), 2422-2424.

Horiguchi, Y., Honda, K., Kato, Y., Nakashima, N., & Niidome, Y. (2008). Photothermal Reshaping of Gold Nanorods Depends on the Passivating Layers of the Nanorod Surfaces. *Langmuir, 24*(20), 12026-12031. doi:10.1021/la800811j

Hou, L., Sun, J., Guo, H., Lin, Q., Wang, Y., Bai, Y., . . . Bai, J. (2018). High-efficiency, high-energy ytterbium-doped Q-switched fibre laser with graphene oxide-COOH saturable absorber. *Laser Physics Letters, 15*(7), 075103.

Huang, J. Y., Huang, S. C., Chang, H. L., Su, K. W., Chen, Y. F., & Huang, K. F. (2008). Passive Q switching of Er-Yb fiber laser with semiconductor saturable absorber. *Opt Express, 16*(5), 3002-3007. Retrieved from http://www.ncbi.nlm.nih.gov/pubmed/18542386

Huang, K.-X., Lu, B.-L., Li, D., Qi, X.-Y., Chen, H.-W., Wang, N., . . . Bai, J.-T. (2017). Black phosphorus flakes covered microfiber for Q-switched ytterbium-doped fiber laser. *Applied Optics, 56*(23), 6427-6431.

Huang, Y., Luo, Z., Li, Y., Zhong, M., Xu, B., Che, K., . . . Weng, J. (2014a). Widely-tunable, passively Q-switched erbium-doped fiber laser with few-layer MoS2 saturable absorber. *Optics Express, 22*(21), 25258-25266. doi:10.1364/OE.22.025258

Huang, Y., Luo, Z., Li, Y., Zhong, M., Xu, B., Che, K., . . . Weng, J. J. O. E. (2014b). Widely-tunable, passively Q-switched erbium-doped fiber laser with few-layer MoS 2 saturable absorber. *22*(21), 25258-25266.

Ikezawa, M., Kondo, Y., & Shirotani, I. (1983). Infrared optical absorption due to one and two phonon processes in black phosphorus. *Journal of the Physical Society of Japan, 52*(5), 1518-1520.

Ismail, E., Zolkopli, S., Lokman, M., Yahaya, H., Harun, S. W., & Ahmad, F. (2018). Q-switched Erbium Doped Fiber Laser Incorporating Antimony (III) Telluride in Polyvinyl Alcohol as Saturable Absorber. *Indonesian Journal of Electrical Engineering and Computer Science, 10*, 409-415. doi:10.11591/ijeecs.v10.i2.pp409-415

Jamieson, J. C. (1963). Crystal Structures Adopted by Black Phosphorus at High Pressures. *Science, 139*(3561), 1291-1292. doi:10.1126/science.139.3561.1291

Jiang, T., Yin, K., Zheng, X., Yu, H., & Cheng, X.-A. (2015). *Black phosphorus as a new broadband saturable absorber for infrared passively Q-switched fiber lasers* (Vol. 1504).

Jones, D. J., Diddams, S. A., Ranka, J. K., Stentz, A., Windeler, R. S., Hall, J. L., & Cundiff, S. T. (2000). Carrier-Envelope Phase Control of Femtosecond Mode-Locked Lasers and Direct Optical Frequency Synthesis. *Science, 288*(5466), 635-639. doi:10.1126/science.288.5466.635

Jung, M., Lee, J., Koo, J., Park, J., Song, Y.-W., Lee, K., . . . Lee, J. H. (2014). A femtosecond pulse fiber laser at 1935 nm using a bulk-structured Bi2Te3 topological insulator. *Optics Express, 22*(7), 7865-7874. doi:10.1364/OE.22.007865

Kaltenbrunner, M., Sekitani, T., Reeder, J., Yokota, T., Kuribara, K., Tokuhara, T., . . . Someya, T. (2013). An ultra-lightweight design for imperceptible plastic electronics. *Nature, 499*, 458. doi:10.1038/nature12314

Kambe, T., Sakamoto, R., Kusamoto, T., Pal, T., Fukui, N., Hoshiko, K., . . . Ishizaka, K. (2014). Redox control and high conductivity of nickel bis (dithiolene) complex π-nanosheet: a potential organic two-dimensional topological insulator. *Journal of the American Chemical Society, 136*(41), 14357-14360.

Kee, H. H., Lee, G., & Newson, T. P. (1998). Narrow linewidth CW and Q-switched erbium-doped fibre loop laser. *Electronics Letters, 34*(13), 1318-1319.

Keller, U. (2003). Recent developments in compact ultrafast lasers. *Nature, 424*, 831. doi:10.1038/nature01938

Keller, U. (2004). Ultrafast solid-state lasers. In *Progress in Optics* (Vol. 46, pp. 1-115): Elsevier.

Keller, U., Miller, D., Boyd, G., Chiu, T., Ferguson, J., & Asom, M. (1992). Solid-state low-loss intracavity saturable absorber for Nd: YLF lasers: an antiresonant semiconductor Fabry–Perot saturable absorber. *Optics Letters, 17*(7), 505-507.

Keren, S., Brand, E., Levi, Y., Levit, B., & Horowitz, M. (2002). Data storage in optical fibers and reconstruction by use of low-coherence spectral interferometry. *Optics Letters, 27*(2), 125-127.

Khazaeinezhad, R., Hosseinzadeh Kassani, S., Paulson, B., Jeong, H., Gwak, J., Rotermund, F., . . . Oh, K. (2017). Ultrafast nonlinear optical properties of thin-

solid DNA film and their application as a saturable absorber in femtosecond mode-locked fiber laser. *Scientific reports, 7*, 41480. doi:10.1038/srep41480

Khilo, A., Spector, S. J., Grein, M. E., Nejadmalayeri, A. H., Holzwarth, C. W., Sander, M. Y., . . . Kärtner, F. X. (2012). Photonic ADC: overcoming the bottleneck of electronic jitter. *Optics Express, 20*(4), 4454-4469. doi:10.1364/OE.20.004454

Khodagholy, D., Gelinas, J. N., Thesen, T., Doyle, W., Devinsky, O., Malliaras, G. G., & Buzsáki, G. (2014). NeuroGrid: recording action potentials from the surface of the brain. *Nature Neuroscience, 18*, 310. doi:10.1038/nn.3905

Kim, C., Facchetti, A., & Marks, T. J. (2007). Polymer Gate Dielectric Surface Viscoelasticity Modulates Pentacene Transistor Performance. *Science, 318*(5847), 76. Retrieved from

Kim, J.-M., Jha, S. K., Lee, D.-H., Chand, R., Jeun, J.-H., & Kim, Y.-S. (2012). A flexible pentacene thin film transistors as disposable DNA hybridization sensor. *Journal of Industrial and Engineering Chemistry, 18*(5), 1642-1646. doi:https://doi.org/10.1016/j.jiec.2012.02.026

Kim, J. Y., Lee, K., Coates, N. E., Moses, D., Nguyen, T.-Q., Dante, M., & Heeger, A. J. (2007). Efficient tandem polymer solar cells fabricated by all-solution processing. *Science, 317*(5835), 222-225.

Kim, O. Y., & Lee, J. Y. (2012). High efficiency deep blue phosphorescent organic light-emitting diodes using a tetraphenylsilane based phosphine oxide host material. *Journal of Industrial and Engineering Chemistry, 18*(3), 1029-1032. doi:https://doi.org/10.1016/j.jiec.2011.11.148

Koester, C. J., & Snitzer, E. (1964). Amplification in a fiber laser. *Applied optics, 3*(10), 1182-1186.

Kong, L., Qin, Z., Xie, G., Guo, Z., Zhang, H., Yuan, P., & Qian, L. (2016). Multilayer black phosphorus as broadband saturable absorber for pulsed lasers from 1 to 2.7 μm wavelength. *Laser Physics Letters, 13*(4), 045801. doi:10.1088/1612-2011/13/4/045801

Kong, Y. C., Yang, H. R., Li, W. L., & Chen, G. W. (2015). Switchable dual-wavelength all-fiber laser mode-locked by carbon nanotubes. *Laser Physics, 25*(1), 015101.

Kurkov, A. S. (2011). Q-switched all-fiber lasers with saturable absorbers. *Laser Physics Letters, 8*(5), 335. Retrieved from http://stacks.iop.org/1612-202X/8/i=5/a=001

Latiff, A. A., Kadir, N. A., Ismail, E. I., Shamsuddin, H., Ahmad, H., & Harun, S. W. (2017). All-fiber dual-wavelength Q-switched and mode-locked EDFL by SMF-THDF-SMF structure as a saturable absorber. *Optics Communications, 389*, 29-34. doi:https://doi.org/10.1016/j.optcom.2016.12.011

Laukamp, C., Salama, W., & González-Álvarez, I. (2016). Proximal and remote spectroscopic characterisation of regolith in the Albany–Fraser Orogen (Western Australia). *Ore Geology Reviews, 73*, 540-554.

Lazaridis, P., Debarge, G., & Gallion, P. (1995). Time–bandwidth product of chirped sech2 pulses: application to phase–amplitude-coupling factor measurement. *Optics Letters, 20*(10), 1160-1162. doi:10.1364/OL.20.001160

Lecourt, J. B., Martel, G., Guezo, M., Labbe, C., & Loualiche, S. (2006). Erbium-doped fiber laser passively Q-switched by an InGaAs/InP multiple quantum well saturable absorber. *Optics Communications, 263*(1), 71-83. doi:10.1016/j.optcom.2006.01.009

Lee, C. W., Kim, O. Y., & Lee, J. Y. (2014). Organic materials for organic electronic devices. *Journal of Industrial and Engineering Chemistry, 20*(4), 1198-1208. doi:https://doi.org/10.1016/j.jiec.2013.09.036

Lee, J., Chopra, N., Eom, S.-H., Zheng, Y., Xue, J., So, F., & Shi, J. (2008). Effects of triplet energies and transporting properties of carrier transporting materials on blue phosphorescent organic light emitting devices. *Applied Physics Letters, 93*(12), 348.

Lee, J., Kim, Y.-J., Lee, K., Lee, S., & Kim, S.-W. (2010). Time-of-flight measurement with femtosecond light pulses. *Nature Photonics, 4*(10), 716-720. doi:10.1038/nphoton.2010.175

Lei, K., Li, F., Mu, C., Wang, J., Zhao, Q., Chen, C., & Chen, J. (2017). High K-storage performance based on the synergy of dipotassium terephthalate and ether-based electrolytes. *Energy & Environmental Science, 10*(2), 552-557.

Li, C.-H., Benedick, A. J., Fendel, P., Glenday, A. G., Kärtner, F. X., Phillips, D. F., . . . Walsworth, R. L. (2008). A laser frequency comb that enables radial velocity measurements with a precision of 1 cm s-1. *Nature, 452*(7187), 610-612. doi:10.1038/nature06854

Li, H., Xia, H., Lan, C., Li, C., Zhang, X., Li, J., & Liu, Y. (2015). Passively -Switched Erbium-Doped Fiber Laser Based on Few-Layer MoS2 Saturable Absorber. *IEEE Photonics Technology Letters, 27*(1), 69-72.

Li, H., Zhang, F., Wang, Y., & Zheng, D. (2003). Synthesis and characterization of tris-(8-hydroxyquinoline) aluminum. *Materials Science & Engineering, B: Solid-State Materials for Advanced Technology, 100*(1), 40-46.

Li, J., Luo, H., Zhai, B., Lu, R., Guo, Z., Zhang, H., & Liu, Y. (2016). Black phosphorus: a two-dimension saturable absorption material for mid-infrared Q-switched and mode-locked fiber lasers. *Scientific reports, 6*, 30361. doi:10.1038/srep30361

Liao, M., Gao, W., Cheng, T., Duan, Z., Xue, X., Suzuki, T., & Ohishi, Y. (2012). Flat and broadband supercontinuum generation by four-wave mixing in a highly nonlinear tapered microstructured fiber. *Optics Express, 20*(26), B574-B580.

Lim, S., Elim, H., Gao, X., Wee, A., Ji, W., Lee, J., & Lin, J. (2006). Electronic and optical properties of nitrogen-doped multiwalled carbon nanotubes. *Physical Review B, 73*(4), 045402.

Lin, D., Xia, K., Li, R., Li, X., Li, G., Ueda, K.-i., & Li, J. (2010). Radially polarized and passively Q-switched fiber laser. *Optics Letters, 35*(21), 3574-3576.

Lin, J., Hu, Y., Chen, C., Gu, C., & Xu, L. (2015). Wavelength-tunable Yb-doped passively Q-switching fiber laser based on WS 2 saturable absorber. *Optics Express, 23*(22), 29059-29064.

Liu, G., Feng, D., Zhang, M., Jiang, S., & Zhang, C. (2015). Mode-locked erbium-doped all fiber laser using few-layer graphene as a saturable absorber. *Optics & Laser Technology, 72*, 70-73.

Liu, H., Chow, K., Yamashita, S., Set, S. J. O., & Technology, L. (2013). Carbon-nanotube-based passively Q-switched fiber laser for high energy pulse generation. *45*, 713-716.

Liu, H., Luo, A.-P., Wang, F.-Z., Tang, R., Liu, M., Luo, Z.-C., . . . Zhang, H. (2014). Femtosecond pulse erbium-doped fiber laser by a few-layer MoS 2 saturable absorber. *Optics Letters, 39*(15), 4591-4594.

Liu, H., Song, W., Yu, Y., Jiang, Q., Pang, F., & Wang, T. (2019). Black Phosphorus-Film with Drop-Casting Method for High-Energy Pulse Generation From Q-Switched Er-Doped Fiber Laser. *Photonic Sensors, 9*(3), 239-245. doi:10.1007/s13320-019-0549-6

Liu, J., Wu, S., Yang, Q.-H., & Wang, P. (2011). Stable nanosecond pulse generation from a graphene-based passively Q-switched Yb-doped fiber laser. *Optics Letters, 36*(20), 4008-4010.

Liu, J., Xu, J., & Wang, P. (2012). Graphene-based passively Q-switched 2 μm thulium-doped fiber laser. *Optics Communications, 285*(24), 5319-5322.

Liu, J., Xu, J., & Wang, P. (2012). High Repetition-Rate Narrow Bandwidth SESAM Mode-Locked Yb-Doped Fiber Lasers. *IEEE Photonics Technology Letters, 24*(7), 539-541. doi:10.1109/LPT.2011.2181992

Liu, X. (2011). Interaction and motion of solitons in passively-mode-locked fiber lasers. *Physical Review A, 84*(5), 053828.

Liu, X., Cui, Y., Han, D., Yao, X., & Sun, Z. (2015). Distributed ultrafast fibre laser. *Scientific reports, 5*, 9101.

Lo, K. K.-W. (2007). Luminescent Transition Metal Complexes as Biological Labels and Probes. In V. W. W. Yam (Ed.), *Photofunctional Transition Metal Complexes* (pp. 205-245). Berlin, Heidelberg: Springer Berlin Heidelberg.

Lu, S. B., Miao, L. L., Guo, Z. N., Qi, X., Zhao, C. J., Zhang, H., . . . Fan, D. Y. (2015). Broadband nonlinear optical response in multi-layer black phosphorus: an emerging infrared and mid-infrared optical material. *Optics Express, 23*(9), 11183-11194. doi:10.1364/OE.23.011183

Luo, A.-P., Luo, Z.-C., Liu, H., Zheng, X.-W., Ning, Q.-Y., Zhao, N., . . . Xu, W.-C. (2015). Noise-like pulse trapping in a figure-eight fiber laser. *Optics Express, 23*(8), 10421-10427.

Luo, Z.-C., Liu, M., Guo, Z.-N., Jiang, X.-F., Luo, A.-P., Zhao, C.-J., . . . Zhang, H. (2015). Microfiber-based few-layer black phosphorus saturable absorber for ultra-fast fiber laser. *Optics Express, 23*(15), 20030-20039.

Luo, Z., Huang, Y., Zhong, M., Li, Y., Wu, J., Xu, B., . . . Weng, J. (2014). 1-, 1.5-, and 2-µm fiber lasers Q-switched by a broadband few-layer MoS 2 saturable absorber. *Journal of Lightwave Technology, 32*(24), 4077-4084.

Luo, Z., Liu, C., Huang, Y., Wu, D., Wu, J., Xu, H., . . . Weng, J. (2014). Topological-Insulator Passively Q-Switched Double-Clad Fiber Laser at 2µm Wavelength. *IEEE Journal of Selected Topics in Quantum Electronics, 20*(5), 1-8. doi:10.1109/JSTQE.2014.2305834

Luo, Z., Zhou, M., Weng, J., Huang, G., Xu, H., Ye, C., & Cai, Z. (2010). Graphene-based passively Q-switched dual-wavelength erbium-doped fiber laser. *Optics Letters, 35*(21), 3709-3711. doi:10.1364/OL.35.003709

Mak, K. F., Lee, C., Hone, J., Shan, J., & Heinz, T. F. (2010). Atomically thin MoS 2: a new direct-gap semiconductor. *Physical review letters, 105*(13), 136805.

Mao, D., Jiang, B., Gan, X., Ma, C., Chen, Y., Zhao, C., . . . Zhao, J. (2015). Soliton fiber laser mode locked with two types of film-based Bi_2Te_3 saturable absorbers. *Photonics Research, 3*(2), A43-A46. doi:10.1364/PRJ.3.000A43

Markom, A. M., Sen-Winson, M. W., Paul, M. C., & Harun, S. W. (2017). *Ultrafast soliton mode-locked Zirconia-based Erbium-doped fiber laser with carbon nanotubes saturable absorber.* Paper presented at the IOP Conference Series: Materials Science and Engineering.

Martin, D. C. (2015). Molecular design, synthesis, and characterization of conjugated polymers for interfacing electronic biomedical devices with living tissue. *MRS Communications, 5*(2), 131-153. doi:10.1557/mrc.2015.17

Mehta, J., Vinayak, P., Tuteja, S. K., Chhabra, V. A., Bhardwaj, N., Paul, A., . . . Deep, A. (2016). Graphene modified screen printed immunosensor for highly sensitive detection of parathion. *Biosensors and Bioelectronics, 83*, 339-346.

Morkel, P., Jedrzejewski, K., Taylor, E., & Payne, D. (1992). Short-pulse, high-power Q-switched fiber laser. *IEEE Photonics Technology Letters, 4*(6), 545-547.

Muccini, M. (2006). A bright future for organic field-effect transistors. *Nature Materials, 5*(8), 605.

Nair, R. R., Blake, P., Grigorenko, A. N., Novoselov, K. S., Booth, T. J., Stauber, T., . . . Geim, A. K. (2008). Fine Structure Constant Defines Visual Transparency of Graphene. *Science, 320*(5881), 1308-1308. doi:10.1126/science.1156965

Nakazawa, M., Kubota, H., Sahara, A., & Tamura, K. (1998). Time-domain ABCD matrix formalism for laser mode-locking and optical pulse transmission. *IEEE Journal of Quantum Electronics, 34*(7), 1075-1081.

Nel, A., Xia, T., Mädler, L., & Li, N. J. s. (2006). Toxic potential of materials at the nanolevel. *311*(5761), 622-627.

Nemitz, N., Ohkubo, T., Takamoto, M., Ushijima, I., Das, M., Ohmae, N., & Katori, H. (2016). Frequency ratio of Yb and Sr clocks with 5 × 10−17 uncertainty at 150 seconds averaging time. *Nature Photonics, 10*(4), 258-261. doi:10.1038/nphoton.2016.20

Ngo, N. Q. (2016). *Ultra-fast fiber lasers: principles and applications with MATLAB® models*: CRC Press.

Nicholson, J. W., Yablon, A., Westbrook, P., Feder, K., & Yan, M. (2004). High power, single mode, all-fiber source of femtosecond pulses at 1550 nm and its use in supercontinuum generation. *Optics Express, 12*(13), 3025-3034.

Nishizawa, N. (2014). Ultrashort pulse fiber lasers and their applications. *Japanese Journal of Applied Physics, 53*(9), 090101.

Nodop, D., Limpert, J., Hohmuth, R., Richter, W., Guina, M., & Tunnermann, A. (2007). High-pulse-energy passively Q-switched quasi-monolithic microchip lasers operating in the sub-100-ps pulse regime. *Opt Lett, 32*(15), 2115-2117. Retrieved from http://www.ncbi.nlm.nih.gov/pubmed/17671554

Novoselov, K. S., Geim, A. K., Morozov, S. V., Jiang, D., Zhang, Y., Dubonos, S. V., . . . Firsov, A. A. (2004). Electric field effect in atomically thin carbon films. *Science, 306*(5696), 666-669. doi:10.1126/science.1102896

O'Mahony, M. J., Simeonidou, D., Hunter, D. K., & Tzanakaki, A. J. I. C. m. (2001). The application of optical packet switching in future communication networks. *39*(3), 128-135.

Obraztsov, A., Obraztsova, E., Tyurnina, A., & Zolotukhin, A. (2007). Chemical vapor deposition of thin graphite films of nanometer thickness. *Carbon.*

Owens, R. M., & Malliaras, G. G. (2011). Organic Electronics at the Interface with Biology. *MRS Bulletin, 35*(6), 449-456. doi:10.1557/mrs2010.583

Pan, H.-C., Liang, F.-P., Mao, C.-J., Zhu, J.-J., & Chen, H.-Y. (2007). Highly Luminescent Zinc(II)−Bis(8-hydroxyquinoline) Complex Nanorods: Sonochemical Synthesis, Characterizations, and Protein Sensing. *The Journal of Physical Chemistry B, 111*(20), 5767-5772. doi:10.1021/jp0703049

Park, S. M., Yu, H., Park, M. G., Han, S. Y., Kang, S. W., Park, H. M., & Kim, J. W. (2012). Quantitative analysis of an organic thin film by XPS, AFM and FT-IR. *Surface and Interface Analysis, 44*(2), 156-161.

Petropoulos, P., Offerhaus, H., Richardson, D., Dhanjal, S., & Zheludev, N. (1999). Passive Q-switching of fiber lasers using a broadband liquefying gallium mirror. *Applied Physics Letters, 74*(24), 3619-3621.

Peumans, P., Uchida, S., & Forrest, S. R. (2011). Efficient bulk heterojunction photovoltaic cells using small-molecular-weight organic thin films. In *Materials for Sustainable Energy: A Collection of Peer-Reviewed Research and Review Articles from Nature Publishing Group* (pp. 94-98): World Scientific.

Philippov, V., Kir'yanov, A., & Unger, S. (2004). Advanced configuration of erbium fiber passively Q-switched laser with Co/sup 2+: ZnSe crystal as saturable absorber. *IEEE Photonics Technology Letters, 16*(1), 57-59.

Popa, D., Sun, Z., Hasan, T., Torrisi, F., Wang, F., & Ferrari, A. (2011). Graphene Q-switched, tunable fiber laser. *Applied Physics Letters, 98*(7), 073106.

Quimby, R. S. (2006). Photonics and lasers. *johnwiley & sons Inc*.

Quintero, O. M. S., Chaparro, W. A., Ipaz, L., Barco, J. E. S., Beltrán, F. E., & Zambrano, G. (2013). Influence of the microstructure on the electrochemical properties of Al-Cr-N coatings deposited by co-sputtering method from a Cr-Al binary target. *Materials Research, 16*(1), 204-214.

Rahman, M. F., Latiff, A. A., Rusdi, M. F., Dimyati, K., & Harun, S. W. (2018). Q-switched ytterbium-doped fiber laser via a thulium-doped fiber saturable absorber. *Applied Optics, 57*(22), 6510-6515.

Ramadurai, K., Cromer, C. L., Lewis, L. A., Hurst, K. E., Dillon, A. C., Mahajan, R. L., & Lehman, J. H. (2008). High-performance carbon nanotube coatings for high-power laser radiometry. *Journal of Applied Physics, 103*(1), 013103.

Razak, N., Yasin, M., Zakaria, Z., Abdul Latiff, A., & Harun, S. W. (2017). Q-switched fiber laser with tungsten disulfide saturable absorber prepared by drop casting method. *Photonics Letters of Poland, 9*, 103. doi:10.4302/plp.v9i3.752

Razak, N. N., Latiff, A. A., Zakaria, Z., & Harun, S. W. (2017). Q-switched Erbium-doped Fiber Laser with a Black Phosphorus Saturable Absorber. *Photonics Letters of Poland, 9*(2), 72-74.

Ren, X., Li, J., Holmes, R. J., Djurovich, P. I., Forrest, S. R., & Thompson, M. E. (2004). Ultrahigh energy gap hosts in deep blue organic electrophosphorescent devices. *Chemistry of materials, 16*(23), 4743-4747.

Rivnay, J., Owens, R. M., & Malliaras, G. G. (2014). The Rise of Organic Bioelectronics. *Chemistry of materials, 26*(1), 679-685. doi:10.1021/cm4022003

Rosol, A. H. A., Rahman, H. A., Ismail, E. I., Jusoh, Z., Latiff, A. A., & Harun, S. W. (2017). Mode-locked fiber laser with a manganese-doped cadmium selenide saturable absorber. *Chinese Optics Letters, 15*(7), 071405. Retrieved from http://col.osa.org/abstract.cfm?URI=col-15-7-071405

Šafaříková, E., Švihálková Šindlerová, L., Stříteský, S., Kubala, L., Vala, M., Weiter, M., & Víteček, J. (2018). Evaluation and improvement of organic semiconductors' biocompatibility towards fibroblasts and cardiomyocytes. *Sensors and Actuators B: Chemical, 260*, 418-425. doi:https://doi.org/10.1016/j.snb.2017.12.108

Saraceno, C. J., Schriber, C., Mangold, M., Hoffmann, M., Heckl, O. H., Baer, C. R., . . . Keller, U. (2011). SESAMs for high-power oscillators: design guidelines and damage thresholds. *IEEE Journal of Selected Topics in Quantum Electronics, 18*(1), 29-41.

Satoh, N., Nakashima, T., Kamikura, K., & Yamamoto, K. (2008). Quantum size effect in TiO_2 nanoparticles prepared by finely controlled metal assembly on dendrimer templates. *Nature Nanotechnology, 3*, 106. doi:10.1038/nnano.2008.2 https://www.nature.com/articles/nnano.2008.2#supplementary-information

Savage, E. (2012). *Carbon-carbon composites*: Springer Science & Business Media.

Schmidt, A., Rivier, S., Steinmeyer, G., Yim, J. H., Cho, W. B., Lee, S., . . . Griebner, U. (2008). Passive mode locking of Yb:KLuW using a single-walled carbon nanotube saturable absorber. *Opt Lett, 33*(7), 729-731. doi:10.1364/OL.33.000729

Schmidt, W., & Schäfer, F. (1968). Self-mode-locking of dye-lasers with saturated absorbers. *Physics Letters A, 26*(11), 558-559.

Shao, Q., Wang, T., Wang, X., & Chen, Y. (2011). Bis-(8-hydroxyquinoline) copper nanoribbons: preparation, characterization, and photoconductivity. *Frontiers of Optoelectronics in China, 4*(2), 195-198.

Sheng, Q., Feng, M., Xin, W., Han, T., Liu, Y., Liu, Z., & Tian, J. (2013). Actively manipulation of operation states in passively pulsed fiber lasers by using graphene saturable absorber on microfiber. *Optics Express, 21*(12), 14859-14866.

Shi-Xiang, X., Wen-Xue, L., Qiang, H., Hui, Z., & He-Ping, Z. (2008). Efficient laser-diode end-pumped passively Q-switched mode-locked Yb: LYSO laser based on SESAM. *Chinese Physics Letters, 25*(2), 548.

Siddiq, N., Chong, W., Pramono, Y., Muntini, M., & Ahmad, H. (2019). C-band tunable performance of passively Q-switched erbium-doped fiber laser using Tin (IV) oxide as a saturable absorber. *Optics Communications, 442*, 1-7.

Siegman, A. E. (1986). Lasers university science books. *Mill Valley, CA, 37*, 208.

Sigm-Aaldrich. (2019). Tris-(8-hydroxyquinoline)aluminum. Retrieved from [cited 9/Dec/2019], https://www.sigmaaldrich.com/catalog/product/aldrich/697737?lang=en&region=MY

Smirnov, S. V., Kobtsev, S. M., & Kukarin, S. V. (2014). Efficiency of non-linear frequency conversion of double-scale pico-femtosecond pulses of passively mode-locked fiber laser. *Optics Express, 22*(1), 1058-1064. doi:10.1364/OE.22.001058

Smith, N. J., Blow, K. J., & Andonovic, I. (1992). Sideband generation through perturbations to the average soliton model. *Journal of Lightwave Technology, 10*(10), 1329-1333. doi:10.1109/50.166771

Snitzer, E. (1961a). Optical Maser Action of Nd+3 in a Barium Crown Glass. *Physical review letters, 7*(12), 444-446. doi:10.1103/PhysRevLett.7.444

Snitzer, E. (1961b). Proposed fiber cavities for optical masers. *Journal of Applied Physics, 32*(1), 36-39.

Sobon, G. (2015). Mode-locking of fiber lasers using novel two-dimensional nanomaterials: graphene and topological insulators [Invited]. *Photonics Research, 3*(2), A56-A63. doi:10.1364/PRJ.3.000A56

Someya, T., Bao, Z., & Malliaras, G. G. (2016). The rise of plastic bioelectronics. *Nature, 540*, 379. doi:10.1038/nature21004

Someya, T., Sekitani, T., Iba, S., Kato, Y., Kawaguchi, H., & Sakurai, T. (2004). A large-area, flexible pressure sensor matrix with organic field-effect transistors for artificial skin applications. *101*(27), 9966-9970. doi:10.1073/pnas.0401918101 %J Proceedings of the National Academy of Sciences of the United States of America

Song, Y.-W., Jang, S. Y., Han, W.-S., & Bae, M.-K. (2010). Graphene mode-lockers for fiber lasers functioned with evanescent field interaction. *Applied Physics Letters, 96*, 051122-051122. doi:10.1063/1.3309669

Sotor, J., Sobon, G., Grodecki, K., & Abramski, K. (2014). Mode-locked erbium-doped fiber laser based on evanescent field interaction with Sb2Te3 topological insulator. *Applied Physics Letters, 104*(25), 251112.

Sotor, J., Sobon, G., Kowalczyk, M., Macherzynski, W., Paletko, P., & Abramski, K. M. (2015). Ultrafast thulium-doped fiber laser mode locked with black phosphorus. *Optics Letters, 40*(16), 3885-3888. doi:10.1364/OL.40.003885

Spühler, G., Paschotta, R., Fluck, R., Braun, B., Moser, M., Zhang, G., . . . Keller, U. (1999). Experimentally confirmed design guidelines for passively Q-switched microchip lasers using semiconductor saturable absorbers. *JOSA B, 16*(3), 376-388.

Spühler, G., Paschotta, R., Kullberg, M., Graf, M., Moser, M., Mix, E., . . . Keller, U. (2001). A passively Q-switched Yb: YAG microchip laser. *Applied Physics B, 72*(3), 285-287.

Steinmetz, T., Wilken, T., Araujo-Hauck, C., Holzwarth, R., Hänsch, T. W., Pasquini, L., . . . Udem, T. (2008). Laser Frequency Combs for Astronomical Observations. *Science, 321*(5894), 1335-1337. doi:10.1126/science.1161030

Stetser, D., & DeMaria, A. (1966). Optical spectra of ultrashort optical pulses generated by mode-locked glass: Nd lasers. *Applied Physics Letters, 9*(3), 118-120.

Sumimura, K., Genda, Y., Ohta, T., Itoh, K., & Nishizawa, N. (2010). Quasi-supercontinuum generation using 1.06 μmultrashort-pulse laser system for ultrahigh-resolution optical-coherence tomography. *Optics Letters, 35*(21), 3631-3633.

Sun, L., Lin, Z., Peng, J., Weng, J., Huang, Y., & Luo, Z. (2014). Preparation of Few-Layer Bismuth Selenide by Liquid-Phase-Exfoliation and Its Optical Absorption Properties. *Scientific reports, 4*, 4794. doi:10.1038/srep04794

Sun, Z., Hasan, T., & Ferrari, A. (2012). Ultrafast lasers mode-locked by nanotubes and graphene. *Physica E: Low-dimensional Systems and Nanostructures, 44*(6), 1082-1091.

Sun, Z., Hasan, T., Torrisi, F., Popa, D., Privitera, G., Wang, F., . . . Ferrari, A. C. (2010). Graphene mode-locked ultrafast laser. *ACS nano, 4*(2), 803-810.

Svelto, O., & Hanna, D. C. (2013). *Principles of Lasers*: Springer US.

Tang, C. W. (1986). Two-layer organic photovoltaic cell. *Applied Physics Letters, 48*(2), 183-185.

Ter-Mikirtychev, V. V. (2014). *Fundamentals of fiber lasers and fiber amplifiers*: Springer.

Tey, K. L., Rahman, M. F. A., Rosol, A. H. A., Rusdi, M. F. M., Mahyuddin, M. B. H., Harun, S. W., & Latiff, A. A. (2017). Q-switched double-clad Ytterbium-doped fiber laser using MoS2 flakes saturable absorber. *IOP Conference Series: Materials Science and Engineering, 210*, 012054. doi:10.1088/1757-899x/210/1/012054

Tran, V., Soklaski, R., Liang, Y., & Yang, L. (2014). Layer-controlled band gap and anisotropic excitons in few-layer black phosphorus. *Physical Review B, 89*(23), 235319.

Travers, J., Rulkov, A., Cumberland, B., Popov, S., & Taylor, J. (2008). Visible supercontinuum generation in photonic crystal fibers with a 400W continuous wave fiber laser. *Optics Express, 16*(19), 14435-14447.

Udem, T., Holzwarth, R., & Hänsch, T. W. (2002). Optical frequency metrology. *Nature, 416*(6877), 233.

Wang, B., Zhang, F., Pang, F., Wang, T. E. D. P. J. M. D. T. J., & Yang, C. (2011, 2011/11/13). *An optical fiber humidity sensor based on optical absorption.* Paper presented at the Optical Sensors and Biophotonics, Shanghai.

Wang, G. (2017). Wavelength-switchable passively mode-locked fiber laser with mechanically exfoliated molybdenum ditelluride on side-polished fiber. *Optics & Laser Technology, 96*, 307-312. doi:https://doi.org/10.1016/j.optlastec.2017.05.030

Wang, J., Chen, L., Dou, C., Yan, H., Meng, L., & Wei, Z. (2018). Mo0.5W0.5S2 for Q-switched pulse generation in ytterbium-doped fiber laser. *Nanotechnology, 29*(22), 224002. doi:10.1088/1361-6528/aab5f2

Wang, L.-Y., Xu, W.-C., Luo, Z.-C., Cao, W.-J., Luo, A.-P., Dong, J.-L., & Wang, H.-Y. (2012). Dark pulses with tunable repetition rate emission from fiber ring laser. *Optics Communications, 285*(8), 2113-2117. doi:https://doi.org/10.1016/j.optcom.2011.12.073

Wang, M., Chen, C., Li, Q., Huang, K., & Chen, H. (2014). *Passively mode-locked Er-doped fiber laser based on a semiconductor saturable absorber mirror.* Paper presented at the Optoelectronic Devices and Integration V.

Wang, Q., Chen, Y., Jiang, G., Miao, L., Zhao, C., Fu, X., . . . Zhang, H. (2015). Drop-Casted Self-Assembled Topological Insulator Membrane as an Effective Saturable Absorber for Ultrafast Laser Photonics. *IEEE Photonics Journal, 7*(2), 1-11. doi:10.1109/JPHOT.2015.2406754

Wang, Q. H., Kalantar-Zadeh, K., Kis, A., Coleman, J. N., & Strano, M. S. (2012). Electronics and optoelectronics of two-dimensional transition metal dichalcogenides. *Nature Nanotechnology, 7*(11), 699.

Wang, S., Yu, H., Zhang, H., Wang, A., Zhao, M., Chen, Y., . . . Wang, J. (2014). Broadband few-layer MoS2 saturable absorbers. *Advanced materials, 26*(21), 3538-3544.

Wang, X., Zhou, P., Wang, X., Xiao, H., & Liu, Z. (2014). 2 µm bright–dark pulses in Tm-doped fiber ring laser with net anomalous dispersion. *Applied Physics Express, 7*(2), 022704. doi:10.7567/apex.7.022704

Warschauer, D. (1963). Electrical and optical properties of crystalline black phosphorus. *Journal of Applied Physics, 34*(7), 1853-1860.

Wei, L., Zhou, D., Fan, H. Y., & Liu, W. (2012). Graphene-Based Q-Switched Erbium-Doped Fiber Laser With Wide Pulse-Repetition-Rate Range. *IEEE Photonics Technology Letters, 24*(4), 309-311. doi:10.1109/LPT.2011.2178821

Wen, M., Xu, J., Liu, L., Lai, P.-T., & Tang, W.-M. (2017). Improved Electrical Performance of Multilayer MoS 2 Transistor With NH 3-Annealed ALD HfTiO Gate Dielectric. *IEEE Transactions on Electron Devices, 64*(3), 1020-1025.

Williams, D. J. (1983). *Nonlinear optical properties of organic and polymeric materials.* Paper presented at the ACS Symposium series 233.

Wilson, J. A., & Yoffe, A. (1969). The transition metal dichalcogenides discussion and interpretation of the observed optical, electrical and structural properties. *Advances in Physics, 18*(73), 193-335.

Wittig, J., & Matthias, B. (1968). Superconducting phosphorus. *Science, 160*(3831), 994-995.

Woodward, R., Howe, R., Runcorn, T., Hu, G., Torrisi, F., Kelleher, E., & Hasan, T. (2015). Wideband saturable absorption in few-layer molybdenum diselenide (MoSe 2) for Q-switching Yb-, Er-and Tm-doped fiber lasers. *Optics Express, 23*(15), 20051-20061.

Woodward, R., & Kelleher, E. J. A. S. (2015). 2D saturable absorbers for fibre lasers. *5*(4), 1440-1456.

Wu, K., Zhang, X., Wang, J., Li, X., & Chen, J. (2015). WS_2 as a saturable absorber for ultrafast photonic applications of mode-locked and Q-switched lasers. *Optics Express, 23*(9), 11453-11461.

Wu, M., Chen, Y., Zhang, H., & Wen, S. (2014). Nanosecond Q-Switched Erbium-Doped Fiber Laser With Wide Pulse-Repetition-Rate Range Based on Topological Insulator. *IEEE Journal of Quantum Electronics, 50*(6), 393-396. doi:10.1109/JQE.2014.2314774

Xia, F., Wang, H., & Jia, Y. (2014). Rediscovering black phosphorus as an anisotropic layered material for optoelectronics and electronics. *Nature communications, 5*, 4458.

Xie, W., He, W.-W., Du, D.-Y., Li, S.-L., Qin, J.-S., Su, Z.-M., . . . Lan, Y.-Q. (2016). A stable Alq3@MOF composite for white-light emission. *Chemical Communications, 52*(16), 3288-3291. doi:10.1039/C5CC08703A

Xu, J., Liu, J., Wu, S., Yang, Q.-H., & Wang, P. (2012). Graphene oxide mode-locked femtosecond erbium-doped fiber lasers. *Optics Express, 20*(14), 15474-15480.

Xu, S. X., Li, W. X., Hao, Q., Zhai, H., & Zeng, H. P. (2008). Efficient laser-diode end-pumped passively Q-switched mode-locked Yb : LYSO laser based on SESAM. *Chinese Physics Letters, 25*(2), 548-551. Retrieved from <Go to ISI>://WOS:000253316600053

Xu, X., Zhai, J., Li, L., Chen, Y., Yu, Y., Zhang, M., . . . Tang, Z. (2014). Passively mode-locking erbium-doped fiber lasers with 0.3 nm single-walled carbon nanotubes. *Scientific reports, 4*, 6761-6761. doi:10.1038/srep06761

Xue, J., Uchida, S., Rand, B. P., & Forrest, S. R. (2004). Asymmetric tandem organic photovoltaic cells with hybrid planar-mixed molecular heterojunctions. *Applied Physics Letters, 85*(23), 5757-5759.

Yan, P., Liu, A., Chen, Y., Wang, J., Ruan, S., Chen, H., & Ding, J. (2015). Passively mode-locked fiber laser by a cell-type WS2 nanosheets saturable absorber. *Scientific reports, 5*, 12587. doi:10.1038/srep12587

Yang, Y., Yang, S., Li, C., & Lin, X. (2019). Passively Q-switched and mode-locked Tm-Ho co-doped fiber laser using a WS2 saturable absorber fabricated by chemical vapor deposition. *Optics & Laser Technology, 111*, 571-574. doi:https://doi.org/10.1016/j.optlastec.2018.10.023

Yap, Y., Kida, S., Aoyama, T., Mori, Y., & Sasaki, T. (1998). Influence of negative dc bias voltage on structural transformation of carbon nitride at 600 C. *Applied Physics Letters, 73*(7), 915-917.

Yawalkar, P., Dhoble, S., Thejo Kalyani, N., Atram, R., & Kokode, N. J. L. (2013). Photoluminescence of Alq3-and Tb-activated aluminium–tris (8-hydroxyquinoline) complex for blue chip-excited OLEDs. *28*(1), 63-68.

Yin, S., Hua, Y., Chen, X., Yang, X., Hou, Y., & Xu, X. (2000). Improved efficiency of molecular organic EL devices based on super molecular structure. *Synthetic Metals, 111-112*, 109-112. doi:https://doi.org/10.1016/S0379-6779(99)00311-2

Yook, K. S., & Lee, J. Y. (2012). Simplified pin organic light-emitting diodes using an universal ambipolar material. *Journal of Industrial and Engineering Chemistry, 18*(1), 309-311.

Zakaria, U., Harun, S., Reddy, P., Dutta, D., Das, S., Dhar, A., . . . Yasin, M. (2018). Q-Switched Hafnium Bismuth Erbium-Doped Fiber Laser With Bismuth (III) Telluride Based Saturable Absorber. *Chalcogenide Letters, 15*(4), 181-186.

Zaytsev, A., Lin, C.-H., You, Y.-J., Chung, C.-C., Wang, C.-L., & Pan, C.-L. (2013). Supercontinuum generation by noise-like pulses transmitted through normally dispersive standard single-mode fibers. *Optics Express, 21*(13), 16056-16062.

Zhang, B. Y., Liu, T., Meng, B., Li, X., Liang, G., Hu, X., & Wang, Q. J. (2013). Broadband high photoresponse from pure monolayer graphene photodetector. *Nature communications, 4*, 1811. doi:10.1038/ncomms2830 https://www.nature.com/articles/ncomms2830#supplementary-information

Zhang, H., Lu, S., Zheng, J., Du, J., Wen, S., Tang, D., & Loh, K. (2014). Molybdenum disulfide (MoS 2) as a broadband saturable absorber for ultra-fast photonics. *Optics Express, 22*(6), 7249-7260.

Zhang, H., Tang, D., Zhao, L., Wu, X., & Tam, H. (2009). Dissipative vector solitons in a dispersion-managed cavity fiber laser with net positive cavity dispersion. *Optics Express, 17*(2), 455-460.

Zhang, H., Tang, D. Y., Wu, X., & Zhao, L. M. (2009). Multi-wavelength dissipative soliton operation of an erbium-doped fiber laser. *Optics Express, 17*(15), 12692-12697. doi:10.1364/OE.17.012692

Zhang, H., Tang, D. Y., Zhao, L. M., Bao, Q. L., Loh, K. P., Lin, B., & Tjin, S. C. (2010). Compact graphene mode-locked wavelength-tunable erbium-doped fiber lasers: from all anomalous dispersion to all normal dispersion. *Laser Physics Letters, 7*(8), 591-596. doi:10.1002/lapl.201010025

Zhang, L., Fan, J., Wang, J., Hu, J., Lotya, M., Wang, G., . . . Wang, J. (2012). Graphene incorporated Q-switching of a polarization-maintaining Yb-doped fiber laser. *Laser Physics Letters, 9*(12), 888.

Zhang, L., Wang, Y., Yu, H., Sun, L., Hou, W., Lin, X., & Li, J. (2011). Passive mode-locked Nd: YVO 4 laser using a multi-walled carbon nanotube saturable absorber. *Laser Physics, 21*(8), 1382-1386.

Zhang, M., Howe, R. C. T., Woodward, R. I., Kelleher, E. J. R., Torrisi, F., Hu, G., . . . Hasan, T. (2015). Solution processed MoS2-PVA composite for sub-bandgap mode-locking of a wideband tunable ultrafast Er:fiber laser. *Nano Research, 8*(5), 1522-1534. doi:10.1007/s12274-014-0637-2

Zhang, M., Hu, G., Hu, G., Howe, R., Chen, L., Zheng, Z., & Hasan, T. (2015). Yb-and Er-doped fiber laser Q-switched with an optically uniform, broadband WS 2 saturable absorber. *Scientific reports, 5*, 17482.

Zhang, U., Popa, D., Sun, Z., Hasan, T., Ferrari, A., & Ilday, F. (2013). *All-fiber Yb-doped laser mode-locked by nanotubes.* Paper presented at the Lasers and Electro-Optics Europe (CLEO EUROPE/IQEC), 2013 Conference on and International Quantum Electronics Conference.

Zhao, C., Zou, Y., Chen, Y., Wang, Z., Lu, S., Zhang, H., . . . Tang, D. (2012). Wavelength-tunable picosecond soliton fiber laser with topological insulator: Bi 2 Se 3 as a mode locker. *Optics Express, 20*(25), 27888-27895.

Zhao, J., Yan, P., Ruan, S., Yu, Y., Du, G., Zhang, G., . . . Luo, J. (2012). Multi-wavelength graphene-based Q-switched erbium-doped fiber laser. *Optical Engineering, 51*(7), 074201.

Zhao, L., Tang, D., Wu, X., Bao, Q., & Loh, K. (2010). Dissipative soliton operation of an ytterbium-doped fiber laser mode locked with atomic multilayer graphene. *Optics Letters, 35*, 3622-3624. doi:10.1364/OL.35.003622

Zhen, T., Kan, W., Lingchen, K., Nan, Y., Yao, W., Rong, C., . . . Yulong, T. (2015). Mode-locked thulium fiber laser with MoS 2. *Laser Physics Letters, 12*(6), 065104. Retrieved from http://stacks.iop.org/1612-202X/12/i=6/a=065104

Zheng, Y., Dong, X., Zhao, C., Li, Y., Shao, L., & Jin, S. (2013). Relative humidity sensor based on microfiber loop resonator. Advances in Materials Science and Engineering, 2013.

Zhou, D. P., Wei, L., Dong, B., & Liu, W. K. (2010). Tunable Passively Q-switched Erbium-Doped Fiber Laser With Carbon Nanotubes as a Saturable Absorber. IEEE Photonics Technology Letters, 22(1), 9-11. doi:10.1109/LPT.2009.2035325

Zuikafly, S. N. F., Khalifa, A., Ahmad, F., Shafie, S., & Harun, S. (2018). Conductive graphene as passive saturable absorber with high instantaneous peak power and pulse energy in Q-switched regime. Results in Physics, 9, 371-375. doi:https://doi.org/10.1016/j.rinp.2018.03.002

LIST OF PUBLICATIONS

List of publications during the study:

1. **Salam, S.**, Al-Masoodi, A., Al-Hiti, A. S., Al-Masoodi, A. H., Wang, P., Wong, W. R., & Harun, S. W. (2019). *FIrpic thin film as saturable absorber for passively Q-switched and mode-locked erbium-doped fiber laser*. Optical Fiber Technology, 50, 256-262.

2. **Salam, S.**, Al-Masoodi, A., Wang, P., & Harun, S. (2020). *Hybrid organic small molecules as a saturable absorber for passive Q-switching in erbium-doped fiber laser*. OSA Continuum, 3(2), 177-185.

3. **Salam, S.**, Al-Masoodi, A. H., Wang, P., & Harun, S. W. (2020). *Femtosecond mode-locked erbium-doped fibre laser with Alq_3 saturable absorber*. IET Optoelectronics.

4. **Salam, S.**, Al-Masoodi, A. H. H., Yasin, M., & Harun, S. W. (2020). *Soliton mode-locked Er-doped fiber laser by using Alq_3 saturable absorber*. Optics & Laser Technology, 123, 105893.

5. **Salam, S.**, Azooz, S. M., Nizamani, B., Najm, M. M., & Harun, S. W. (2020). *Mode-locked laser at 1066 nm by using Alq_3 as saturable absorber in all-fiber based cavity*. Optik, 165179.

6. **Salam, S.**, Harun, S. W., Al-Masoodi, A. H., Ahmed, M. H., Al-Masoodi, A. H., Alani, I. A., . . . Yasin, M. (2019). *Tris-(8-hydroxyquinoline) aluminium thin film as saturable absorber for passively Q-switched erbium-doped fibre laser*. IET Optoelectronics, 13(5), 247-253.

7. **Salam, S.**, Sulaiman, S., Al-Masoodi, A., Al-Azzawi, A. A., & Harun, S. (2019). *Q-switched ytterbium-doped fiber laser by using FIrpic as a saturable absorber*. OSA Continuum, 2(7), 2145-2152.

8. **Salam, S.**, Wong, W. R., Al-Masoodi, A., & Harun, S. W. (2019). *High-energy Q-switched ytterbium-doped all-fiber laser with tris-(8-hydroxyquinoline) aluminum as saturable absorber*. Optical Materials Express, 9(8), 3215-3225.

9. Nizamani, B., Jafry, A., **Salam, S.**, Najm, M. M., Khudus, M. A., Hanafi, E., & Harun, S. (2020). *Mechanical exfoliation of indium tin oxide as saturable absorber for Q-switched Ytterbium-doped and Erbium-doped fiber lasers*. Optics Communications, 126217.

10. Nizamani, B., Memon, F., Umar, Z., **Salam, S.**, Najm, M., Khudus, M. A., . . . Harun, S. (2020). *Q-switched erbium-doped fiber laser with silicon oxycarbide saturable absorber*. Optik, 165234.

11. Nizamani, B., **Salam, S**., Jafry, A., Zahir, N., Jurami, N., Khudus, M. A., . . . Harun, S. (2020). *Indium Tin Oxide Coated D-Shape Fiber as a Saturable Absorber for Generating a Dark Pulse Mode-Locked Laser*. Chinese Physics Letters, 37(5), 054202.